Lipocalin 2 as a pathologic mediator of cancer cachexia and neurocognitive decline

By Brennan G. Olson

A DISSERTATION

Presented to:
The Physiology and Pharmacology Graduate Program
and the Oregon Health & Science University School of Medicine

In partial fulfillment of the requirements for the degree:

Doctor of Philosophy

April 30th, 2021

School of Medicine

Oregon Health & Science University

CERTIFICATE OF APPROVAL

This is to certify that the PhD dissertation of

Brennan G. Olson

has been approved

Daniel Marks, MD, PhD
Mentor

Aaron Grossberg, MD, PhD
Committee Chair

Shuih-Wen Luoh, MD, PhD
Member

David Jacoby, MD
Member

Jonathan Brody, PhD
Member

Table of Contents

Acknowledgements

I owe a great debt to several individuals that enabled me to complete the work described in this document. I will start with my wife, Ashley, as she is a constant source of motivation and a pillar of strength that I leaned on throughout my graduate studies. Whether it was long days or nights in the lab, weekends spent in the mouse room, or simply eating dinner in front of my computer at home in order to read and analyze data in the evenings, Ashley is continually supportive of my vocation. Additionally, Ashley goes above and beyond, having helped me dissect mouse tissues on several occasions when short-handed, critically reading and assessing my manuscripts herein (many of which she is acknowledged for), and pushing me to reach deadlines. Having spent several years in a basic science lab focused on breast cancer progression, written a thesis for her master's program, and now a practicing provider in a urologic oncology setting, I may have received the most qualified, yet grossly underpaid (zero dollars to be precise), assistance during my graduate studies through her. Her brilliance, work ethic, and perseverance continue to inspire me, and I am incredibly fortunate to have her as my life partner.

Ashley and I welcomed our beautiful baby boy, Griffin, to the world during my second year of graduate school. While the COVID-19 pandemic certainly reduced my experimental production, the timing of the pandemic could not have been better—lab access was restricted less than three weeks after Griffin was born, and I was sitting on a mound of data that needed to be analyzed and put into words. What resulted was a wonderful allowance of time at home with our son, along with experiment-free writing time, in which I wrote the majority of Chapters 1 and 4 of this dissertation. I will forever

cherish those months at home with my family, as I realize my free time will continue to dwindle as I progress to residency and beyond. Having Griffin join our family is not only the best thing that has happened to me, but has ultimately pushed me to think in the context of the “bigger picture” more regularly, as I believe parenthood has made me realize how trivial many of my daily concerns really were. Thank you, Griffin, for being a beaming light in the darkness of 2020, and I promise to not make you read this document as a form of reprimand.

My parents, Karen and Brian Olson, are owed much more than a simple thank you. Growing up, I thought I would simply take over the family farm—a small scale cash-crop operation in rural Wisconsin. After my parents recognized my academic potential, they constantly pushed me to pursue higher education. I believe my current trajectory was ultimately achieved by securing a basketball scholarship after high school, allowing me to attend a great college, and ultimately a path to MD and PhD training. My mom worked full days as a home-care nurse, commuted home to make dinner for the family, then drove me to Minneapolis (a 1.5-hour drive) several days throughout the week in order to play basketball in front of college recruiters. She sacrificed her weekends throughout grade school to coach my basketball team, made sure I was completing my schoolwork, and constantly put me in positions to succeed. I truly believe I would not be where I am now without my mom’s complete selflessness in raising me and my siblings, and I am forever grateful to have grown up in such a nourishing environment. I hope I can provide the same supporting environment for Griff—I certainly have the blueprint. Thank you, mom and dad, for allowing me to flourish as a student, athlete, husband, and now father.

My mentor, Dr. Daniel Marks, also deserves much more than a simple thank you. Dan's lab was my final laboratory rotation, and after completing two laboratory rotations with excellent PIs performing exciting research, I thought I would be going through the motions in completing my last rotation before choosing one of the first two labs. Furthermore, and to be frank, I did not think I would find myself studying "everything but the cancer" in the context of neoplastic disease (quite the opposite in fact). However, I quickly realized how exceptional of a mentor Dan was, and I found myself thoroughly enjoying the neuroscience of cancer-associated cachexia. Dan immediately set the precedent for our would-be mentor-mentee relationship, allowing me a substantial amount of intellectual and experimental freedom, but always being available for discussion and guidance concerning data and directions. I realized Dan's mentorship style was a perfect match for me, as I believe I am at my best without barraging oversight. Dan has been wholeheartedly supportive and allowed me to grow immensely in thinking like an independent investigator. I am extremely grateful for Dan's constant generosity and sincere mentorship—thank you for everything Dan. I hope I can repay the favor with my own mentees someday.

I would also like to thank several other individuals for providing mentorship and guidance during my training. I would thank Dr. David Jacoby for providing our program with unwavering leadership and support. Dr. Jacoby is always available to us students no matter the circumstances. It is unsurprising that our MSTP program has been able to almost double in size with him at the helm given his work ethic (I received a letter of support from him at 4:45 in the morning) and ability to attract exceptional students. Despite his clear success in leading our program, you would never know from talking

with him. He is continually attributing our program's success to the students, faculty, and staff, never relishing or sitting on his laurels. Thank you for being a brilliant leader Dr. Jacoby. I would like to thank Alexis Young for her diligence, hard work, and thoughtfulness in taking over an extremely difficult and demanding role in Program Coordinator. I would like to thank Dr. Shiuh-Wen Luoh for providing constant mentorship throughout the preclinical and graduate phase of my studies, always encouraging and asking questions that almost always lead me to an interesting observation. I would thank Dr. Aaron Grossberg for mentorship on several fronts, including career guidance, clinical research, bench research, and life advice. Finally, I owe an enormous thank you to Dr. Xinxia Zhu, Mason Norgard, and Peter Levasseur of the Marks lab for their continuous technical and scientific support concerning the manuscripts described in chapters 3, 4, and 5.

Abstract

Illness behaviors, metabolic disturbances, and cognitive injury are common in cancer patients and frequently lead to wasting or cachexia. This devastating state of malnutrition is brought about by a synergistic combination of decreased appetite and increase in metabolism of fat and lean body mass. The severity of cachexia is often the primary determining factor in both quality of life and ultimate survival. There are currently no effective treatments for cachexia, and its mechanisms are poorly understood. Our lab has previously elucidated the actions of inflammatory cytokines, including IL-1β and TNF-α, on hypothalamic neurons and their roles in driving cachexia symptoms. However, chronic administration of these cytokines results in desensitization and loss of cachexia symptoms, demonstrating canonical inflammatory cytokines alone are insufficient for sustaining cachexia. These observations and more demonstrate that the molecular pathways responsible for driving chronic central nervous system (CNS) derangement and cachexia symptoms remain unknown.

Lipocalin 2 (LCN2) is a secreted protein produced during numerous acute and chronic diseases, yet its role in cachexia is unexplored. Lcn2 is described as an important mediator of cell viability and is able to access appetite-regulating brain regions found near circumventricular structures. I found that, in several murine models of pancreatic ductal adenocarcinoma (PDAC)-associated cachexia, Lcn2 is robustly upregulated in the circulation and brain. Chronic central administration of Lcn2 results in appetite suppression that does not desensitize, and *lcn2* knockout mice are protected from cachexia-anorexia, fatigue, and lean and fat mass loss. The primary source of Lcn2 during PDAC cachexia was the bone marrow compartment, and restoration of

Lcn2 in this compartment alone was sufficient in rescuing the appetite-suppression phenotype of PDAC cachexia.

In addition to Lcn2's appetite-regulating effects, I observed a distinct alteration in hippocampal neuron dynamics of mice receiving pathologic levels of Lcn2 in the brain, including a reduction in mature neuron density and an increase in newborn neurons. Indeed, mice receiving chronic central Lcn2 treatment displayed a reduction in spatial recognition memory. These results suggest that while Lcn2 is able to regulate food consumption during cachexia, it may also mediate cognitive decline associated with chronic systemic inflammatory disease, including cancer.

Collectively, these results demonstrate that Lcn2 is a pathologic mediator of both appetite suppression and cognitive decline in the setting of chronic exposure. Further work is needed to identify the precise cellular mechanisms that elicit these pathologic features of cachexia, including receptor-specific effects of Lcn2 and intracellular signaling pathways.

Introduction

Overview

This dissertation explores the role of Lipocalin 2 in cancer-associated cachexia, a devastating metabolic syndrome characterized by appetite suppression, accelerated fat and lean mass catabolism, fatigue, and cognitive decline. Since a large portion of this dissertation focuses on behavioral manifestations of cachexia, Section 1 of the Introduction provides a broad overview of illness behaviors and their evolutionary relevance in the context of disease. Section 2 provides an overview of cachexia, including definitions, etiology, and inadequacy of treatment options. Since my studies lead me to focus on appetite suppression and neurocognitive decline symptoms of cachexia, I devote Section 3 of the introduction to providing background on CNS-based mechanisms of cachexia. Finally, Section 4 of this Introduction provides a more in-depth review of Lipocalin 2, which will be an emphasis of Chapters 3 and 4 of this dissertation.

1. Illness behaviors: an evolutionary perspective

The behaviors of both humans and animals are considerably changed during the course of infection. Specifically, ill individuals maintain little motivation to eat or ambulate, and frequently complain of symptoms of fatigue, anhedonia, and cognitive impairment. These illness behaviors, including anorexia and fatigue, are evolutionarily-conserved responses for combating pathogens through both minimizing macronutrients for pathogen proliferation (i.e. anorexia), yet sparing energy for immunologic response

that would otherwise be diverted toward unnecessary locomotor activities (i.e. fatigue) (1). Illness behaviors broadly comprise a component life history theory, an organizing principle in biology that attempts to understand how natural selection molded an organism's ability to enjoy reproductive success (2, 3). Ultimately, life history theory is a framework for understanding how an organism's environmental challenges (extrinsic challenges; including nutritional availability, predation, pathogens, and toxins) influence intrinsic behavioral, reproductive, and molecular programs, such as metabolic trade-offs and fight-or-flight response (3). Since the dawn of life history theory in the 1950's, over half a century of research has clearly demonstrated the precedent of this organizing principle in the context of inflammatory disease. For instance, when challenged by a pathogen, mammals enact responses that optimizes its finite environmental resources into reproductive, growth, metabolic, and survival strategies.

Broadly, the illness behaviors observed in the context of acute infectious disease represent a highly coordinated, yet extremely energy-expensive, response in mitigating pathogen proliferation (4). This response can be likened to an "all in" approach to ridding the host of the pathogen, resulting in a huge apportionment of energy to mount a robust immune response and modify host metabolism to create an unfavorable growth environment for the pathogen. The degree and type of responses are closely associated with level of inflammation, type of pathogen encountered (bacteria vs virus), and metabolic state of the organism. Interestingly, rodents exposed to bacterial or viral mimetics display similar illness behaviors, yet benefit differentially from illness programs (5). Specifically, anorectic behaviors are observed under both contexts, yet opposing this specific illness behavior improves metabolic status, mitigates inflammation, and

prolongs survival in the context of viral infection (2, 5). This study and others generally agree with the old adage of “starve a fever, stuff a cold,” but also points out a flaw in our evolutionary history in combating disease. Why would mammals develop similar behavioral responses to viral infection as bacterial infection when certain aspects of this response, specifically anorexia, is to the detriment of the host? This conundrum remains a highly-debated and studied topic, and raises several questions concerning illness behaviors observed in other disease settings. Of those many questions raised, a single question particularly stood out to me at the beginning of my graduate studies and remains fundamental to this thesis: are illness behaviors beneficial or detrimental during non-infectious disease, including cancer?

Since our evolutionary history of life-threatening encounters—in which the predominant extrinsic drivers of death included pathogens (namely bacteria), predation, toxins, and undernutrition—were consequential in the development of life-preserving metabolic, immunologic, and behavioral responses, it stands to reason that some of these responses are teleologically inappropriate in the context of modern-day disease. Put plainly, we humans die very differently today than we did some 0.2-25 million years ago during our hominid chronology. The inception of sanitation, agriculture, scientific advancement, and modern medicine are allowing us to live far beyond our ancestors and the evolutionary code levied upon them over millions of years. As a result, we are now experiencing new diseases at an ever-increasing rate, such as cancer and neurocognitive pathologies, that are also associated with the aforementioned illness behaviors, yet represent distinct inflammatory challenges. For instance, cancers generally result in sterile inflammation and can impose illness behaviors for months or

years. This is in stark contrast with bacterial infection, which represents an acute inflammatory state in which the illness behaviors rapidly subside after the clearance of the pathogen. Indeed, life history theory strongly implicates bacterial infection and acute inflammation as the principal driver of our allostatic metabolic and behavioral responses. Herein lies the conundrum and primary topic of investigation for this thesis: since illness behaviors are observed in both the context of acute and chronic inflammation, are these evolutionarily conserved responses observed during acute inflammatory insult beneficial or pathologic in the context of relatively "newer" chronic inflammatory diseases—such as cancer?

2. Cancer-associated cachexia

Cachexia is a devastating metabolic syndrome that incites severe muscle and fat wasting, fatigue, and cognitive decline (6). Cachexia has been alluded to for centuries, including illustrious descriptions of the syndrome by Hippocrates around 400 BC: "the flesh is consumed and becomes water… the abdomen fills with water, the feet and legs swell, the shoulders, clavicles, chest, and thighs melt away… the illness is fatal" (7). Cachexia is associated with numerous chronic diseases, including cancer, heart failure, cystic fibrosis, kidney disease, and Alzheimer's disease (6). Indeed, cachexia is an irreversible metabolic syndrome that is critically linked to poor prognosis in cancer, as it is estimated to account for up to 80% of fatalities depending on the specific cancer (8). The current international consensus definition for cachexia, defined in 2011, is: "….a multifactorial syndrome characterised by an ongoing loss of skeletal muscle mass (with or without loss of fat mass) that cannot be fully reversed by conventional nutritional

support and leads to progressive functional impairment. The pathophysiology is characterised by a negative protein and energy balance driven by a variable combination of reduced food intake and abnormal metabolism" (8). Current diagnostic criteria for clinically-defined cachexia include: weight loss greater than 5%, or weight loss greater than 2% in individuals already showing depletion according to current body weight and height (body-mass index [BMI] <20 kg/m^2)) or skeletal muscle mass (sarcopenia) (8).

Cachexia is particularly prevalent amongst cancer patients as a result from not only primary tumor growth and metastases, but also the cytotoxic therapy used to treat the cancer, where it significantly contributes to reduced survival, accelerated disease progression, and limits patients' ability to tolerate therapy (9-12). It is estimated that nearly half of patients suffering from hematological cancers, colorectal cancer, lung cancer, and head and neck cancers experience clinically-defined cachexia, while up to 70% of patients with gastroesophageal and pancreatic cancer experience cachexia (6). Although an in-depth comparison of cachexia, simple starvation, and malnutrition is detailed in Chapter 1, it is important to highlight the unique metabolic and wasting profile imposed by cachexia here. Specifically, cachexia results in a progressive wasting even in the context of nutritional support, whereas starvation and malnutrition are completely reversed by appropriate caloric intake (13). While an important component of the treatment of cachexia, conventional nutritional support used to offset reduced caloric intake is only marginally effective, demonstrating that the progressive tissue catabolism observed in cachexia patients cannot be explained solely by a reduction in food intake. As such, the cachexia field has focused on alternative mechanisms and pathways that

drive cachexia symptoms, including inflammation, endocrine alterations, and immune dysfunction to name a few. Despite recent advances on a basic science front, as well as the completion of numerous clinical trials, no approved therapeutic intervention for cachexia exists. These observations and more illustrate the fields lack of mechanistic understanding of this complex metabolic syndrome and highlights the need for new approaches for studying cachexia.

Cachexia imposes a significant burden on our health system, as it is estimated that nearly 530,000 patients experience cancer-related cachexia yearly in the United States alone (14). Given these staggering numbers, clear economic burden on our health systems, and fact that no approved therapy for cachexia exists, it is unsurprising that the National Cancer Institute recently issued a cachexia-focused provocative question request for application titled “How can cancer cachexia be reversed? (PQ6; FY2020)” This increasing recognition and focus on cachexia research is incredibly exciting, and will hopefully result in the discovery of new therapies. As I write this, the past two years of cachexia research alone provided several new insights into cancer-associated cachexia, many of which include mechanisms by which peripherally-derived signals interface with the central nervous system (CNS) to mediate behavioral and metabolic disturbances. Since our laboratory and this thesis work focuses on CNS-based mechanisms of cancer cachexia, an in-depth discussion of CNS mechanisms of cachexia is warranted.

3. Central nervous system mechanisms of cachexia

Although cachexia is a multi-organ syndrome involving complex inter-organ interactions during its progression, the CNS is uniquely equipped in exerting overarching homeostatic control of peripheral tissues through its direct control of illness behaviors (such as anorexia and fatigue), efferent engagement of the autonomic nervous system, and regulation of neuroendocrine axes (13, 15, 16). Furthermore, several decades of research demonstrate that the CNS is both a receiver and amplifier of peripheral inflammatory signals, and that this amplification of peripheral signals is responsible, in part, for regulating several metabolic and behavioral manifestations of cachexia (17, 18). Research dedicated to unveiling CNS mechanisms of cachexia has historically focused on the hypothalamus, a central coordinator of several homeostatic processes that are known to be awry during cachexia, including appetite, sleep, activity level, wakefulness, and macronutrient distribution to name a few. However, recent work in this field has implicated additional CNS structures involved in cachexia symptoms, including the brain stem (15, 19, 20). These advances in the field imply that not only is our understanding of hypothalamic mechanisms incomplete at this time, but our knowledge of how other brain structures and their CNS circuitry influence cachexia is in its infancy. Nevertheless, given the clear role of the CNS in the development of the signs and symptoms of cachexia, combined with recent advances in CNS-based mechanisms of cachexia, research devoted to unveiling aberrant CNS pathways during cachexia represents a promising approach in identifying therapeutic targets for this metabolic syndrome. This section will highlight studies investigating how the brain

mediates cancer cachexia, with a particular focus on foundational work in inflammatory, autonomic nervous system, and neuroendocrine mechanisms.

3.1 Central inflammation: lessons from IL-1β

Cancer, as well as the cytotoxic chemotherapy utilized to treat the cancer, is often accompanied by prolonged systemic inflammation. As such, it is generally accepted that inflammation is a key component in the development and progression of cancer cachexia (21-23). Indeed, increased circulating levels of inflammatory cytokines and innate immune cells, including IL-6 (24), TNF-α (25), C-reactive protein (24), and neutrophils (26) are all associated with cachexia in humans. These systemic inflammatory mediators are derived from several tissue sources, including the liver, fat, skeletal muscle, and bone marrow, as well as the developing tumor, including nearby stromal cells in response to the tumor, infiltrating immune cells, and neoplastic cells themselves (27-31). In addition to peripherally-derived inflammatory molecules, a recent report describes a distinct neuroimmune axis in driving cachexia by which peripheral myeloid cells directly invade the CNS (20). Once produced in the circulation, these molecular and cellular inflammatory mediators are able to either interface with the brain by directly crossing the blood-brain barrier (BBB) (32) or through direct blood-borne sampling by circumventricular organs.

Seminal work describing the cachexia-inducing potential of systemic inflammatory mediators originate from simple experiments in which cytokines were administered directly to the brain of rodents. Specifically, intracerebroventricular (ICV) injection of pathophysiological levels of interleukin 1 beta (IL-1β) or tumor necrosis

factor alpha (TNF-α) result in anorexia, weight loss, increased energy expenditure, and accelerated catabolism of fat and lean mass (33, 34). Furthermore, the central administration of these cytokines also results in a paracrine loop, through which their administration into the brain results in an increase in endogenous production, both maintaining and propagating a local inflammatory milieu in the CNS (35-37). These foundational experiments demonstrate that when inflammatory cytokines produced during cachexia interface with the CNS, 1) illness behaviors consistent with cachexia are individually produced, and 2) the brain not only receives these inflammatory signals, but interprets and amplifies these signals near CNS nuclei integral for energy homeostasis.

Of the inflammatory cytokines produced peripherally and centrally during cachexia, possibly no other is more studied that IL-1β. Indeed, several studies show that IL-1β is the major cytokine induced in the mediobasal hypothalamus as a result of peripheral tumor development (16, 38, 39). These reports and more formed the precedent for the study IL-1β in the development of illness behaviors and cachexia over the past two decades. Indeed, it was recently demonstrated that brain-endothelial expression of the interleukin-1 receptor (IL-1R) individually enhances leukocyte recruitment, mediates sickness behavior, and impairs neurogenesis (40). Brain endothelial cells respond to IL-1β in a myeloid differentiation primary response protein MyD88-dependent manner, which amplifies and propagates inflammatory signals to glial cells (41). The role of IL-1β in cachexia is further demonstrated by cachexia studies in which MyD88, which is the universal adaptor protein to all Toll-like receptors (TLRs) except TLR3 and the interleukin 1 receptor family, is implicated in the pathogenesis of

cancer cachexia. In two separate reports utilizing different models of cancer cachexia, *MyD88* deletion attenuated several measures of cachexia, including anorexia, muscle catabolism, fat loss, hypothalamic inflammation, and fatigue (42, 43). Although a recent report demonstrated that genetic deletion *Il-1β* failed to improve fatigue symptoms in several different rodent models of cancer, suggesting that while IL-1β signaling may initiate or drive some cachexia symptoms, it is unlikely to be an all-encompassing therapeutic target (44). Given the robust induction of several inflammatory cytokines in the context of cancer cachexia, it is plausible that combinatorial blockade of central-acting inflammatory mediators is requisite in mitigating cachexia. While we utilized IL-1β as a conceptual framework for CNS bioamplification of peripheral signals during cachexia, there are undoubtedly other inflammatory cytokines that undergo similar amplification events by the brain, including TNF-α, IL-6, and LIF—mechanistic review of these cytokines in the brain can be found in recent reviews (15, 18).

In addition to cytokines being received and amplified in the CNS during cachexia, a recent report from our lab demonstrates a clear role for myeloid cell invasion in the CNS in driving pancreatic cancer cachexia symptoms, including anorexia and lean mass catabolism, that is predominantly driven by the CCR2-CCL2 axis (20). Prior reports demonstrate a clear role for CNS-infiltrating immune cells in both health and disease, having either beneficial or detrimental effects depending on the underlying pathology (45). In this study, the majority of the CNS-invading immune cells were neutrophils, which accumulated at a unique CNS structure called the velum interpositum (VI). Interestingly, a large percentage of neutrophils in this region expressed CCR2, which is typically considered a monocyte chemotaxis receptor. CCR2 deletion

attenuated cachexia and prevented neutrophils from infiltrating the VI during pancreatic cancer cachexia. Furthermore, these CNS-invading neutrophils expressed a transcriptome that is dissimilar from that of neutrophils invading peripheral tissues, implicating a distinct neutrophil population infiltrates the brain during cancer cachexia. Although future investigation is needed, this study demonstrates that the inflammatory mediators during cachexia may extend beyond canonical cytokines and to CNS-invading immune cells, by which myeloid cells (namely neutrophils) enter the CNS through a unique meningeal portal to incite inflammation in CNS structures important in energy homeostasis.

Although blockade of inflammatory signaling in rodent models of cancer cachexia has yielded promising results, concomitant clinical trials have broadly failed to attenuate cachexia in humans (46). Thus, while systemic inflammatory mediators may be important in the initiation of illness behaviors and cachexia, current data suggest that they are insufficient in sustaining cachexia (47-50). These results demonstrate the complexity of cancer cachexia, and although they do not preclude anti-inflammatory therapies in its treatment, they suggest they may have limited utility as a monotherapy.

3.2 Sympathetic nervous system engagement

In response to stress, the CNS coordinates an evolutionarily conserved fight-or-flight response, a metabolically costly physiologic program that rapidly liberates energy stores for muscle use. This program is directed within the central nervous system, where neurons in the paraventricular nucleus of the hypothalamus (PVH) integrate environmental and neuronal input and project to noradrenergic centers in the brainstem

and preganglionic neurons in the spinal cord (51). Furthermore, extensive remodeling of the SNS during chronic inflammatory stress greatly modifies end-organ responses to SNS inputs (38, 52, 53). Acting through sympathetic ganglia throughout the body, the SNS regulates end organs via the release of norepinephrine (NE) at synapses and release of epinephrine (EPI) from the adrenal medulla into the circulation. These neurotransmitters elevate metabolic rate by increasing heart rate (HR) and cardiac contractility, engaging lipolysis in white adipose tissue (WAT), and inducing non-exercise thermogenesis in brown adipose tissue (BAT) by uncoupling electron transport from ATP generation in the mitochondria (6). Indeed, independent studies demonstrated that sympathetic tone is elevated in patients and mice with cachexia, and a sustained elevation in basal metabolic rate (BMR) is repeatedly described as a critical energy-expenditure mechanism during cancer cachexia. Despite clear precedent for SNS activation in the progression of cancer cachexia, the precise mechanisms of SNS engagement in cachexia remain incompletely understood (54, 55). Here we will summarize known and potential mechanisms by which the CNS orchestrates SNS activation, tissue remodeling, and energy wasting in cachexia.

Increased BAT thermogenesis in cachectic mice was first reported 40 years ago and has since been reported in multiple murine models of cachexia (54, 56, 57). In addition to increased BAT thermogenesis, excess energy expenditure in cachexia can be mediated by “browning” of WAT, in which WAT takes on some of the molecular characteristics and thermogenic capability of BAT—a process mediated by SNS input (58, 59). Indeed, it was recently demonstrated that the β3-adrenergic receptor blockade—the receptor responsible, in part, for establishing sympathetic tone in

tissues—ameliorated adipose wasting, browning, and cachexia-associated weight loss (52). While this study implicates the SNS in remodeling adipose tissue, resulting in the upregulation energetically-expensive thermogenesis programs, it remains unclear which CNS pathways are responsible for this increased SNS tone during cachexia development. Recently, a brain circuit was identified that potently regulates metabolism in WAT and BAT (58). This circuit is initiated in the arcuate nucleus (Arc) of the MBH via the interaction of pro-opiomelanocortin (POMC) and Agouti-related peptide (AgRP) neurons with the adipokine leptin, then relayed via PVH Brain-derived neurotrophic factor (BDNF) neurons that ultimately regulate SNS tone in peripheral adipose tissues. Interestingly, these authors demonstrate remarkable plasticity in SNS innervation of adipose depots, and this plasticity is dependent on chronic (rather than acute) signaling in the Arc. Additionally, a recent report by Kim et al show a precise and rapid activation of adipose tissue lipolysis by the brain-fat axis in the context of bacterial infection, and that this axis that is entirely dependent on hypothalamic Arc TNF receptor activation and sympathetic nerve outflow to fat (60). Since TNF, also known as cachectin, is strongly implicated as a mediator of CNS inflammation during cachexia, it is plausible that this described brain-fat axis mediates some of the adipose tissue remodeling and wasting observed during cancer cachexia. Even though the authors described this phenomenon in the context of adaptive immune response and did not investigate browning signatures in WAT, it seems plausible that the chronic inflammatory state induced by cachexia could induce sustained activation of this brain-fat axis through hypothalamic TNF signaling, resulting in prolonged lipolysis and progressive fat wasting typical of cachexia.

Further evidence of SNS activation in cachexia is derived from studies of HR variability (HRV) in cachectic patients. HRV is measured as variance in time between successive beats and is a measure of autonomic tone. Imbalances in autonomic tone (most commonly elevated sympathetic input) decrease HRV and are associated with increased mortality. Cachectic cancer patients were found to have substantially decreased HRV, indicating elevated SNS tone (61, 62). A recent report by Luan et al demonstrate a brain-fat-heart axis in the maintenance of stroke volume and overall cardiac output in the context of acute inflammation after LPS challenge (63). The authors identify Growth and Differentiation Factor 15 (GDF15) as the critical mediator of this axis. Specifically, GDF15 is produced in the liver during acute inflammation and secreted into circulation where it then binds to its receptor in the area postrema of the brainstem, resulting in SNS outflow back to hepatic tissue and subsequent mobilization of lipids. The authors demonstrate that this lipid mobilization is critical in the maintenance of cardiovascular function during acute inflammation, and intricately demonstrate that hepatic β-adrenergic signaling is central to this process (63). Since GDF15 is known to be upregulated in numerous rodent cachexia models and humans with cancer, it is likely that GDF15-driven SNS engagement mediates wasting during cancer cachexia as a recent report suggests (64-66). As such, GDF15 represents a promising therapeutic target for the treatment of cancer cachexia, due to not only its potential SNS modulating effects, but also its robust anorectic effects through activation of the area postrema (also known as the vomiting center of the brain) (67).

During acute stress, transient activation of the stress response elicits metabolic and behavioral adaptations that are beneficial to the organism over the short term. In chronic

disease states, prolonged activation of the stress response is maladaptive and leads to loss of physiologic reserve and cachexia. Given the SNS plays an imperative role in the acute stress response, and recent work implicates SNS engagement in the pathogenesis of cancer-associated wasting, the identification of molecular mediators and pathways in which the SNS is chronically activated represents a promising approach to treating this debilitating wasting syndrome. Further research in this space is needed.

3.3 Neuroendocrine modulation

The CNS is also a central regulator of endocrine organ function through the release of several hypothalamic-pituitary hormones, including corticotropin-releasing hormone (CRH), thyroid releasing hormone (TRH), and gonadotropin-releasing hormone (GnRH) to name a few. These hypothalamic endocrine neurons all send projections to the fenestrated capillaries of the ME, where they secrete hormones into the portal system, which act on the pituitary gland to amplify additional hormone secretion into peripheral circulation. While the neuroendocrine regulation of behavioral aspects of cachexia is well established (for reviews, see (68, 69)), the cachexia field is still unveiling mechanisms by which aberrant endocrine function leads to the direct catabolism of lean and fat tissues. Here we will review these recent reports and mechanisms by which CNS control of endocrine response mediates cachexia-associated wasting.

The hypothalamic-pituitary-adrenal (HPA) axis is activated by a wide array of stressors, including fear, fasting or undernutrition, acute illness, and injury. Since many of these stressors exist in the context of cachexia, the field hypothesized that the HPA

axis is engaged during cachexia. Indeed, several reports show an increase in the glucocorticoid (GC) corticosterone—the rodent analog of human cortisol—in mice with cancer cachexia (38, 70). GCs are released as the systemic effector molecules of the neuroendocrine arm of the CNS stress response beginning with activation of CRH neurons in the PVH and leading to the release of cortisol (in humans) or corticosterone (in mice) from the adrenal cortex. GCs are a primary driver of skeletal muscle catabolism due to acute inflammation and denervation injury, and exogenous GCs are sufficient to drive muscle catabolism in both mouse and human (16, 71). Our laboratory showed that GC ablation, antagonism or deletion of the GC receptor (GR) in the muscle all prevented inflammation-, lung cancer-, or chemotherapy-associated muscle wasting (16, 71, 72). Thus, GCs act as a required permissive factor to allow pathological muscle catabolism. Mechanistically, GCs induce muscle wasting by both promoting catabolism by transactivation of *Foxo1* and *Trim63* and by blocking the activity of the mammalian target of rapamycin (mTOR), a regulator of muscle anabolism (73, 74). These reports strongly implicate GC signaling in driving cancer-associated muscle wasting, and demonstrate that the CNS maintains endocrine control of, at a minimum, skeletal muscle wasting.

In addition to CNS control of the HPA axis, induction of GCs, and subsequent muscle atrophy during cancer cachexia, recent reports also suggest dysfunction of the hypothalamic-pituitary-gonadal (HPG) axis in cancer patients (75, 76). These reports detail a significant decrease in testosterone levels in male cancer patients, both prior to and after the initiation of cancer treatment, estimating between 40-90% of cancer patients suffer from low testosterone levels (77, 78). These results also extend to pre-

clinical models of cachexia, as a recent report demonstrated that male mice engrafted with pancreatic cancer display a loss of over 97% of circulating free testosterone relative to control mice (38). Given the known anabolic properties of testosterone, this hypogonadal state likely contributes to the propagation of cachexia symptoms, including fatigue, weight loss, and muscle catabolism. Indeed, Skipworth and colleagues recently demonstrated that hypogonadal cancer patients experienced significantly greater weight loss than eugonadal patients (79), while Dev et al demonstrated low testosterone levels were associated with increased systemic inflammation, weight loss, and decreased overall survival (80). Despite the acknowledgement of hypogonadism in cancer cachexia, little mechanistic advancement has been made into how cancer and its therapeutics disrupt the HPG axis. A recent review by Burney and Garcia postulated several potential mechanisms by which the HPG axis could be altered during cancer cachexia, and included inflammation and hypothalamic leptin upregulation as potential modulators of the HPG (75) . However, future mechanistic research is needed to determine how cancer enacts neuroendocrine change through the HPG.

The hypothalamus is the master regulator of the endocrine system through its ability to detect peripheral signals and produce a robust systemic hormonal response through several axes, including the HPA and HPG. Since endocrine dysfunction is now recognized in cachexia as a potent regulator of peripheral tissue catabolism, it is plausible that other endocrine aberrations contribute to cachexia-associated wasting.

3.4 Summary of CNS mechanisms in cachexia

Herein, we explored past and present research of CNS-based mechanisms of cancer cachexia, providing a conceptual framework for inflammatory, autonomic, and neuroendocrine pathways of energy homeostasis. Although we presented inflammatory, autonomic, and neuroendocrine concepts of cachexia individually, it is undeniable that their modulation during health and disease are interdependent. For instance, CRH neurons regulate activity of the HPA axis and simultaneously provide regulatory projections to brainstem and spinal cord neurons that regulate sympathetic outflow (81). CRH neurons are known to regulate SNS inputs to the heart, adipose tissue, liver, and other peripheral tissues, all of which are also sensitive to GC levels established by the HPA axis (59, 61, 81). Additionally, hypothalamic IL-1β exposure is sufficient for activation of the HPA axis, GC production, and subsequent muscle catabolism (16). Therefore, components of the CNS-based inflammatory, autonomic, and neuroendocrine pathways activated by cancer progression are mechanistically interdependent and display functional redundancy in regulating peripheral tissue catabolism during cachexia. This instance of redundancy also highlights the CNS's ability to amplify biological programs in the periphery, such as muscle catabolism, through multiple efferent effector mechanisms. Therefore, promising cachexia therapeutics that target the brain are likely to modulate several of these CNS processes of cachexia.

4. Lipocalin 2: a pleiotropic mediator of inflammation, metabolism, and cell viability

Shortly after joining Dr. Marks' lab, I came across a paper by Mosialou et al titled "MC4R-dependent suppression of appetite by bone-derived lipocalin 2," which immediately piqued my interest in the molecule (82). Since Dr. Marks' is very familiar with the hypothalamic type 4 melanocortin (MC4R) system in cachexia, combined with this recent report detailing an appetite-regulating effect of Lcn2, we collectively thought it prudent to perform a quick literature review and conceive simple pilot experiments to determine if Lipocalin 2 is regulated in the context of cancer cachexia. This literature review revealed just how diverse of a molecule Lcn2 truly is, having disparate roles in various physiologic and pathologic settings. Lipocalin 2 (Lcn2), also known as neutrophil gelatinase-associated lipocalin (NGAL), siderocalin, or 24p3, is a member of the lipocalin superfamily and a pleotropic mediator of several immunologic, metabolic, and inflammatory processes (83, 84). Further evidencing Lcn2's multifaceted role is that it has three known receptors: Solute Carrier Family 22 Member 17 (SLC22A17), the MC4R, and megalin (82, 85, 86). Lcn2 was originally identified as a 25-kD protein purified from human neutrophilic granules in 1993 (83, 87-89). Since this molecule has only recently been discovered, it is likely that there is still much to be discovered about its biological function.

One of the first molecular functions unveiled of Lcn2 was its iron-trafficking capacity (90). At the time, this was a remarkable study, as the delivery of iron to cells was solely attributable to their ability to capture iron-loaded transferrin (91, 92). With this recent discovery of Lcn2 and its iron-trafficking role, it was postulated that Lcn2 would

be a multifaceted mediator of cellular processes, as intracellular iron processing is a unique regulation mechanism of inflammation, immune system function, and gene expression to name a few (93-96). What would follow in the decade after this initial discovery and characterization of Lcn2 would embody these initial hypotheses, in which Lcn2 mediates several molecular functions. Here I provide a comprehensive review of Lcn2 during health and disease, and end with a discussion about its potential intersections with cancer cachexia.

4.1 Bacteriostatic and Inflammatory properties

In 2004, the first definitive study concerning the iron-trafficking role of Lcn2 during disease was published in *Nature* (97). Flo et al demonstrated that Lcn2 was robustly induced in the serum of mice after lipopolysaccharide (LPS) challenge, and that mice deficient in Lcn2 experienced significantly increased blood, liver, and splenic *E. coli* proliferation (97). The authors go on to demonstrate that Lcn2 specifically inhibits enterochelin-dependent growth of *E. coli* through the binding of Lcn2 to catecholate-type siderophores, and that increasing concentrations of Lcn2 inhibits *E. coli* growth *in vitro*–an effect that is promptly counteracted by adding equimolar amounts of enterochelin (97). Finally, they show that *lcn2*-KO mice succumb to *E. coli* infection much faster than WT mice, and that this survival effect is siderophore-specific (97). This hallmark study was the first line of evidence for the acute induction of Lcn2 being a beneficial response in the context of acute disease.

Since its initial characterization in the context of bacteria-induced inflammation, Lcn2 is shown to be increased in expression in a variety of inflammatory states,

including acute kidney injury (98-100), reperfusion injury (101, 102), lupus nephritis (103), acute liver injury (98, 104), acute hepatic failure (105), autoimmune myocarditis (106), and several cancers (107-110). Similarly, Lcn2 is also shown to be highly expressed in numerous neuropathologies that result in CNS inflammation, including inflammatory conditions like fever (111), primary neurodegeneration (112-114), autoimmune disease (115-117), brain injury (118, 119), schizophrenia (120), spinal cord injury (121), and vascular disease (122, 123) amongst others. Given many of these inflammatory conditions occur in a sterile setting, the principle anti-bacterial effects of Lcn2 are seemingly dispensable in this context, suggesting Lcn2 act beyond a simple anti-bacterial molecule during disease. Indeed, numerous reports have come to light characterizing the tolerance function (defined below) of Lcn2 in the context of acute inflammation. These reports include Lcn2's influence on immune cell function (124, 125), chemotaxis and migration (126), and amelioration of CNS inflammation (127), although refuting reports describing an exact opposite effect are prevalent (128, 129).

When considering a molecule's "resistance" effects, defined as a molecule's ability to fight a pathogen, another term that now comes into biological consideration is "tolerance," defined as biological mechanisms employed to protect the host from secondary inflammatory damage produced from both the pathogen and the hosts inflammatory response in fighting the pathogen (i.e. fever) (130, 131). This line of thought can be applied to the progression of Lcn2's scientific study, in which the focus of Lcn2 research is generally now focused beyond its anti-bacterial properties (tolerance mechanisms). One such field of investigation is the role Lcn2 may play in the regulation of inflammation, which we will now discuss.

The case for Lcn2 being an anti-inflammatory molecule, and thus a molecular mediator of host tolerance during infection, was illustrated through a simple experiment in which LPS was injected intraperitoneally in rodents (132). Guo and colleagues demonstrated that *lcn2*-deficient bone marrow-derived macrophages were more sensitive to LPS simulation, ultimately leading to an increase in the activation of nuclear factor kappa-light-chain-enhancer of activated B cells (NF-κB), c-Jun, and STAT3 signaling pathways and concomitant up-regulation of expression of NF-κB and STAT3 target genes such as *Il-1β, Il-6, Inos, and Mcp-1* (132). Similarly, Zhang et al demonstrated that when added to macrophages, Lcn2 suppressed LPS-induced cytokine production (133). These studies demonstrates that Lcn2 expression plays an important anti-inflammatory role during macrophage activation (132). In addition to potential peripheral anti-inflammatory effects of Lcn2, a publication by Kang et al in 2018 demonstrated Lcn2 is uniquely protective in the CNS during LPS challenge (127). Specifically, the authors demonstrate that *lcn2*-KO mice injected with LPS displayed a unique transcriptome in the CNS with significantly higher levels of several pro-inflammatory molecules, including cytokine and chemokines, nucleotide-binding oligomerization domain-like receptor signaling molecules, and Janus kinase signaling molecules (127). These studies and more suggest Lcn2 acts in a protective capacity during sterile inflammation, while a large body of literature suggests the exact opposite effect of Lcn2 during sterile inflammatory disease, in which Lcn2 propagates disease-related inflammation.

The literature for Lcn2 being a pro-inflammatory agent is more abundant than that suggesting it serves as an anti-inflammatory molecule as discussed above. In direct

contrast with the aforementioned Kang study in which Lcn2 is protective in the CNS during LPS challenge, Jin et al observe a neurotoxic role of Lcn2 in the brain, detailing the inflammation-inciting effects of Lcn2 on glia and endothelium in the brain, which in turn resulted in a reduction in neuronal viability (134). In addition to Lcn2 aggravating CNS inflammation in LPS models, over a decade of work from the Kyoungho Suk lab details several other instances in which Lcn2 is broadly pathological when induced in the CNS, including models of peripheral nerve injury (135), formalin-induced nociception and pathologic pain (136), stroke (119), encephalomyelitis (116), optic neuritis (137), parkinsonism (138), vascular dementia (139), diabetic encephalopathy (140), and diabetic neuropathy (141). Additionally, Shin et al recently reported a dual oxidative stress and inflammatory effect of Lcn2 when induced in the hippocampus after kainic acid-induced seizure rodent model (142). Another putative mechanism by which Lcn2 may induce CNS inflammation is through its chemotactic properties, in which the upregulation of Lcn2 in the brain results the induction of chemokines (particularly CXCL10) and subsequent recruitment of inflammatory immune cells (126, 143). Indeed, Lcn2 is known to individually induce neutrophil chemotaxis (96, 144).

In peripheral inflammatory models, Lcn2 has also been demonstrated to exacerbate inflammation. In an imiquimod-induced psoriasiform skin model, exogenous Lcn2 treatment resulted in a significant induction of numerous inflammatory cytokines and chemokines in the plaque compared to vehicle treated mice (145). These trends extend to other peripheral inflammatory disease models, including nonalcoholic steatohepatitis (146), alcoholic liver disease (147), and atherosclerosis (148). A recurring theme in these reports is an acute induction of Lcn2 in their respective tissue

of study, followed by an increase in inflammatory immune cell infiltration (predominantly neutrophils) and subsequent increase in inflammatory tissue damage. As mentioned previously, the litany of research demonstrating a pro-inflammatory effect of Lcn2 outweighs that of its anti-inflammatory effects. As I write this, a PubMed search for "Lipocalin 2" results in 3,522 articles, while searching "Lipocalin 2 inflammation" results in 812 reports. Given nearly a quarter of the Lcn2 literature concerns its influence on inflammatory processes, and since systemic and central inflammation is described as a critical component of cachexia progression, investigations into Lcn2's inflammatory effect in the context of cancer cachexia was warranted and is examined in-depth in Chapter 3 of this thesis.

4.2 Metabolic properties: insights from models of obesity

Lcn2 is also highly regulated in several metabolic disorders, with the preponderance of the literature describing various functions of Lcn2 in the progression of obesity (84). Obesity reflects a metabolic state of low-grade chronic inflammation, hypothalamic dysregulation, and a mismatch in caloric intake-to-use. In this sense, obesity represents a similar metabolic inflammatory state as cachexia, although presents in a dialectical opposite phenotype. The first reports demonstrating Lcn2's upregulation during high-fat diet (HFD) induced obesity attributed its expression to white adipocytes (149), while dexamethasone was also shown to rapidly induce *lcn2* in cultured 3T3-L1 adipocytes (150). Indeed, serum Lcn2 levels are significantly increased in obese patients and closely correlated with measures of insulin resistance (151), and *lcn2* expression in visceral and subcutaneous adipose tissue was found to correlate with

circulating proinflammatory cytokines (152). In addition to the regulation of adipose expression of *lcn2* by inflammatory cytokines, a report by Zhang et al demonstrated *lcn2* was also highly regulated by other metabolic stressors, including fasting, excess glucose, insulin-tolerance test, and exogenous fatty acids (palmitate and oleate) (153). Interestingly, after performing a whole-body tissue analysis for Lcn2 production, I observe no such regulation of Lcn2 in the fat of cachectic mice (See Chapter 3, Figure 2a). Therefore, while *lcn2* is robustly induced in the fat during obesity, my data suggest alternative immunometabolic pathways are responsible for its induction in the context of cancer cachexia, and imply a distinct biological role for Lcn2 during cachexia when compared to obesity. Furthermore, white adipose expression of *lcn2* was demonstrated to activated brown adipose tissue (BAT) via a norepinephrine-independent pathway, as BAT from *lcn2*-KO mice is less thermogenically active (154). A recent report by Meyers et al expanded upon this notion of Lcn2 activating thermogenic programs using an *in vitro* approach, demonstrating exogenous Lcn2 increases beiging (*Tbx1* and *Zic1)* and thermogenic markers (*Ucp1* and *Ppar-γ*) in cultured 3T3-L1 cells (155). Since increased adipose tissue "browning" and increased thermogenesis is a purported mechanism of energy imbalance in cachexia, I also performed detailed analyses of adipose tissue browning in *lcn2*-KO mice after cachexia development in Chapter 3. These early studies demonstrate that Lcn2 is robustly regulated in the context of obesity and serves to increase adipose tissue thermogenesis and tissue remodeling. However, these early studies were broadly observational. Whether or not the induction of this evolutionarily conserved anti-bacterial molecule in the context of obesity is beneficial or pathological was unknown until recently.

As mentioned in the opening paragraph of this section, Mosialou et al demonstrated an anorectic effect of Lcn2 through its actions in the paraventricular nucleus of the hypothalamus in 2017, but a significant component of that work also detailed a glucose-handling effect of bone-derived Lcn2 (82). Specifically, the authors demonstrate osteoblast-derived Lcn2 improves insulin secretion and glucose clearance after glucose-tolerance test (82). The authors logically followed up this interesting observation in a report published just last year, demonstrating that osteoblast-specific deletion of *lcn2* resulted in glucose intolerance, insulin resistance, and pancreatic β-cell dysfunction (156). Using a streptozotocin-induced diabetes model, the authors demonstrate that exogenous Lcn2-treated mice displayed improved blood glucose handling, increased islet number, β-cell area, β-cell mass, insulin secretion, and ultimate survival (156). This report suggests an adaptive role of Lcn2 in the context of obesity, in which HFD, obesity, and type 2 diabetes results in the induction of Lcn2 in osteoblasts, which is then capable of curbing appetite, increasing pancreatic β-cell islet function, and subsequent glucose handling. Collectively, these data and more support the notion that Lcn2 regulates metabolism in some capacity.

4.3 Cell viability properties

Seminal work by Devireddy and colleagues demonstrated a clear role for Lcn2 in the regulation of programmed cell death (85, 157). In 2001, the authors showed that *lcn2* was the most upregulated gene after IL-3 deprivation of hematopoietic cells—an experimental paradigm known to induce apoptosis in all non-immortalized hematopoietic cells (158). Using several molecular assays and overexpression systems,

the authors intricately demonstrate that the induction of *lcn2* is required for apoptosis in cultured hematopoietic cells, but several nonhematopoietic cells and monocyte-derived macrophages were resistant to Lcn2-mediated apoptosis, demonstrating that the apoptotic effects of Lcn2 are cell type-specific (157). Four years after this discovery, these authors demonstrated that Lcn2's ability to regulate programmed cell death is dependent on the iron-loading status of the molecule, and that this iron-binding is dependent on an associated siderophore (85). Using clever *in vitro* overexpression systems of Lcn2 and its identified receptor (SLC22A17 or 24p3R), the authors imply that the synthesis and release of Lcn2 is performed in a siderophore-free state, and siderophore-free extracellular Lcn2 binds its endogenous receptor, is endocytosed, and can then associated with intracellular siderophore-iron complex (85, 159). If Lcn2 is loaded with an iron-siderophore complex prior to receptor binding and endocytosis, the siderophore-iron complex can be donated intracellularly, initiating an anti-apoptotic program dependent on the downregulation of *Bim* (85). The opposite occurs in the context of siderophore-iron-free Lcn2 binding to its receptor, in which unbound Lcn2 is endocytosed and is able to complex with intracellular iron and an unidentified endogenous siderophore; this intracellular iron-removal pathway results in an upregulation of pro-apoptotic *Bim* and subsequent activation of apoptosis (85). Despite these heroic efforts in describing Lcn2's iron trafficking properties, the precise mechanisms by which Lcn2 binds to iron remains mysterious. Specifically, it remains unclear if siderophilic binding to extracellular iron is required for its recognition by Lcn2, and if non-bacterial siderophores—specifically mammalian homologs—are capable of binding iron and forming the Lcn2-iron-siderophore complex (90).

Since this initial characterization of the apoptotic-regulatory effects of Lcn2, several reports have suggested both pro- and anti-apoptotic effects of Lcn2 dependent on the pathology, cell type, and iron-binding status of the molecule. Wen et al demonstrated that Lcn2 induced during obesity is protective of gastric mucosa through the its ability to reduce endoplasmic reticulum stress (160). In cultured cardiomyocytes, Holo-Lcn2 (Lcn2-siderphore-iron complex) was recently shown to induce mitochondrial reactive oxygen species production and impair oxidative phosphorylation, while Apo-Lcn2 (Lcn2 moiety alone) did not individually influence mitochondrial dynamics (161). Utilizing an *in vitro* rat brain slice culture model, Bi et al demonstrate that reactive astrocytes are able to secrete Lcn2 in the context of TDP-43 overexpression (the pathologic disease protein in tau- and alpha-synuclein negative frontotemporal dementia), and this astrocyte-derived Lcn2 is selectively toxic to cultured cortical neurons (112, 162). These results were corroborated in models of methamphetamine-abuse related neuronal apoptosis (163) and vascular dementia (139).

The apoptotic-regulatory effects of Lcn2 are well established. However, the past 10 years of research on this topic demonstrates Lcn2 is able to activate endoplasmic reticulum stress, generate mitochondrial reactive oxygen species, and prevent ferroptosis (164), demonstrating this molecule's versatility in regulating intracellular processes. Furthermore, Lcn2 has three putative receptors, two iron-bound forms (Apo- and Holo-Lcn2), and differential intracellular effects dependent on cell type. The permutations in which Lcn2 can enact cellular change is vast, and presents an incredibly complex biological situation for the study of Lcn2 *in vivo.*

4.4 Lcn2 and cachexia: a promising therapeutic target?

Since our laboratory is focused on CNS-based mechanisms of cachexia, my first exploratory study concerning Lcn2 was quantitative PCR of the hypothalamus in mice with pancreatic cancer cachexia. I observed a near 60-fold increase in *lcn2* in cachectic mice and was full of glee (Figure 1). After this initial observation, confirming *lcn2* was robustly upregulated in the hypothalamus of cachectic mice, I was completely dedicated to unveiling what this highly evolutionarily conserved anti-bacterial molecule was doing in the brain during cancer. These investigations are the focus of Chapter 3 of this dissertation.

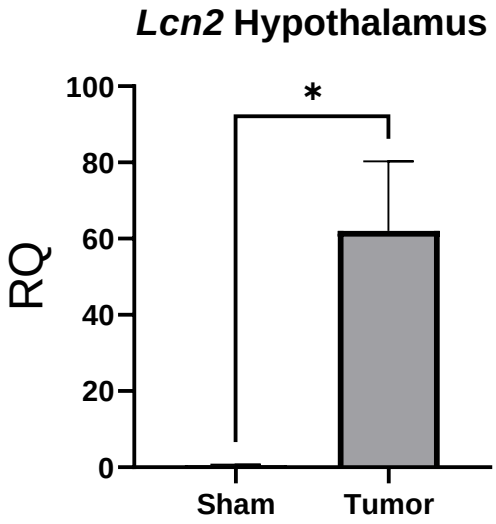

Figure 1. qPCR of *lcn2* in the hypothalamus of sham and pancreatic cancer cachexia mice. n = 4 per group.

After this initial characterization of *lcn2* expression in the hypothalamus of cachectic mice, I performed a more thorough examination of the expression pattern of

lcn2 in the brain of mice by *in situ* hybridization. To my surprise, an area ventral to the hippocampus, and not the hypothalamus, exhibited the largest induction of *lcn2* during cachexia. Given Lcn2's known role in regulating cell viability, over a decade of research by the Kyoungho Suk lab demonstrating a neurotoxic effect of Lcn2 in the brain in several neuropathologic conditions, along with neurocognitive decline being a known symptom of cachexia (165), we hypothesized that this specific induction of *lcn2* adjacent to the hippocampus plays a role in cognition. This line of thought forms the basis of Chapter 4 of this dissertation.

Collectively, my initial literature review of Lcn2 left me with far more questions than answers. The literature is fraught with conflicting reports of the role of Lcn2 during disease, and at the time, there were no reports concerning the role of Lcn2 in the context of cachexia. Since Lcn2 is strongly implicated in the regulation of inflammation, metabolism, and cellular stress and death—all processes central to the pathogenesis of cachexia—I thought Lcn2 represented an exciting and promising research avenue for my graduate studies.

5. Summary

Cachexia represents a formidable metabolic syndrome that is observed in several chronic diseases, including cancer, and consists of anorexia, progressive fat and lean mass catabolism, fatigue, and cognitive decline. The mechanisms of cachexia remain unclear, and while over one hundred clinical trials of human cancer cachexia have been conducted to date, none have resulted in the approval of an effective therapy (166-170). In this dissertation, I characterize the role of Lipocalin 2 in driving the

appetite-suppressive and cognitive impairment features of cachexia through its actions on the mediobasal hypothalamus and hippocampus, respectively (Figure 2). Throughout my medical and scientific training, I have realized my affinity to head and neck oncology, and recognized a significant lack of basic science tools for the study of cachexia in a head and neck cancer setting. As such, I end this dissertation with my future career directions in mind, describing and characterizing a novel murine model of head and neck cancer cachexia. I hope to utilize these newly established tools as I advance in my academic career.

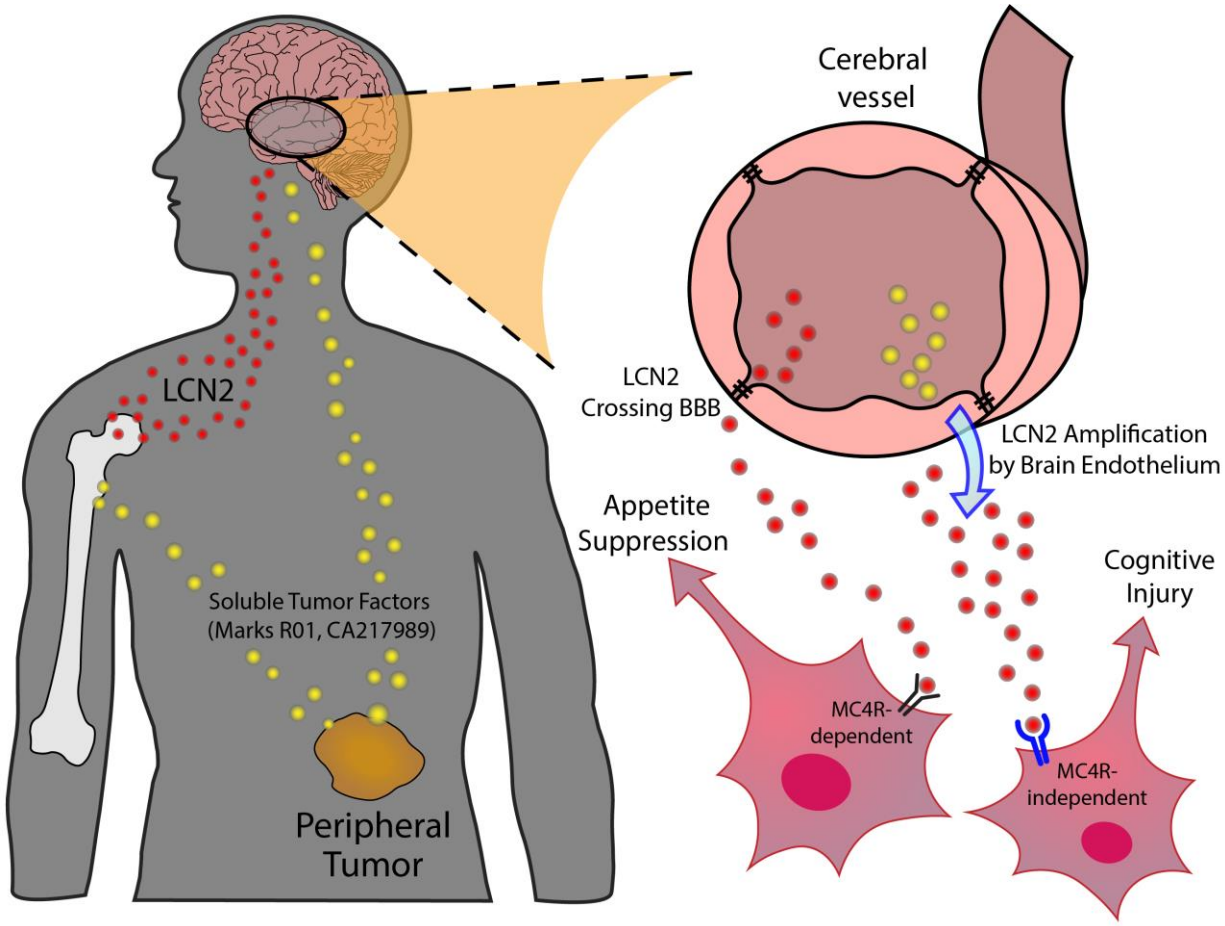

Figure 2. A model of Lcn2 production and action in the brain during cancer cachexia. During the evolution of cancer cachexia, the bone marrow and brain endothelium produce Lipocalin 2 (red circles) that is able to enter the brain parenchyma. Once in the brain, Lipocalin 2 acts through distinct neuron receptors to cause anorexia and cellular stress which drives cachexia symptoms.

Chapter 1: Diverging metabolic programs and behaviors during states of starvation, protein malnutrition, and cachexia.

A manuscript published in *Journal of Cachexia, Sarcopenia, and Muscle*

Olson B, Marks DL, Grossberg AJ. Diverging metabolic programmes and behaviours during states of starvation, protein malnutrition, and cachexia. *J Cachexia Sarcopenia Muscle.* 2020;11(6):1429-1446.

Diverging metabolic programs and behaviors during states of starvation, protein malnutrition, and cachexia

Brennan Olson[1,2], Daniel L. Marks[2,3], and Aaron J. Grossberg[3,4,5*]

[1] Medical Scientist Training Program, Oregon Health & Science University, Portland, OR, USA
[2] Papé Family Pediatric Research Institute, Oregon Health & Science University, Portland, OR, USA
[3] Brenden-Colson Center for Pancreatic Care, Oregon Health & Science University, Portland, OR, USA
[4] Department of Radiation Medicine, Oregon Health & Science University, Portland, OR, USA
[5] Cancer Early Detection Advanced Research Center, Oregon Health & Science University, Portland, OR, USA

**Corresponding Author Information*

Aaron J. Grossberg, MD, PhD

3181 SW Sam Jackson Park Road

L 481

Portland, OR 97239

Email: grossber@ohsu.edu

Abstract

Background

Our evolutionary history is defined, in part, by our ability to survive times of nutrient scarcity. The outcomes of the metabolic and behavioral adaptations during starvation are highly efficient macronutrient allocation, minimization of energy expenditure, and maximized odds of finding food. However, in different contexts, caloric deprivation is met with vastly different physiologic and behavioral responses, which challenge the primacy of energy homeostasis.

Methods

We conducted a literature review of scientific studies in humans, laboratory animals, and non-laboratory animals that evaluated the physiologic, metabolic, and behavioral responses to fasting, starvation, protein- or essential amino acid-deficient diets, and cachexia. Studies that investigated the changes in ingestive behavior, locomotor activity, resting metabolic rate, and tissue catabolism were selected as the focus of discussion.

Results

Whereas starvation responses prioritize energy balance, both protein malnutrition and cachexia present existential threats that induce unique adaptive programs which can exacerbate the caloric insufficiency of undernutrition. We compare and contrast the behavioral and metabolic responses and elucidate the mechanistic pathways that drive state-dependent alterations in energy seeking and partitioning.

Conclusion

The evolution of energetically inefficient metabolic and behavioral responses to protein malnutrition and cachexia reveal a hierarchy of metabolic priorities governed by discrete regulatory networks.

Graphical Abstract

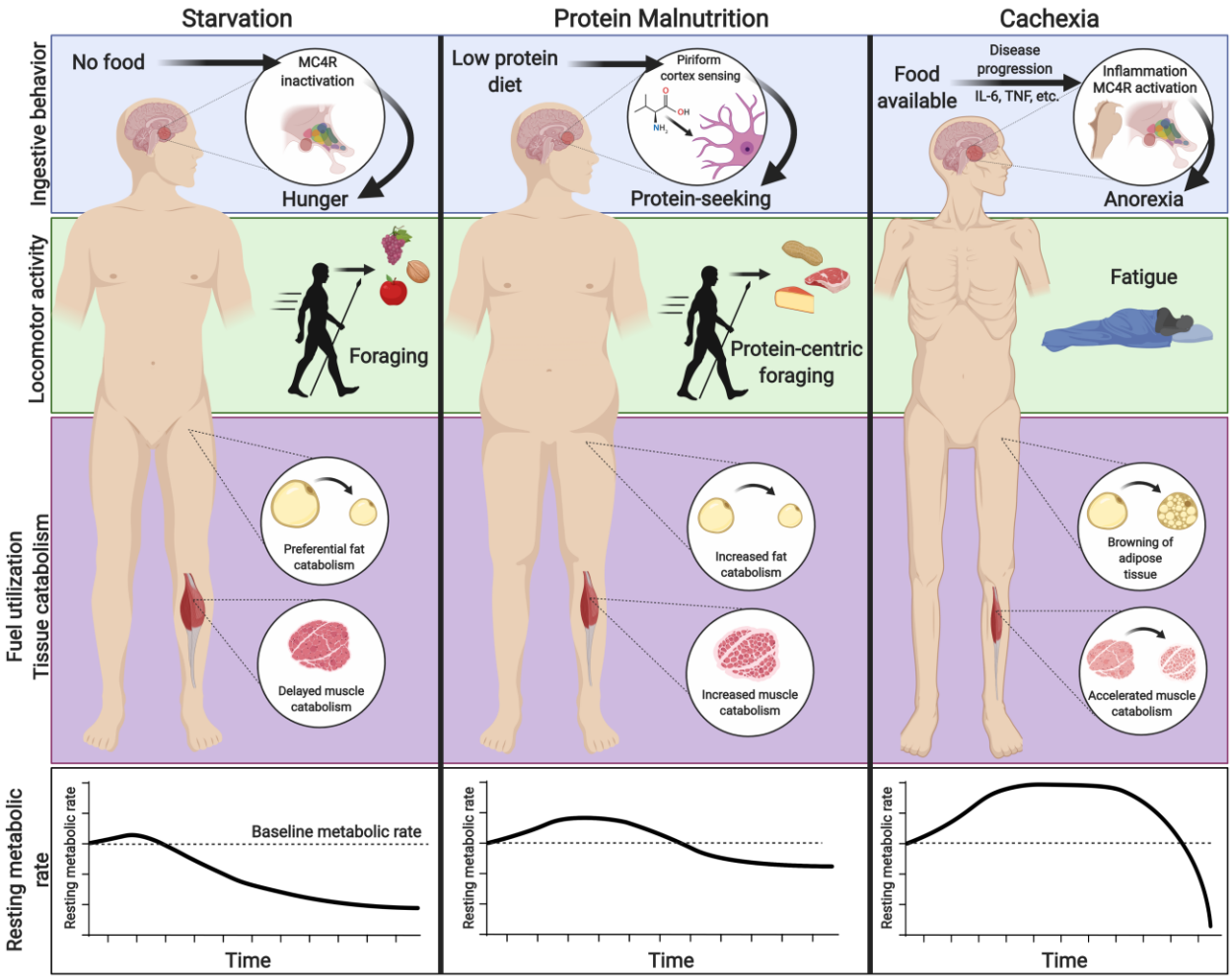

Keywords: starvation, cachexia, metabolism, evolution, protein malnutrition

1. Introduction

Appropriate nutrient consumption is an essential process in sustaining normal biological processes. Both small and extreme fluctuations in caloric intake result in changes in metabolism and behavior in effort to maintain organismal homeostasis. During calorically plentiful states, organisms activate energy-consuming anabolic pathways and satiety behaviors, while states of caloric deprivation result in energy-liberating catabolic pathways and foraging behaviors (171, 172). These metabolic programs and behaviors are evolutionarily conserved responses that were shaped to endure periods of famine (173). Specifically, starvation results in metabolic adaptations that decrease energy expenditure and conserve protein stores in order to preserve organ function, while increasing appetite and foraging behaviors in attempt to correct the underlying nutritional deficiency. However, in the context of protein-specific malnutrition or disease-associated cachexia, the metabolic and behavioral responses to nutrient insufficiency differ from simple starvation. For example, in both protein malnutrition and cachexia, catabolic processes are activated and macronutrient intake is paradoxically suppressed, violating the rule of energy conservation. While decades of research demonstrate that the physiologic and behavioral responses activated during starvation serve to spare energy stores and restrict energy expenditure, recent discoveries regarding the physiology and behavioral neuroscience of protein malnutrition and cachexia reveal additional levels of metabolic regulation that lend insight into the pressures that guided metabolic pathway evolution.

Simple starvation, defined herein as pure caloric deficit in an otherwise healthy organism, activates programs that prioritize metabolic efficiency, thereby promoting

resilience and survival. Less is known about protein malnutrition and cachexia, and recent evidence suggests the metabolic programs of these states in response to caloric deficit are broadly inefficient. Furthermore, these three states of nutrient deprivation result in unique behavioral responses that either complement, or contradict, the overall nutrient requirement of the organism (Figure 1). In this review, we will discuss the disparate physiologic responses of the metabolic states of simple starvation, protein malnutrition, and cachexia, with a particular focus on our current understanding of metabolism, neurophysiology, and behavioral outputs.

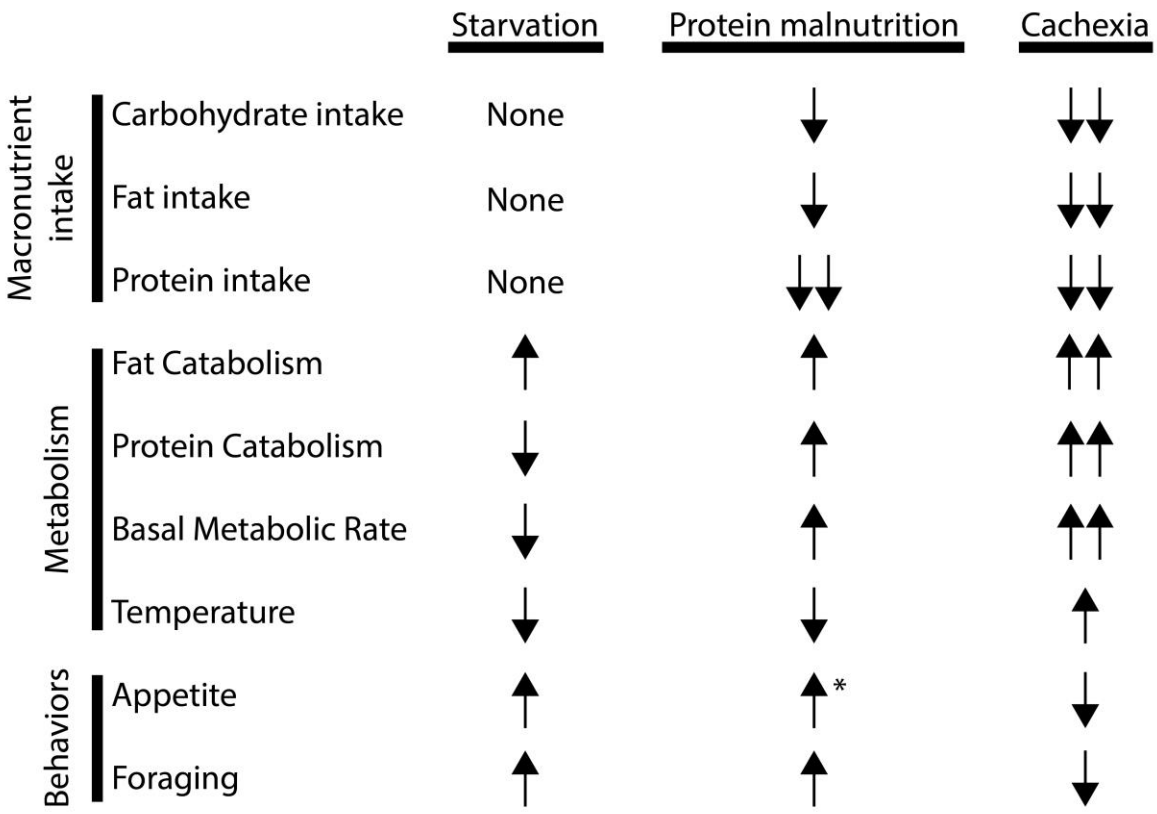

Figure 1. An overview of macronutrient intake, tissue metabolism, and behavioral changes observed during simple starvation, protein deficiency, and cachexia. *Increased appetite to protein-rich foods, yet active rejection of protein-poor foods.

2. Starvation

Metabolic homeostasis is maintained by a well-described network involving regions in the hypothalamus and brainstem that respond to hormonal and metabolic signals of both short- and long-term energy supply and engage appropriate behavioral and physiologic programs (174). Under physiologic conditions, mammals are able match cumulative energy intake with energy expenditure with exceptional precision due to tight control of tissue metabolism and feeding behaviors by the central nervous system (175, 176). Because nutrient scarcity represented an existential threat to organisms throughout their evolution, these systems prioritize efficiency and energy storage to maximize both countermeasures against and resilience to undernutrition. This response is defined behaviorally by an increase in appetite and foraging behavior, and metabolically by a decrease in basal metabolism and preferential catabolism of adipose over lean tissue (177, 178). Although this imbalanced response to nutrient availability likely made humans more vulnerable to obesity in the context of high nutrient availability, it ensures that the long-term effects of nutrient insufficiency are minimized. In this review, we use simple starvation to introduce the homeostatic response to nutritional insufficiency, which will then serve as our comparator when discussing the respective situations of protein malnutrition and cachexia.

2.1 Ingestive Behavior

Secreted peripheral factors alter neuronal activity and feeding behaviors during starvation, with decades of research demonstrating the influence of gut- and fat-secreted neuropeptides on the mediobasal hypothalamus (MBH) (179). Here, we will briefly discuss the well-studied endocrine molecules ghrelin and leptin that are known to play roles in driving behaviors of feeding at least in part through their direct, yet opposing, mechanisms on hypothalamic neurons. Other peripherally secreted hormones that influence food intake under physiologic conditions are summarized in Table 1. During fasting and starvation, the stomach releases the peptide hormone ghrelin, the only known circulating hormone that stimulates appetite. After secretion by the stomach, acylation of ghrelin is required for its binding to its receptor, the growth-hormone-secretagogue receptor, and for its ability to cross the blood-brain barrier (180). Once in the brain, ghrelin stimulates appetite through interaction with appetite-regulating neurons in the MBH. These include neurons that inhibit food intake (pro-opiomelanocortin (POMC) neurons), and appetite-stimulating neurons expressing neuropeptide Y (NPY) and agouti-related protein (AgRP), known collectively as the melanocortin system. The melanocortin system exerts many of its effects through regulation of activity at the type 4 melanocortin receptor (MC4R), which is expressed in numerous brain regions. POMC neurons release the MC4R agonist neurotransmitter alpha-melanocyte stimulating hormone (MSH), whereas AgRP neurons directly inhibit POMC neuronal activity and also release the MC4R inverse agonist AgRP at most MC4R expressing neurons. Ghrelin induces food intake primarily via activation of

NPY/AgRP neurons in the arcuate nucleus (ARC) of the MBH (181-183), which in turn send projections to numerous nuclei within the hypothalamus, including the paraventricular, ventromedial, dorsomedial, and lateral hypothalamus, as well as nuclei outside of the hypothalamus, including the nucleus of tractus solitarii and parabrachial nucleus (PBN) (184). Conversely, the anorexigenic adipokine leptin is markedly reduced during starvation (185). Leptin functions as a long-term signal of energy status, with circulating levels proportional to total adipose stores (186). Whereas the presence of leptin is permissive of normal caloric intake and neuroendocrine function, a fall in leptin levels signals a loss of long term energy stores. Correspondingly, decreased leptin is associated with decreased anorexigenic POMC neuronal activity, thereby triggering hunger and accompanying physiologic responses during starvation (187). This neuroendocrine interplay between rising levels of ghrelin and falling levels of leptin synergistically increase appetite during starvation. This intricate balance between upregulation of orexigenic and downregulation of anorexigenic molecules is a unifying theme of starvation neurophysiology.

Table 1. Additional endocrine molecules that mediate food intake

Hormone	**Source**	**Signaling mechanism(s)**
Cholecystokinin (CCK)	enteroendocrine cells of the duodenum and jejunum	Peripheral vagal afferent receptors and transmission of signals to nucleus of the solitary tract; Melanocortin system(188)
Glucacon-like peptide-1 (GLP1)	L cells of distal small and large intestine	nucleus of the solitary tract in the brainstem and the paraventricular nucleus of the hypothalamus; glucose regulation(189, 190)
Peptide YY (PYY)	endocrine L cells of the gut	Hypothalamic melanocortin system*; Aversive response; protein-dependent satiety(191, 192)

Glucocorticoids	Adrenal gland	Unclear, but potentially permissive in the orexigenic effect of AgRP in the hypothalamus(193, 194)
Insulin	Endocrine pancreas	Hypothalamic melanocortin system(195, 196)

2.2 Locomotor Activity

The regulation of activity in response to starvation is somewhat more complex than that of appetite. On one hand, voluntary activity increases energy usage and exacerbates energy debt in the absence of food intake. Yet, for nearly all of human existence, survival depended on the ability to forage, or to efficiently locate, acquire, and consume food (197). As such, foraging is deemed an obligate life history strategy, and a species' ability to recognize when foraging is beneficial or detrimental is a part of its evolutionary code (198). In general, starvation increases foraging behaviors when the likelihood of a meal is increased, yet limits foraging and movement when prey or food is limited (199, 200). During calorie deprivation, hyperactivity and increased foraging behavior is readily observed in rodents, wherein they exhibit stereotypic food anticipatory activity in the hours preceding mealtime (201). Although the neural pathways underlying this response are incompletely understood, this behavior is associated with concurrent increases in hypothalamic turnover of norepinephrine, dopamine, and serotonin (202). The neuropeptide orexin-A, released by neurons located in the lateral and perifornical hypothalamus, is required for fasting-associated activity increases. Furthermore, recent mouse work demonstrated that AgRP neurons in the mediobasal hypothalamus are themselves activated during starvation and are capable of driving foraging behavior (203). Orexin neurons reciprocally regulate both hypothalamic AgRP neurons and catecholaminergic neurons in the locus coeruleus,

establishing a brainstem-to-hypothalamus arousal loop that appears to mediate fasting-associated foraging (204, 205). The degree of hyperactivity and foraging is balanced between fear of predation and likelihood of feeding, and these processes are influenced, in part, through amygdala circuitry (206).

Rodents will increase their locomotor activity (foraging) when calorie availability is restricted, but access to at least some nutrition is maintained. In contrast, complete removal of food causes a triphasic response in weight loss and locomotor activity in rodents (207-209). The short-lived first phase is defined by early rapid weight loss and a decline in daily activity within 24 hours of fasting initiation. During a prolonged second phase, ongoing suppression of activity is associated with low rates of protein turnover, high dependence on lipid oxidation, and relatively steady body mass. Upon exhaustion of adipose depots, fasted rodents then show a profound rise in locomotor activity in the third phase, associated with rapid weight loss and protein catabolism (210). The duration of the energy-conserving second phase is age-dependent, longest in older animals that have larger adipose depots. Similar responses were shown in other species, most notably migratory birds and emperor penguins, in which the metabolic shift from lipid to protein catabolism is a signal of expiring energy stores that switches behavioral program from conservation to active foraging (211, 212). Collectively, these observations demonstrate the clear link between voluntary activity and energy balance and reveal an evolutionarily conserved mechanism whereby activity is regulated both by food availability and long-term energy stores.

2.3 Resting Metabolic Rate

Energy conservation is a key component of the adaptive response to starvation. Resting metabolic rate (RMR), the energy used to maintain body temperature, repair organs and tissues, maintain ion gradients, and support cardiorespiratory function, accounts for approximately two-thirds of total energy expenditure (213). Therefore, the RMR represents the greatest potential reservoir for energy conservation. Indeed, decades of research demonstrate that one of the main adaptations in humans and other species to nutrient deprivation is to reduce RMR. RMR is proportional to an animal's lean body mass, as lean tissues are far more metabolically active than adipose tissue. The suppression of RMR seen in response to even prolonged starvation exceeds that which can be explained by pure loss of lean mass, indicating that RMR depression is an active conservation strategy. This is known as "adaptive thermogenesis", because heat generation is the principal component of resting energy expenditure that is modulated in response to feeding. One of the earliest reports of this process showed the basal metabolic rate (equal to the RMR upon waking, while fasted and at rest) of a man who fasted for 42 days, with intake limited to water, lemonade, or beer. Basal metabolism progressively decreased until the end of his fast, at which time his resting energy expenditure was approximately half of that in the fed state (214). Similarly, the Minnesota Experiment challenged normal weight participants through stages of semi-starvation, restricted refeeding, and *ad libitum* refeeding, demonstrating excess suppression of RMR during undernutrition (215). Rats and mice also reduce thermogenesis response to fasting, suggesting that this is an evolutionarily conserved mechanism to preserve body mass (216, 217). Suppression of thermogenesis can

preserve mass over a large range of caloric deficits, perhaps most recognizably in the context of failure to lose weight during dieting (218).

The RMR is largely under the control of the sympathetic nervous system (SNS). Catecholamines released into the synapse from noradrenergic nerve terminals or systemically from the adrenal medulla increase the rate of cellular metabolism and mobilize fuel stores by stimulating lipolysis in adipocytes and glycogenolysis and gluconeogenesis from the muscle and liver (219). The SNS is responsive to nutritional status—engaged by overfeeding and suppressed by fasting (220). This response is seen in the human studies cited above, wherein fasting decreased resting heart rate, a surrogate for decreased sympathetic tone, in addition to its effects on thermogenesis. Indeed, fasting mice and rats also exhibit decreases in heart rate and blood pressure, consistent with decreased SNS activity (221, 222). Fasted rats have lower levels and turnover of norepinephrine in the heart, liver, pancreas, and other sympathetically innervated tissues as compared to fed rats (223). Although these cardiovascular effects can themselves conserve energy, the SNS has direct effects on thermogenesis mediated primarily by brown and white adipose tissue (WAT) via the β3 adrenoceptor (224). SNS activation stimulates uncoupled oxidative respiration via the expression of uncoupling protein 1 (UCP1), leading to nonshivering thermogenesis in brown adipose tissue (BAT) (225). Simultaneously, adrenergic input induces lipolysis in WAT, thereby providing a fuel source for BAT thermogenesis (226). Although previously thought to only be found in infants, BAT has recently been identified as an important thermogenic tissue in adult humans, as well (227-231). Thus, the decreases in RMR induced by

fasting appear to be largely mediated by decreased SNS activity and the resultant restriction of thermogenesis and cardiac output.

2.4 Fuel Utilization and Tissue Catabolism

The primary purpose of the metabolic response during fasting and starvation is to provide sufficient energy to the brain and other tissues critical for survival. During starvation, energy in the form of glucose is mobilized during early starvation, with ketone bodies serving as the primary energy source for the heart and brain in prolonged starvation (232). If fasting proceeds beyond one day in humans, or 8-12 hours in mice, hepatic stores of glycogen are rapidly depleted and catabolism of adipose and muscle tissue serve as the major sources of energy (233, 234). Since fat stores are limited in their ability to generate glucose, muscle catabolism is the primary source of hepatic and renal glucose production during starvation through liberation of gluconeogenic amino acids (235). However, proteins are not a substantial stored energy reserve, and humans evolved to preserve protein by shifting our fuel utilization from glucose to ketone bodies after just two days of starvation (236). These ketone bodies are produced by the liver from lipolysis-liberated fatty acids and significantly curtail muscle catabolism during starvation (237). Indeed, humans preferentially catabolize fat stores over skeletal muscle mass during prolonged caloric deficit (171). If starvation persists after fat stores are depleted, protein catabolism accelerates and can lead to severe wasting, organ failure, and ultimately death (238, 239). The preferential catabolism of adipose tissue is largely driven by the endocrine response to starvation. In the short term, falling blood sugar is met with the counter-regulatory endocrine response, including release of

glucocorticoids, glucagon, and growth hormone, and a concomitant decrease in insulin (240, 241). This stimulates both gluconeogenesis and lipolysis, engaging a catabolic program that redistributes stored energy in the absence of food intake (242). Although full discussion is outside of the scope of this review, a review of the major changes in circulating hormone levels is summarized in Table 2. Taken together, this strategic triaging of energy store utilization during starvation serves to reduce breakdown of proteins while providing adequate energy substrates for the brain and other tissues critical for survival (Figure 2A).

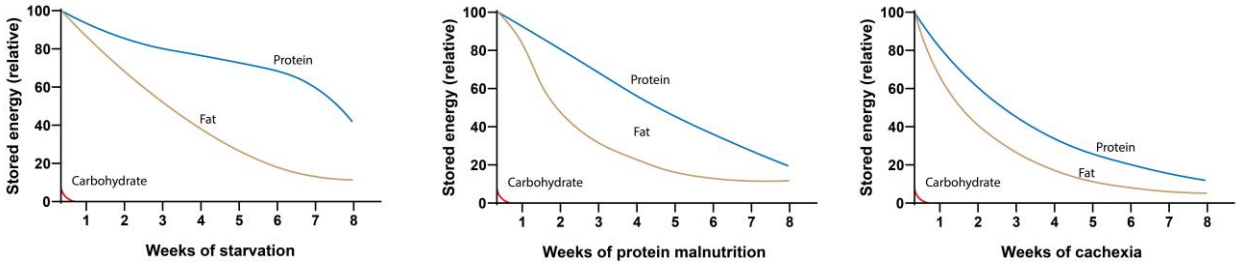

Figure 2. Relative rates of carbohydrate, fat, and protein catabolism during simple starvation, protein malnutrition, and cachexia.

Table 2. Overview of peripheral hormone response during starvation, protein malnutrition, and cachexia. Data are compared to healthy (all human studies) or pair-fed controls. Trends reported from human studies are italicized. *Compared to non-cachectic cancer patients.

	Starvation	**Protein Malnutrition**	**Cachexia**
Cortisol	Increased(242)	Increased(243, 244)	Increased(16, 245)

Thyroid hormone	Decreased(246-248)	Decreased(249)	Increased*(250)
Parathyroid hormone	Increased(251)	Increased(252)	Increased(253, 254)
Renin-angiotensin aldosterone	Increased(255, 256)	Increased; minimal excretion(257)	Increased(258, 259)
Norepinephrine	Increased peripherally(260); reduced action centrally(261)	Increased peripherally; reduced action centrally(262)	Increased(259)
Growth Hormone	Increased(240, 241)	Increased(263)	Increased(264)
Insulin	Decreased(260, 265)	Increased(266)	*Decreased(259, 267-269); impaired secretion
IGF1	Decreased(270)	Decreased(271)	Decreased(272)

3. Protein Malnutrition

Protein malnutrition represents a special case of undernutrition, in which specific adaptations evolved to ensure adequate intake of amino acids essential for growth, reproduction, and survival (273). In contrast to simple starvation, which is defined as caloric insufficiency, in protein malnutrition an imbalance in amino acid content or inadequacy of one or more amino acids drives behavioral and metabolic responses designed to correct the imbalance. Protein malnutrition can refer to a broad range of protein-deficient diets from total lack of protein content to specific amino acid shortages. For the sake of this review, we will define protein malnutrition as either overall inadequate protein intake—a low protein (LP) diet—or the dietary absence of a single essential amino acid (EAA-deficient diet), a scenario which best exemplifies the protein-specific homeostatic circuit. Absence or excess of single amino acids elicit powerful

feeding and behavioral effects, which in some cases can exacerbate overall energy imbalance. Imbalances in amino acids are then recovered via the increased catabolism of lean tissues, which may rely upon pathways that increase resting metabolic rate. This highlights a graded system in which regulation of nutritional composition preferentially drives the response program over pure caloric content. Below, we discuss the parallel mechanisms that mediate these processes and their interactions with homeostatic systems employed during starvation.

3.1 Ingestive Behavior

Animals fed a LP diet display alterations in appetitive behaviors that vary depending on protein content. For example, rats fed a moderately LP diet, with 8-10% of energy as protein, display sustained hyperphagia, prioritizing normalizing protein levels over caloric homeostasis (274-276). However, rodents consuming either very LP diet (<8% of energy in rats or <5% in mice) or EAA-deficient diets become hypophagic, even in the context of negative energy balance (277, 278). When exposed to such a diet, rats will decrease meal size and increase interfeeding intervals within 20 minutes of meal onset, mediated by neuronal detection of the EAA imbalance (279, 280). Within hours, the rats then develop conditioned taste aversion to the deficient diet while also developing preference for the missing amino acid (281, 282). Thus, despite undernutrition, laboratory rodents will paradoxically sustain hypophagia in the presence of EAA-deficient foods. When given access to foods containing the missing amino acid, or if the deficient EAA is injected into the brain, feeding behavior rapidly resumes with preference shown for the nutritionally replete food (283). Upon refeeding, rats will even

prefer a protein-free meal to an amino acid-imbalanced chow, reinforcing the importance of amino acid composition as a driver of food preference (284). Chronic hypophagia is therefore driven by aversion to EAA-deficiency, not lack of appetite. These observations translate somewhat to human studies, as moderate restriction of dietary protein induces adaptive changes in food intake to restore adequate protein status, but people will not overeat a very low protein diet to the point of protein repletion (285, 286). These findings led to the hypothesis of a “protein-centric” feeding paradigm, in which dietary amino acid composition is proposed to be the primary determinant of ingestive behavior, superseding the drive for energy homeostasis.

The sensing of amino acid deficiency during protein malnutrition is complex, and involves both the hypothalamus and the anterior piriform cortex (APC), a region involved in olfaction that is among the most primitive parts of the mammalian cortex (287, 288). The APC detection mechanism relies on the accumulation of uncharged transfer RNA, which activates the general amino acid control non-derepressing kinase 2 (GCN2). Mice and drosophila lacking GCN2 do not detect or avoid EAA-deficient diets, unless this exposure is prolonged (287). GCN2 phosphroylates eukaryotic initiation factor 2 (EIF2A) in APC neurons, initiating a signaling cascade that functions to block general protein synthesis (287, 289). The net effect of this pathway is to reduce GABAergic inhibition in the APC circuit and increase glutamatergic transmission (290). Although it remains unclear which targets of APC mediate the anorectic response, fMRI assessments in rats show rapid activation of both the ventromedial and lateral hypothalamus, two regions involved in feeding behaviors that receive APC axonal projections (290, 291). However, recent conflicting studies question the GCN2/EIF2A-

dependent mechanism in the APC, suggesting neuronal sensing of amino acids remain incompletely understood (292). A similar mechanism for EAA detection in the MBH was proposed, supported by the blunting of the anorectic response to a leucine-deficient diet following adenoviral knockdown of GCN2 in the ARC of mice (293). Although appetite-regulating neurons in the hypothalamus may directly detect EAA deficiencies, central melanocortin signaling appears to only play a minor role in the acute feeding response. Mice depleted of the MC4R have a slightly attenuated acute anorectic response to EAA-deficient diet, but neither pharmacologic or genetic blockade impacts the chronic hypophagia induced by dietary EAA deficiency (294). This observation illustrates the mechanistic and behavioral divergence between feeding responses—driven principally by aversion—and appetite, which is preserved.

3.2 Locomotor Activity

Rodents fed EAA-deficient diets develop rapid and sustained anorexia yet display increased foraging behaviors in effort to find foods containing the needed essential amino acid (290). This supports the observation that hypophagia observed during EAA deficient diet consumption is not reflective of a global decrease in appetitive behaviors. Similar to fasting, both LP diet and EAA-deficiency significantly increase locomotor activity compared to rodents fed normal chow (295). During the initial EAA-deficient meal, increased activity corresponds temporally to meal termination and is characterized by digging in their food cup, suggesting that the purpose of this activity is to seek new foods (296). Accordingly, this behavior is rapidly extinguished upon reintroduction of the deficient EAA, in a process dependent upon normal protein synthesis in the APC (297).

As with the regulation of food intake, the regulation of foraging behavior due to protein malnutrition is complex. The key site of signal integration appears to be orexin neurons in the lateral hypothalamus, which receive both excitatory projections from the APC and peptidergic projections from the MBH. Disinhibition of APC neurons in response to EAA-deficiency then directly activates lateral hypothalamic orexin neurons, which coordinate the locomotor appetitive behaviors (reviewed in (290)). Karnani and colleagues demonstrate that orexin neurons are also activated by non-essential amino acids, which may be increased in the context of EAA deficiency, leading to increased foraging activity (298). These authors were further able to show that non-essential amino acids at physiologic concentrations were able to overcome glucose inhibition of orexin neurons, providing a mechanistic explanation for the activation of foraging in the EAA deficient setting despite adequate calorie intake (298). Collectively, it is clear that protein malnutrition induces foraging behaviors similar to that of a starving animal and, combined with a strong preference for amino acid replete food sources, serve to maximize the animal's chances of rectifying nutrient imbalances.

3.3 Resting Metabolic Rate

The central sensing of amino acid deprivation can regulate energy expenditure and autonomic outflow through mechanisms that are independent of other macronutrients. Dietary leucine deprivation increases thyrotropin-releasing hormone (TRH) expression in the hypothalamus, ultimately increasing energy expenditure as indicated by measures of locomotor activity, oxygen consumption, and temperature regulation (299). This collective increase in TRH observed during leucine deprivation results in

sympathetic nervous system (SNS) activation and autonomic outflow to peripheral tissues that increases resting metabolic rate and lipid catabolism, as reviewed above. Specifically, leucine deprivation increases the expression of the β3-adrenoceptor, *Adrb3,* as well as *Ucp1* in BAT consistent with sympathetic activation of thermogenesis (300, 301). Similarly, we found that *Ucp1* expression was increased in mice and rats fed a valine-deficient diet, and Guo and colleagues showed that both valine and isoleucine deficiency increase lipid mobilization and energy expenditure suggesting that hypermetabolism is a conserved response to amino acid imbalance (277, 295). Other investigators demonstrated that leucine deprivation induced the induction of *Ucp1* and other markers of thermogenic activation (generally known as "browning") in WAT, via a CNS pathway and activation of sympathetic outflow (302). The evolutionary benefit of this increase in metabolic rate and metabolic reprogramming of adipose tissue in an undernourished animal is not immediately clear, but may be important to balance the energy demands of foraging, via SNS mediated activation of lipolysis (300).

3.4 Fuel Utilization and Tissue Catabolism

When compared to starvation, protein malnutrition is broadly associated with an earlier-onset and increased protein and fat catabolism (Figure 2B). After being fed a diet deficient in EAA, rodents quickly deplete carbohydrate stores similar to that observed during simple starvation. However, rodents catabolize muscle at a significantly higher rate than their normal chow pair-fed counterparts, demonstrating that a distinct and independent catabolic pathway is associated with EAA deficiency (277). Active muscle catabolism releases EAAs into the blood, thereby providing a source of diet-limited

EAAs and allowing for ongoing protein synthesis to maintain essential physiological processes. Mechanistically, this process is driven by the induction of catabolism-inducing E3 ubiquitin ligases (MuRF1 and MAFbx) in skeletal muscle. These catabolic proteins are upregulated in the muscle of rodents fed an EAA-deficient diet after just 3 days and remain elevated after nearly 3 weeks (277). To a lesser extent, this increased catabolic state observed in the muscle compartment for EAA-deficient animals is also observed in fat tissues. Specifically, rodents on an EAA-deficient diet catabolize fat stores similarly to pair-fed controls for the first week, but burn fat at a much higher rate after 2 weeks (277). This catabolic program is likely to be influenced both by increased energy expenditure described above, along with the actions of circulating glucocorticoids. Although the general trends of hormonal changes associated with protein malnutrition are similar to those found in starvation (Table 2), administration of a valine deficient diet increased plasma corticosterone compared with pair-fed control mice and rats (277). In response to a leucine-deficient diet, Xia and colleagues define a novel role of p70 S6 kinase 1 (S6K1) in modulating expression of corticotropin-releasing hormone (CRH) in MC4R-positive hypothalamic neurons. This induction of hypothalamic CRH expression is essential for stimulating lipolysis in response to leucine deprivation (303). Furthermore, glucocorticoids play a well-established role in mediating skeletal muscle catabolism via the induction of the E3 ubiquitin ligases referenced above in multiple pathophysiologic conditions (16, 71, 72). Although the dependence of muscle catabolism in response to EAA deficiency upon glucocorticoid elevation has not been directly confirmed, the associative data provide compelling evidence that glucocorticoids serve as a unifying endocrine mediator of macronutrient mobilization.

Conversely, the levels of the anabolic hormones insulin and insulin like growth factor-1 are decreased in rodents on an EAA-deficient diet compared to pair fed animals, further shifting the metabolic balance toward catabolism (294). In total, EAA-deficiency results in a sustained catabolic state of peripheral tissues, liberating fat and muscle stores at a faster pace than simple starvation.

4. Cachexia

Cachexia is a wasting syndrome associated with a broad range of acute and chronic illnesses, including infection, heart disease, cancer, and chronic inflammatory conditions. Unlike starvation and protein malnutrition, which are dictated by environmental nutrient availability, cachexia results from internal factors and cannot be fully reversed by nutritional supplementation. Cachexia is characterized by the co-occurrence of anorexia, lethargy, hypermetabolism, and accelerated catabolism (15). This program is the result of inflammatory and metabolic signals that reorient the homeostatic mechanisms employed during starvation and protein malnutrition, establishing a hierarchy of context-specific afferent signals. That cachexia is conserved across species and inflammatory conditions suggests that it likely evolved as an adaptive response to life-threatening illness. Indeed, several studies demonstrate survival benefits of this catabolic state during acute infectious processes (63, 304). These benefits are traditionally thought to result from the redirection of valuable metabolic resources from the brain and gut to the immune response (305). Recent work adds that this metabolic program aids in tissue tolerance during the immune response, preventing end organ dysfunction (63, 304). Proinflammatory cytokines are common among cachectic conditions and sufficient to

drive much of the metabolic physiology. Recent work has expanded the list of afferent mediators contributing to wasting and offered new insights into its etiology. Below we contrast the CNS response to cachexia from those of starvation and protein malnutrition and discuss the mediators that drive these divergent programs.

4.1 Ingestive Behaviors

Due the increase in resting energy expenditure during cachexia, an increase in energy intake would be required to offset the overall catabolic state. However, cachexia induces appetite suppression that amplifies the overall energy deficit (Figure 3). In some cases this presents as frank anorexia, whereas in other cases a more subtle failure to appropriately increase feeding is observed (38, 52, 306, 307). The resistance to the effects of energy debt are most notable after substantial weight is lost, when the hypothalamic feeding rheostat would be under increased pressure to reestablish homeostasis. The disinterest in feeding during cachexia is in direct opposition to what is observed in simple starvation or protein malnutrition, each of which results in behaviors that attempt to restore macronutrient homeostasis.

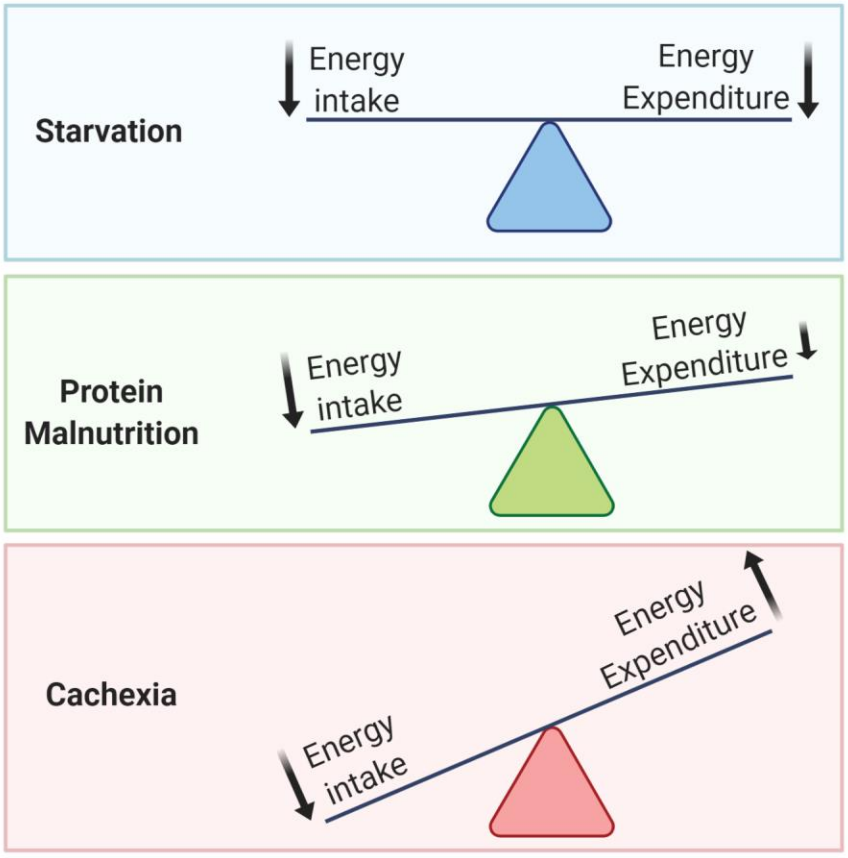

Figure 3. Energy intake and expenditure during starvation, protein malnutrition, and cachexia.

Multiple systemic and central factors converge to inhibit ingestive behaviors, with the hypothalamus and brainstem thought to be the major sites of signal integration. Principal among anorectic factors are inflammatory cytokines, including interleukin-1β (IL-1β), tumor necrosis factor (TNF), leukemia inhibitory factor (LIF), type 1 interferon (IFN), and prostaglandins (2, 15). Each of these molecules is independently capable of inducing anorexia when administered either peripherally or directly in the brain. Research in our laboratories and others' over the past two decades demonstrated that a

principal site of action for these cytokines is in the MBH, where specialized fenestrated endothelium and localized inflammatory cells allow for the transmission and amplification of peripheral inflammatory signals (reviewed in (18)). These cytokines then act directly or indirectly to increase signaling through the MC4R, in a fashion similar to leptin (306). Pharmacologic or genetic ablation of MC4R signaling reverses cachexia in multiple acute and chronic laboratory rodent models of cachexia (308-313).

More recent work implicates two populations of neurons in the brainstem in the anorectic component of cachexia. The first consists of neurons in the PBN, located in the pons, which relays noxious stimuli from the viscera to the amygdala as a component of the threat circuit. Activation of PBN calcitonin gene-related peptide (CGRP)-expressing neurons potently suppresses appetite (314). These neurons were activated in two murine models of cancer cachexia and sterile inflammation, and their chemogenetic inhibition was sufficient to reverse the anorexia and weight loss associated with each model (314, 315). As PBN CGRP neurons are inhibited by hypothalamic AgRP neurons and express MC4R, they may function as a downstream effector of hypothalamic-mediated cachexia (316, 317). Given their role in relaying aversive signals, these neurons may also have non-overlapping influences on cachexia-anorexia, generating redundancy in this system. A second brainstem site involved in the transmission of noxious signals is located in the area postrema, a circumventricular organ most well-known for its role in nausea. A population of neurons there express the GDNF family receptor alpha like (GFRAL), the only known receptor for growth differentiation factor 15 (GDF-15), a member of the transforming growth factor beta ligand family that suppresses food intake (318-320). Elevated serum levels of GDF-15

are found in multiple cachectic states and serum levels correlate with weight loss in prostate cancer (63, 321). Treatment of mice with GDF-15 or implantation with a GDF-15 overexpressing tumor is sufficient to induce cachexia, whereas treatment with a neutralizing antibody reversed cachexia in multiple murine cancer models (307, 322, 323). Although there is some integration of these anorectic pathways, the existence of multiple disparate mediators represents a level of redundancy found in few biological systems, suggesting that suppression of food intake during illness is an essential response. Indeed, a provocative study by Wang and colleagues demonstrated that improvement in survival in mice with a *Salmonella* infection, required fasting-induced ketogenesis (304). Whether decreased nutrient intake provides an adaptive advantage in the contexts of cancer or other conditions remains unclear.

4.2 Locomotor Activity

Unlike starvation or protein malnutrition, cachexia is associated with a profound lethargy and decrease in both foraging and non-foraging locomotor activity. Lethargy is among the first signs of sickness, often observed prior to the onset of fever in patients with microbial infections or murine models of sterile inflammation (324). From an evolutionary perspective, this response makes sense both to reserve metabolic resources for the fight against infection and to avoid exposure to the elements or predation while in a weakened state. Cachectic rodents neither exhibit the increase in foraging behavior seen in other states of undernutrition nor do they develop anticipatory activity when entrained with time-restricted feeding paradigms (325). As described above, foraging behavior is mediated by perifornical/lateral hypothalamic orexin neurons,

which receive input from the MBH, APC, and brainstem arousal centers. Orexin neuron activity is decreased in mice treated with LPS and sarcoma-bearing rats, and intracerebroventricular administration of orexin can restore normal locomotor activity in these models, suggesting that the inhibition of orexin neuron activity underlies sickness-associated lethargy (325). This inhibition appears to be mediated by an increase in the activity of local interneurons that express neurotensin, but the link between inflammation and the activity of these neurons remains poorly described (325). Within the MBH, AgRP neuron activity is necessary to engage in foraging behavior, yet AgRP neuron activity and peptide release are reduced in cachectic rodents (203, 326, 327). As AgRP neurons are known to share reciprocal projections with the lateral hypothalamus and thought to drive foraging via activation of orexin neurons, the loss of AgRP neuron activity may mediate the downregulation of orexin neuron activity. The aforementioned study that evaluated PBN CGRP neurons also found that their chemogenetic inhibition reversed lethargy (315). Neurons in the lateral PBN send projections to orexin neurons that then innervate the locus coeruleus, but it remains unclear whether orexin neurons play a role in lateral PBN CGRP-mediated lethargy or these are two parallel pathways (328).

Decreased activity in cachectic humans and rodents appears to be multifactorial, involving peripheral mechanisms, as well. Muscles from cachectic mice exhibit decreased mass, strength, function, and exhibit early fatigability (329, 330). Because inflammatory signaling can drive both skeletal muscle wasting and lethargy, it can be difficult to attribute the decrease in locomotor activity specifically to muscle wasting. However, transgenic mice overexpressing the transcription factor Forkhead box protein

O1 (FoxO1), a driver of skeletal muscle catabolism, show reduced muscle mass and spontaneous locomotor activity, suggesting that skeletal muscle loss is sufficient to suppress activity (331). Cachexia is further associated with metabolic changes that alter fuel mobilization and utilization. Recent work in mice bearing head and neck cancers shows that decreases in locomotor activity can occur independent of central inflammation and prior to significant muscle loss (44). Metabolic phenotyping in these mice revealed significant changes in carbohydrate metabolism associated with lower blood glucose levels and increased skeletal muscle lactate accumulation, positing an additional contribution of metabolic exhaustion to hypoactivity in cachexia (332).

4.3 Resting Metabolic Rate

The regulation of resting metabolic rate in cachexia is most thoroughly studied in the context of cancer, with the majority of studies demonstrating normal or increased energy expenditure in a variety of different cancer types (333-336). Cancer patients frequently have reduced caloric intake and weight loss, so even “normal” energy expenditure should be considered excessive in this context. RMR is related to the degree of cachexia, with elevated energy expenditure documented prior to overt weight loss, sustained through early cachexia, then declining in those most severely affected (refractory cachexia) (333, 337), perhaps due to depletion of available metabolic substrates. Indeed, increased fat oxidation is observed in cancer patients, irrespective of weight loss, and browning of WAT is observed in murine cachexia models and in humans with cachexia (52, 338). Although direct action of circulating factors (e.g. parathyroid hormone related peptide [PTHrP]) can activate thermogenesis and

browning of adipose tissue in a subset of cancer types, the most robust and consistent driver of this process is chronic activation of adrenergic sympathetic inputs. A number of studies demonstrate activation of pre-autonomic neurons in the paraventricular nucleus of the hypothalamus (PVH) during both the early and late stages of cachexia, suggesting that this is a common mechanism of induction of thermogenesis in this disease (339, 340). Although few in number, studies that explored the impact of glucocorticoids on human adipose tissue thermogenesis demonstrated an increase in BAT activation by glucocorticoids, suggesting that this is another mechanism driving increased energy utilization during cachexia (341, 342). Furthermore, the hormonal changes associated with cancer cachexia are characterized by increased release of thyroid hormone as compared to non-cachectic patients, indicating that this may further increase the resting metabolic rate (250) (Table 2). Collectively, existing data argue that increased metabolic rate (or lack of compensatory metabolic response to insufficient caloric intake) is an important feature of cachexia, driven by a combination of metabolic inefficiency ("futile" metabolic cycles) and tissue reprogramming. However, the afferent signals driving these events, as well as the relative contribution of CNS vs. peripheral mechanisms remain poorly described.

4.4 Fuel Utilization and Tissue Catabolism

As in starvation and protein malnutrition, cachexia is associated with a global shift from carbohydrate to lipid oxidation in both patients and rodent models of disease (343-345). Levels of both glucose and lipids are frequently elevated in the blood of cachectic patients and rodents, indicating adequate substrate availability, particularly in

early stages of cachexia (346, 347). That hyperglycemia is common in cancer patients despite the tumor's increased glucose avidity, implies a global metabolic reprogramming favoring lipid as a substrate. The relative fuel utilization can be measured by indirect calorimetry, and is expressed as the respiratory exchange ratio (RER)—the ratio between the amount of carbon dioxide generated and the amount of oxygen consumed. Multiple studies show a decrease in RER of cachectic patients and rodents, indicating a preference for lipid oxidation over glucose (52, 343, 348). Evidence from models of early cachexia suggests that this transition occurs before substantial weight loss occurs (343). Lipid oxidation appears to be elevated principally in the skeletal muscle, where excess lipid oxidation may be sufficient to drive muscle wasting (343, 349). However, hepatic lipid oxidation, required for ketone generation, is decreased in multiple models of cachexia, demonstrating a tissue-dependent reprogramming (350, 351). This impaired ketogenesis is hypothesized to be a driver of tissue wasting, but conflicting data exist, with dietary or pharmacologic activation of ketogenesis shown to reverse cachexia in mouse models of lung and pancreatic cancer, but not in a rat sarcoma model or human cancer patients (350, 352-354). The use of proteins as a metabolic fuel is more difficult to measure, as RER does not take them into account, and they generally constitute a small contribution to overall metabolism. Although muscle wasting is a cardinal feature of cachexia, levels of serum amino acids and urinary nitrogen excretion are largely unaltered or paradoxically decreased in cachectic patients and rodents (355-357). Much of the protein mobilized from muscles during cachexia is thought to provide substrate for the hepatic acute phase response to inflammation, a metabolically costly process involving the synthesis and release of bioactive proteins

involved in modifying the metabolic environment of the threatened host. Because the amino acid composition of muscle differs substantially from acute phase reactants, it is hypothesized that this drives further wasting to supply adequate levels of the limiting amino acids (358).

In comparison to both starvation and protein malnutrition, cachexia is associated with the greatest muscle and fat catabolism relative to the degree of caloric deficiency (Figure 2C) (38, 359). Using computational models of cachexia in humans, it is estimated that lipolysis increases by up to 30-80% over baseline (360-362), while reports suggest muscle catabolism may increase by 40-60% (363-366). Muscle loss in cachexia owes to a combination of reduced protein synthesis and increased protein catabolism (367). The relative influence of altered synthesis and degradation to wasting varies among studies, with early reports suggesting that decreased synthesis played a dominant role (368, 369). More recent studies clearly established that cachectic patients retain anabolic potential, with a clinical trial showing net gain in muscle mass with the ghrelin mimetic (anamorelin) in patients with cancer cachexia (370-374). Amino acid supplementation in cachectic tumor-bearing rats increased protein synthesis, yet degradation outpaced gains in protein synthesis (375). This catabolic program in skeletal muscle is mediated through the activation of the ubiquitin proteasome pathway and enhanced *Mafbx*, *Murf1*, and *Foxo1* expression (376). Although common to all three states of undernutrition, the ubiquitin proteasome pathway is activated to a greater degree in cachexia than in either starvation or protein malnutrition (38, 294). The activation of the ubiquitin proteasome pathway in cachexia reflects the influences of direct inflammatory cytokine signaling on muscle, persistently elevated glucocorticoid

signaling, and disuse (377). Multiple *in vitro* and preclinical studies confirm that inflammatory cytokines, including IL-1, TNF, and IFNγ, and glucocorticoids, are independently sufficient to induce E3 ubiquitin ligase expresion in skeletal muscle, thereby amplifying the catabolic effect of undernutrition (378-380).

Autophagy, the digestion and recycling of cellular contents by the lysosome, also contributes to muscle catabolism. This process is an important component of cellular homeostasis, allowing for the degradation of damaged organelles, toxic protein aggregates, and misfolded proteins (381). Autophagy is increased following prolonged fasting in mice, but notably is elevated in the muscles of cachectic humans mice as well, as evidenced by increased levels of autophagy mediators BNIP3 and LC3B and the autophagy-promoting transcription factor FOXO3 (382-388). Similar to the ubiquitin-proteasome pathway, autophagy can be activated in skeletal muscle by metabolic (calorie restriction), hormonal (glucocorticoid) or inflammatory (cytokine) challenges, illustrating the high degree of conservation in muscle-intrinsic catabolic mechanisms across contexts (384). As in skeletal muscle, cardiac wasting can be driven by both the ubiquitin protesasome pathway and increased autophagy. Few extant data support the role of increased MAFbx and MuRF-1 in hearts from cachectic mice, however, with conflicting reports in mice with cancer cachexia (38, 389, 390). Conversely, autophagy markers LC3-II, cathepsin L, and beclin are elevated in hearts from rodents with cancer cachexia (389, 391, 392). The relative roles for these pathways in cardiac wasting remain unclear and a topic of active investigation. Ultimately, the cachectic humoral milieu, characterized by increased levels of proinflammatory mediators and

glucocorticoids, is able to augment physiologic activation of these catabolic pathways in skeletal and cardiac muscle beyond that of undernutrition alone.

Loss of WAT in cachexia is due to enhanced lipolysis, associated with elevated levels of circulating free fatty acids and glycerol (393). Lipolysis is mediated by two enzymes in adipocytes—adipose triglyceride lipase (ATGL), which catalyzes the initial hydrolysis of triglycerides to diacylglycerol, and hormone sensitive lipase (HSL), which is responsible for the subsequent hydrolysis of diacylglycerol. Although HSL is generally considered the main inducible driver of lipolysis, deletion of *Atgl* prevented lipolysis in the B16 melanoma murine model of cancer cachexia (394). Lipolysis in cachexia is mediated by increased SNS activation and a host of humoral mediators, including TNF, IL-6, and zinc alpha glycoprotein, each of which is commonly elevated in the serum of cachectic patients or rodents (393). Cachexia is also associated with browning of WAT to promote thermogenesis via the expression of the UCP1 (52, 254). In this way, cachexia modifies adipocyte biology both to induce WAT atrophy via lipolysis and increase metabolic rate through excess energy dissipation. Fat and muscle catabolism are largely studied as independent events in cachexia, however several murine studies demonstrate that preventing adipose wasting also reversed skeletal muscle loss (254, 394). The link between adipose wasting and muscle loss remains unclear but may owe to oxidative stress associated with the increase in fatty oxidation seen in cachectic muscle (349). When compared to simple starvation and protein malnutrition, the metabolic programs of cachexia are broadly more catabolic and energetically inefficient, leading to an increase in resting energy expenditure and depletion of metabolic reserves.

5. Conclusion

Throughout our evolutionary history, humans developed behavioral and biochemical strategies to cope with nutrient scarcity in the context of famine. However, starvation was not the only threat to survival associated with undernutrition, as changes in ingestive behaviors and metabolism are seen in the contexts of protein malnutrition and infection or inflammation, as well. Herein, we sought to summarize general macronutrient utilization and tissue catabolism shifts observed amongst these three metabolic states, as well as the associated deviations in neurophysiology and behaviors that serve to rectify (or propagate) nutritional imbalances. In the context of simple starvation and protein malnutrition, the metabolic and neuroendocrine responses induce changes in behavior and metabolism that facilitate correction of the nutritional deficiencies. Throughout the spectrum of starvation and protein malnutrition, the brain receives both local and distant neuroendocrine signals to interpret the body's overall nutritional state, and modulates behaviors and motivations in attempt to balance energy needs, with the requirement to balance amino acid composition eclipsing the drive to maintain overall caloric sufficiency. This hierarchy may seem somewhat surprising, and suggests that EAAs and not simple energy equivalents are the limiting nutritional reagent for organismal survival and replication.

The constellation of metabolic and behavioral responses observed during cachexia represent a highly coordinated series of adaptations designed to survive acute insults by shifting priorities to both combat and tolerate the inflammatory challenge. As systemic infection represented the most salient existential threat to animals in the pre-

antibiotic era, the reorganization of metabolism around disease survival provides a teleological narrative for this paradoxical response to energy depletion. From an evolutionary perspective, humans rarely lived long enough to develop chronic diseases associated with cachexia. Because the metabolic alterations of cachexia, including browning of adipose tissue, skeletal muscle and adipose catabolism, and elevated basal metabolic rate lead to a severe mismatch in energy balance, it is commonly thought that these responses become maladaptive when engaged over a prolonged period, as during chronic disease. Furthermore, the sickness behaviors of cachexia (including appetite suppression, fatigue, and debility) significantly impact patients' quality of life, stimulating efforts to develop treatments aimed specifically toward reversing cachexia. However, future research may yet show advantages to this physiology in chronic cachectic conditions.

We recognize the important contributions that cognitive, emotional, and hedonic inputs play in feeding motivation during both normal physiology and pathology. Due to the widely varying influences these psychosocial inputs play in both energy metabolism and feeding, we chose to focus solely on the brain's integration of metabolic and neuroendocrine cues during starvation, protein malnutrition, and cachexia, with a particular focus on neurological pathways that are distinct amongst these three metabolic states. Nearly all of the mechanistic data discussed in this review is derived from studies in rodents. It is clear that these responses are likely to be heavily modified by telencephalic inputs in humans, which may provide an additional level of context-matching to enhance survival.

In starvation, classical neuroendocrine cues, such as gut- and fat-derived hormones, are predominantly responsible for organismal metabolic and behavioral outputs. During protein malnutrition, the direct sensing of amino acid imbalances through recently identified neuronal pathways in the APC likely play a direct role in driving peripheral tissue catabolism. The neuroscience of cachexia is defined by the production of cachexia-promoting factors that are not regulated by nutritional stress alone, but by systemic inflammation due to the underlying disease. The CNS-based pathways that regulate energy homeostasis during cachexia remains an area of active investigation, but a growing body of evidence demonstrates the capacity of the brain to recognize peripheral mediators of sickness, amplify these signals in circumventricular structures, and modulate energy homeostasis through appetite regulation and neuroendocrine and autonomic control of peripheral tissue metabolism (15, 18, 395). Collectively, the neurophysiology of cachexia exacerbates energy losses, whereas the neurophysiology of simple starvation and protein malnutrition ultimately serve to rectify energy imbalances (Figure 3). As evolution is driven by competing pressures, these divergent responses are the result of a natural hierarchy of needs and illustrate the profound impact that disease had in shaping animal physiology. Future investigations into the metabolism and neuroscience of these metabolic states may identify distinct diverging points in our evolutionary history, unique neurobiological pathways of CNS metabolic control, and offer new insights into the physiologic plasticity needed for long term survival of a species.

Acknowledgements

This work is supported by the National Cancer Institute grants F30 CA254033 (BO), R01 CA217989 (DLM), R01 CA234006 (DLM), and K08 CA245188 (AJG), and the Brenden-Colson Center for Pancreatic Care (DLM and AJG). The authors of this manuscript certify that they comply with the ethical guidelines for authorship and publishing in the Journal of Cachexia, Sarcopenia and Muscle (396).

The authors have no conflict of interests to disclose.

Chapter 2: Pretreatment cancer-related cognitive impairment—mechanisms and outlook

A manuscript published in *Cancers*

Olson B, Marks DL. Pretreatment Cancer-Related Cognitive Impairment Mechanisms and Outlook. *Cancers.* 2019;11(5).

Pretreatment Cancer-Related Cognitive Impairment—Mechanisms and Outlook

Brennan Olson [1,2] and Daniel L. Marks [2,3,*]

[1] Medical Scientist Training Program, Oregon Health & Science University, 3181 SW Sam Jackson Park Rd, Portland, OR 97239, USA; olsobr@ohsu.edu
[2] Papé Family Pediatric Research Institute, Oregon Health & Science University, 3181 SW Sam Jackson Park Rd, Portland, OR 97239, USA
[3] Brenden-Colson Center for Pancreatic Care, Oregon Health & Science University, 3181 SW Sam Jackson Park Rd, Portland, OR 97239, USA
***** Correspondence: marksd@ohsu.edu

* Corresponding Author:

Daniel Marks, MD, PhD

3181 SW Sam Jackson Park Road

L 481

Portland, OR 97239

Email: marksd@ohsu.edu

Abstract

Cognitive changes are common in patients with active cancer and during its remission. This has largely been blamed on therapy-related toxicities and diagnosis-related stress, with little attention paid to the biological impact of cancer itself. A plethora of clinical studies demonstrates that cancer patients experience cognitive impairment during and after treatment. However, recent studies show that a significant portion of patients with non-central nervous system (CNS) tumors experience cognitive decline *prior* to treatment, suggesting a role for tumor-derived factors in modulating cognition and behavior. Cancer-related cognitive impairment (CRCI) negatively impacts a patient's quality of life, reduces occupational and social functioning, and increases morbidity and mortality. Furthermore, patients with cancer cachexia frequently experience a stark neurocognitive decline, suggesting peripheral tumors exert an enduring toll on the brain during this chronic paraneoplastic syndrome. However, the scarcity of research on cognitive impairment in non-CNS cancers makes it difficult to isolate psychosocial, genetic, behavioral, and pathophysiological factors in CRCI. Furthermore, clinical models of CRCI are frequently confounded by complicated drug regimens that inherently affect neurocognitive processes. The severity of CRCI varies considerably amongst patients and highlights its multifactorial nature. Untangling the biological aspects of CRCI from genetic, psychosocial, and behavioral factors is non-trivial, yet vital in understanding the pathogenesis of CRCI and discovering means for therapeutic intervention. Recent evidence demonstrating the ability of peripheral tumors to alter CNS pathways in murine models is compelling, and it allows

researchers to isolate the underlying biological mechanisms from the confounding psychosocial stressors found in the clinic. This review summarizes the state of the science of CRCI independent of treatment and focuses on biological mechanisms in which peripheral cancers modulate the CNS.

Keywords: Cancer; cachexia; cognitive decline; cytokines; extracellular vesicles; blood-brain barrier; neuroinflammation

1. Introduction

Advances in cancer treatments have greatly improved the overall survival of patients. However, the use of cancer therapies, including radiation, chemotherapy, and immunotherapies, are commonly associated with toxicities. A multitude of studies demonstrates that patients treated with systemic therapy or radiotherapy experience neurocognitive decline (397-400). However, a new wave of research demonstrates that even prior to treatment, a significant portion of patients with non-CNS malignancies experience cognitive impairment (401, 402). Furthermore, patients with cancer cachexia frequently experience cognitive decline, suggesting tumor factors chronically affect cognition throughout the disease course. With 1.7 million new cases of cancer in 2018 in the US alone and due to an aging population, the prevalence of cancer is on the rise as is the population of patients in remission or cured of disease (403). Consequently, as patients continue to live longer after their cancer is cured, the focus is shifting towards understanding long-term sequelae caused by cancer therapeutics or surgery, and special attention to the quality of life measurements has become paramount for patient care. While much of the focus is centered around mitigating therapy-related toxicities, there is a paradoxical under-appreciation of inherent cancer-related toxicities. The precise mechanisms by which peripheral tumors communicate to the CNS to cause cognitive and behavioral change remain elusive, but almost certainly consist of a complex interplay between the immune system, genetic factors, host behavior, and psychosocial state.

Overall, an estimated 30% of cancer patients have detectable cognitive impairment prior to treatment, up to 75% of patients experience cognitive impairment during

treatment, and 35% of patients experience cognitive impairment several years after the completion of treatment (397-402). Defining and measuring cancer-related cognitive impairment (CRCI) is a challenge, as there are multiple neuropsychological measures to assess cognitive function. Testing cognition within the clinic is complicated and measures multiple domains, including executive function, visual memory, psychomotor speed, attention, and concentration, to name a few. There is currently no “gold standard” for measuring cognitive function in cancer patients or survivors, and there is no general consensus on the methodology for the testing of cognitive decline (404). The clinical presentation of CRCI varies between cancer types and is affected by several factors of the tumor alone, including the stage during diagnosis. As we review the recent clinical data of CRCI, it is worth noting that the clinical tests of cognitive dysfunction in cancer are not currently validated for this patient cohort. Furthermore, the definition of “cognitive impairment” encompasses several aspects of cognitive function and is not universal across studies. In addition to cognitive impairment, patients may also experience cancer-related fatigue prior to treatment (405, 406). Although out of the scope of this review, it is worth noting that cancer-related fatigue—defined as a persistent sense of tiredness related to cancer or cancer treatment that interferes with usual functioning—is biologically distinct from cognitive dysfunction (407, 408). While the neurocognitive decline may occur in the context of cancer-related fatigue, CRCI frequently occurs in isolation or precedes fatigue (409-411). Additionally, the clinical course of fatigue is a notable experience that impairs both mind and body, while CRCI is often insidious in nature, and patients may not universally recognize their cognitive decline during clinical presentation (412, 413). Furthermore, defining cognitive decline

requires knowledge of patients' baseline cognitive function. Rodent models confirmed the temporal distinction between cognitive impairment, fatigue, and other sickness behaviors. Memory impairment, as measured by novel object recognition, significantly precedes fatigue and other classical sickness behaviors (414). Indeed, repeated intraperitoneal injection of breast cancer cell-conditioned medium is sufficient to induce cognitive decline, but not other sickness behaviors (414), providing direct evidence of the ability of soluble tumor factors to cause cognitive impairment.

In patients, fatigue is associated with poor clinical outcomes and is taken into consideration when creating treatment plans (415, 416). However, less was known about the prognostic utility of CRCI until recently. Cognitive impairment (deficits in working memory) prior to cancer treatment is an important predictor of survival in hematologic cancers (417) and pancreatic cancer (418). Furthermore, CRCI is not limited to older patients, as it is also observed in younger patients with Hodgkin lymphoma (419). Taken together, recent clinical studies demonstrate that cognitive impairment is an underappreciated symptom of cancer that affects both quality of life as well as survival. Furthermore, these studies emphasize the need for robust clinical testing of cognitive impairment in patients recently diagnosed with cancer, as CRCI is a risk factor that should guide clinicians in creating individualized treatment plans.

As the population continues to age, the prevalence of cognitive impairment in cancer patients will continue to escalate, creating a serious need for targeted approaches for patients with CRCI. A recent article by Horowitz et al. highlights the importance of future studies to investigate CRCI in a basic science context, efforts that are requisite for developing rational therapeutic targets (420). As patients experience

varying degrees of CRCI throughout their disease course, assessing the differential impact of the tumor and treatment on cognition remains challenging. A better pathophysiological understanding of CRCI will aid in the development of effective treatment strategies while providing a broader framework for mechanisms by which peripheral cancers communicate to the brain to modulate behavior. Consequently, animal models are necessary to uncouple tumor versus treatment effects on the CNS. This review summarizes recent clinical studies concerning CRCI and highlights advances in our understanding of the biological mechanisms by which peripheral tumors modulate the CNS.

2. Epidemiology of Pre-Treatment CRCI and Recent Clinical Studies

Cognitive impairment during cancer is most studied in the context of therapy-related cognitive impairment. However, pre-treatment CRCI was recently demonstrated in several cancer types, including acute myelogenous leukemia or myelodysplastic syndrome (407), breast cancer (401, 421, 422), colorectal cancer (423), and testicular cancer (424) (Table 1). Longitudinal studies observed between 11 (425) and 33% of breast cancer patients experienced cognitive impairment prior to chemotherapy (401, 402, 426). More recently, a nationwide, prospective, observational study identified that patients with stage I-IIIC breast cancer experience significant cognitive impairment prior to treatment, particularly in the domains of memory, attention, and executive function (427).

Table 1. Human studies reporting a significant cognitive decline in cancer patients prior to treatment.

Study	Cancer Type	Tested Cognitive Domains	Neuropsychological Assessments	% With Pre-Treatment Cognitive Impairment[1]
Meyers et al. 2005	Acute Myelogenous Leukemia, Myelodysplastic Syndrome	Attention, motor function, memory, executive function, verbal fluency, visual-motor scanning speed, fine motor dexterity	Digit Span, Digit Symbol, HVLT, Controlled Oral Word Association, TMTA+B, Grooved Pegboard	>40%
Jansen et al. 2011	Breast	Attention, motor function, memory, executive function, visuospatial skill, language	RBANS, Stroop Test, Grooved Pegboard, AFI, CES-D Scale, STAI-S, LFS	23%
Vardy et al. 2015	Colorectal	Attention, memory, working memory capacity, task switching	Digit Span, Letter-Number, Spatial Span, Digit Symbol, TMTA+B, HVLT, Brief Visuospatial Memory Test	43%
Wefel et al. 2011	Nonseminamatous Testicular	Attention, motor function, memory, executive function, psychomotor speed, language	Digit Span, Digit Symbol, TMTA+B, MAE Controlled Oral Word Association, HVLT, Grooved Pegboard	46%
Baekelandt et al. 2016	Pancreatic	Self-reported assessment of cognitive function[2]	EORTC QLQ-C30 Questionnaire	32%
Hsheih et al. 2018	Hematologic Cancers	Memory, executive function	Clock-in-the-Box (CIB), Five-Word Delayed Recall	>35%

[1] Cognitive impairment as defined by significantly lower function in any one cognitive domain

[2] The raw scores from EORTC QLQ-30 on the two questions that together constitute the cognitive function scale were transformed to a score range from 0 to 100%. Low cognitive function was defined as a score <66.67%

Abbreviations: HVLT, Hopkins Verbal Learning Test; TMTA+B, Trail Making Test Part A + B; RBANS, Repeatable Battery of Adult Neuropsychological Status; AFI, Attentional Function Index; CES-D, Center for Epidemiological Studies-Depression; STAI-S, Spielberger State Anxiety Inventory; LFS, Lee Fatigue Scale; MAE, Multilingual Aphasia Examination; EORTC QLQ, European Organisation for Research and Treatment of Cancer Quality of life Questionnaire

In the past 25 years, several studies explored neuroimaging approaches in assessing cognitive impairment during cancer (428). A recent magnetic resonance imaging (MRI) study in patients with various non-CNS cancers noted significant differences in cortical surface area or cortical thickness in multiple brain regions between non-treated cancer patients and controls (429). Specifically, decreases in cortical surface area or thickness were observed in untreated cancer patients in the temporal and frontal lobes, including the parahippocampal region, an area important in memory encoding and retrieval. Scherling and colleagues also observed smaller white matter volumes in breast cancer patients compared to healthy controls in several regions of the parietal, frontal, and limbic regions (430). These two studies provide compelling data describing baseline neuroanatomic differences, independent of treatment, between cancer patients and healthy controls. However, contrary results were reported in breast cancer brain MRI studies, revealing only a chemotherapy-related reduction in a gray

matter (431, 432). It is worth noting that the atrophy observed in these studies was not directly associated with cognitive impairment. Importantly, these studies are not without limitations, as the sample size was limited and baseline performance status varied considerably amongst groups.

The notion that pre-treatment cancer patients experience neurocognitive decline more readily than age-matched controls is gaining attention. Furthermore, recent clinical studies demonstrate that cognitive decline prior to cancer treatment is a significant independent predictor of survival (417, 418). Taken together, the clinical studies to date suggest that peripheral tumors and blood cancers affect several domains of cognitive function and modulate white matter neuroanatomy. However, the mechanisms by which cancer interfaces with the brain to enact cognitive and structural change remain unclear. Here, we explore the putative mechanisms by which peripheral cancers interact with the brain to affect cognitive function.

3. Theory of Soluble Tumor Factors' Ability to Communicate with the CNS

3.1 Inflammatory Cytokines

Perhaps the most established and studied facet of cancer and behavior is the inflammatory capacity of the tumor microenvironment. Tumors contain a complex network of tissue stroma, infiltrating immune cells, and neoplastic cells, all capable of generating cytokines (27-31). Several peripheral cancers are associated with increased circulating inflammatory cytokines, indicating this phenomenology is not specific to any

one cancer (433-441). Furthermore, unique serum cytokine profiles were identified during neurocognitive decline in cancer: in patients with acute myelogenous leukemia or myelodysplastic syndrome, increased interleukin (IL)-6 was associated with poor executive function, while concurrent increases in serum IL-6, IL-1 receptor, and tumor necrosis factor (TNF)-alpha were associated with fatigue (407). Interestingly, IL-8 levels positively correlated with memory function, suggesting that not all pro-inflammatory cytokines are deleterious to the CNS during cancer. Indeed, one study of breast cancer patients demonstrated that IL-17 and Granulocyte-colony stimulating factor (G-CSF) were positively correlated with psychomotor speed prior to treatment (442). While several clinical studies have demonstrated that peripherally-derived cytokines correlate with cognitive decline (443-446), the precise biological mechanisms of cytokine-mediated communication with the CNS to affect cognition are still being unveiled.

Inflammatory cytokines produced within the tumor environment enter the circulation and interface with the brain by directly crossing the blood-brain barrier (BBB) (32) or through direct blood-borne sampling by circumventricular organs (CVOs) (305, 447, 448). After crossing the BBB or highly-permeable capillaries of the CVOs, these inflammatory cytokines activate glial cells (40, 449) or directly influence neuronal circuits important in homeostatic functions and cognition (450-452). However, even before entering the brain parenchyma, inflammatory cytokines within the choroid plexus and meningeal vessels are capable of activating quiescent perivascular macrophages (453) and dendritic cells (454). Activation of these antigen-presenting cells promotes further inflammatory response by recruiting cytokine-producing adaptive immune cells (455).

For instance, CNS-infiltrating T effector cells are especially prevalent in multiple sclerosis and secrete interferon (IFN)-gamma and IL-17A (456), cytokines that induce glial cell activation and apoptosis of myelin-producing oligodendrocytes (457). Xiaoyu and colleagues recently demonstrated that brain-endothelial expression of the interleukin-1 receptor (IL-1R) enhances leukocyte recruitment, mediates sickness behavior, and impairs neurogenesis (40). Indeed, brain endothelial cells respond to IL-1B in a myeloid differentiation primary response protein MyD88-dependent manner, which amplifies and propagates inflammatory signals to glial cells (41). These studies demonstrate that the BBB serves to sense, interpret, and amplify peripheral cues to the CNS (41), potentially through further production of inflammatory cytokines at the BBB. During the progression of cancer, the cytokine array produced by both distant intratumoral cells and CNS-invading immune cells presents a unique challenge to the brain. The constant production of cytokines activates meningeal and choroid plexus immune cells**,** promotes inflammatory glial polarization, and ultimately inflicts pathological structural and biochemical changes in neuron populations central to cognitive function. Indeed, neuroinflammation caused by circulating cytokines during cancer progression parallels the emerging story of inflammation in primary neurodegenerative diseases (458)**.**

Peripheral cytokines also mediate behavioral responses by influencing the vagus nerve. Vagal afferent fibers richly innervate peripheral organs and relay inflammatory, satiety, and metabolic cues to the brain. In the brainstem, these afferent fibers terminate in the nucleus tractus solitarius (NTS), which then sends fibers projecting to regions important in behavior and cognition. These regions include the locus coeruleus, hypothalamus, thalamus, and amygdala (459). Electrophysiological recordings of the

vagus nerve following peripheral IL-1B or TNF-alpha administration demonstrate that these pro-inflammatory cytokines robustly induce nerve activation (460). Although no direct evidence exists connecting vagal nuclei to hippocampal structures, damage to the subdiaphragmatic vagus in rats results in microgliosis and impaired neurogenesis in the dentate gyrus (461). While there is a large body of literature suggesting that direct vagal nerve stimulation (VNS) may improve cognitive function in rodent models of CNS disease (462, 463), stimulation of the vagus nerve in these models is intermittent and independent of a systemic inflammatory milieu. It is conceivable that continuous vagal stimulation via the inflammatory tumor microenvironment is an exhaustive process on CNS circuits, while irregular stimulation through VNS treatment “jump starts” neurons during depression and neurodegenerative diseases.

Murine studies involving the injection of single cytokines into the periphery demonstrate the significance of peripheral inflammation on cognitive processes. Here, we review the literature of cytokines that are dysregulated during cancer and mechanisms by which these individual molecules alter cognition.

3.1.1 IL-1β

IL-1β remains one of the most studied cytokines during inflammatory diseases, yet direct connections between IL-1β and cognition lack, particularly in a behavioral neuroscience context. Intraperitoneal administration of IL-1β alone leads to cerebral release and catabolism of serotonin, norepinephrine (464), dopamine (465), and tryptophan (466)—vital neurotransmitters and molecules in cognitive processes. Indeed, brief exposure of cornu ammonis (CA1) pyramidal neurons to sub-femtomolar

concentrations of IL-1β causes profound decreases in excitatory glutamatergic transmission, yet leaves inhibitory gamma-aminobutyric acid (GABA)ergic signaling unabated (467). Furthermore, IL-1β and TNF-alpha can directly inhibit the ability of astrocytes to convert excess glutamate to glutamine, a process critical in the prevention of neuron excitotoxicity (468).

3.1.2 IL-2

IL-2 is implicated in hippocampal neurodegeneration, as repeated peripheral injections in rats suppress long-term potentiation (469). Mechanistically, IL-2 inhibits the hippocampal release of acetylcholine (470), a neurotransmitter important in attention, recall, and memory formation (471). Axonal degeneration, demyelination, and alterations in the cerebrovascular structure are observed as early as 6 hours after peripheral IL-2 administration in rats (472). These neuron structural changes persist and compound after repeated injections. IL-2 is a Food and Drug Administration (FDA)-approved treatment for metastatic melanoma and renal cell carcinoma, and it is associated with psychiatric manifestations and cognitive decline. Denicoff et al. demonstrated that 22 of 44 patients receiving IL-2 therapy became disoriented over the course of treatment and demonstrated cognitive deterioration (473). Cognitive decline and other neuropsychiatric symptoms were dose- and time-dependent, as patients treated with higher doses presented with symptoms earlier, while nearly all patients exhibited neurologic symptoms at the end of the study. During the progression of CRCI, the secretion of IL-2 by intratumoral dendritic cells, CD4+ T cells, and CD8+ T cells aids in the immunologic response against the tumor. However, the rapid and sustained

release of tumoral IL-2 results in spillage of the cytokine into circulation and migration to the CNS, potentially resulting in cognitive deficits.

3.1.3 IL-6

IL-6 is recognized as a versatile cytokine in various CNS processes, proving to be beneficial for normal CNS physiology, yet deleterious during several neurological diseases (474). Despite being classified as a pro-inflammatory cytokine, nearly 30 years ago evidence emerged demonstrating that IL-6 is a neurotrophic factor (475). Indeed, several studies implicate IL-6 in neuronal differentiation (476-478). However, IL-6 contributes to chronic neuropathologies by enhancing N-methyl-D-aspartic acid (NMDA) receptor neurotoxicity (479). IL-6 is also capable of indirectly modulating neuronal activity by differentially activating microglia; IL-6-stimulated microglia co-cultured with neurons drastically reduce neuronal survival (480). This translates behaviorally, as overexpression of IL-6 within astrocytes results in impaired avoidance learning behavior in mice (481). Conversely, mice deficient in IL-6 display sensory dysfunction and impaired axonal regenerative capacity (482). While the literature is full of conflicting evidence for the role of IL-6 in normal neuronal function and pathologies, it is clear that a delicate balance of IL-6 exists during basal physiology, while states of inflammation result in IL-6 aberrations that subdue the CNS and cause cognitive decline.

3.1.4 TNF-alpha

Peripheral TNF-alpha is robustly induced during several peripheral inflammatory diseases, including cancer (483-486), and the significance of TNF-alpha signaling in the brain on cognitive function has gained attention in recent years. Terrando and colleagues demonstrated that TNF-alpha is an upstream target of IL-1B production in the brain, synergizes with MyD88 signaling, and sustains cognitive decline after surgical intervention in mice (487). When TNF-alpha crosses the BBB, it can activate the astrocytic TNF-alpha receptor 1 (TNFR1), resulting in hippocampal synaptic alterations and subsequent memory impairment (488).

3.1.5 Interferon

The interferons (IFN) provide a compelling human example in which single cytokines in the periphery can cause cognitive dysfunction. IFN-alpha, beta, and gamma are all FDA approved drugs used to treat cancer, hepatitis, multiple sclerosis, and chronic granulomatous disease. Patients treated with IFN-alpha, beta, or gamma routinely exhibit depression, disordered sleep, malaise, and impaired memory (489). The molecular cascade in which IFN-B regulates behavior and cognitive impairment was recently unveiled by Blank and colleagues: circulating IFN-B binds to luminal brain endothelial IFN receptor chain 1 and mediates the release of C-X-C motif ligand 10 (CXCL10) into the brain parenchyma, which, in turn, causes neuronal dysfunction (490). Furthermore, there is a strong correlation between prefrontal cortex (PFC) levels of CXCL10 and cognitive decline in humans (491). The PFC is uniquely positioned to orchestrate several facets of cognition through its extensive neural network (492), and its activation is significantly reduced in breast cancer survivors irrespective of treatment

(493). During cancer, it is possible that the peripheral up-regulation of IFN-B induces CXCL10 expression in cerebral vessels of the PFC in a chronic fashion, ultimately leading to dysfunction of PFC circuits critical in cognitive processes.

Recent studies have greatly improved our understanding of the tumor-brain axis in the context of inflammation and cytokine release. While it is clear that cytokines play a central role in the normal development of the CNS (494, 495), it is also apparent that the marked and sustained production of cytokines during the progression of cancer exerts negative consequences on the brain, including cognitive decline.

3.2 Brain-Infiltrating Immune Cells

Although the CNS was classically described as an immune-privileged organ, it is now accepted that peripheral immune cells infiltrate the brain during pathologic states. The early work characterizing brain-infiltrating immune cells was in the context of infectious disease, and a specific requirement for CNS immune cells during infection exists for controlling pathogen proliferation (496). Although these brain immune cells limit pathogen proliferation, the CNS immunologic response is not universally beneficial when prolonged or exaggerated. Specifically, activated immune cells in the CNS cause inflammation and swelling of CNS structures and meninges. The collateral cerebral damage alters neuronal circuits to cause changes in behavior and cognition. While the role of infiltrating immune cells during CNS infections is well characterized, only recently their role has been explored in non-infectious diseases.

Over the past 15 years, various studies demonstrated that neuroinflammation secondary to non-infectious pathology leads to robust infiltration of peripheral immune

cells into the brain. Conditions in which this phenomenon was observed include epilepsy (497), Alzheimer's disease (498), Parkinson disease (499), multiple sclerosis (MS) (500, 501), stroke (502, 503), and pancreatic cancer (504). However, the biological impact of these invading leukocytes during non-infectious disease has been unrecognized until recently. Several studies demonstrate mitigated brain inflammation, reduced disease progression, and improved functional outcomes by blocking leukocyte infiltration into the brain (498, 505, 506). One such study demonstrated that preventing the entry of myeloid cells via chemokine receptor type 2 (CCR2) blockade was protective in a status-epilepticus murine model (505). These studies demonstrated the close correlation between CNS disease progression and immune cell infiltrate. The identity of infiltrating immune cells in the CNS is heterogeneous and context-dependent, with varying immune cells populations within distinct regions of the CNS (507). Nonetheless, it is clear that infiltrating immune cells are independently capable of driving neuroinflammation and could alter cognitive function when trafficked to specific areas of the CNS.

Until recently, little was known about how peripheral immune cells potentiate cognitive decline and sickness behaviors during systemic inflammation. During advanced liver disease, microglia recruitment of monocytes through TNF-alpha signaling correlates with sickness behaviors and generalized neuronal excitability (508). Burfeind and colleagues recently described a unique population of neutrophils that invade the brain in a murine pancreatic cancer cachexia model (504). The authors identified a distinct population of neutrophils that specifically infiltrate the velum interpositum (VI), an area immediately adjacent to the hippocampus and habenula.

When inflamed, the VI is uniquely positioned to drive cognitive decline and sickness behavior by virtue of its proximity to structures critical in memory and appetite regulation. Furthermore, the recruitment of this inflammatory population of neutrophils relies heavily on the CCR2-CCL2 axis, as genetic ablation of CCR2 reduces CNS neutrophil infiltration and ameliorates symptoms of cachexia. These findings present a novel mechanism by which peripheral tumors subjugate the brain and cause cognitive decline.

3.3 Tumor-Derived Extracellular Vesicles

Extracellular vesicles (EVs) are cell-derived membranous structures and include apoptotic bodies, microvesicles, and exosomes. Initially described as carriers of cellular waste (509), we now recognize EVs' signaling potential through their exchange of lipids, nucleic acids, and protein products between cells (510). Our knowledge of the molecular biology of EVs has expanded over recent years, shedding light on signaling functions of these extracellular molecules during both normal physiology and pathology. Recent studies demonstrate that tumor cells secrete EVs carrying oncogenic signaling molecules that are responsible, in part, for the pathogenesis and growth of cancer (511-514). In the CNS, EVs shuttle cellular products important in synaptic plasticity, neurovascular permeability, and glial cell morphology (515). Furthermore, it is now accepted that peripherally-derived EVs can readily cross the BBB both via endothelial transcytosis and through CVOs (516, 517). With the recent advances in EV biology, a thorough examination of mechanisms by which peripherally-derived EVs signal to the CNS may provide therapeutic insight for CRCI.

During cancer and other states of peripheral inflammation, a heterogeneous population of EVs containing inflammatory mediators are released into the circulation. One group of signaling molecules within EVs that have garnered attention in recent years is the inflammation-related microRNAs (miRs). EVs containing inflammatory miRs are significantly elevated in the serum of mice 1 hour after intraperitoneal injection of low dose lipopolysaccharide (LPS) (518). When inflammatory EVs that are isolated from the serum of LPS-injected mice are reintroduced peripherally to a healthy animal, a distinct inflammatory response ensues within the brain. Specifically, hippocampal and neocortex microgliosis and astrocytosis are observed with concurrent increases in brain TNF-alpha and IL-6 (519). These inflammatory changes within the brain correlate with EV levels of miR-155 and miR-146a within the cerebrospinal fluid (CSF) (519, 520). These studies demonstrate that peripheral EVs can cross the BBB and induce inflammatory responses in CNS structures important for cognition.

In a mouse model of peripheral inflammation induced by pancreatic ductal adenocarcinoma (PDAC), EVs containing miR-30 are up-regulated and abrogate tumor-suppressing mechanisms (521). Interestingly, cerebral miR-30 directly impairs synaptic transmission and plasticity of hippocampal neurons (522). The release of tumor-derived miR-30 into the circulation and subsequent localization to the CNS could provide an uninterrupted mechanism of tumor-induced cognitive impairment. During carcinogenesis, tumors that are more densely innervated are more aggressive and lead to increased mortality (523), and denervation of tumors in mouse models of PDAC slows the progression of the disease (524). Consequently, it has been hypothesized that tumors signal to the peripheral nervous system to directly promote their innervation, a term

called axonogenesis. The molecular mediators that control axonogenesis have remained poorly defined until recently. Indeed, tumor-derived exosomes containing EphrinB1 drive nervous system innervation of head and neck squamous cell tumors (525). This study exemplifies how tumor-derived EVs exert systemic control of nervous tissue to dictate remodeling and signaling. Although not explored in the CNS, EV-driven axonogenesis and neuronal remodeling may prove to be important mechanisms for altering cognition during cancer progression. As our understanding of the basic biology of EVs continues to improve with the development of new technologies, identifying molecular targets of “inflammatory” EVs may provide therapeutic targets for cancer and its associated CNS sequelae.

3.4 Blood-Brain Barrier Integrity

The observation that water-soluble dyes injected systemically stain all organs except CNS structures provided the first piece of evidence that the brain is compartmentally distinct from the periphery (526). These pioneering studies by Paul Ehrlich and his students demonstrated that a BBB exists during normal physiologic states. We now recognize the BBB as a critical gatekeeper preventing the unrestricted movement of micro and macromolecules to and from the CNS. Disruption of this barrier is generally accompanied by changes in CNS physiology. The BBB cellular components include endothelial cells, pericytes, and astrocytic end-feet, while an acellular basement membrane further divorces the luminal surface from the brain parenchyma. Disruption of any one component of the BBB exposes neurons to higher concentrations of circulatory molecules, which would otherwise remain tightly regulated under normal

conditions. CNS exposure to higher circulating solute concentrations results in abnormal neuronal signaling and compromises synapse integrity, processes that may result in cognitive decline. Specifying whether BBB dysfunction results from or precedes neuroinflammatory insult is a difficult task. Consequently, little is known about how the BBB is affected by peripheral tumors. As reviewed below, recent murine models demonstrate that peripheral cytokine dysregulation, a common feature of non-CNS cancers, is sufficient to disrupt the BBB and induce cognitive decline.

BBB dysfunction is observed during several neurodegenerative and neurovascular conditions and is considered a driver of disease progression (527-529). BBB breakdown is also observed during systemic inflammation, including states of endotoxemia induced by LPS (530, 531) and polyinosinic-polycytidylic acid (532). Models of colitis (533) and pancreatitis (534) also revealed unique alterations in BBB integrity. In a rat model of pancreatic encephalopathy, a severe complication of acute pancreatitis which presents with confusion and cognitive impairment, serum TNF-alpha and IL-6 significantly correlate with BBB permeability (534). Indeed, TNF-alpha is partly responsible for the generation of reactive oxygen species, down-regulation of endothelial junction proteins, and induction of IL-6 in human brain microvascular endothelial cells (535, 536). Conversely, peripheral injection of the anti-inflammatory cytokine IL-10 lessens BBB attenuation during the progression of acute pancreatitis (537), demonstrating the necessity of chronic inflammatory cytokine production for attenuating the BBB. As discussed earlier, peripheral tumors produce inflammatory cytokines which enter the circulation and travel to the BBB. BBB disruption has been observed in response to TNF-alpha (538), IL-1B, IL-6 (539), and IFN-gamma (540), all cytokines are up-

regulated during the progression of cancer. Although the BBB remains poorly studied in the context of cancer independent of treatment, it is plausible that these inflammatory cytokines play a dual role in attenuating the BBB and directly influencing neuronal plasticity during cancer. As our understanding of the BBB in the context of peripheral inflammation continues to grow, the development of therapies that adjust BBB permeability may be a useful therapeutic approach for mitigating cancer symptoms that are augmented in the CNS.

4. Conclusions and Future Directions

The chronic and compounding nature of inflammatory mediators created by peripheral tumors creates a formidable challenge for the CNS. Our knowledge of the associated symptoms during acute and chronic disease has boomed in recent years, and we now understand that the symptomology of disease profoundly impacts the survival of the organism. Cognitive alterations and sickness behaviors observed in acute disease primarily serve a protective role (541). The principles of life history theory suggest that the shunting of energy from cognitive processes and general locomotion to the immune system aids in eliminating pathogens (2, 542). However, less is understood about cognitive decline and sickness behaviors during chronic non-infectious diseases, particularly cancer. Humans evolved to develop methods to survive bacterial and viral infections, rarely living long enough to develop tumors. We now understand that shunting of energy away from the brain and into survival functions is acutely beneficial, but detrimental during chronic diseases, such as cancer. This is exemplified during the pathogenesis of cancer cachexia, as the symptoms and metabolic aberrations exert

devastating effects on quality of life, ability to tolerate treatment, and ultimate survival of the patient. While the classical sickness behaviors associated with cancer, including fatigue, anorexia, and lethargy, are well recognized as deleterious symptoms, only recently the clinical evidence for the cognitive decline has emerged as a negative predictor of survival. As a result, several biological questions related to CRCI remain unexplored, as the field has remained largely studied in a clinical context. In this article, we have reviewed recent clinical evidence of peripheral tumors affecting cognition and the putative biochemical mechanisms by which peripheral tumors directly subjugate the brain (Figure 1, Table 2).

Several challenges remain in defining, identifying, and measuring cognition in the clinic. Standardized assessments of cognitive decline in the context of cancer are lacking. Furthermore, proper assessment of cognitive decline requires knowledge of baseline cognitive performance and multiple follow-up visits. Assessing the biological mechanisms of CRCI remains a challenging, yet valuable endeavor of future investigation. A serious need exists for the development of murine models of CRCI. Specifically, a curable murine tumor model that exhibits cognitive decline and other sickness behaviors will aid in identifying tumor factors that cause pre-treatment cognitive decline as well as enduring memory impairment after the cancer is cured.

As the clinical course of CRCI becomes more apparent, our understanding of the biological mechanisms of cancer-CNS communication becomes ever more important. Identifying CRCI in the clinic remains challenging, and no unifying standardized exam for diagnosing CRCI exists. Ideally, detecting CRCI would entail both clinical examination and an objective imaging approach. Further elucidation of the mechanisms

by which tumors cause cognitive decline will allow oncologists to tailor treatment regimens to mitigate CRCI, improve quality of life, and ultimately increase survival of future patients.

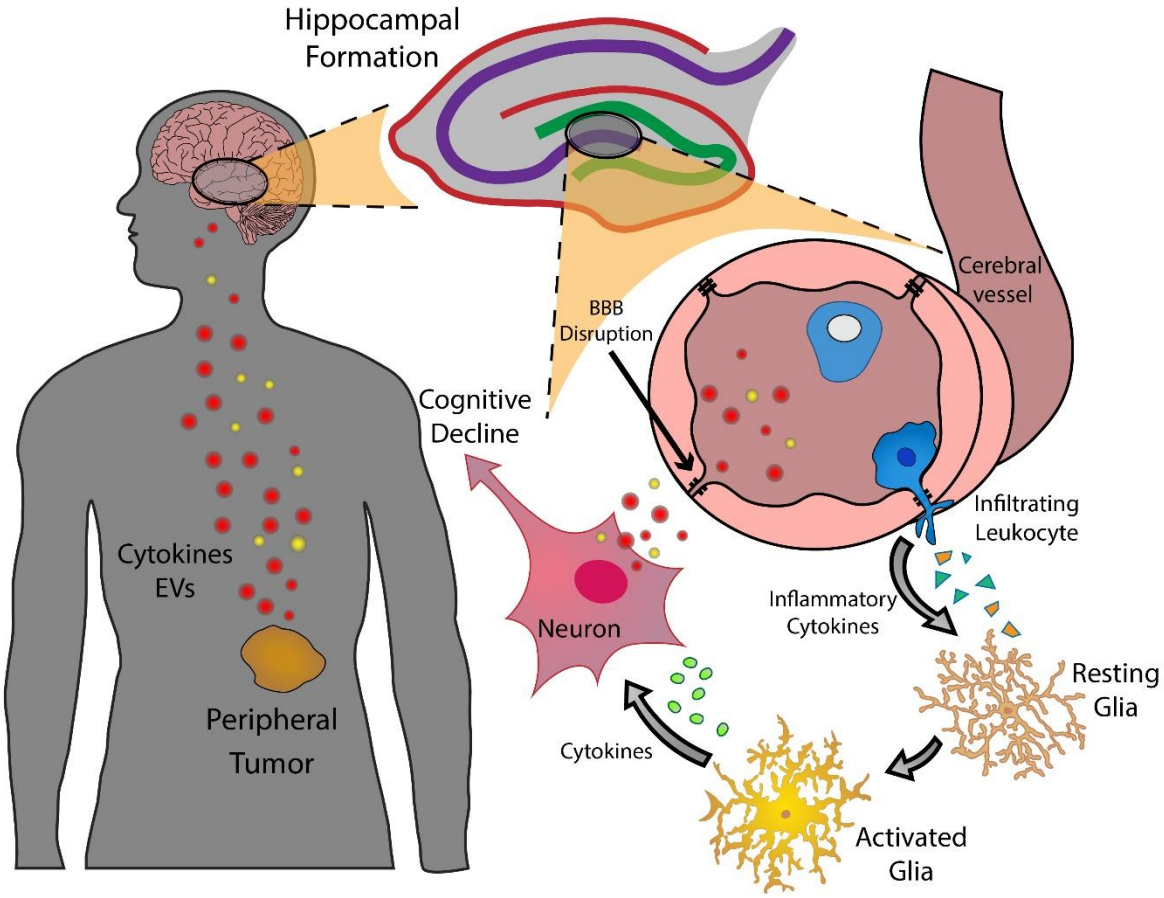

Figure 1. A model of putative mechanisms by which peripheral tumors interface with the CNS to initiate and sustain cognitive decline. EVs, extracellular vesicles; BBB, blood-brain barrier.

Table 2. Key mechanisms of the peripheral inflammation-CNS interface in cognitive decline.

Biological Target/Mechanism	Effect on CNS Function	References
Cytokines		
IL-1B	Modulation of neurotransmitter secretion, decrease in glutamatergic transmission	76–80
IL-2	Attenuation of Ach release, axonal degeneration, demyelination	81–83
IL-6	NMDA receptor neurotoxicity, microglial activation, impaired axonal regeneration	90,91,93
TNF-alpha	Promotes cerebral IL-1B production, MyD88 signaling, inflammatory astrocyte polarization	98,99
IFN-beta	Mediates cerebral endothelial release of CXCL10	101
Immune cells		
CD4+ T cells	Fas-Fas ligand-mediated dopaminergic toxicity	112
Neutrophils	NETosis, IL-17 secretion, cytotoxic granule spillage	111,117
Extracellular vesicles	Micro-RNA signaling, impairs synaptic transmission, axonogenesis	135,138
Blood-brain barrier disruption	Exposure of the brain to a higher concentration of peripheral solutes	143,146,147

Abbreviations: IL, interleukin; TNF, tumor necrosis factor; Ach, acetylcholine; NMDA, N-methyl-D-aspartate; MyD88, myeloid differentiation primary response protein 88; IFN, interferon; CXCL10, C-X-C motif ligand 10

Acknowledgments

We would like to thank Dr. Stephanie Krasnow and Ashley J. Olson for their critical reading of the manuscript.

Author Contributions: Conceptualization—B.O., D.L.M.; writing—original draft preparation, B.O., D.L.M.; writing—review and editing, B.O., D.L.M.; supervision, D.L.M.; funding acquisition, D.L.M.

Funding: This work is supported by NIH R01CA217989 and the Brenden-Colson Center for Pancreatic Care.

Conflicts of Interest: The authors declare no conflict of interest.

Chapter 3: Lipocalin 2 mediates appetite suppression during pancreatic cancer cachexia

A manuscript published in *Nature Communications*

Olson B, Zhu X, Norgard MA, et al. Lipocalin 2 mediates appetite suppression during pancreatic cancer cachexia. Nat Commun. 2021;12(1):2057.

Brennan Olson[1,2], Xinxia Zhu[1], Mason A Norgard[1], Peter Levasseur[1], John T Butler[1,2], Abigail Buenafe[1], Kevin G Burfeind[1,2], Katherine A Michaelis[1,2], Katherine R Pelz[4], Heike Mendez[4], Jared Edwards[1], Stephanie M Krasnow[1], Aaron J Grossberg[3,4,5], and *Daniel L Marks[1,4,6]

Lipocalin 2 mediates appetite suppression during pancreatic cancer cachexia

1. Papé Family Pediatric Research Institute, Oregon Health & Science University, Portland, OR USA
2. Medical Scientist Training Program, Oregon Health & Science University, Portland, OR USA
3. Department of Radiation Medicine, Oregon Health & Science University, Portland, OR USA
4. Brenden-Colson Center for Pancreatic Care, Oregon Health and & Science University Portland, OR USA
5. Cancer Early Detection Advanced Research Center, Knight Cancer Institute, Oregon Health & Science University, Portland, OR USA
6. Knight Cancer Institute, Oregon Health & Science University, Portland, OR USA

*Corresponding Author Information

Daniel L. Marks, MD, PhD

3181 SW Sam Jackson Park Road

L 481

Portland, OR 97239

Email: marksd@ohsu.edu

Abstract

Cancer cachexia is a disorder characterized by excessive tissue catabolism and wasting, ultimately leading to increased mortality. Cachexia imposes a significant caloric deficit through a synergistic decrease in food intake and increased basal metabolic rate, and reversal of cachexia is a promising strategy for improving cancer survival. Since decreased nutrition is an essential component of cachexia, identification of factors that influence the anorectic response of cachexia is a rational approach for improving patient outcomes. Recently, the pleotropic molecule Lipocalin 2 (Lcn2) was identified as a physiologic mediator of appetite. However, it remains unknown if this molecule influences energy balance during cancer-associated cachexia. Herein, we identify Lcn2 as a novel pathologic mediator of cachexia-anorexia through its recently identified actions on the melanocortin 4 receptor (MC4R) in the central nervous system. We demonstrate Lcn2 is robustly upregulated in numerous murine models of pancreatic cancer cachexia, and its expression is closely associated with reduced food consumption and both fat and lean mass loss. The preponderance of circulating Lcn2 during pancreatic cancer cachexia is derived from the bone marrow compartment, partially due to neutrophil expansion and their elevated expression of *lcn2*. We demonstrate that *lcn2*-knockout mice are robustly protected from cachexia-anorexia and have improved fat and lean mass. Pharmacologic inhibition of Lcn2-MC4R signaling through cerebral injection of agouti-related peptide (AgRP), an inverse agonist of MC4R, improves feeding behaviors during pancreatic cancer cachexia. Through adoptive transfer techniques, we demonstrate that restoration of *lcn2* expression in the bone marrow compartment is sufficient to restore the anorexia feature of pancreatic cancer

cachexia. Finally, we observe that circulating Lcn2 levels correlate with neutrophil expansion in patients with pancreatic cancer, is associated with both fat and lean mass wasting, and is associated with increased mortality. Together, we show that plasma Lcn2 levels are robustly elevated during pancreatic cancer in rodents and humans, Lcn2 readily crosses the blood brain barrier, and mediates appetite suppression and concomitant fat and lean mass wasting through a melanocortin-dependent mechanism.

Keywords: Cachexia, lipocalin 2, metabolism, appetite, anorexia, pancreatic cancer, sarcopenia, melanocortin 4 receptor, neutrophils, neutrophil to lymphocyte ratio, NLR

1. Introduction

Cachexia, or disease-associated wasting, is a metabolic state consisting of a paradoxical decrease in appetite, yet increase in basal metabolic rate (6, 8, 543). This mismatch in caloric intake and expenditure imposes a significant energy imbalance, leading to excessive wasting, reduced quality of life, and decreased patient tolerance to therapy (544, 545). Since decreased nutrition is an essential component of cancer cachexia (351, 546), improving cachexia-related anorexia remains an important aspect in treating this metabolic disorder. Indeed, nutritional interventions and pharmacologic improvement of appetite are emerging as promising treatment paradigms for patients with cachexia (547-549). Therefore, identification of the pathways that influence nutritional deficits associated with cachexia could provide new therapeutic options for this otherwise debilitating metabolic disorder.

To this end, significant efforts are being made to identify the mechanism of appetite dysregulation during cancer-associated cachexia. Lipocalin 2 (Lcn2), also known as neutrophil gelatinase-associated lipocalin, siderocalin, or 24p3, is a pleiotropic mediator of several inflammatory and metabolic processes that is secreted into circulation during a variety of diseases associated with cachexia (84), including cancer (550), chronic kidney disease (551), and heart failure (552). Recently published data demonstrate Lcn2 suppresses appetite through its binding to the melanocortin 4 receptor (MC4R) in the paraventricular nucleus (PVN) of the hypothalamus (82), a nucleus essential in regulating feeding behaviors and energy homeostasis (553). These studies demonstrate a role for Lcn2 in regulating appetite during non-pathologic states. However, whether the dysregulation of Lcn2 produces meaningful changes in energy balance during cancer-associated cachexia is not known.

Here, we explore the relationship between Lcn2 production, feeding behaviors, and tissue catabolism during pancreatic cancer cachexia. In five separate rodent models of pancreatic cancer cachexia, we demonstrate a large induction of circulating and central Lcn2 levels that negatively correlate with food intake and muscle mass. Since the literature supports the notion that *lcn2* tissue expression is disease dependent (84), we identify the bone marrow and myeloid compartment, namely neutrophils, as the predominant source of Lcn2 during pancreatic cancer cachexia. We show that the genetic deletion of *lcn2* mitigates cachexia-anorexia and lean and fat mass loss, while restoration of Lcn2 in the bone marrow compartment alone reestablishes the anorexia and muscle catabolism features of cachexia. Importantly, we detect Lcn2 in the brain after restoring expression in the bone marrow compartment, demonstrating Lcn2 readily crosses the blood brain barrier (BBB). Although inflammation is sufficient to induce anorexia, the increased food intake during Lcn2 blockade is independent of systemic inflammatory state and immunologic activation. Through pair-feeding studies, we show that the muscle-sparing effects of Lcn2 blockade are attributable to increased food intake alone, not differential regulation of ubiquitin- and autophagy-related catabolic pathways. Analogous to our murine models, we present human data showing associations between rising Lcn2 levels and neutrophil expansion, fat and lean mass wasting, and mortality during pancreatic cancer. Taken together, we present a novel immunometabolic mechanism of appetite regulation during cachexia in which Lcn2 is derived from the bone marrow compartment, crosses the blood brain barrier, and binds to the MC4R in mediobasal hypothalamic neurons to mediate long-term anorexia and subsequent loss of lean and fat mass.

2. Results

Lcn2 *is upregulated in the circulation and CNS in multiple murine models of pancreatic cancer cachexia and correlates with anorexia and muscle loss*

Using five separate murine models of pancreatic ductal adenocarcinoma-associated cachexia, we measured daily food intake, skeletal and cardiac muscle mass, and circulating and central Lcn2 levels. These models follow distinct daily food intake trajectories, total food consumption, and terminal skeletal and cardiac muscle masses over the course of disease (Figures 1A-D). Similarly, the transcriptional regulation of catabolic and inflammatory genes associated with cachexia varied considerably amongst these five models of pancreatic cancer cachexia. Consistent with previous reports of pancreatic cancer cachexia, skeletal muscle catabolism was associated with elevated expression of E3 ubiquitin ligase-related genes, including *Mafbx, Murf1, and Foxo1,* while cardiac atrophy was associated with increased autophagy-related genes, including *Bnip3, Ctsl,* and *Gabarapl* (Figures 1E-F) (38). Other features of cachexia, including hypothalamic inflammation and induction of acute-phase proteins by the liver, varied amongst these five models of pancreatic cancer cachexia. We observed significantly higher hypothalamic *Il1b* mRNA in two models (KPC and FC1245), while *Il1r1* was elevated in all models but FC1242 (Figure 1G). The liver contributes to the overall systemic inflammatory phenotype during cachexia through production of acute-

phase proteins and pro-inflammatory signals; acute-phase proteins *Apcs* and *Orm1* were transcriptionally elevated in all models, while variable increases in *Il1b, Il6, and Selp* mRNA were observed amongst models. Despite the varying degrees of cachexia symptoms (anorexia and muscle catabolism), as well as inflammatory and catabolic gene signatures, we observed increased Lcn2 protein in the circulation and cerebrospinal fluid (CSF) in all models of pancreatic cancer cachexia (Figures 1I-J). Furthermore, we observed a negative correlation between both peripheral and central Lcn2 levels and food intake, as well as skeletal muscle mass, when comparing all models (Figure 1K-N; Figure S1).

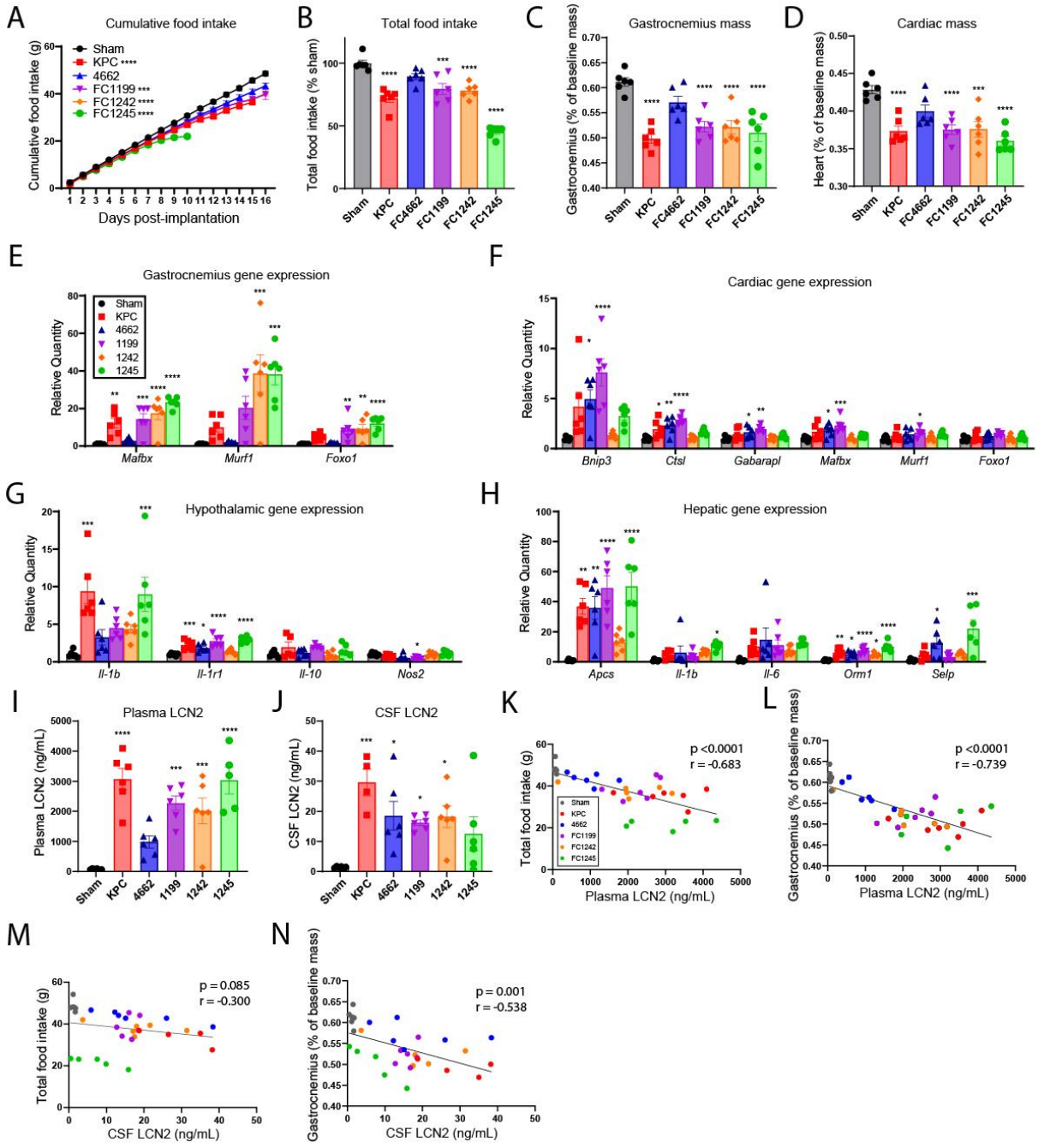

Figure 1. Lcn2 is upregulated across several models of pancreatic cancer cachexia and correlates with food consumption and muscle loss. (A) Cumulative food intake in five models of pancreatic cancer cachexia and sham operation controls. (B) Total food intake normalized to sham control group. (C) Skeletal muscle catabolism as indicated by terminal gastrocnemius mass normalized to body mass. (D) Cardiac muscle

catabolism as indicated by terminal heart mass normalized to body mass. (E) Gastrocnemius, (F) heart, (G) hypothalamus, and (H) liver gene expression profiles in pancreatic cancer cachexia models (represented as relative quantity to sham control). Terminal (I) plasma and (J) CSF Lcn2 levels. Linear regression analysis between plasma Lcn2 levels and (K) total food intake or (L) gastrocnemius mass. Linear regression analysis between CSF Lcn2 levels and (M) total food intake or (N) gastrocnemius mass. A-I, K-L; N = 6 per group. J, M-N; N = N = 6 per group except KPC (N = 4 per group). All data are expressed as mean ± SEM. Data represented in B-J were analyzed with one-way ANOVA with Bonferroni multiple comparisons comparing tumor experimental groups to sham operation control. K-N were analyzed by simple linear regression and two-tailed correlation analyses. *$p \leq 0.05$, **$p \leq 0.01$, and ***$p \leq 0.001$, ****$p \leq 0.0001$. Sham operation controls = grey/black, KPC = red, 4662 = blue, FC1199 = purple, FC1242 = orange, FC1245 = green.

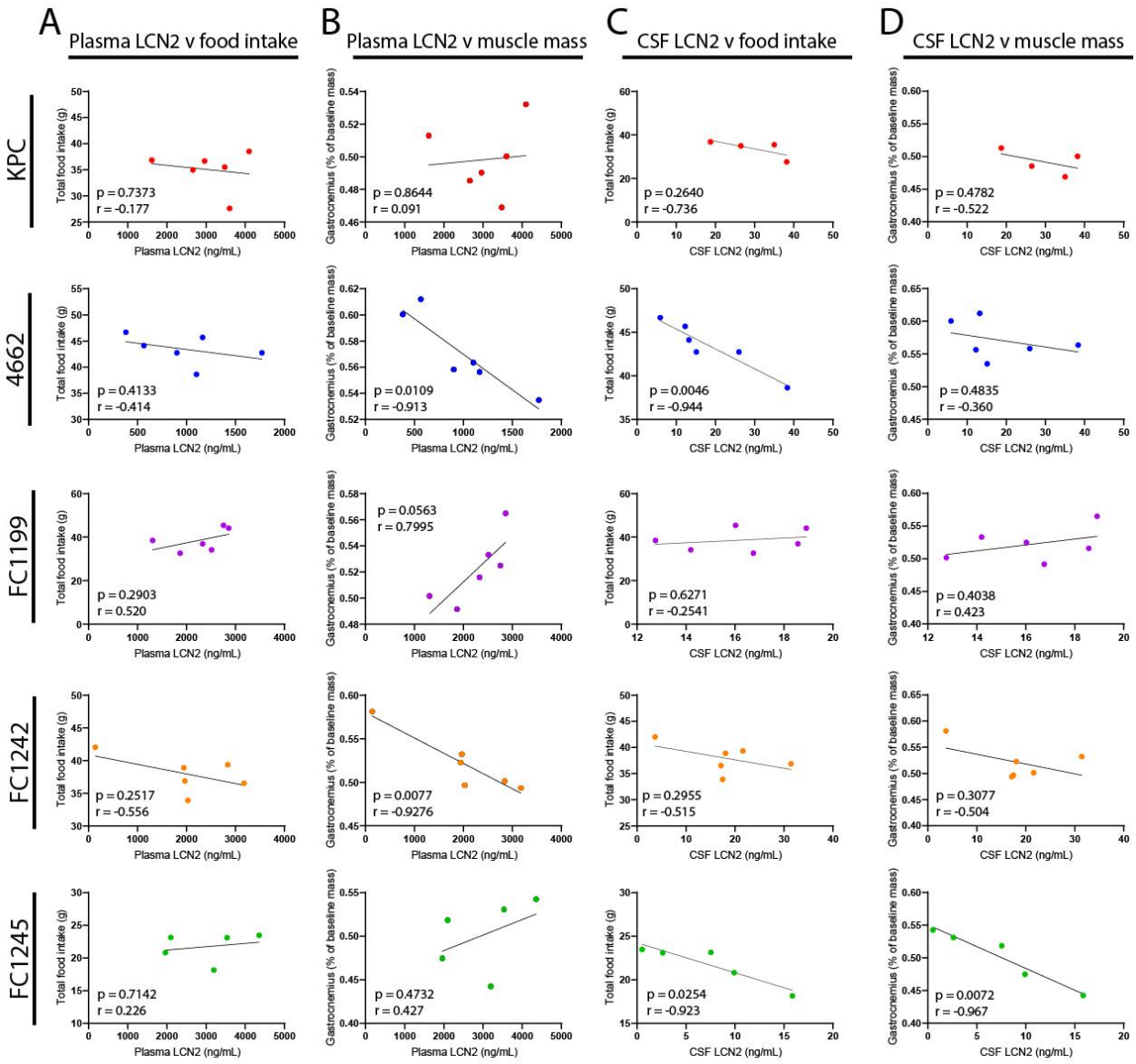

Supplementary Figure 1. Related to Figure 1K-N. Linear regression analysis between plasma Lcn2 levels and (A) total food intake or (B) gastrocnemius mass for each individual pancreatic cancer cell line analyzed in Figure 1K-L. Linear regression analysis between CSF Lcn2 levels and (C) total food intake or (D) gastrocnemius mass for each individual pancreatic cancer cell line analyzed in Figure 1M-N. Data were analyzed by simple linear regression and two-tailed correlation analyses. Sham operation controls =

grey/black, KPC = red, FC4662 = blue, FC1199 = purple, FC1242 = orange, FC1245 = green.

Lcn2 ***is predominantly produced in the bone marrow compartment and neutrophils during pancreatic cancer cachexia***

To determine the meaningful source of Lcn2 during pancreatic cancer cachexia, we analyzed Lcn2 levels across tissues utilizing the KPC model described in Figure 1. During both normal physiology and cachexia, we observed Lcn2 principally in the bone marrow compartment, with much smaller quantities observed in the spleen, lung, and liver (Figure 2A). We observed significantly higher Lcn2 protein levels in the lung, liver, and spleen during pancreatic cancer cachexia. However, we did not observe an increase in bone marrow Lcn2 during pancreatic cancer cachexia (Figure 2B; Figure S2A), potentially owing to a saturating level in both sham and cachexia conditions. Production of Lcn2 in the bone marrow compartment was confirmed by immunohistochemical staining (Figure 2C). Importantly, we validated the specificity of the Lcn2 antibodies used in our studies, as staining is absent in *lcn2-KO* mouse tissue, including the bone marrow (Figure S2A). The induction of Lcn2 has been attributed to several canonical inflammatory cytokines, including lFNγ (554), TNFα (554), IL-1β (153), and IL-6 (555) to name a few. To determine if Lcn2 is an inflammation induced mediator of cachexia, we examined circulating Lcn2 levels in both IL-6 and MyD88 knockout mice, as these two inflammatory signaling pathways are critical in the development of several features of cachexia (351, 556). Indeed, circulating levels of Lcn2 are significantly

reduced in both MyD88 and IL-6 knockout tumor-bearing mice (Figure S2B-C). Since the bone marrow appeared to be the largest producer of Lcn2 and is a major primary lymphoid organ responsible for immunologic response during disease, we hypothesized that circulating and tissue-resident immune cells were responsible, in part, for the observed increase in Lcn2. To address this question, we analyzed the composition of circulating immune cells during cachexia. We observed a large expansion of the myeloid cell population, with a relative and absolute decrease in the lymphocyte population (Figure 2D). This myeloid expansion in murine pancreatic cancer cachexia is composed principally of circulating neutrophils, with relative decreases in Ly6C+ high and low expressing monocytes (Figure 2E; Figure S2D-E). Consistent with previous reports (88), nearly all neutrophils stain positive for Lcn2 during both normal physiology and cachexia (Figure 2F). However, we detected a significant increase in *lcn2* transcripts in circulating neutrophils of cachectic mice by RNA sequencing (Figure 2G).

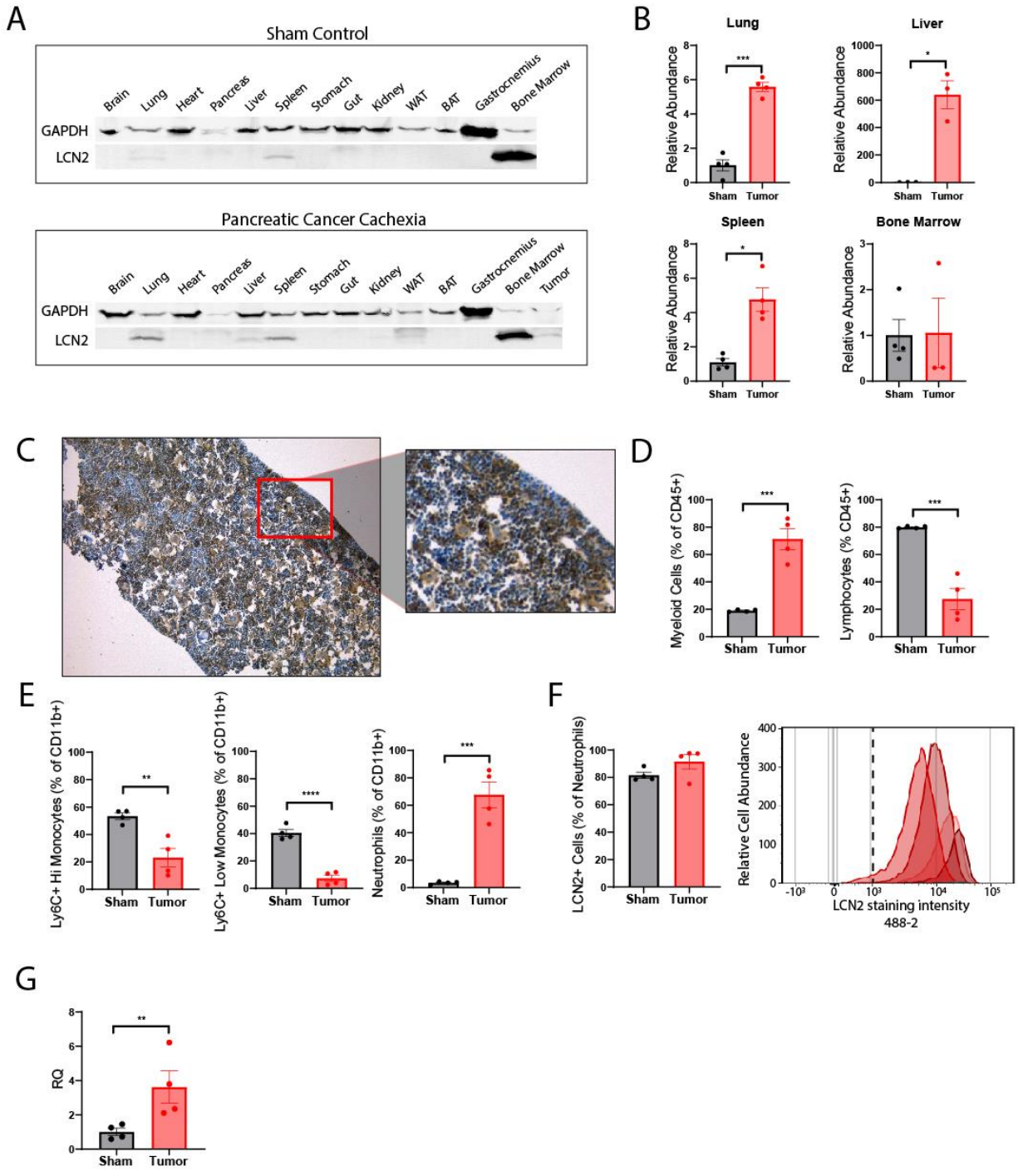

Figure 2. Lcn2 is predominantly produced by the bone marrow compartment and neutrophils during cachexia. (A) Representative tissue Western blot analysis of Lcn2 in sham operated or pancreatic cancer cachexia mice (orthotopic KPC pancreatic cancer

cell implantation). (B) Western blot quantification of Lcn2 in lung, liver, spleen, and bone marrow compartments (n = 4 per group, except in KPC-engrafted liver and bone marrow samples [n = 3 per group]). (C) Representative immunohistochemistry staining images of Lcn2 in the bone marrow of cachectic mice; 10x and high-resolution inset (scale bar = 50 μm). (D and E) Flow cytometry analysis to detect myeloid and lymphoid populations and myeloid cell subpopulations. (F) Flow cytometry quantification of intracellular Lcn2 in Ly6G+ neutrophils; accompanying fluorescent intensity histogram, capturing relative abundance of Ly6G+ Lcn2+ neutrophils between sham (gray lines) and cachectic (red lines) groups. The Ly6G+ cell population in the sham group is suppressed to the X axis by the relative abundance found in the cachectic group. Each curve represents a single subject. Vertical dotted line approximates gating threshold for positive intracellular Lcn2 staining. (G) FACS-sorted neutrophil RNASeq analysis of Lcn2 transcripts. D-G; N = 4 per group. B, D-G were analyzed by two-tailed Students t-tests. A; Lcn2 molecular weight = 23 kDa, GAPDH = 37 kDa. All data expressed as mean ± SEM. Quantitative data analyzed by Student's t test. *$p \leq 0.05$, **$p \leq 0.01$, ***$p \leq 0.001$, and ****$p \leq 0.0001$. Sham operation controls = grey/black, KPC = red.

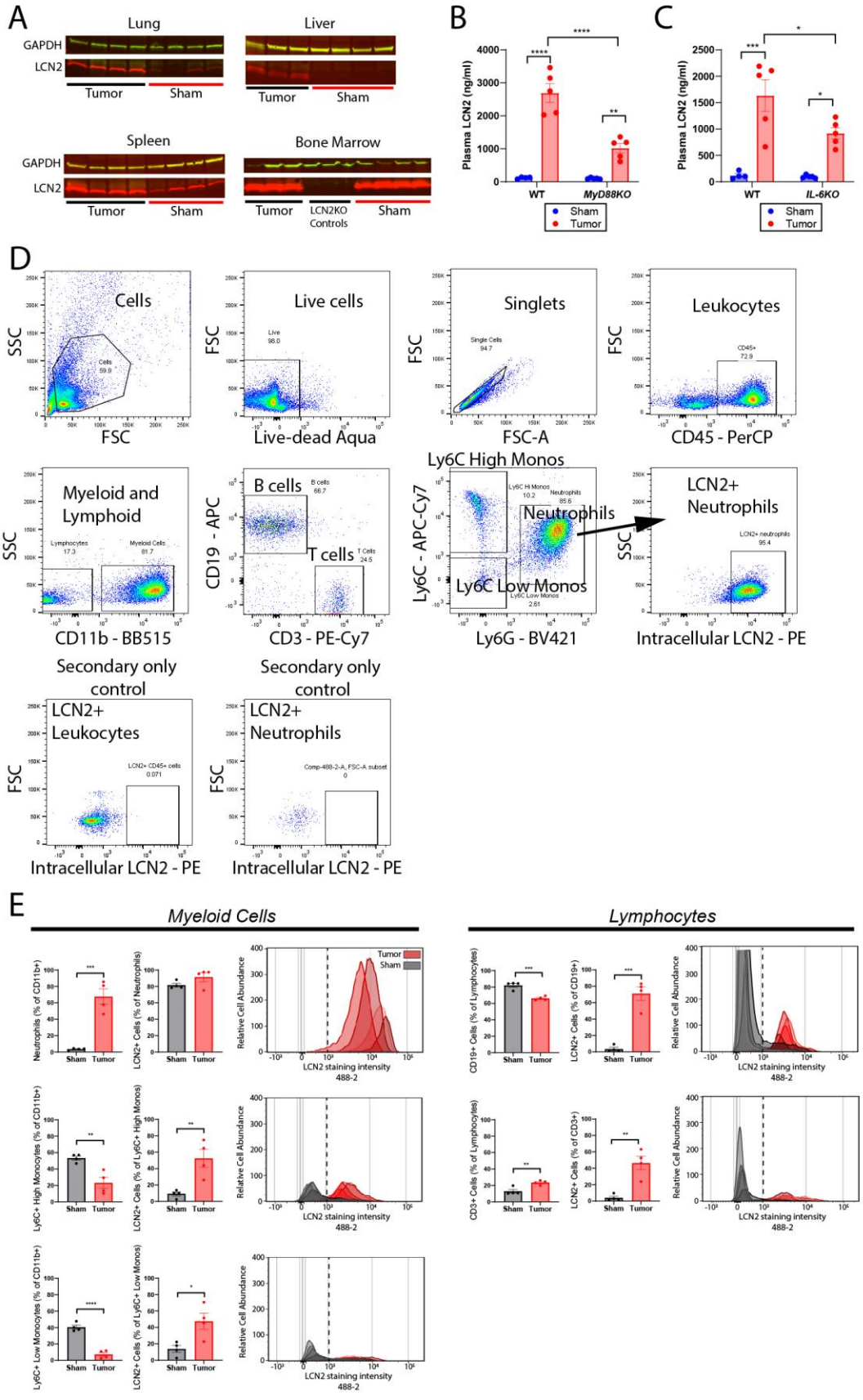
A
Lung
Liver
GAPDH
LCN2
Tumor
Sham
Spleen
Bone Marrow
LCN2KO Controls
B
Plasma LCN2 (ng/ml)
WT
MyD88KO
Sham
Tumor
C
IL-6KO
D
Cells
SSC
FSC
Live cells
Live-dead Aqua
Singlets
FSC-A
Leukocytes
CD45 - PerCP
Myeloid and Lymphoid
CD11b - BB515
B cells
T cells
CD19 - APC
CD3 - PE-Cy7
Ly6C High Monos
Neutrophils
Ly6C Low Monos
Ly6C - APC-Cy7
Ly6G - BV421
LCN2+ Neutrophils
Intracellular LCN2 - PE
Secondary only control
LCN2+ Leukocytes
E
Myeloid Cells
Lymphocytes
Neutrophils (% of CD11b+)
LCN2+ Cells (% of Neutrophils)
Relative Cell Abundance
LCN2 staining intensity
488-2
Ly6C+ High Monocytes (% of CD11b+)
LCN2+ Cells (% of Ly6C+ High Monos)
Ly6C+ Low Monocytes (% of CD11b+)
LCN2+ Cells (% of Ly6C+ Low Monos)
CD19+ Cells (% of Lymphocytes)
LCN2+ Cells (% of CD19+)
CD3+ Cells (% of Lymphocytes)
LCN2+ Cells (% of CD3+)

Supplementary Figure 2. Related to Figure 2. (A) Western blots used to quantify densitometry values for lung, liver, spleen, and bone marrow (n = 3-4 per group). Terminal plasma Lcn2 levels in sham and tumor-bearing (B) WT and *Myd88-KO* mice (N = 5 per group for *Myd88*-KO sham, *Myd88*-KO tumor, and WT tumor groups; N = 4 for the WT sham group) and (C) WT and *IL6-KO* mice (N = 5 per group for *Il6-KO* sham, *Il6-KO* tumor, and WT tumor groups; N = 4 for the WT sham group). (D) Flow cytometry gating strategy for circulating immune cell populations and intracellular Lcn2. (E) Quantification of peripheral myeloid and lymphoid cell subtypes (as a percentage of total myeloid or lymphoid cells) stained for intracellular Lcn2; accompanying fluorescent intensity histograms for Lcn2 staining intensity and relative cell abundance in sham and cachectic groups. Vertical dotted lines approximate gating threshold for positive intracellular Lcn2 staining. Histograms represent combined overlays of individual mice (sham or tumor). For neutrophil histogram overlay, the sham control mice display minimal cell abundance, thus are marginally visible (n = 4 per group). A; Lcn2 molecular weight = 23 kDa, GAPDH = 37 kDa. All data are expressed as mean ± SEM. B; blue = sham operation controls, red = KPC engrafted mice. E; Sham operation controls = grey/black, KPC = red.

Genetic deletion of lcn2 ameliorates pancreatic cancer cachexia-anorexia

After observing upregulation of Lcn2 in the periphery and CNS of mice that develop pancreatic cancer cachexia, we wanted to determine if genetic deletion of *lcn2*

would reverse the behavioral and physiologic manifestations of cachexia. After KPC tumor implantation, we observed increased food consumption in *lcn2-KO* mice relative to WT control (Figures 3A-B). Furthermore, we observed a statistically non-significant increase in skeletal muscle mass in tumor-bearing *lcn2-KO* mice compared to WT, while cardiac tissue was significantly spared in tumor-bearing *lcn2-KO* mice (Figure 3C-D). Similar to the tissue-specific measurements, nuclear magnetic resonance (NMR) body composition analysis of the lean compartment also demonstrates a non-significant improvement in lean mass of *lcn2-KO* tumor-bearing mice (Figure 3E). NMR-based body composition analysis of the fat compartment demonstrated consistent increase in fat mass of *lcn2-KO* tumor-bearing mice throughout the study, including early (day 4 post-implantation), mid (day 8 post-implantation), and late-stage (day 11 post-implantation) cachexia for *lcn2-KO* tumor-bearing mice (Figure 3F-H). Similarly, *lcn2-KO* tumor-bearing mice had a significantly increased inguinal fat pad mass at the end of the study when normalizing to sham controls (Figure 3I). Despite observing an elevation in fat mass of *lcn2-KO* tumor-bearing mice, there was no difference in white adipose browning between WT and *lcn2-KO* mice as indicated by browning genes *Ucp1, Prdm16,* and *Cidea* (Figure S3A-D). Although there was a significant increase in *Ppar-γ* of *lcn2-KO* mice, controlling for baseline genotypic expression did not result in a significant reduction in tumor-bearing mice between genotypes (Figures S3C). Histologically, there appears to be an increase in cellularity in WT tumor-bearing mice compared to *lcn2-KO* tumor-bearing mice, suggestive of increased cellular infiltrates known to be important in fat wasting in viral cachexia models (Figure S3E) (557). While this particular model of cancer cachexia results in significant lean and fat mass loss,

tumor-free body mass is unchanged owing to abdominal ascites and third-spacing edema (Figure S3F) (38).

lcn2 deletion improved voluntary wheel running and trended toward improved survival duration (Figure S3G-J). These behavioral effects were independent of tumor growth and basic histologic appearance, as tumor mass and key histopathological tumor characteristics (including ragged parenchymal infiltrations, focal necrotic loci, and acute inflammation) were similar between WT and *lcn2-KO* mice (Figure S3K-N). The impacts on feeding behavior and voluntary wheel running were also observed in animals with a less precipitous disease course (by orthotopic implantation of fewer pancreatic cancer cells) (Figure S3O-P). Since it is suggested that gastrointestinal malabsorption may play a role in energy balance during cancer cachexia, we analyzed fecal lipid, protein, and protease concentrations and did not detect changes during cachexia nor genotype-specific alterations, except for an increase in fecal lipids of *lcn2-KO* mice at the final 5 days of the study (days 7-11), although this may be due to increased food intake as these animals were not pair-fed (Figure S3Q-U). We also monitored blood glucose of WT and *lcn2*-KO mice and observed a significant increase in *lcn2-KO* tumor-bearing mice compared to WT at the end of the study, likely due to the increased food consumption of *lcn2-KO* tumor-bearing mice, as WT and *lcn2-KO* sham controls remained similar throughout the study (Figure S3V-X). We did not detect Lcn2 in the circulation or CSF of tumor-bearing *lcn2-KO* mice, demonstrating that tumor-derived Lcn2 does not meaningfully contribute to circulating or central Lcn2 levels during cachexia (Figure 3J-K). Furthermore, genetic deletion of *lcn2* did not affect the myeloid to lymphocyte ratio during pancreatic cancer cachexia, demonstrating a similar

immunologic profile amongst *lcn2-KO* and WT genotypes (Figure 3L-M). Despite improvements in skeletal and cardiac tissue mass, deletion of *lcn2* did not alter ubiquitin ligase or autophagy-related transcripts during cachexia (Figure 3N-O). Finally, *lcn2* deletion did not alter acute-phase- and inflammatory-related transcripts in the liver and hypothalamus during the development of cachexia (Figure 3P-Q).

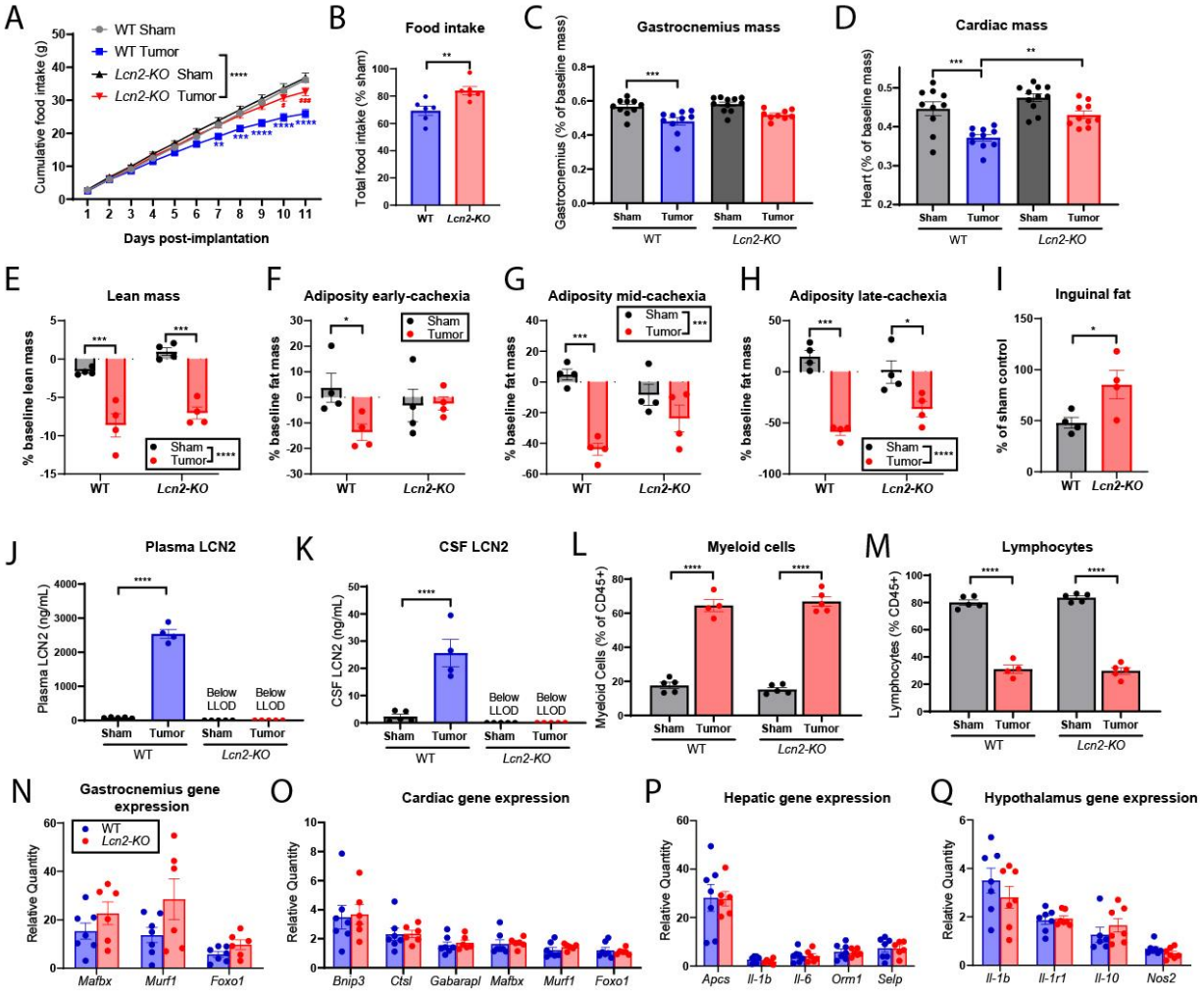

Figure 3. Genetic deletion of Lcn2 ameliorates cachexia-anorexia. (A) Cumulative and (B) total food intake for WT and *lcn2-KO* mice after receiving tumor implantations or sham operations (n = 6 per group for WT sham, WT tumor, and *lcn2-KO* tumor groups;

n = 7 for *lcn2-KO* sham controls). (C) Terminal gastrocnemius and (D) heart mass as a percentage of baseline body mass (n = 10 per group in WT sham, WT tumor, and *lcn2-KO* tumor groups; n = 11 in *lcn2-KO* sham controls). (E) NMR body composition analysis of terminal tumor-free lean (n = 4 per group). (F-H) NMR body composition analysis of fat mass at early (study day 4), mid (study day 8), and late (study day 11) cachexia (n = 4 per group). (I) Terminal inguinal fat pad mass normalized to genotype control (n = 4 per group). (J) Terminal plasma and (K) cerebrospinal fluid Lcn2 levels (n = 5 per group for WT Sham, *lcn2-KO* sham, and *lcn2-KO* tumor groups; n = 4 for the WT tumor group). (L) Proportions of myeloid and (M) lymphoid cells as a percentage of CD45+ cells (n = 5 per group for WT Sham, *lcn2-KO* sham, and *lcn2-KO* tumor groups; n = 4 for the WT tumor group). (N) Ubiquitin proteasome pathway gene expression in the gastrocnemius. (O) Ubiquitin proteasome and autophagy-related gene expression in cardiac muscle. (P) Hepatic expression of acute-phase- and inflammatory-related transcripts. (Q) Hypothalamic gene expression of inflammation-related transcripts. For N-Q, n = 6 per group for WT sham and *lcn2-KO* tumor groups; n = 7 for *lcn2-KO* sham and WT tumor, groups. All gene expression data represented as fold change over genotype-matched controls. No difference was observed in baseline expression of transcripts between WT and *lcn2-KO* mice. All data expressed as mean ± SEM. Cumulative food intake data were analyzed by a repeated-measures Two-way ANOVA followed by Bonferroni's post hoc test. Food intake and inguinal fat mass as % of sham was analyzed by two-tailed Student's t test. All other data (C-H, J-Q) were analyzed by ordinary Two-way ANOVA followed by Bonferroni's post hoc test. *$p \leq 0.05$, **$p \leq 0.01$, ***$p \leq 0.001$, and ****$p \leq 0.0001$. LLOD = lower limit of detection. A-D, J-K, N-Q; Gray =

WT sham operation control; Black = *lcn2-KO* sham operation control; Blue = WT KPC-engrafted mice; Red = *lcn2-KO* KPC-engrafted mice. E-I, L-M; Sham operation controls = grey/black, KPC-engrafted mice = red.

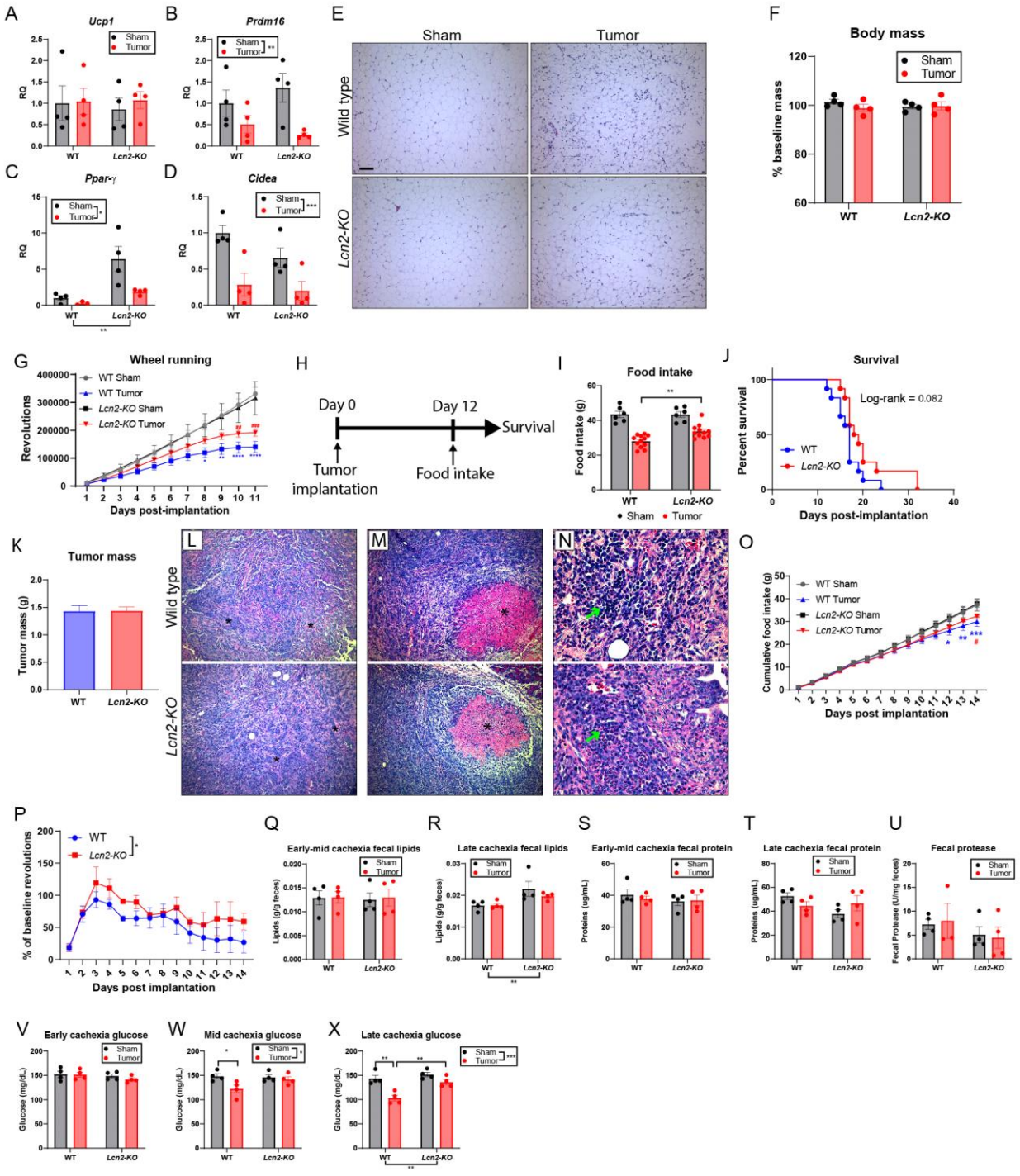

Supplementary Figure 3. Related to Figure 3. (A-D) Inguinal white adipose tissue gene expression analysis of browning genes *Ucp1, Prdm16, Ppar-γ,* and *Cidea* (N = 4 per group for all groups, except the WT tumor group in Figure C [N = 3]). (E) Representative H&E histochemical images of inguinal white adipose tissue of WT and *lcn2-KO* mice after sham or tumor implantation (10x magnification, scale bar = 100 μm). (F) Terminal tumor-free mass of WT and *lcn2-KO* mice after sham or tumor implantation (n = 4 per group). (G) Cumulative voluntary wheel running after tumor implantation or sham operation in WT and *lcn2-KO* mice (N = 6 per group for WT sham, WT tumor, and *lcn2-KO* tumor groups; N = 7 for the *lcn2-KO* sham group). (H) Experimental design for survival study and food consumption assessments. (I) Day 12 total food intake during survival study. (J) Kaplan Meier survival curve comparing WT and *lcn2-KO* tumor-engrafted mice compared by log rank test. n = 6-12 per group for B-D. (K) Terminal tumor mass for WT and *lcn2-KO* mice (n = 6 per group). Histopathologic characteristics of KPC allografts showing (L) ragged stromal infiltration, (M) geographical necrosis, and (N) acute inflammatory infiltrates after implantation into WT and *lcn2-KO* mice (scale bar = 100 μm). (O) Cumulative food intake in WT and *lcn2-KO* mice implanted with fewer KPC pancreatic cancer cells (0.75 x10^6) than in Figure 3 (n = 4 per group). (P) Normalized voluntary wheel running data in WT and *lcn2-KO* mice orthotopically implanted with 0.75x10^6 KPC cells after a 3-week acclimation period (n = 4 per group). (Q) Early-mid and (R) late-stage cachexia fecal lipid levels in WT and *lcn2-KO* mice (n = 4 per group). (S) Early-mid (days 1-6) and (T) late-stage (days 7-11) cachexia fecal protein levels in WT and *lcn2-KO* mice (n = 4 per group). (U) Terminal fecal protease

activity in WT and *lcn2-KO* mice (n = 4 per group). (V) Early (day 4), (W) mid (day 8), and (X) late-stage (day 11) blood glucose levels in WT and *lcn2-KO* mice (n = 4 per group). Repeated food intake and wheel running data were analyzed by a repeated-measures Two-way ANOVA followed by Bonferroni's post hoc test (G, O, P). Total food intake, gene expression data, body mass, fecal analyses, and glucose levels were analyzed by ordinary Two-way ANOVA followed by Bonferroni's post hoc test (A-D, F, I, Q-X). (J) Data was analyzed by a log-rank test (two-tailed). All data are expressed as mean ± SEM. A-F, I, Q-X; Sham operation controls = grey/black, KPC-engrafted mice = red. G, J, K, O, P; Gray = WT sham operation control; Black = *lcn2-KO* sham operation control; Blue = WT KPC-engrafted mice; Red = *lcn2-KO* KPC-engrafted mice.

The central melanocortin 4 system mediates appetite suppression during pancreatic cancer cachexia

Based on recent literature demonstrating that Lcn2 binds to hypothalamic MC4R (82) and our observation that feeding behavior improves in *lcn2-KO* mice during cachexia, we hypothesized that MC4R antagonism (or inverse agonism) would improve appetite during the development of cancer cachexia. To address this hypothesis, we examined whether intracerebroventricular (ICV) infusion of agouti-related peptide (AgRP), an inverse agonist of the MC4R, improved appetite during the progression of pancreatic cancer cachexia. After the development of the signs and symptoms of cachexia (lethargy, decreased food intake, minimal grooming), we began ICV administration of AgRP (Figure 4A). Mice consumed equivalent amounts of food prior to

ICV AgRP treatment (Figure 4B). However, after the development of cachexia symptoms, mice receiving ICV AgRP treatment increased food intake compared to their vehicle-treated counterparts (Figure 4C-D). Similar to the *lcn2-KO* tumor-bearing mice, AgRP treated mice had improved skeletal and cardiac tissue mass at the end of the study (Figure 4F-E). Furthermore, these muscle-sparing effects were independent of ubiquitin-proteasome and autophagy related pathways, suggesting the increased food consumption alone was responsible for the sparing of muscle mass (Figure S4A-B). Tumor burden was equivalent between AgRP- and vehicle-treated groups (Figure S4C).

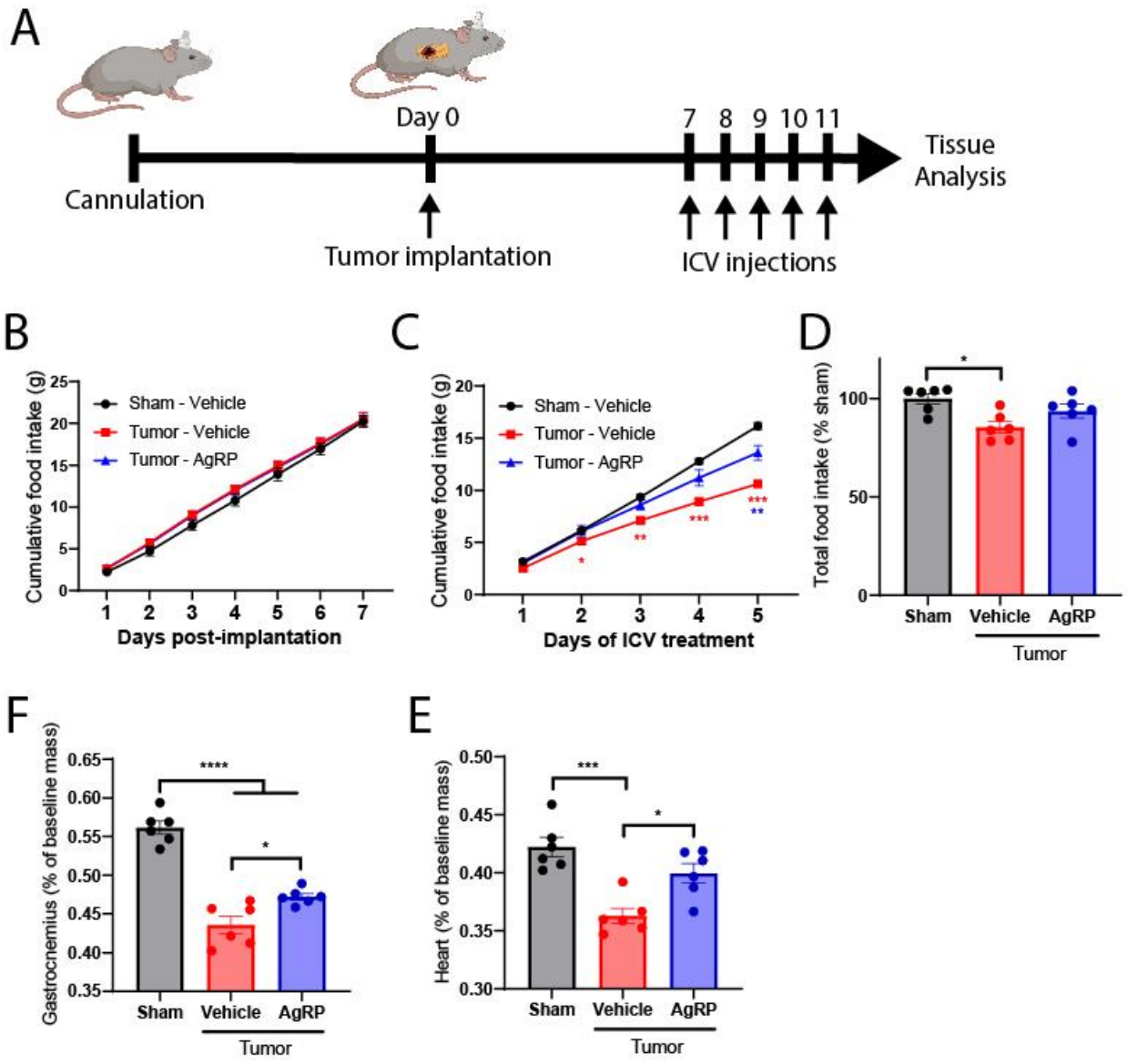

Figure 4. MC4R inverse agonism improves feeding behaviors and muscle mass during pancreatic cancer cachexia. (A) Experimental design and protocol of cannulation, tumor implantation, and ICV treatment. Cumulative food intake after tumor implantation (B) before and (C) after initiation of daily ICV AgRP (1 nmol) or vehicle treatments. In B, the Tumor – AgRP group is masked immediately behind the Tumor – Vehicle group. (D) Total food intake as a percentage of sham control for entire study. (F) Terminal gastrocnemius and (E) cardiac tissue mass normalized to baseline mass. n = 6 per

group. All data expressed as mean ± SEM. Cumulative food intake data were analyzed by a repeated-measures Two-way ANOVA followed by Bonferroni's post hoc test. All other data were analyzed by ordinary One-way ANOVA followed by Bonferroni's post hoc test. *p ≤ 0.05, **p ≤ 0.01, ***p ≤ 0.001, and ****p ≤ 0.0001. Black/grey = sham operation control, Red = KPC-engrafted, ICV vehicle treated mice, Blue = KPC-engrafted, ICV AgRP treated mice.

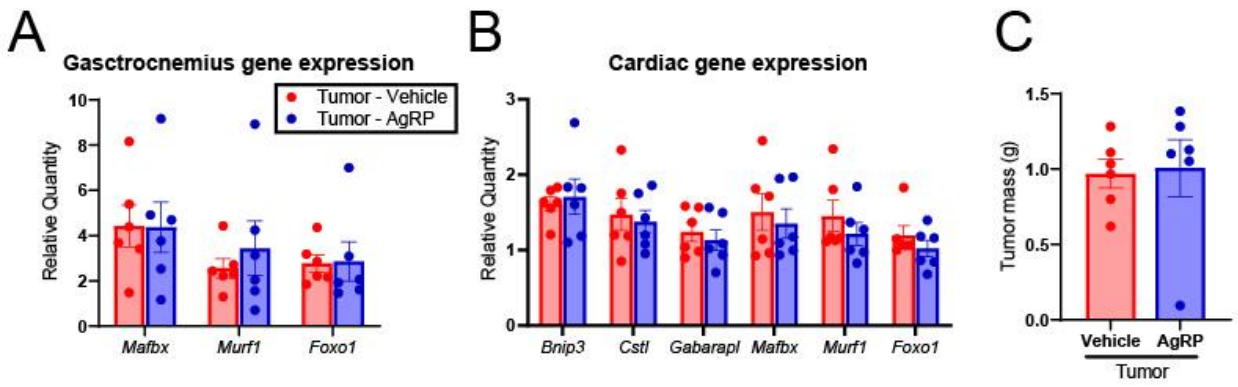

Supplementary Figure 4. Related to Figure 4. (A) Gastrocnemius and (B) cardiac tissue ubiquitin ligase and autophagy pathway gene analysis. (C) Terminal tumor mass. n = 6 per group. All data are expressed as mean ± SEM. Red = KPC-engrafted, ICV vehicle treated mice, Blue = KPC-engrafted, ICV AgRP treated mice.

Lcn2 *crosses the blood-brain barrier and regulates feeding behaviors during cancer cachexia*

Since we observed that the bone marrow is the predominant location of Lcn2 protein production, we hypothesized that restoring *lcn2* expression in this compartment

would result in significant production and secretion of Lcn2 into circulation, and that this circulating Lcn2 is capable of crossing the blood-brain barrier (BBB) to regulate appetite through its recently identified actions in the CNS. Using an adoptive transfer technique that gently conditions the bone marrow while sparing the integrity of the BBB, we transplanted WT bone marrow into *lcn2-KO* mice (Figure 5A). Indeed, restoration of *lcn2* in the bone marrow compartment alone resulted in a significant rescue of peripheral Lcn2 levels during both normal physiology (sham operation mice) and cancer cachexia (Figure 5B). Furthermore, restoration of *lcn2* expression in the bone marrow yielded a near 50% restoration of Lcn2 levels in the CSF during both normal physiology and cachexia (Figure 5C). We then tested whether cerebral Lcn2 is sufficient to alter feeding behavior. Consistent with previous reports, we demonstrated that chronic ICV injection of Lcn2 is capable of inducing appetite suppression and concurrent weight loss (Figure S5A-E) (82). Furthermore, we observed elevated cFos expression in paraventricular neurons following ICV administration of Lcn2; this cFos expression profile is similar to that of mice treated with ICV Melanotan-II (MT-II), a potent synthetic analogue of α-MSH and agonist of the MC4R (Figure S5F-G). To ensure Lcn2's anorectic response is dependent on MC4R signaling, we repeatedly administered Lcn2 to the lateral ventricle of WT and *Mc4r*-KO mice, and observed a significant reduction in food intake, body mass, and fat mass in WT compared to *Mc4r*-KO mice (Figure S5H-L).

Restoration of lcn2 in the bone marrow compartment suppresses food intake during pancreatic cancer cachexia

To examine whether restoration of *lcn2* expression in the bone marrow compartment influences energy balance during pancreatic cancer cachexia, we engrafted WT bone marrow into *lcn2-KO* mice, allowed transplanted animals to recover for eight weeks, then orthotopically implanted pancreatic cancer cells and monitored feeding behavior. Using this bone marrow transplantation method, we regularly achieve high levels of chimerism (>80%) as indicated by GFP expression in circulating immune cells in both genotypes (WT and *lcn2-KO*) and experimental groups (sham operation and tumor implantation) (Figure S6A-D). After bone marrow transplantation and subsequent tumor implantation, we observed a decrease in daily cumulative food intake and a trend towards decreased total food intake for *lcn2-KO* mice receiving *lcn2*-replete bone marrow (Figure 5D-E). As we observed previously, there was a modest improvement in skeletal and cardiac muscle catabolism in the pure *lcn2-KO* genotype (*lcn2-KO* mice receiving *lcn2-KO* bone marrow) compared to the WT genotype (WT mice receiving WT bone marrow) (Figure 5F-G). In *lcn2-KO* mice receiving WT bone marrow, we observed an intermediate skeletal and cardiac muscle wasting phenotype compared to the pure WT (WT mice receiving WT marrow) and *lcn2-KO* (*lcn2-KO* mice receiving *lcn2-KO* marrow) genotypes. Successful bone marrow engraftment and expression of *lcn2* was validated through Western blot analysis of the bone marrow at the end of the study (Figure S6C). Finally, we did not observe a difference in tumor burden, as indicated by terminal tumor mass, amongst the three experimental groups (Figure S6E).

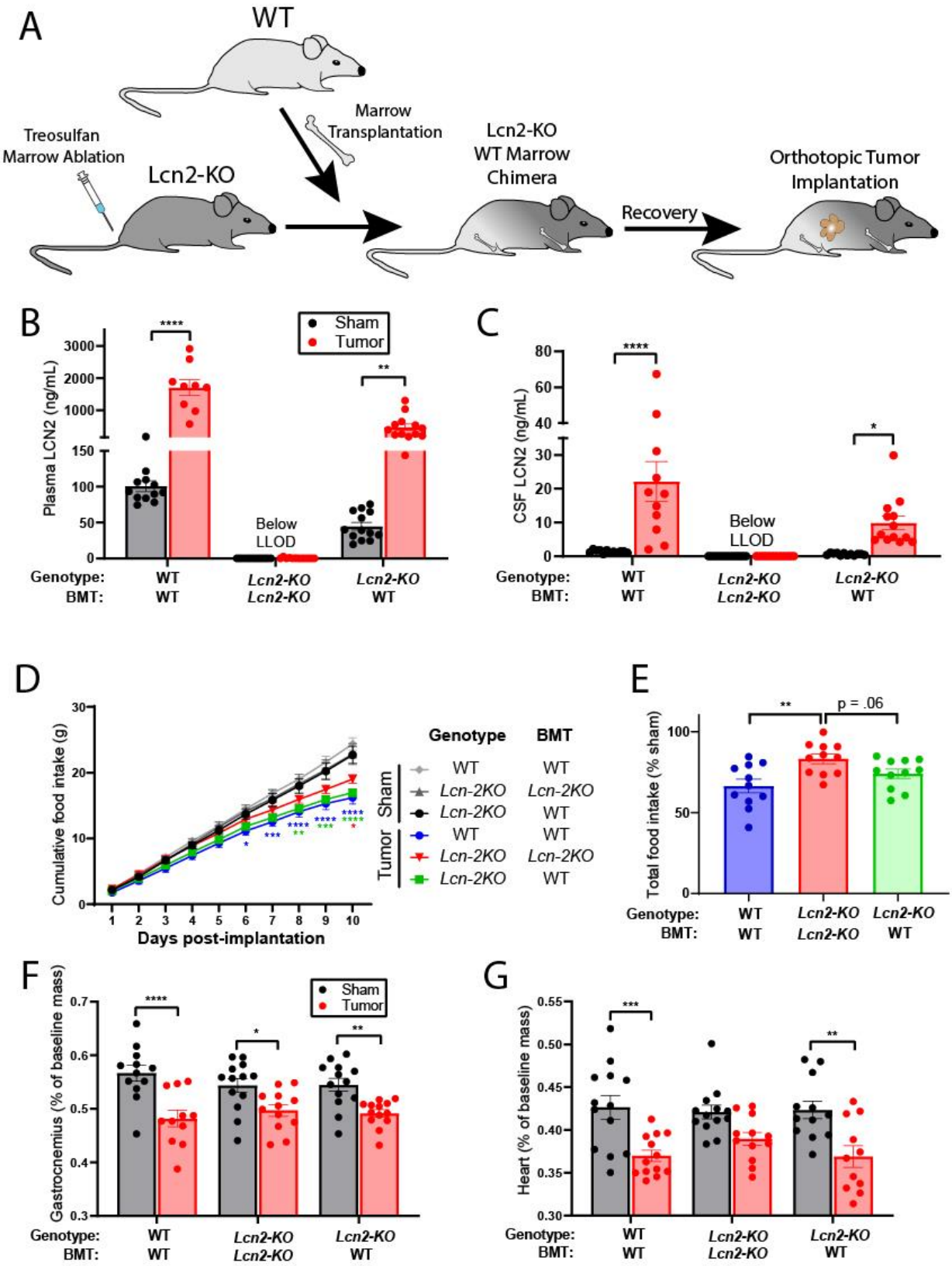
A
WT
Marrow Transplantation
Treosulfan Marrow Ablation
Lcn2-KO
Lcn2-KO WT Marrow Chimera
Recovery
Orthotopic Tumor Implantation
B
Plasma LCN2 (ng/mL)
Sham
Tumor
Below LLOD
Genotype: WT Lcn2-KO Lcn2-KO
BMT: WT Lcn2-KO WT
C
CSF LCN2 (ng/mL)
Below LLOD
Genotype: WT Lcn2-KO Lcn2-KO
BMT: WT Lcn2-KO WT
D
Cumulative food intake (g)
Days post-implantation
Genotype BMT
Sham WT WT
Lcn-2KO Lcn-2KO
Lcn-2KO WT
Tumor WT WT
Lcn-2KO Lcn-2KO
Lcn-2KO WT
E
Total food intake (% sham)
p = .06
Genotype: WT Lcn2-KO Lcn2-KO
BMT: WT Lcn2-KO WT
F
Gastrocnemius (% of baseline mass)
Sham
Tumor
Genotype: WT Lcn2-KO Lcn2-KO
BMT: WT Lcn2-KO WT
G
Heart (% of baseline mass)
Genotype: WT Lcn2-KO Lcn2-KO
BMT: WT Lcn2-KO WT

Figure 5. Lcn2 readily crosses the BBB and its expression in the bone marrow is sufficient to induce appetite suppression during pancreatic cancer cachexia. (A) Experimental design of bone marrow transplantation experiments. (B) Terminal peripheral and (C) central Lcn2 levels. (D) Cumulative food intake and (E) total food intake as a percent of sham control. (F) Terminal gastrocnemius and (G) cardiac tissue mass normalized to baseline mass. B-C; N = 12 for WT/WT-BM sham, *lcn2-KO*/KO-BMT sham, and *lcn2-KO*/KO-BMT KPC-engrafted mice; N = 9 for WT/WT-BM tumor group; N = 13 for *lcn2-KO*/WT-BMT sham and *lcn2-KO*/WT-BMT KPC-engrafted mice. D-G; N = 12 per group for WT/WT-BM sham and *lcn2-KO*/KO-BMT sham groups; N = 13 for the *lcn2-KO*/WT-BMT sham group; N = 11 per group for WT/WT-BM tumor, *lcn2-KO*/WT-BMT tumor, and *lcn2-KO*/KO-BMT tumor groups. All data expressed as mean ± SEM. Cumulative food intake data were analyzed by Mixed Model ANOVA with continuous measures followed by Bonferroni's post hoc test. Total food intake data were analyzed by One-way ANOVA followed by Bonferroni's post hoc test. All other data were analyzed by Mixed Model ANOVA followed by Bonferroni's post hoc test. Main column effects were calculated amongst tumor groups in panel D and are represented in the figure legend. *p ≤ 0.05, **p ≤ 0.01, ***p ≤ 0.001, and ****p ≤ 0.0001. LLOD = lower limit of detection. BMT = Bone marrow transplantation. B-C, F-G; Sham operation controls = grey/black, KPC-engrafted mice = red. D-E; Light grey = WT/WT-BMT sham operation control, Dark grey = *lcn2-KO*/*lcn2-KO*-BMT sham operation control, Black = *lcn2-KO*/WT-BMT sham operation control, Blue = WT/WT-BMT KPC-engrafted mice, Red = *lcn2-KO*/*lcn2-KO*-BMT KPC-engrafted mice, Green = *lcn2-KO*/WT-BMT KPC-engrafted mice.

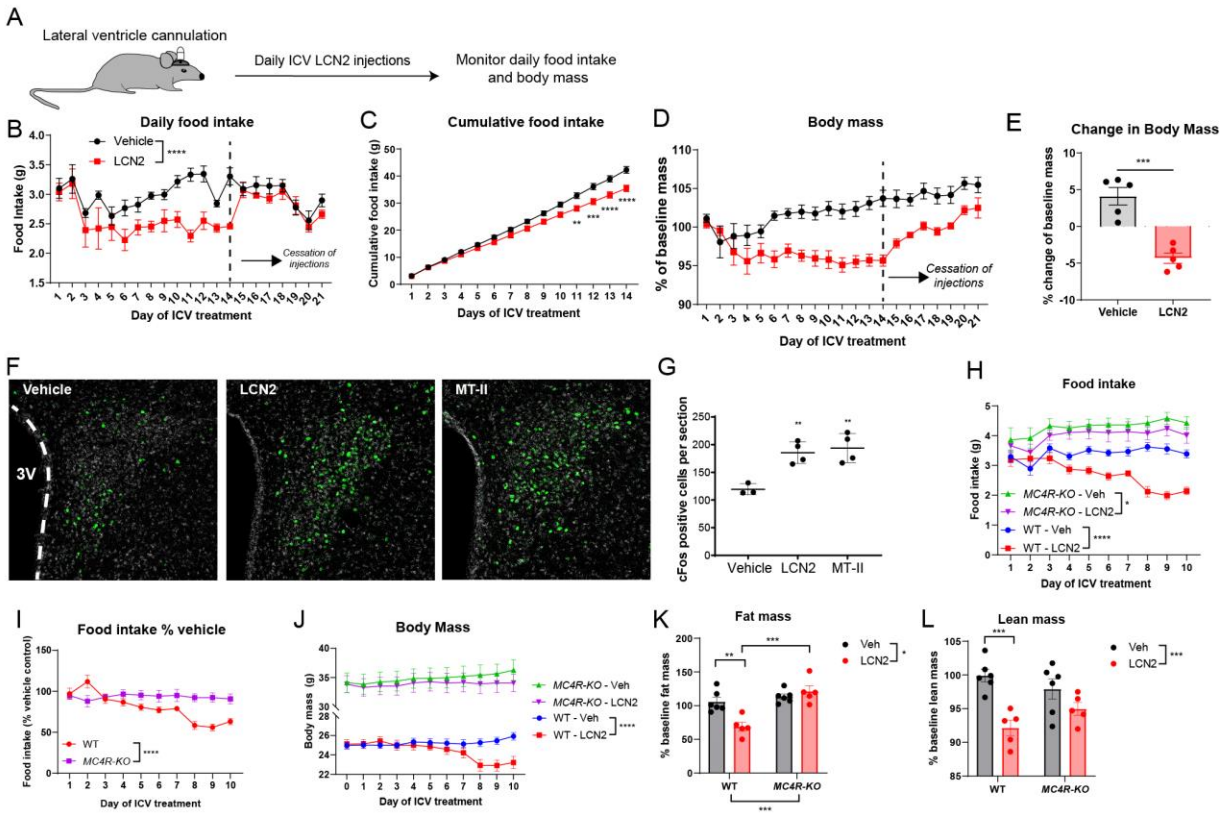

Supplementary Figure 5. Related to Figure 5. (A) Experimental protocol for ICV administration of Lcn2 (40 ng) or vehicle control. (B) Daily and (C) cumulative food intake. (D) Daily change in body mass as a percentage of baseline mass. (E) Change in body mass at the end of the ICV treatment period (14 days). B-E; N = 5 per group. After day 14, ICV treatment was stopped and food intake and body weight data were collected for another week. (F) Representative images of paraventricular nucleus cFos staining 90 minutes after ICV administration of Lcn2 (40 ng), MT-II (1 nmol), or vehicle (scale bar = 100 µm). (G) Quantification of cFos positive cells using the average count in three consecutive sections per mouse (N = 3 for the ICV vehicle group; N = 4 for the ICV Lcn2 and MT-II groups). 3V = third ventricle. ICV = intracerebroventricular. (H) Daily

food intake, (I) genotype-normalized food intake, (J) daily body mass, and terminal (K) fat and (L) lean mass in WT and *Mc4r-KO* mice receiving ICV vehicle or Lcn2 (40 ng). H-L; N = 6 per group for WT ICV vehicle and Mc4rKO ICV vehicle groups; N = 5 per group for WT ICV Lcn2 and Mc4rKO ICV Lcn2 groups). All data are expressed as mean ± SEM. ICV = intracerebroventricular. A-E, K-L; Black = ICV Vehicle, Red = ICV Lcn2. H-J; Blue = WT ICV vehicle injection, Red = WT ICV Lcn2 injection, Green = Mc4r-KO ICV vehicle injection, Purple = Mc4r-KO ICV Lcn2 injection.

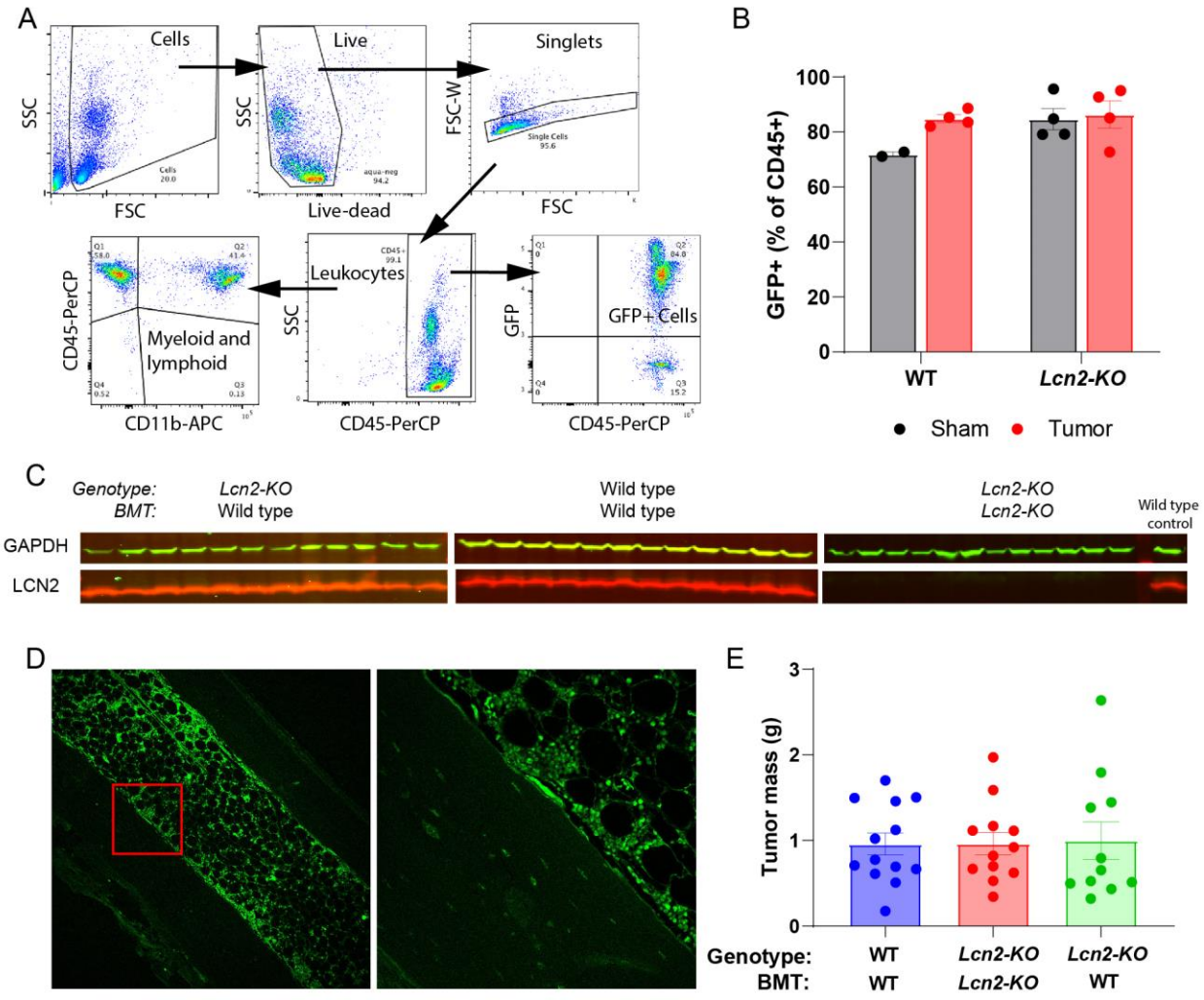

Supplementary Figure 6. Related to Figure 5. (A) Gating strategy for flow cytometry analysis of circulating GFP+ immune cells after generation of GFP+ bone marrow chimeras. (B) Quantification of GFP+ as a percentage of CD45+ cells in WT and *lcn2-KO* mice after sham operation or tumor implantation. (C) Representative bone marrow Western blots confirming successful bone marrow engraftment and expression of Lcn2. (D) Representative confocal images of cortical and spongy bone in a WT mouse after receiving Ly5.1 eGFP bone marrow transplantation (scale bar = 50µm). (E) Terminal tumor mass for all mice included in the bone marrow transplantation studies. C; Lcn2 molecular weight = 23 kDa, GAPDH = 37 kDa. All data are expressed as mean ± SEM. BMT = bone marrow transplantation. For B, no statistics were performed, as only n = 2 was achieved for the WT sham operation control. E was analyzed by one-way ANOVA. B; Grey = sham operation control, Red = KPC-engrafted mice. E; Blue = WT/WT-BMT KPC-engrafted mice, Red = *lcn2-KO*/*lcn2-KO*-BMT KPC-engrafted mice, Green = *lcn2-KO*/WT-BMT KPC-engrafted mice.

Lean mass sparing effect of lcn2 ablation is mediated by increased food intake

To formally test whether the muscle-sparing effects of *lcn2* ablation are mediated through food intake, rather than a combination of food intake and tissue-specific metabolic alterations, we performed pair-feeding studies in which we matched the tumor-bearing *lcn2-KO* food intake to that of their tumor-bearing WT counterparts (Figure 6A). After pair feeding, we observed no difference in skeletal or cardiac tissue

catabolism between *lcn2-KO* and WT tumor-bearing mice (Figure 6B, C). Collectively, this observation supports the hypothesis that the muscle-sparing effects of Lcn2 are largely mediated through increased energy consumption, but not a direct effect of Lcn2 on muscle.

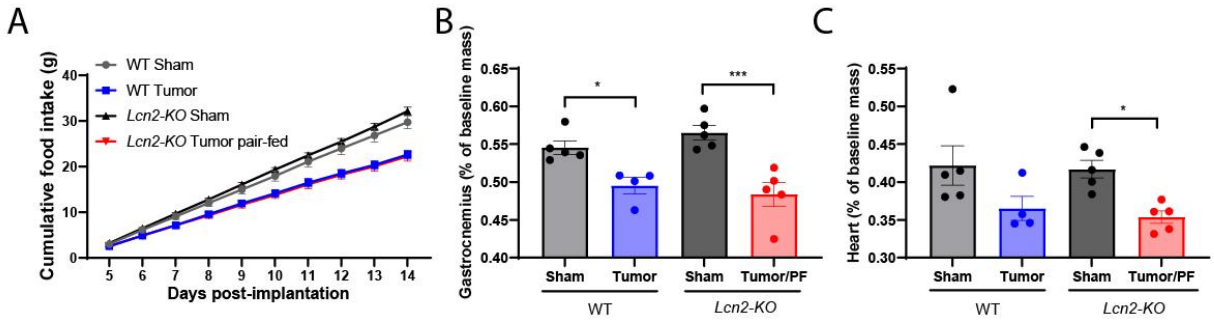

Figure 6. Pair feeding abolishes muscle gain in *lcn2-KO* mice during cachexia. (A) Cumulative food intake after the initiation of cachexia symptoms. N = 5 per group (B) Terminal gastrocnemius and (C) cardiac tissue mass normalized to baseline mass. N= 5 per group for WT sham, *lcn2-KO* sham, and *lcn2-KO* tumor groups; N = 4 for the WT tumor group. Cumulative food intake data were analyzed by a repeated-measures Two-way ANOVA followed by Bonferroni's post hoc test. Data presented in B-C were analyzed by a Two-way ANOVA followed by Bonferroni's post hoc test. *p ≤ 0.05, **p ≤ 0.01, ***p ≤ 0.001, and ****p ≤ 0.0001. PF = pair-fed. All data are expressed as mean ± SEM. Gray = WT sham operation control; Black = *lcn2-KO* sham operation control; Blue = WT KPC-engrafted mice; Red = *lcn2-KO* KPC-engrafted, pair-fed mice.

Circulating Lcn2 *correlates with neutrophil expansion, lean and fat mass wasting, and mortality in patients with pancreatic cancer*

To test whether our observations in these preclinical models of cachexia extend to human disease, we measured plasma LCN2 levels in patients with pancreatic cancer at diagnosis and, in several cases, follow-up visits. Since we observed an increase in circulating neutrophils, as well as their transcriptional upregulation of *lcn2* in our rodent models of pancreatic cancer cachexia, we hypothesized that neutrophil expansion would be associated with an increase in circulating LCN2 levels during human disease. Indeed, we observed a concurrent increase in peripheral neutrophils, decrease in lymphocytes, and elevation of neutrophil to lymphocyte ratio (NLR) as circulating LCN2 levels rise, recapitulating the immunologic shift we observed in our rodent models (Figure 7A-C, Supplemental table 1). Next, we sought to determine if an increase in LCN2 in patients diagnosed with pancreatic cancer corresponded with alterations in fat and lean mass, as these were consistent findings in our rodent models. We measured the amount of skeletal muscle and visceral adipose tissue in axial images at the third lumbar vertebrae for patients with pancreatic cancer at diagnosis, as well as follow-up visits (Figure 7D) (558). We observed a significant association between increasing LCN2 levels and loss of both visceral fat and skeletal muscle (Figure 7E-F; Supplemental table 2). Finally, we identified a 240 ng/mL plasma LCN2 cutoff that stratifies patients by survival outcomes (559). In this patient population, a plasma LCN2 level of greater than 240 ng/mL at diagnosis was associated with significantly decreased overall survival compared to patients with LCN2 values under this threshold

(Figure 7G, Supplemental table 3: HR = 1.81; 95% CI = 1.07-3.05; p = 0.03). Taken together, our data demonstrate that elevated LCN2 levels during human pancreatic cancer is associated with neutrophil expansion, increased fat and skeletal muscle catabolism, and decreased survival. In general, these findings recapitulate what we observed in our pancreatic cancer cachexia mouse models.

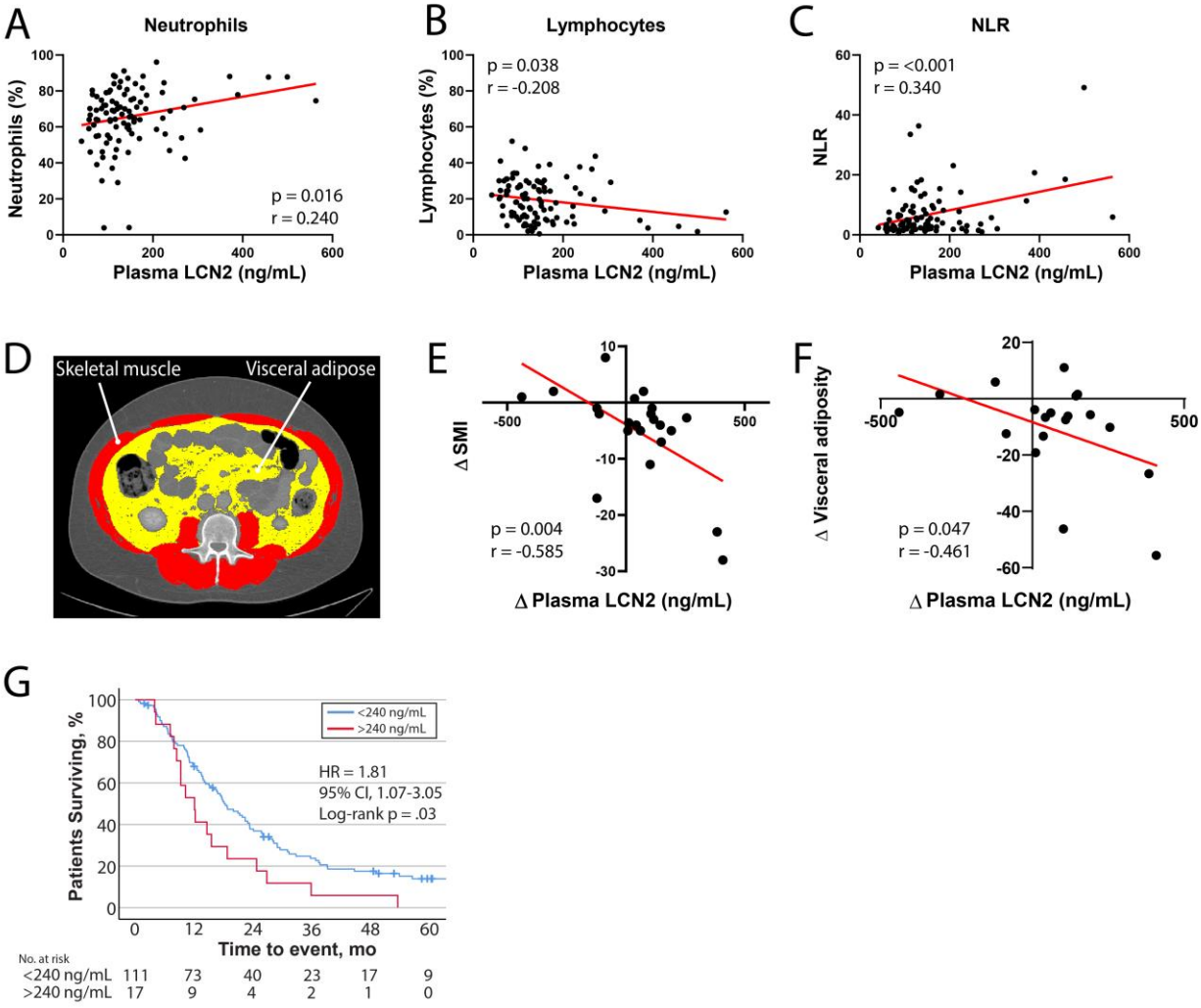

Figure 7. LCN2 is regulated during pancreatic cancer in humans and is associated with neutrophil expansion, skeletal muscle catabolism, and increased mortality. (A-C) Scatter

plot of plasma LCN2 levels and (A) circulating neutrophil percentage, (B) lymphocyte percentage, and (C) neutrophil to lymphocyte ratio (n = 100). (D) Representative axial computed tomography scan at the third lumbar vertebrae highlighting visceral adipose tissue in yellow and skeletal muscle in red. (E) Correlation plot of change in skeletal muscle index and change in LCN2 levels after diagnosis (n = 22). (F) Correlation plot of change in visceral adiposity and change in LCN2 levels after diagnosis (n = 19). (G) Overall survival for patients with pancreatic cancer dichotomized by 240 ng/mL LCN2 levels at diagnosis (n = 128; 2 patients with less than 1.5 months of follow-up were excluded from analysis). SMI = skeletal muscle index; both SMI and visceral adiposity calculated by dividing total cross-sectional area at L3 (cm^2) by patient height squared (m^2). Data from E-F represent a subset of patients from A-C which have baseline and follow computed tomography scans. Please see Supplementary tables for demographics information for each patient population in A-C, E-F, and G. A-C, E-F; were analyzed by simple linear regression and two-tailed correlation analyses. Data represented in G analyzed by log-rank Mantel-Cox test (two-sided). NLR = Neutrophil-to-lymphocyte ratio. G; Blue = <240 ng/mL LCN2, Red = >240 ng/mL LCN2.

			Total (N = 100)
Age			62.3 (11.3)
Sex	Male		51
	Female		49
BMI (kg/m2)	Mean		27.2 (5.6)
	Binned	<18.5	4
		18.5-24.9	33
		25-29.9	39
		29.9-34.9	16
		>35	8

Days from diagnosis to treatment			32.6 (20.3)
Tumor location		Head	62
		Body	6
		Tail	4
		Overlapping	5
		NOS	23
Cancer Stage		0	2
		IA	0
		IB	4
		IIA	19
		IIB	41
		III	10
		IV	23
		Unknown	1
Neoadjuvant Therapy	Chemo	No	72
		Yes	12
		Unknown	16
	RT	No	81
		Yes	10
		Unknown	9
Tumor resection		No	33
		Yes	67
Adjuvant Chemotherapy		No	18
		Yes	49
Chemotherapy regimens		Gemcitabine	32
		FOLFIRINOX	14
		Gemcitabine/nab-paclitaxel	17
		FOLFIRIONX + Gemcitabine/nab-paclitaxel	2
		FOLFOX	1
		Gemcitabine/cisplatin	1
		Gemcitabine/HAP	4
		Unknown	11
Immune cell		NEUTROPHIL %	65.8 (16.6)
		LYMPHOCYTE %	19.3 (11.5)
		Neutrophil/Lymphocyte ratio	6.6 (7.7)
Plasma Lcn2 (ng/mL)			150.3 (90.8)
CA19-9			890.8 (2838.3)

Supplementary table 1. Related to Figure 7A-C. Patient demographics, treatment, and biomarker data. Abbreviations: BMI, body mass index; NOS, not otherwise specified; HAP, hypoxic abdominal perfusion; FOLFIRINOX, 5-fluorouracil, leucovorin, irinotecan, and oxaliplatin; FOLFOX, 5-fluorouracil, leucovorin, and oxaliplatin. RT, radiotherapy; CA19-9, cancer antigen 19-9. Standard deviation presented in parentheses where appropriate.

			N = 22
Age			62.2 (12.9)
Sex	Male		13
	Female		9
BMI (kg/m2)	Mean		26.9 (4.8)
	Binned	<18.5	1
		18.5-24.9	6
		25-29.9	10
		29.9-34.9	5
Days from diagnosis to treatment			36.2 (23.8)
Tumor location		Head	12
		Body	2
		Tail	0
		Overlapping	0
		NOS	8
Cancer Stage		IA	1
		IB	0
		IIA	2
		IIB	5
		III	5
		IV	9
Neoadjuvant Therapy	Chemo	No	9
		Yes	4
		Unknown	9
	RT	No	16
		Yes	4
		Unknown	2
Tumor resection		No	15

		Yes	7
Adjuvant Chemotherapy		No	1
		Yes	6
Chemotherapy regimens		Gemcitabine	3
		FOLFIRINOX	5
		Gemcitabine/nab-paclitaxel	9
		FOLFIRIONX + Gemcitabine/nab-paclitaxel	1
		FOLFOX	1
		Unknown	2
Plasma LCN2 (ng/mL)		Baseline	217.5 (175.9)
		Follow up	263.5 (138.2)
CA19-9			1537.9 (4670.1)
Body Composition	SMI	Baseline	38.8 (8.1)
		Follow up	33.8 (13.8)
	Visceral adipose	Baseline	33.2 (27.9)
		Follow up	22.6 (38.6)

Supplementary table 2. Related to Figure 7E-F. Patient demographics, treatment, and biomarker data. Abbreviations: BMI, body mass index; NOS, not otherwise specified; FOLFIRINOX, 5-fluorouracil, leucovorin, irinotecan, and oxaliplatin; FOLFOX, 5-fluorouracil, leucovorin, and oxaliplatin. RT, radiotherapy; CA19-9, cancer antigen 19-9. Standard deviation presented in parentheses where appropriate.

			Lcn2 <240 ng/mL (N = 111)	Lcn2 >240 ng/mL (N = 17)	P value
Age			63.8 (10.9)	59.4 (13.9)	0.14
Sex	Male		56	7	0.480
	Female		55	10	
BMI (kg/m2)	Mean		27.3 (5.6)	27.8 (6.0)	0.73
	Binned	<18.5	4	0	0.930
		18.5-24.9	36	6	

		25-29.9	43	7	
		29.9-34.9	16	2	
		>35	10	2	
Days from diagnosis to treatment			34.1 (27.2)	31.9 (17.8)	0.75
Tumor location		Head	71	8	0.040
		Body	5	2	
		Tail	6	0	
		Overlapping	3	3	
		NOS	26	4	
Cancer Stage		0	2	0	0.590
		IA	1	0	
		IB	7	1	
		IIA	20	4	
		IIB	43	3	
		III	12	4	
		IV	26	5	
Median survival time (mo)			17.44	11	
Neoadjuvant Therapy	Chemo	No	82	11	0.670
		Yes	12	2	
		Unknown	17	4	
	RT	No	93	14	0.850
		Yes	9	2	
		Unknown	9	1	
Tumor resection		No	35	9	0.100
		Yes	76	8	
Adjuvant Chemotherapy		No	20	3	0.680
		Yes	56	5	
Chemotherapy regimens		Gemcitabine	36	3	0.110
		FOLFIRINOX	16	0	
		FOLFIRI	1	0	
		Gemcitabine/nab-paclitaxel	17	5	
		FOLFIRIONX + Gemcitabine/nab-paclitaxel	1	2	
		FOLFOX	1	0	
		Gemcitabine/cisplatin	2	1	
		Gemcitabine/HAP	3	1	
		Unknown	14	2	
Plasma LCN2	Diagnosis		125.9 (46.8)	400.4(136.5)	<0.01

(ng/mL)			
CA19-9	929.6 (2845.4)	997.2 (2092.5)	0.93

Supplementary table 3. Related to Figure 7G. Patient demographics, treatment, and biomarker data dichotomized by a 240 ng/mL baseline Lcn2 threshold. Abbreviations: BMI, body mass index; NOS, not otherwise specified; HAP, hypoxic abdominal perfusion; FOLFIRINOX, 5-fluorouracil, leucovorin, irinotecan, and oxaliplatin; FOLFOX, 5-fluorouracil, leucovorin, and oxaliplatin; FOLFIRI, 5-fluorouracil, leucovorin, and irinotecan. RT, radiotherapy; CA19-9, cancer antigen 19-9. Standard deviation presented in parentheses where appropriate. P-values calculated using Student's t-test for continuous variables, $\chi 2$ or Fisher's Exact Test for categorical variables. When applicable, all statistical tests were two-tailed.

3. Discussion

The purpose of this work was to evaluate the role of Lcn2 in mediating the anorectic component of pancreatic cancer cachexia. Herein, we describe an immunometabolic pathway, in which bone marrow upregulation and secretion of Lcn2 results in appetite suppression through its action in the CNS. This direct effect on food intake results in an accompanying decrease in fat and lean mass in our rodent models (Figure 8). In humans, we observe a similar immunologic shift and upregulation of Lcn2 during the progression of pancreatic cancer. Although caloric intake is not readily captured in the clinic, we observed that an increase in circulating Lcn2 is associated with fat and lean mass loss by computational analysis of fat and lean tissue using

computed tomographic scans. Collectively, these studies support the notion that the pathologic upregulation of Lcn2 contributes to the development of cancer-associated anorexia and both fat and lean mass wasting.

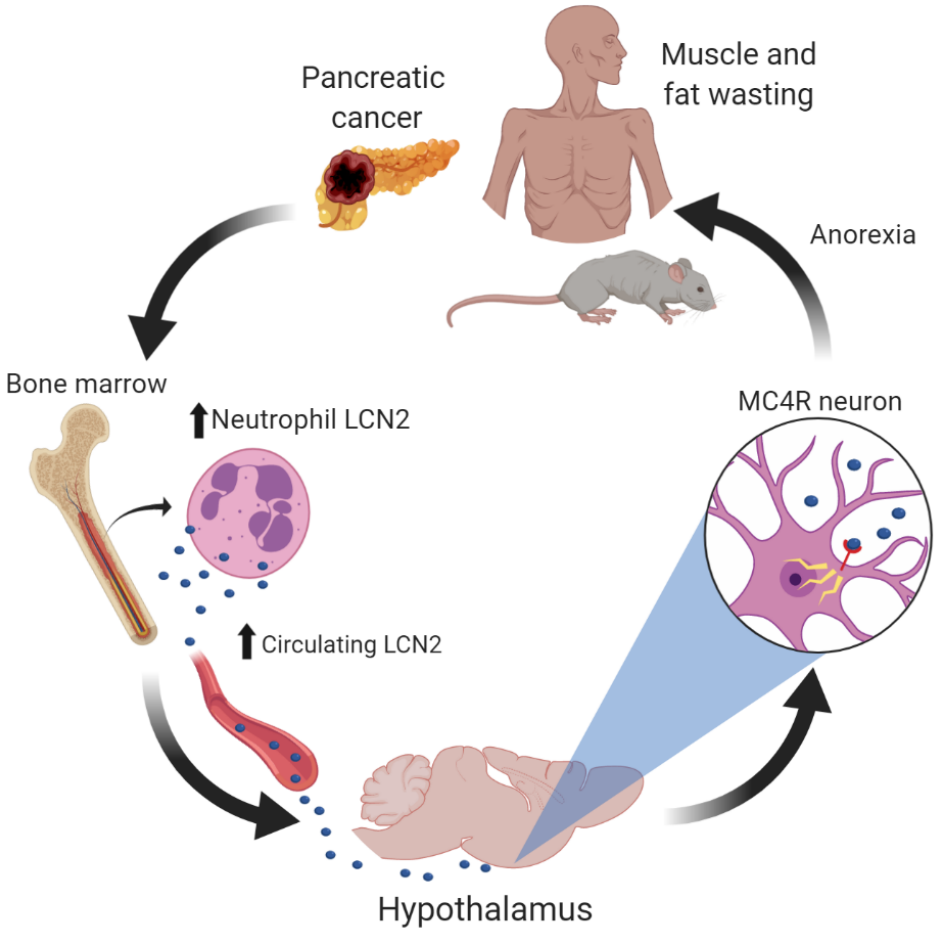

Figure 8. Graphical summary of findings. We report that the pathogenesis of pancreatic cancer cachexia is associated with increased circulating levels of Lcn2, which is an anorectic molecule that potentiates muscle and fat wasting associated with cachexia.

With the recent identification of Lcn2 as a neuroendocrine hormone that binds to MC4R under normal physiologic conditions, we sought to expand upon this axis in the context of appetite dysregulation during neoplastic disease (82). It is well described that Lcn2 is upregulated during infectious inflammatory conditions (97), and since systemic inflammation is a hallmark feature of cancer cachexia, we hypothesized that the underlying sterile inflammatory state would result in a sustained elevation of circulating Lcn2. Our data show a consistent elevation of circulating and central Lcn2 levels in five separate rodent models of pancreatic cancer that induce variable degrees of cachexia. This elevation in circulating and central Lcn2 levels is negatively correlated with food consumption and lean muscle mass. After our initial characterization of Lcn2 production across five separate models of cachexia, we focused on the well-characterized KPC model for ensuing genetic and pharmacologic studies. Since several inflammatory mediators are shown to regulate Lcn2 levels in various pathologies, we demonstrate that mice devoid of *IL-6* and *MyD88*, two inflammatory pathways known to mediate host metabolism during cachexia (351, 556), have reduced circulating Lcn2 levels, demonstrating Lcn2 is an inflammation-induced protein during cancer cachexia. We identified the bone marrow compartment as the largest source of Lcn2 protein. As the bone marrow is a primary lymphoid organ responsible for the generation of immune cells, we went on to identify neutrophils as a significant source of Lcn2 during cachexia. Notably, we also observed an increase in lung, liver, and splenic Lcn2 production during pancreatic cancer progression, likely attributable to increased neutrophilic infiltration during cachexia (560) and other systemic inflammatory states (561). Finally, RNA sequencing of circulating neutrophils of sham and tumor-bearing mice demonstrated a

significant increase in *lcn2* transcripts of cachectic mice. Taken together, the robust increase in neutrophil count, along with the modest elevation of intracellular Lcn2 levels and increase in *lcn2* expression in neutrophils, all support the notion that neutrophils are a significant source of circulating Lcn2 levels during cachexia.

We next showed that genetic deletion of *lcn2* significantly increased food consumption and modestly spared both lean and fat mass loss during pancreatic cancer cachexia. Notably, these appetite and tissue-sparing effects were independent of central and peripheral inflammatory status, as hypothalamic and hepatic inflammatory gene expression profiles were unchanged in mice with and without intact *lcn2* expression. We also showed that the muscle-sparing effects of *lcn2* deletion were independent of ubiquitin-proteasome and autophagy-related pathways, two well-described catabolic pathways associated with lean mass wasting during chronic disease (378, 379, 562-564). Furthermore, we did not detect significant alterations in white adipose browning genes *Ucp1, Cidea, Ppar-γ, and Prdm16*. Recent studies have also concluded that *lcn2* is dispensable in central and peripheral inflammatory response using LPS-based sepsis models (565). However, opposing studies exist, and suggest Lcn2 is a critical anti-inflammatory factor during sepsis (127), acute liver injury (98), and nephritic disease (566). Thus, the role of Lcn2 during disease is likely multifactorial and context-specific, with distinct physiologic roles depending on cellular source, underlying inflammatory insult, chronicity of disease, and molecular form of Lcn2 (bound or unbound to a siderophore-iron complex). Furthermore, these disparate findings suggest that alternative epigenetic or post-translational regulation could be involved in the regulation and function of Lcn2 during states of metabolic stress. As it relates to the

well-defined role of Lcn2 in iron trafficking (97, 567), Song and colleagues identified that holo-Lcn2 (Lcn2 bound to a bacterial siderophore-iron complex) promotes the generation of reactive oxygen species to impair oxidative phosphorylation in rat cardiomyocytes (161). However, apo-Lcn2 (Lcn2 moiety alone) did not alter mitochondrial processes, demonstrating distinct molecular roles for the two forms of Lcn2 (161). Future studies should account for apo- and holo- forms of Lcn2 when discussing biological significance during disease. As it relates to the present study, it is likely that Lcn2 exists almost exclusively in the apo- form in our cachexia models, as we have no evidence of bacterial proliferation during disease progression.

There is support for appetite and macromolecule regulating effects of Lcn2 in disease models associated with systemic inflammation. *lcn2-KO* animals fed high fat diets display a consistent increase in food consumption (568), while other reports suggest Lcn2 plays a direct role in insulin sensitivity and glucose metabolism (82, 569-571). Since restricted feeding and caloric restriction are effective in improving metabolic stress during disease (572-574), it is plausible that Lcn2 upregulation during diet-induced obesity is an adaptive response that serves to reduce appetite and improve glucose handling. Our data are seemingly consistent with this idea of a prolonged inflammatory state (pancreatic cancer) increasing Lcn2 production to regulate appetite. However, our data agree with prior reports suggesting that the reduced caloric intake during pancreatic cancer is detrimental, as the catabolic and energy-wasting programs of cachexia logically require increased caloric intake to achieve organismal energy homeostasis (6, 38).

With recent literature demonstrating that Lcn2 binds to the MC4R in mediobasal hypothalamic neurons (82), we tested whether disruption of this signaling cascade through ICV injection of AgRP, an inverse agonist of MC4R, would improve appetite during cachexia progression. Similar to *lcn2-KO* tumor-bearing mice, AgRP-treated mice demonstrated a significant improvement in food intake and modest improvements in muscle mass. Consistent with *lcn2-KO* tumor-bearing mice, ICV AgRP treatment did not alter ubiquitin-ligase or autophagy related catabolic pathways in skeletal muscle or cardiac tissue, suggesting that improved caloric intake improves muscle mass through alternative pathways during cachexia. Using an adoptive transfer technique that spares the integrity of the BBB, we demonstrate that reintroducing Lcn2 production in the bone marrow compartment alone results in a large induction of Lcn2 in the circulation and brain, validating that peripherally-derived Lcn2 readily crosses the BBB (82). Furthermore, restoration of *lcn2* in the bone marrow compartment is sufficient to rescue the cachexia-anorexia phenotype. Since we consistently observe a muscle-sparing effect in tumor-bearing animals devoid of Lcn2, we investigated whether this improvement in muscle mass is mediated by improved food intake or through a direct effect of Lcn2 on muscle. To address this, we pair-fed tumor-bearing *lcn2-KO* mice to their tumor-bearing WT counterparts, and observed equivalent skeletal and cardiac tissue mass at the end of the study.

We then explored the biological significance of our observations in human pancreatic cancer. Similar to our preclinical model, we observed a close association between increasing neutrophils and increased circulating Lcn2 levels, suggesting neutrophil expansion is accompanied by increased Lcn2 production and secretion.

Conversely, the opposite trend was observed in the lymphocyte population, with increased circulating lymphocytes being associated with decreased Lcn2 levels. Indeed, increased neutrophil-to-lymphocyte ratio is associated with worsened morbidity and mortality outcomes for patients with pancreatic cancer (575, 576). For patients that had consecutive positron emission tomographic (with computed tomographic) scans and accompanying blood draws, we performed skeletal muscle and visceral fat analyses at the level of the third lumbar vertebrae to define cross sectional area. Using these data, we identify a close negative correlation between changes in circulating Lcn2 levels and loss of both fat and skeletal muscle mass. Since caloric intake is not readily captured in the clinic, we took a logical step in assessing both fat and muscle mass, tissues that are particularly sensitive to prolonged caloric deprivation during chronic disease (577). Thus, it is conceivable that the fat and lean mass loss we observed in patients with elevated Lcn2 levels is partially due to a decrease in appetite and food intake through the molecule's anorectic effects in the brain, as this is the case in our preclinical models. Finally, after dichotomizing pancreatic cancer patients into high (>240 ng/mL) and low (<240 ng/mL) Lcn2 levels at diagnosis, we observed that patients with elevated Lcn2 at the time of diagnosis had reduced overall survival.

Taken together, key observations we make in our rodent models, including neutrophil expansion, increased circulating Lcn2, and lean mass loss, also occur in patients with pancreatic cancer. Indeed, an elevation of the neutrophil to lymphocyte ratio (NLR) is shown to predict poor prognosis in patients with both resectable and unresectable pancreatic cancer (578, 579). It is hypothesized that an elevation in circulating neutrophils may suppress the activity of cytotoxic T cells and other adaptive

immune cell responses, an immunologic shift that could lessen systemic therapeutic efficacy and promote metastatic progression (580). While most of the literature concerning innate and adaptive immunity in an oncologic setting are focused on immune cells influencing the tumor itself, little is known about how, or if, engagement of the immune system in normal tissue during cancer influences cachexia and tissue wasting. It is clear that an elevation of NLR is associated with poor prognosis in several cancer types, yet, to our knowledge, no mechanistic studies explain (1) how this immunologic shift occurs or (2) what facets of this immunologic shift contribute to, or improve, disease symptoms. Sarcopenia, or lean mass wasting, is richly described as a negative prognostic marker in nearly all neoplastic diseases, including pancreatic cancer (581). However, the mechanisms that drive muscle and fat wasting during disease are incompletely understood. Based on our data, we would propose that the increased Lcn2 levels, partly as a result of neutrophil expansion and increased expression of *lcn2* during cachexia, partially explain the increased morbidity and mortality outcomes of cancer patients through its effects on caloric intake and subsequent lean and fat mass wasting.

In summary, the data presented here illustrate that pancreatic cancer-associated Lcn2 mediates appetite suppression through its actions in the CNS. Despite having recognized cachexia as a serious medical problem for over a thousand years (582), effective therapies remain elusive. The development of cancer ominously influences homeostatic control of energy balance through alterations in resting metabolic tone and, in many cancers associated with cachexia, energy intake. It stands to reason that prolonged anorexia, a sickness behavior frequently observed in patients suffering from

cachexia, is not a sustainable strategy for combating neoplastic disease and contributes to ultimate mortality. While improving nutritional intake is likely to improve quality of life and, in some cases, lessen lean and fat wasting, a 2011 international consensus recognized that conventional nutritional support alone is inadequate in treating cachexia (6, 8). Thus, as with most diseases associated with cachexia, we believe addressing nutritional deficiencies is an important facet of treating cachectic patients, but is not a comprehensive approach for improving all cachexia symptoms, including muscle and fat wasting. Nevertheless, identification of factors that influence this seemingly maladaptive anorectic response to pancreatic cancer remains an important component of improving patient outcomes. Based on our data presented here, we propose Lcn2 as a potential therapeutic target for the improvement of appetite during pancreatic cancer cachexia.

Limitations

Here, we have shown that Lcn2 is elevated during pancreatic cancer in humans and mice and induces appetite suppression through its actions in the CNS. However, a limitation of this study is that it is unclear if Lcn2 regulates appetite during other chronic diseases associated with cachexia, or if there are permissive factors in the appetite-regulating effects of Lcn2 that are specific to pancreatic cancer. Although we do not observe a difference in disease burden between WT and *lcn2-KO* groups through terminal tumor mass or histologic features of the cancer, it is possible that Lcn2 affects tumor growth as described previously (550). The orthotopic model we employed is rapidly progressive, and may not allow enough time to recapitulate this finding. However, since we and others observe an independent effect of Lcn2 on appetite when

administered to the CNS (82), and if Lcn2 blockade also mitigates tumorigenesis, these observations only bolster the notion that targeting Lcn2 during pancreatic cancer could prove beneficial through multiple therapeutic means. While we believe the majority of Lcn2 during cachexia is neutrophil-derived, it is conceivable that our bone marrow transplantation experiments also repopulated bone-resident cells (583, 584). In this case, it is plausible that bone-derived Lcn2, as described previously (82), contributes significantly to circulating levels during cachexia.

4. Methods

Mice

C57BL/6J wild type (WT, JAX catalog number 000664), Lipocalin 2 knockout (*lcn2-KO*, JAX catalog number 024630), Melanocortin 4 receptor knockout (*Mc4r*-KO, JAX catalog number 032518), Interleukin 6 knockout (*Il-6*-KO, JAX catalog number 002650), and Myeloid differentiation primary response gene 88 knockout (*MyD88*-KO, JAX catalog number 009088) mice were purchased from The Jackson Laboratory (Bar Harbor, ME) and maintained in our animal facility. All mouse strains used in this paper were generated on a C57BL/6J background. All mice were housed and bred in a dedicated mouse room with a temperature 26˚C with a 12-hour light/dark cycle. Animals were provided *ad libitum* access to food and water (Rodent Diet 5001; Purina Mills) unless otherwise stated. Mice were genotyped according to the standard protocol from The Jackson Laboratory. Sex-, age-, and body weight-matched WT and *lcn2-KO* (as well as

Il-6-KO and *MyD88-KO*) mice at 7-10 weeks old were used unless otherwise stated. Only age-and sex-matching was possible with *Mc4r-KO* due to their profound obesity phenotype. In behavioral studies, animals were individually housed for acclimation at least 7 days prior to procedures. Except in survival studies, tumor-bearing animals were euthanized according to the end points of tumor study policy. Mouse studies were conducted in accordance with the National Institutes of Health Guide for the Care and Use of Laboratory animals, and approved by the Institutional Animal Care and Use Committee (IACUC) of Oregon Health & Science University.

Human samples

After IRB review, human plasma samples obtained in this study were deemed non-human subjects research due to their retrospective and anonymized nature. Plasma samples from men and women age 40-82 years old diagnosed with pancreatic cancer were procured through the Brenden Colson Center for Pancreatic Care (Portland, Oregon) through the Oregon Pancreatic Tumor Registry (OPTR). These samples were collected at the time of diagnosis, and for some patients, in follow-up visits. Age- and sex-matched control samples were procured from the Oregon Clinical and Translational Research Institute. Briefly, blood was drawn through venipuncture and plasma and the buffy coat were separated. Samples were then stored at -80˚C until assayed.

Pancreatic ductal adenocarcinoma cachexia models

The five separate models of PDAC cachexia utilized herein are clonogenic cell lines derived from separate C57BL/6J mice with pancreatic-specific conditional alleles

$KRAS^{G12D}$ and $TP53^{R172H}$ expression driven by the PDX-1-Cre promoter. Since the KPC model is a highly characterized and published model of PDAC cachexia due to its close biological semblance of human disease, we performed all subsequent studies (Figures 2-6) utilizing this model generously provided by Dr. Elizabeth Jaffee (38, 556, 585, 586). The remaining four PDAC cell lines were generously provided by Drs. David Tuveson (FC1242, FC1199, and FC1245) and Robert Vonderheide (4662). All cell lines were maintained in RPMI 1640 supplemented with 10% fetal bovine serum, 1% minimum essential medium non-essential amino acids, 1 mM sodium pyruvate, and 50 U/mL penicillin/streptomycin (Gibco), in cell incubators maintained at 37˚ Celsius and 5% CO_2. All cell lines were routinely tested and confirmed negative for mycoplasma contamination. Under isoflurane anesthesia, a small surgical incision was made in the upper-left quadrant of the abdomen, reflecting the skin layers, fascia, and muscle wall to expose the pancreas. The tail of the pancreas was injected with either 1 million cancer cells suspended in 40 ul of PBS or an equal volume of cell-free PBS. After tumor implantation, the abdominal wall and fascia layers were sutured, followed by two surgical skin clips to close the incision site.

Analysis of cachexia

Food intake, body mass, and post-procedure health status were monitored daily, with sifting of bedding to collect spilled food. Voluntary wheel running was measured continuously utilizing low-profile running wheels (Med Associates Inc) and lab-constructed wheels. In pair-feeding experiments, *lcn2-KO* mice were implanted with KPC cells one day behind to WT KPC mice, and were pair-fed daily with the amount of

food that WT KPC mice consumed within the previous 24 hours. Survival in KPC mice was observed twice daily until death, and tumor appearance was confirmed by necropsy. Necropsy tissue analysis included tumor, gastrocnemius, and heart mass by observers blinded to treatment groups. Additionally, hypothalamus, heart, gastrocnemius, and liver tissues were immediately flash frozen for gene expression analysis.

Nuclear magnetic resonance imaging

Nuclear magnetic resonance (NMR) measurements were taken at baseline (day of tumor implantation), as well as early (day 4), mid (day 8), and late cachexia (day 11) according to the manufacturers protocol (EchoMRI LLC, Houston, TX).

Fecal analyses

Fecal lipids were harvested and analyzed using a protocol modified from Kraus et al. (587). Briefly, cage-collected feces were collected using a sieve and pulverized using a pepper grinder. Finely ground feces then underwent a chloroform:methanol (2:1) extraction via centrifugation at 1,300 x g for for 20 min at RT. After the phase reaction, the organic phase containing the extracted lipids were collected and allowed to evaporate.

Fecal protein concentration was determined using a procotol adapted from Danai et al. (546). Briefly, 10 mg of pulverized feces was resuspended in 500 uL of lysis buffer (2% SDS, 150 mM NaCl, 0.5 M EDTA), sonicated, and centrifuged at 10,000 rpm for 15 mins at 4C. The protein concentration was then assessed using a BCA assay according to the manufacturer's instructions.

Fecal protease activity was determined from fresh terminal colonic feces at the time of sacrifice. Briefly, feces were suspended to a 10 mg/mL suspension in Protein Buffer A (0.1% Triton X-100, 0.5M NaCl, 100mM $CaCl_2$), homogenized and sonicated, then centrifuged at 14,000 RPM for 15 minutes. 100 uL of the resulting supernatant was added to 200 uL of 3% azocasein, vortexed briefly and incubated for 1 hour at 37C. After incubation, 500 uL of 8% tri-chloroacetic acid was added to each sample, vortexed, centrifuged at 9,000 RPM for 5 minutes, and the resulting supernatant was assayed for absorbance at 366 nm.

Bone marrow transplantation

WT and *lcn2-KO* mice aged 8-12 weeks were administered the alkylating chemotherapeutic treosulfan (Ovastat®, a generous gift provided by Joachim Baumgart at Medac GmbH, Germany) at a dose of 1,500 mg/kg/day for 3 days prior to bone marrow transplantation (BMT). Donor bone marrow was harvested from 8-12 week old WT, *lcn2-KO*, or Ly5.1-EGFP mice from femurs, tibias, and humeri by flushing dissected bone cavities with Isocove's modified Dulbecco's medium supplemented with 10% FBS. Bone marrow preparations were then treated with RBC lysis buffer and filtered across a 70 µm cell strainer. $3x10^6$ cells were resuspended in 200 µL HBSS and injected through the tail vein of recipient mice. After initiation of treosulfan treatment, mice received amoxicillin supplemented water (150 mg/L) for two weeks to prevent infection. All mice were allowed a minimum of 8 weeks of recovery after BMT to ensure successful bone marrow engraftment with daily monitoring for signs and symptoms of graft rejection.

Chimerism was determined at the end of animal experiments by blood flow cytometry analysis.

Intracerebroventricular cannulation and injections

Mice were anesthetized using isoflurane and gently placed on a stereotactic alignment instrument (Kopf Instruments). Using sterile technique, bregma was exposed with a 3 mm incision and a 26-gauge lateral ventricle cannula was placed at 1.0 mm X, -0.5 mm Y, and -2.25 mm Z relative to bregma. Cannulas were secured to the skull with embedded screws and crosslinked flash acrylic. Mice were allowed one week for recovery after cannulation surgery. Recombinant mouse Lcn2 (R&D Systems, 40 ng), AgRP (Phoenix Pharmaceuticals, 1 nmol), and MT-II (Phoenix Pharmaceuticals, 1 nmol) were diluted in artificial CSF and injected in a total volume of 2 uL. For repeated or single injection experiments of Lcn2, MT-II, and vehicle, mice received injections under restriction, and received restriction training 5 days prior to initial injections. For ICV AgRP studies, all mice were conditioned to isoflurane anesthesia for 4 days prior to AgRP or vehicle injections.

Cerebrospinal fluid extraction

Mice were anesthetized using isoflurane and placed on a stereotactic alignment instrument (Kopf Instruments). A 2 cm incision was made over the cisterna magna and the trapezius and paraspinal muscles were reflected. Blood and extracellular fluid lying over the cisterna magna were carefully removed to avoid CSF contamination. A glass

micropipette (tip diameter of approximately 400-800 μm) was stereotactically inserted into the cisterna magna for capillary action-based CSF collection.

Histology and immunohistochemistry

Mice were deeply anesthetized using a ketamine/xylazine/acepromazine cocktail and sacrificed by transcardial perfusion with 20 mL PBS followed by ice cold 4% paraformaldehyde (PFA). Tissues were post-fixed in 4% PFA overnight at 4˚C prior to sectioning protocols. **Tumor and inguinal white adipose tissue samples**: paraffin embedded histological sections were stained for hematoxylin and eosin, followed by followed by 10 μM cryostat sectioning. **Bone marrow samples**: transferred to 70% ethanol for 4 hours prior to a gentle decalcification (Decal™, StatLab) for 1 hour. Bone was then paraffin embedded, cryostat sectioned to 50 uM, blocked for 30 minutes in blocking solution (5% normal donkey serum in 0.01 M PBS and 0.3% Triton X-100), followed by VENTANA staining (Roche) with primary and secondary antibodies (listed below). **Brain samples:** after post-fixation, brains were cryoprotected in 20% sucrose for 24 hours at 4˚C prior to 30 μM microtome sectioning. Free-floating sections were incubated in blocking solution (see bone marrow) for 1 hour at room temperature, followed by primary antibody incubation (listed below) overnight at 4˚C. Sections were thoroughly washed with PBS between steps. Sections were mounted on gelatin-coated slides and coverslipped with Prolong Gold anti-fade media (Thermofisher).

Fluorescent-based images were acquired on a Nikon confocal microscope, while chromogen-based images were acquired using a Leica microscope (model DM 4000B).

cFos-positive cells were quantified in the paraventricular nucleus of the hypothalamus in three consecutive sections and averaged by a blinded observer.

Primary antibodies utilized above are listed with company, clone, host, species, and concentration defined in parentheses, respectively: Lcn2 (R&D Systems, AF1857, goat, 1:800) and cFos (Santa Cruz, sc-166940, goat, 1:25000). A donkey anti-goat AF488 (1:500) secondary antibody from Invitrogen was utilized for fluorescent images, while a horse anti-goat IgG (peroxidase) from VECTOR laboratories (MP-7405-15) was used for bone marrow chromagen-based imaging.

Enzyme linked-immunosorbent assays

Whole blood was harvested from mice by cardiopuncture and plasma was isolated using K_2EDTA tubes (BD 365974). Mouse plasma and CSF Lcn2 concentrations were assayed by ELISA according to the manufacturer's protocol (R&D Systems, Catalog # DY1857). Human plasma Lcn2 concentrations were assayed by ELISA according to the manufacturer's protocol (R&D Systems, Catalog # DY1757).

Flow cytometry

Mice were anesthetized using a ketamine/xylazine/acepromazine cocktail and whole blood was collected by cardiopuncture. 200 µL of whole blood was then treated with 1x RBC lysis buffer (Invitrogen) for 10 minutes then incubated in 100 µL of PBS containing antibodies for 45 minutes at 4˚C. For intracellular Lcn2 staining, cells were then fixed and permeabilized for 10 minutes, washed with 1x permeabilization buffer (Invitrogen), and stained with primary antibody for 45 minutes at 4˚C. Cells were stained with a

secondary antibody for 1 hour at 4˚C and resuspended in 200 µL of RPMI +5% FBS for analysis. Cells were thoroughly washed between steps with either RPMI +5% FBS (prior to fixation/permeabilization) or 1x permeabilization buffer (after fixation/permeabilization).

Antibodies and reagents utilized for flow cytometry analysis can be found in **supplementary table 4**. All flow cytometry was performed on a BD LSR II and data were analyzed in FlowJo software.

Quantitative real time PCR

Snap-frozen tissues were rapidly homogenized and RNA was purified with the RNeasy Mini Kit (Qiagen). Samples were then reverse-transcribed with the High Capacity cDNA Reverse Transcription Kit (Life Technologies). qRT-PCR was performed using reagents and TaqMan primer probes listed in **supplementary table 5**. Tissues were normalized to 18S using the ddCT method.

Western blot

Protein was extracted from snap-frozen tissues by homogenization followed by brief sonication. 60 µg of protein was loaded in each lane and run on Novex 6-18% Tris-Glycine gels (Life Technologies). Gels were transferred to PDVF membranes (Millipore) and blocked with 5% BSA for 1 hour. Membranes were incubated with primary antibodies overnight at 4˚C with gentle agitation. Blots were then washed with TBST and incubated in secondary antibodies for 1 hour prior to imaging using the Li-Cor

Odyssey imaging system. A complete list of antibodies and reagents can be found in **supplementary table 6**.

RNA-seq of circulating neutrophils

Whole blood was isolated from mice by cardiopuncture, and total RNA was isolated from FACS-sorted $CD11b^{high}Ly6G^{high}$ neutrophils using an RNAeasy Plus Micro kit (Qiagen). Integrity of RNA was verified by an Agilent Bioanalyzer prior to cDNA preparation using the SMART-Seq v4 Ultra Low Input kit (Takara). RNA libraries were prepared using a TruSeq DNA Nano kit (Illumina) and verified by Tapestation (Agilent). Library concentrations were measured by real-time PCR with StepOnePlus Real Time PCR System (ThermoFisher) followed by a Kapa Library Quantification Kit (KapaBiosystems/Roche). Libraries were then sequenced with a 100 cycle single-read protocol using a HiSeq 2500 sequencer (Illumina). Quality control checks were performed using the FastQC package and raw reads were normalized using the DESeq2 Bioconductor package.

Computed tomography-based body composition analysis

Access to CT scans was approved by the OHSU IRB, as all patients were consented to the OPTR protocol. For each patient, a single contrast-enhanced axial image at the third lumbar vertebrae (L3) was selected, anonymized, and saved in DICOM format using Osirix (Pixmeo). The images underwent first-pass segmentation by an automated algorithm in MATLAB R2016a (MathWorks) (588), which labels skeletal muscle and visceral fat based upon its pre-established radiodensity range (−29 to +150 and −190 to

−30 Hounsfield Units, respectively) (558, 589). The images were then processed with Sliceomatic 5.0 (Tomovision) for manual corrections. Skeletal muscle index (SMI) and normalized visceral fat measures for each patient was calculated by dividing total skeletal muscle and fat cross-sectional area at L3 (cm^2) by patient height squared (m^2).

Statistics

All statistical analyses for murine data were performed in GraphPad Prism 8.0 software. Quantitative data are reported as mean +/- standard error. Two-tailed Students t-tests were performed when comparing two groups. When comparing more than two groups of a single genotype, One-way ANOVA was utilized. Correlation analysis were performed after assessment of normality using Shapiro-Wilk tests, demonstrating all data analyzed followed a Gaussian distribution (Pearson correlation, parametric data). Two-way ANOVA with Bonferroni multiple comparisons test was utilized when comparing multiple genotypes and treatment groups (sham and tumor) unless otherwise specified in figure legends. Data from human studies were analyzed using both GraphPad Prism 8.0 and IBM SPSS Statistics Suite (version 25), with Kaplan Meier survival curve comparison using log-rank Mantel-Cox test. Determination of dichotomizing cutpoints of plasma Lcn2 levels and survival outcomes utilized the Evaluate Cutpoints adaptive algorithm software in RStudio as described previously (559). For all analyses, a p value of < 0.05 was considered to be statistically significant. All measurements were from distinct samples and not taken from the same sample more than once.

Acknowledgments

We thank members of the Oregon Clinical and Translational Research Institute and Brenden Colson Center for Pancreatic Care for providing pancreatic cancer blood samples. We thank Drs. Elizabeth Jaffee (KPC), David Tuveson (FC1242, FC1199, and FC1245), and Robert Vonderheide (4662) for graciously providing the syngeneic pancreatic cancer cell lines used for our studies. The graphical abstract and panel A of Figure 4 were made using BioRender (BioRender.com). Finally, we thank Ashley J Olson, PA-C for technical assistance with the ICV AgRP study. This work was supported by NIH R01CA217989 (Marks), the Brenden-Colson Center for Pancreatic Care at OHSU (Marks), and NIH 1F30CA254033-01 (Olson).

DM is a consultant for Pfizer, Inc. This potential COI is managed by the Oregon Health & Science University integrity office.

Author contributions

B.O. and D.M. designed the study, analyzed the data, and wrote the manuscript with input from the other authors. B.O., X.Z., M.N., P.L., J.B., A.B., K.P., H.M., and S.K. performed experiments and analyzed data. K.B., K.M., J.E., and A.G. contributed with discussion, data abstraction, and data interpretation.

Data availability

All data associated with this study are available in the main text or the supplementary materials. Extended information associated with flow cytometry are available as a Source Data file.

Code availability

Custom code associated with this manuscript, created by Ogulszka and colleagues, is publicly available through their associated manuscript (559).

Chapter 4: Chronic cerebral lipocalin 2 exposure elicits hippocampal neuronal dysfunction and cognitive impairment

A manuscript in review

Chronic cerebral lipocalin 2 exposure elicits hippocampal neuronal dysfunction and cognitive impairment

Brennan Olson[1,2], Xinxia Zhu[1#], Mason A Norgard[1#], Parham Diba[1, 2], Peter R Levasseur[1], Abby C Buenafe[1], Christian Huisman[1], Kevin G Burfeind[1,2], Katherine A Michaelis[1,2], Garth Kong, Theodore Braun, *Daniel L Marks[1,3,4]

1. Papé Family Pediatric Research Institute, Oregon Health & Science University, Portland, OR USA
2. Medical Scientist Training Program, Oregon Health & Science University, Portland, OR USA
3. Brenden-Colson Center for Pancreatic Care, Oregon Health and & Science University Portland, OR USA
4. Knight Cancer Institute, Oregon Health & Science University, Portland, OR USA

# These authors contributed equally to this work

**Corresponding Author Information*

Daniel L. Marks, MD, PhD

3181 SW Sam Jackson Park Road

L 481

Portland, OR 97239

Email: marksd@ohsu.edu

Abstract

Lipocalin 2 (Lcn2) is a pleiotropic molecule that is induced in the central nervous system (CNS) in several acute and chronic pathologies. The acute induction of Lcn2 evolved as a beneficial process, aimed at combating bacterial infection through the sequestration of iron from pathogens, while the role of Lcn2 during chronic, non-infectious disease remains unclear, and recent studies suggest that Lcn2 is neurotoxic. However, whether Lcn2 is sufficient to induce behavioral and cognitive alterations remains unclear. In this paper, we sought to address the role of cerebral Lcn2 on cognition in both acute and chronic settings. We demonstrate that Lcn2 is robustly induced in the CNS during both acute and chronic inflammatory conditions, including LPS-based sepsis and cancer cachexia. *In vivo,* LPS challenge results in a global induction of Lcn2 in the central nervous system, while cancer cachexia results in a distribution specific to the vasculature. Similar to these *in vivo* observations, *in vitro* modeling demonstrated that both glia and cerebral endothelium produce and secrete Lcn2 when challenged with LPS, while only cerebral endothelium secrete Lcn2 when challenged with cancer-conditioned medium. Chronic, but not short-term, cerebral Lcn2 exposure resulted in reduced hippocampal neuron density, an increase in newborn neurons, microglial activation, and increased CNS immune cell infiltration. RNA sequencing analyses of primary hippocampal neurons revealed a distinct transcriptome associated with prolonged Lcn2 exposure, and ontology analysis was suggestive of impaired neuronal function and abnormal spatial learning. Indeed, mice exposed to prolonged cerebral Lcn2 levels experienced a reduction in spatial reference memory as

indicated by Y-maze assessment. These findings implicate Lcn2 as a pathologic mediator of cognitive decline in the setting of chronic disease.

Keywords: Lipocalin 2, hippocampus, cognitive decline, spatial reference memory, cachexia, sepsis, gliosis

1. Introduction

Neurocognitive decline is a common feature in patients suffering from chronic inflammatory diseases, including primary neurodegenerative diseases, cancers, and autoimmune manifestations (165, 590, 591). Since cognitive decline reduces quality of life and ultimate survival, identification of novel mediators and pathways that incur cognitive deterioration is imperative in improving patient outcomes. As the population continues to age, the prevalence of disease-related cognitive decline will continue to rise, further necessitating the development of rational drug targets.

To this end, several studies describe elevated levels of Lipocalin 2 (Lcn2) in the central nervous system (CNS) during both acute and chronic insults (122, 127, 565), yet the literature is discordant concerning the biological role of Lcn2 on behavioral and cognitive processes during disease (127, 565). Since Lcn2 is richly described as an anti-bacterial protein through its siderophilic properties, the acute induction of Lcn2 during infectious disease is described as a beneficial process for clearing the pathogen (97). However, in the context of chronic, non-infectious inflammatory conditions, the precise role of Lcn2 is less clear, and recent evidence suggests Lcn2 may be neuropathological (112, 592). Given the clear utility of Lcn2 in the context of acute disease, yet unclear role in a prolonged disease setting, we sought to address the temporal role of Lcn2 on central nervous system (CNS) health and cognitive function.

Herein, utilizing both *in vivo* and *in vitro* models, we demonstrate that Lcn2 is induced and secreted in the CNS in the context of LPS and pancreatic cancer cachexia, with a unique neuroanatomical distribution dependent on the inflammatory insult. Mice given chronic intracerebrovascular (ICV) Lcn2 displayed a reduction in hippocampal

density of mature neurons, while concurrently demonstrating an increase in newborn dentate gyrus neurons. In addition to hippocampal neuronal alterations, mice receiving ICV Lcn2 displayed an increase in hippocampal microglia, as well as an increase in lymphoid and myeloid cells in the velum interpositum (VI) and nearby hippocampal structures. We observe a distinct transcriptional profile in primary hippocampal neurons treated with Lcn2 that demonstrates an unambiguous temporal effect of Lcn2 exposure on the transcriptome, with an associated ontology analyses of abnormal spatial learning. Finally, mice receiving chronic ICV Lcn2 demonstrated a reduction in spatial reference memory as indicated by Y-maze assessment. Our results implicate cerebral Lcn2 as a pathologic mediator of cognitive decline in the setting of chronic, but not acute, exposure.

2. Results

Lcn2 *is robustly upregulated in the central nervous system during chronic and acute disease*

While Lcn2 is known to be induced in the CNS during inflammatory conditions (116, 129), its neuroanatomical distribution and cellular source is widely variable depending on the underlying pathology. Using both chronic (cancer cachexia) and acute (LPS-based sepsis) murine models of neuroinflammation, we identified unique patterns of *lcn2* expression in the CNS. Specifically, *lcn2* is upregulated in the cerebral

vasculature during cancer cachexia (Figure 1a), while LPS-sepsis resulted in an expression pattern that is consistent with global expression, including both vasculature and glial expression (Figure 1a). On closer examination, we noticed a particular region of high *lcn2* expression immediately ventral to the hippocampal formation under cachectic conditions (Figure 1b). By immunohistochemistry (IHC), we confirmed Lcn2 staining in the cerebral vasculature during cachexia through its localization to CD31+ endothelial cells (Figure 1c-d; Supplementary figure 1), while we observe both vessel and diffuse parenchymal staining during LPS-based sepsis (Figure 1c-d). Utilizing a neuroinflammation transcript panel, we indeed identified *lcn2* as the most highly expressed gene in the hippocampus of cachectic mice (Figure 1e), while it was previously demonstrated that *lcn2* is the most elevated protein in the CNS after LPS challenge(127). Finally, we also detect a large induction of Lcn2 in the cerebrospinal fluid (CSF) during both cachexia and LPS (Figure 1f), suggesting that CNS cells not only produce, but also secrete Lcn2 during acute and chronic inflammatory conditions.

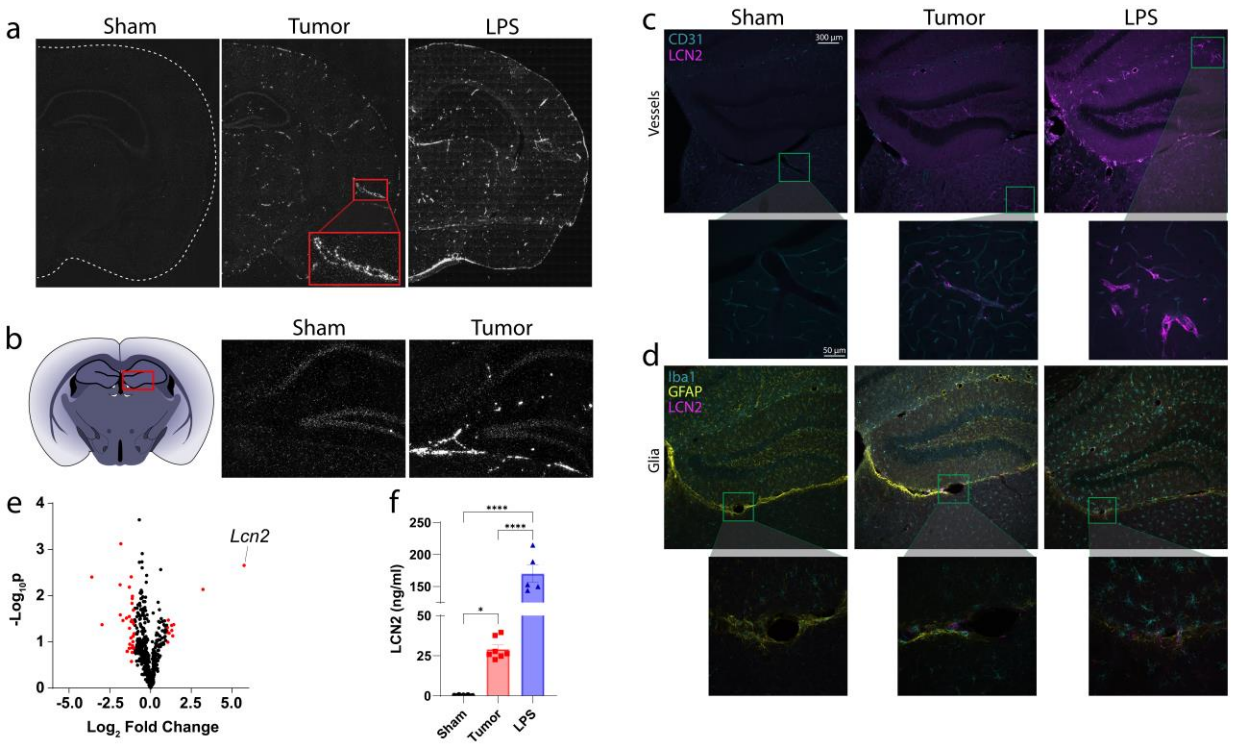

Figure 1. Lipocalin 2 is robustly upregulated in the central nervous system during LPS-based sepsis and cancer cachexia. (a) Representative coronal images of *In situ* hybridization of the brain of sham-operation controls, cancer cachexia, and LPS treated mice. (b) *lcn2 In-situ* hybridization of the velum interpositum in sham operation controls, cancer cachexia, and LPS treated mice. (c) Representative immunohistochemistry images staining for CD31+ blood vessels (teal) and Lcn2 (magenta), and (d) Iba1+ microglia (teal), GFAP+ astrocytes (yellow), and Lcn2 (magenta) in sham operation controls, cancer cachexia, and LPS treated mice. (e) Inflammation-related transcript expression in the hippocampus of cancer cachexia mice compared to sham-operation controls using Nanostring™ neuroinflammation gene panel (n = 3 per group). (f) Terminal CSF levels in sham operation controls (n = 5), cachectic (n = 7) or LPS-treated (n = 5) mice. Data in (e) are expressed as mean ± SEM. Data represented in (e) were

analyzed with one-way ANOVA with Bonferroni multiple comparisons. *p ≤ 0.05 and ****p ≤ 0.0001. LPS = lipopolysaccharide.

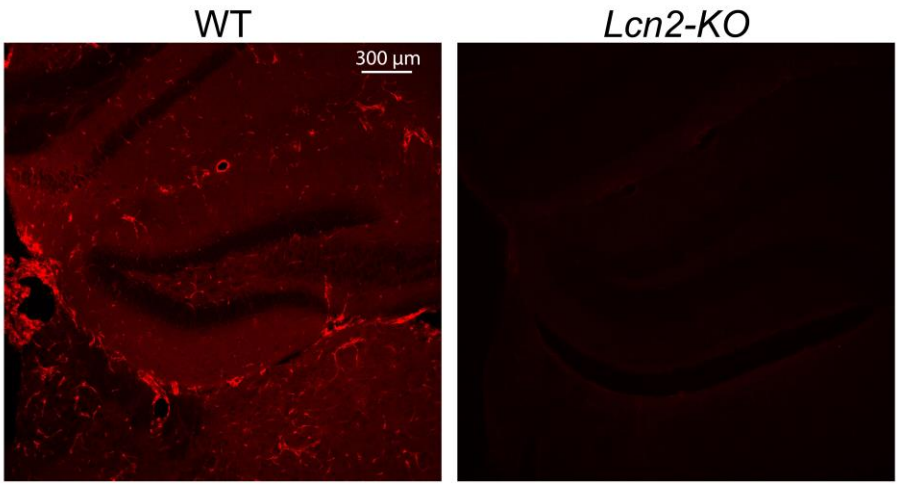

Supplementary Figure 1. Related to figure 1. Confirmation of Lcn2 antibody specificity by IHC in WT and *lcn2*-KO mice were injected with 200 µg/kg LPS. Images representative of 3 independently injected mice.

Soluble tumor factors induce* Lcn2 *production and secretion in brain endothelial cells, while LPS results in both endothelial and glial expression patterns

Since we observed a robust induction of Lcn2 in the brain in the context of both acute and chronic inflammatory disease, we sought to model Lcn2 expression and secretion patterns in response to the respective *in vitro* inflammatory stimuli (pancreatic cancer or LPS). Specifically, we treated bEnd.3 brain endothelial cells and primary

mixed glia with either cancer conditioned medium or LPS and performed an array of molecular assays to determine the expression, production, and secretion profiles of Lcn2 in response to these inflammatory challenges (Figure 2a). As observed *in vivo*, we observe a specific amplification of *lcn2* in cultured brain endothelial cells, but not glia, in the context of cancer challenge by conditioned medium (CM; Figure 2b). Protein production and secretion patterns follow this RNA expression profile closely, as endothelium, but not glia, robustly produce and secrete Lcn2 in response to CM (Figure 2c-e). Conversely, we observed a significant upregulation of *lcn2* in both endothelium and mixed glia in response to LPS challenge (Figure 2b), with a concurrent increase in Lcn2 production and secretion (Figure 2c-e). These data confirm the unique expression and production pattern of Lcn2 in the brain of mice under cachectic and LPS-treated conditions and suggests Lcn2 may serve a distinct biological role amongst these conditions.

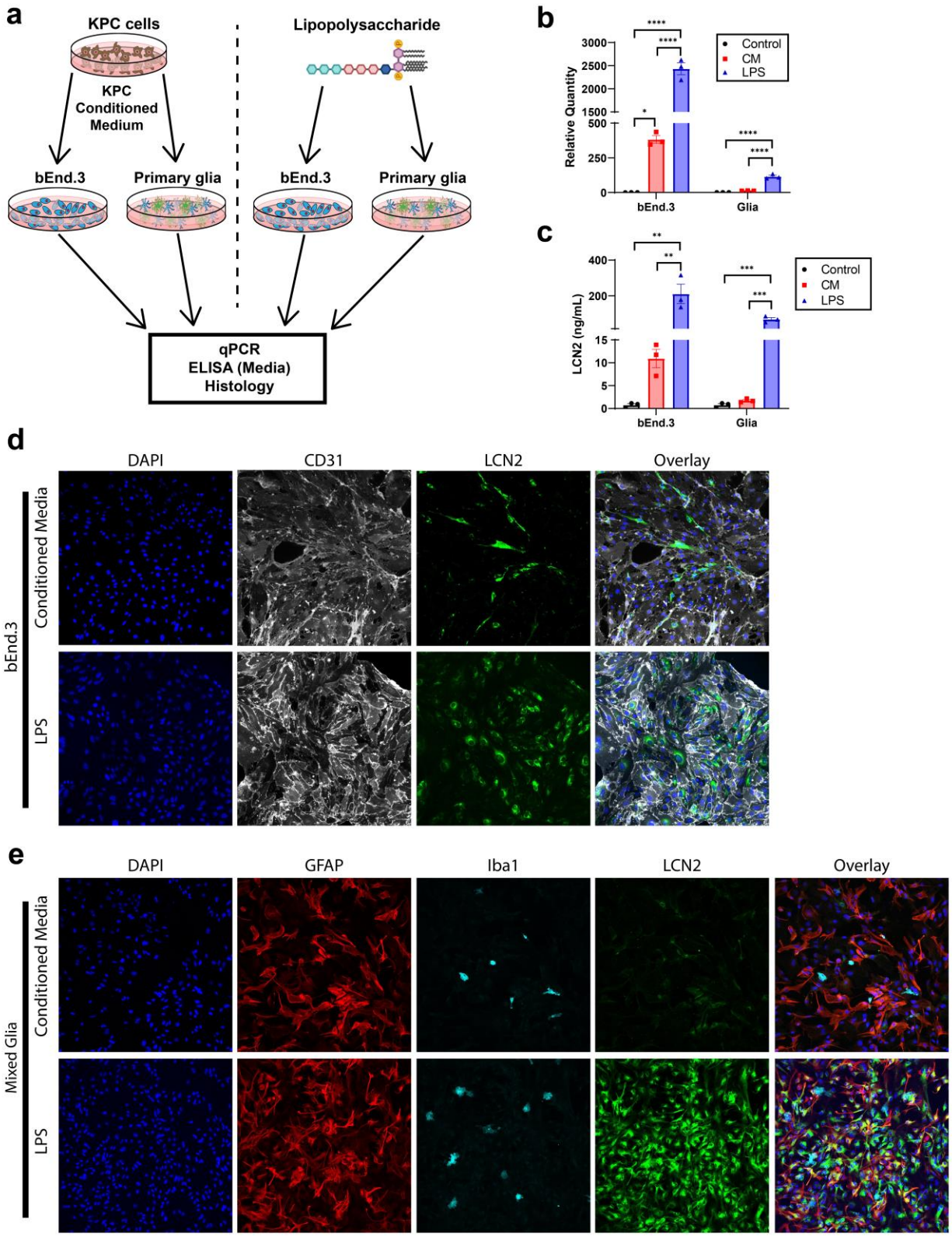
a
KPC cells
KPC Conditioned Medium
Lipopolysaccharide
bEnd.3
Primary glia
bEnd.3
Primary glia
qPCR
ELISA (Media)
Histology
b
Relative Quantity
Control
CM
LPS
bEnd.3
Glia
c
LCN2 (ng/mL)
Control
CM
LPS
bEnd.3
Glia
d
DAPI
CD31
LCN2
Overlay
bEnd.3
Conditioned Media
LPS
e
DAPI
GFAP
Iba1
LCN2
Overlay
Mixed Glia
Conditioned Media
LPS

Figure 2. Soluble tumor factors and LPS challenge results in unique Lcn2 expression, production, and secretion profiles in brain endothelium and glia *in vitro*. (a) Experimental design for b-e. (b) *lcn2* gene expression in bEnd.3 endothelial cells and primary mixed glia after treatment with control media, cancer conditioned media or LPS (n = 3 biological replicates). (c) Lcn2 ELISA of bEnd.3 endothelial cells and primary mixed glia after treatment with control media, cancer conditioned media or LPS (n = 3 biological replicates). Representative immunohistochemistry images of (d) bEnd.3 cells and (e) mixed glia after cancer conditioned media or LPS challenge (20x objective). [LPS] = 10 ng/mL. Data in b-c are expressed as mean ± SEM. Data represented in b-c were analyzed with one-way ANOVA with Bonferroni multiple comparisons per cell type. *p ≤ 0.05, **p ≤ 0.01, and ***p ≤ 0.001, ****p ≤ 0.0001. b.End3 = Brain endothelium 3 cell line; CM = conditioned medium; LPS = lipopolysaccharide.

Genetic deletion of Lcn2 *improves sickness behaviors in chronic, but not acute, inflammatory disease*

Since we observe a large induction of Lcn2 in the CNS of both cancer cachexia and LPS-injected mice, and Lcn2 is implicated as a neuropathologic agent, we sought to address whether genetic deletion of Lcn2 broadly influences illness or cognitive behaviors during these acute and chronic inflammatory insults. To this end, we utilized home-cage nest building as a measure of overall well-being and cognitive function, as nest building is known to be impaired in various mouse models of illness, infection, and

brain injury (including lesions to the hippocampus) (593-596). We observed an improvement in nest building behaviors of *lcn2-KO* mice under cancer cachectic conditions, but no such improvement in the context of LPS injection Figure 3a-c; Supplementary figure 2a). We previously reported the improved nutritional status of *lcn2-KO* mice during cancer cachexia (597), but whether *lcn2* deletion improves nutrition after LPS challenge is not well described. We found that *lcn2* deletion did not improve illness behaviors of food consumption and body mass and showed no effect on mortality (Supplementary Figure 2b-d). Consistent with these results, we previously reported that cerebral injection of Lcn2 did not influence food intake or body mass until after 4 days of exposure (597). Since Lcn2 was recently reported to be elevated after meal intake in fasted mice (82), this presented a conundrum in the current context, as chronic and repeated elevations in Lcn2, but not acute exposure, would be expected to induce neurotoxicity as demonstrated below. We ultimately observed results that are discordant with prior reports, as fasting and refeeding did not result in an increase in Lcn2 release (Supplementary figure 2e-f). With the known protective role of acute Lcn2 induction during bacterial infection through its ability to sequester siderophore-bound iron away from the live pathogen (97), combined with these data demonstrating *lcn2* deletion improved illness behaviors in the chronic inflammatory setting of cachexia but was dispensable during LPS challenge, we hypothesized Lcn2 acts in a temporal fashion in the CNS on neurons regulating cognitive function.

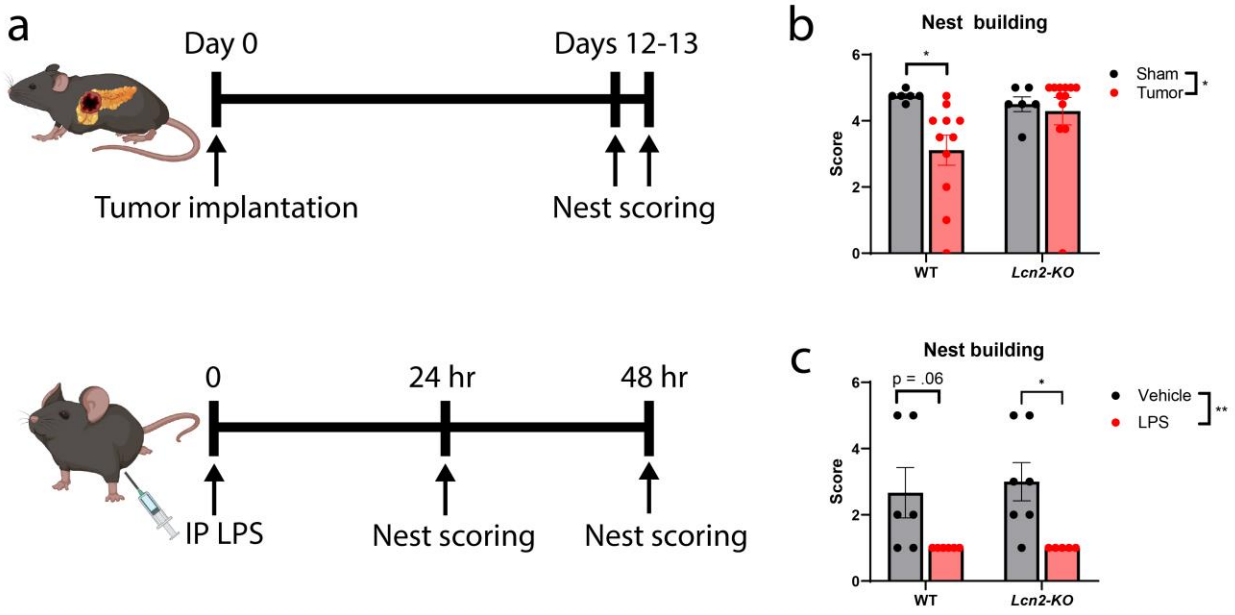

Figure 3. Genetic deletion of Lcn2 improves nest building during cancer cachexia, but not LPS challenge. (a) Experimental design for pancreatic tumor and LPS studies. (b) Nest building scores in *lcn2*-KO and WT mice after sham operation or tumor implantation (n = 6-12 per group). (c) Nest building scores in *lcn2*-KO and WT mice 24 hours after LPS treatment (n = 5-7 per group). Data in b-c are expressed as mean ± SEM. Data represented in b-c were analyzed with two-way ANOVA with Bonferroni multiple comparisons per cell type. LPS dose was 1 mg/kg. *p ≤ 0.05, **p ≤ 0.01, and ***p ≤ 0.001, ****p ≤ 0.0001. LPS = lipopolysaccharide; IP = intraperitoneal.

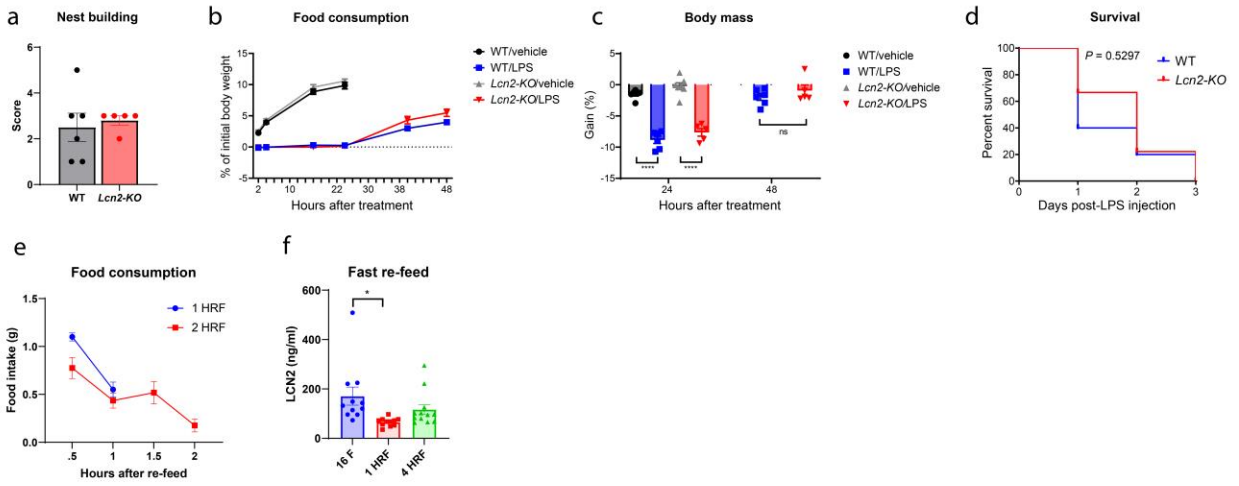

Supplementary Figure 2. Related to Figure 3. (a) Nest building score in *lcn2*-KO and WT mice 48 hours after LPS challenge (n = 5-6 per group). (b) Food intake as a percentage of initial body mass in *lcn2*-KO and WT mice 48 hours after vehicle injection or LPS challenge (n = 5-7 per group). (c) Body mass change body mass in *lcn2*-KO and WT mice 24 and 48 hours after vehicle injection or LPS challenge (n = 5-7 per group). (d) Survival analysis of *lcn2*-KO and WT mice after a lethal dose of LPS (n = 10 per group). (e) Hourly food intake after re-feeding mice after 16 hour fast (n = 4-5 per group). (f) Plasma Lcn2 levels in mice after 16 hour of fasting (16 F), 16 hour fasting + 1 hour after re-feeding (1 HRF), and 16 hour fasting + 4 hours after re-feeding (4 HRF) (n = 11-12 per group).

Chronic cerebral exposure to* Lcn2 *induces hippocampal neuron alterations

While we observed differences in nest building amongst *lcn2*-KO and WT mice under cachectic conditions, it is difficult to disentangle the direct effects of Lcn2 on cognitive outcomes during cancer cachexia since the robust inflammatory processes incurred during cachexia, including fatigue, are known to confound the results of advanced cognitive testing. For this reason, we sought to explore the individual effects of cerebral Lcn2 in the CNS by using an intracerebroventricular (ICV) treatment paradigm (Figure 4a). We also chose to focus on hippocampal alterations in these studies, since we observed a particularly large induction of *lcn2* immediately ventral to the dentate gyrus of the hippocampus *in vivo* (Figure 1a-b; Figure 4b). We observed that mice receiving pathologic levels of ICV Lcn2 for 10 days, but not 4 days, displayed a significant reduction in NeuN positive neuron density in the dentate gyrus (Figure 4c-e). Specifically, we administered 40 ng of Lcn2 (2 ul injections) to achieve a similar degree of concentration-time exposure as cachectic mice (Figure 1e). Utilizing the Pomc-EGFP transgenic mouse, in which newborn neurons in the dentate gyrus express EGFP by the pro-opiomelanocortin (Pomc) promoter, we observed an increase in newborn neurons after 10 days, but not 4 days, of Lcn2 treatment (Figure 4f-h)(598). These data demonstrate that Lcn2 acts in a temporal fashion to alter hippocampal neuron dynamics.

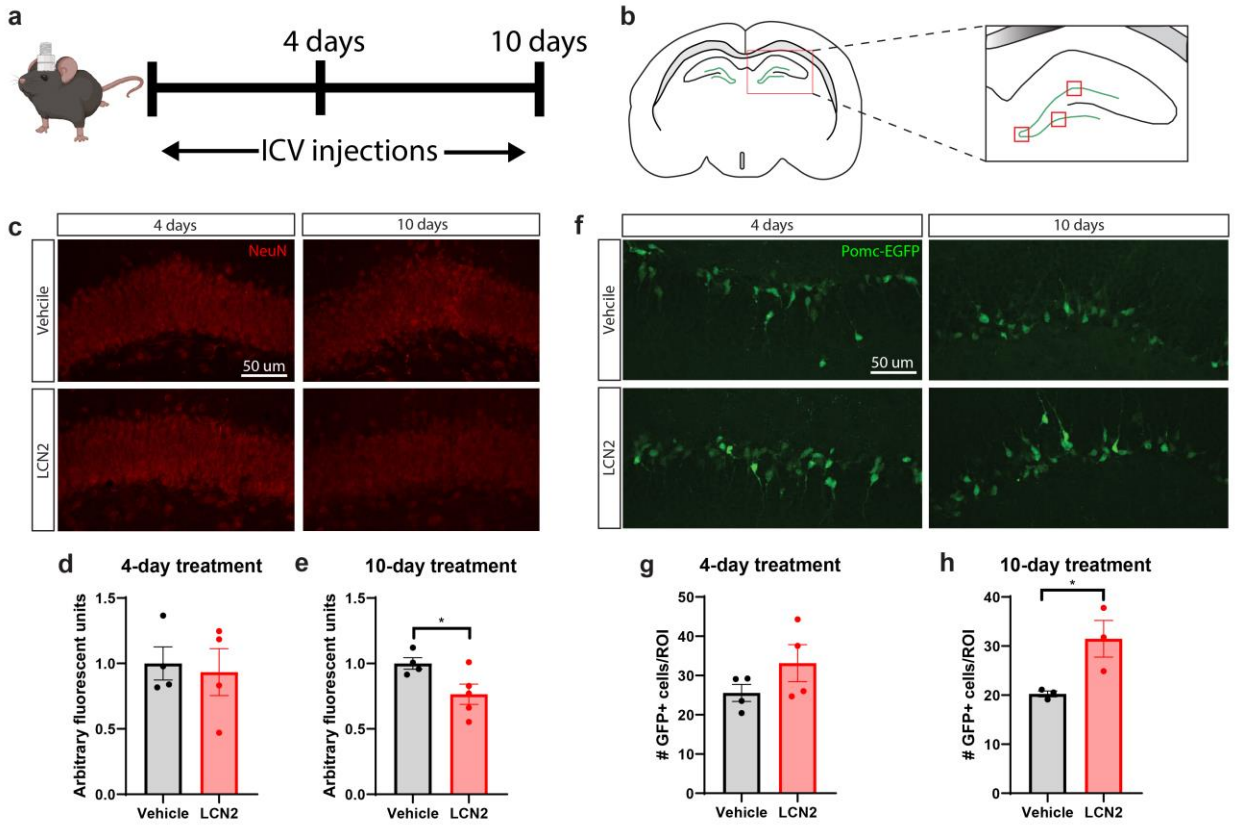

Figure 4. Prolonged cerebral exposure to Lcn2 results in reduced hippocampal density of mature neurons, but an increase in newborn neurons. (a) Experimental design of ICV Lcn2 experiment. (b) Cartoon coronal section of the hippocampus and dentate gyrus, highlighting the quantified regions in d, e, g, h; the three red boxes on the dentate gyrus are the areas imaged on every slice at 40X for quantification analysis. (c) Representative images of NeuN+ neurons in the dentate gyrus of mice given ICV vehicle or Lcn2 (. (d-e) Quantification of NeuN+ neuronal density in selected regions of the dentate gyrus (n = 3-4 images per region of interest; n = 4-5 mice per group). (f) Representative images of Pomc-EGFP neurons in the dentate gyrus of mice given ICV vehicle or Lcn2. (g-h) Quantification of Pomc-EGFP neuron density in selected regions of the dentate gyrus (n = 3-4 images per region of interest; n = 3-4 mice per group).

Data in d-e, g-h are expressed as mean ± SEM. Data represented in d-e, g-h were analyzed by two-tailed Students t-tests. Scale bar = 50 μm. *p ≤ 0.05. ICV = intracerebroventricular; ROI = region of interest.

Chronic Lcn2 *exposure induces hippocampal microgliosis*

After observing changes in neuronal density and populations in the hippocampus, we sought to determine if other cell types in the hippocampus were influenced by Lcn2 administration. Examining the same regions analyzed for neuronal alterations, we observed no change in microglial and astrocyte number or morphology after 4 days of cerebral Lcn2 treatment (Figure 5a-e). After 10 days of cerebral Lcn2 treatment, we observed an increase in microglial number and modest, but non-significant, increase in microglial morphology score compared to vehicle only controls (Figure 5a-e) (599). We next isolated primary microglia and treated them directly with Lcn2 *in vitro* to determine if Lcn2 is directly influencing microglial polarization (Figure 5f). Microglia treated with Lcn2 displayed no change in inflammatory-related genes, including *Il6, Tnf-α, Nos2, and Arg1,* but demonstrated a significant upregulation of several immune cell recruitment genes, including *Ccl2, Ccl3, Cxcl1, Cxcl2, and Cxcl10* (Figure 5g-h). These data suggest that Lcn2 mediates a distinct microglial polarization phenotype *in vivo,* characterized by increased microglial number and expression of immune cell recruitment genes, but does not impact expression of inflammation-related genes.

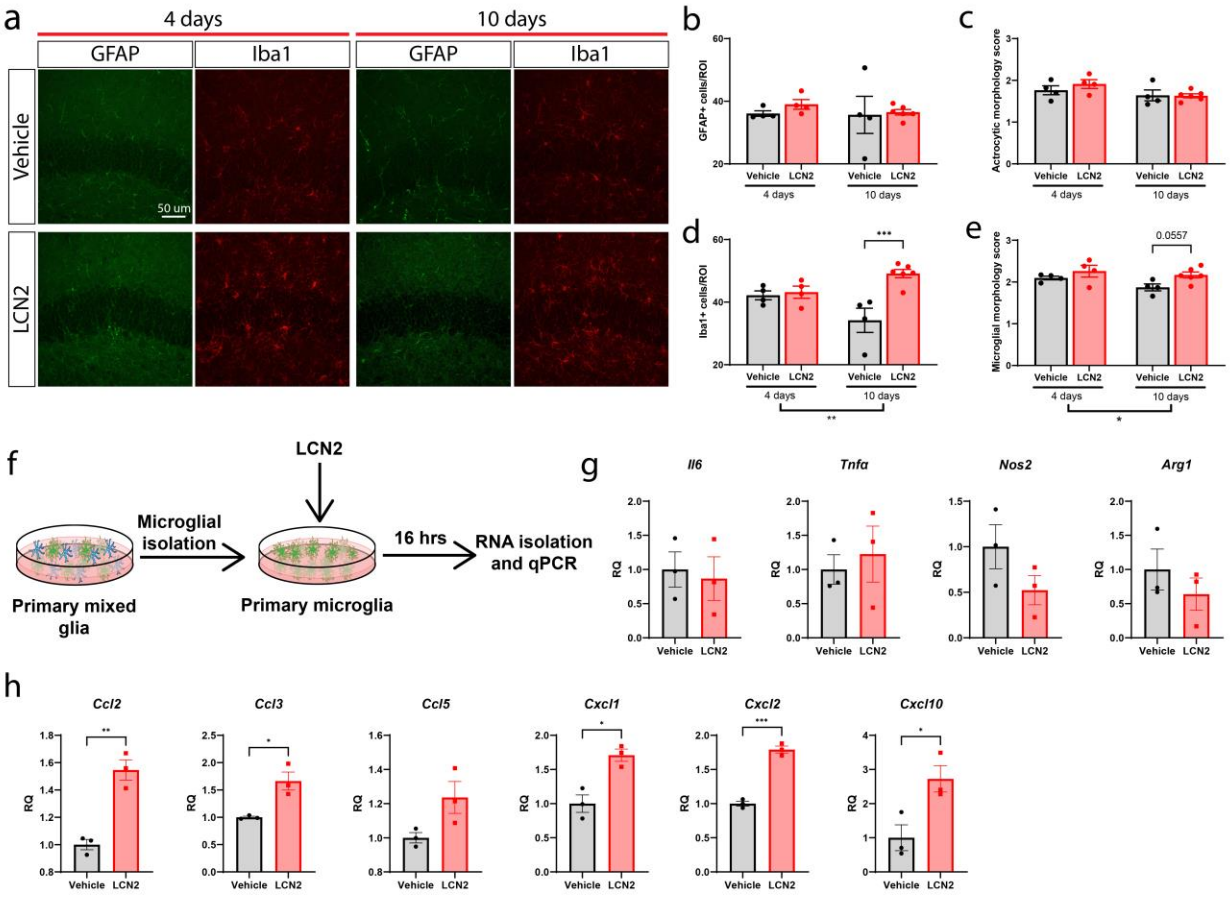

Figure 5. Chronic cerebral Lcn2 exposure results in an increase in hippocampal microglia and expression of chemokines. (a) Representative images of microglia (Iba1+) and astrocytes (GFAP+) around the dentate gyrus after 4 or 10 days of ICV vehicle or Lcn2 treatment. (b) Quantification and (c) morphologic scoring of GFAP+ cells around the dentate gyrus after 4 and 10 days of ICV vehicle or Lcn2 treatment. (d) Quantification and (e) morphologic scoring of Iba1+ cells around the dentate gyrus after 4 and 10 days of ICV vehicle or Lcn2 treatment. (n = 4-5 per group). (f) Experimental design of primary microglia cultures treated with Lcn2 for g-h. (g) Inflammatory transcriptional profile of primary microglia cultures treated with vehicle or Lcn2 (100 ng/mL). (h) Immune cell recruitment transcriptional profile of primary microglia cultures

treated with vehicle or Lcn2 (100 ng/mL). n = 3 biological replicates per condition for g-h. Data in b-e, g-h are expressed as mean ± SEM. Data represented in b-e were analyzed with Two-way ANOVA with Bonferroni multiple comparisons. Data represented in g-h were analyzed by two-tailed Students t-tests. *p ≤ 0.05, **p ≤ 0.01, and ***p ≤ 0.001. ROI = region of interest. RQ = relative quantity.

Lcn2 *is a chemoattractant for immune cells in the CNS*

Given the consistent upregulation of immune cell recruitment genes in microglia treated with Lcn2, we hypothesized that in addition to the observed neuronal and microglial changes, animals treated with cerebral Lcn2 would demonstrate a concomitant increase in CNS immune cells. Indeed, we observed a modest increase in CD45+ cells in the hippocampus after 4 days of ICV Lcn2 treatment, with a robust elevation after 10 days of treatment (Figure 6a,c,e,g,i). Notably, we observed a non-significant increase in myeloperoxidase-positive neutrophils after 4 days of Lcn2 treatment, but this increase disappeared after 10 days of treatment. (Figure 6b,d,f,h,j). To broadly determine which types of CD45+ leukocytes were infiltrating the CNS in the context of elevated Lcn2, we performed flow cytometry on brain samples from animals treated with either Lcn2 or vehicle for 10 days. Consistent with our histological analyses, we observed a robust increase of CD45+ cells in the brain of mice treated with Lcn2 (Figure 6k; Supplementary figure 3). Furthermore, Lcn2-treated mice displayed a significant increase in both lymphoid and myeloid immune cell populations (Figure 6l,o). Amongst the lymphocyte population, we observed a significant increase in CD3+ T-cells,

and modest elevation of CD19+ B cells (Figure 6m-n), while CD11b-mid and non-neutrophil myeloid cells were both elevated amongst the myeloid cell subpopulations (Figure 6o-p). Consistent with our histological observations in the hippocampus, neutrophil count was unchanged between Lcn2 and vehicle treated mice by flow cytometry (Figure 6r).

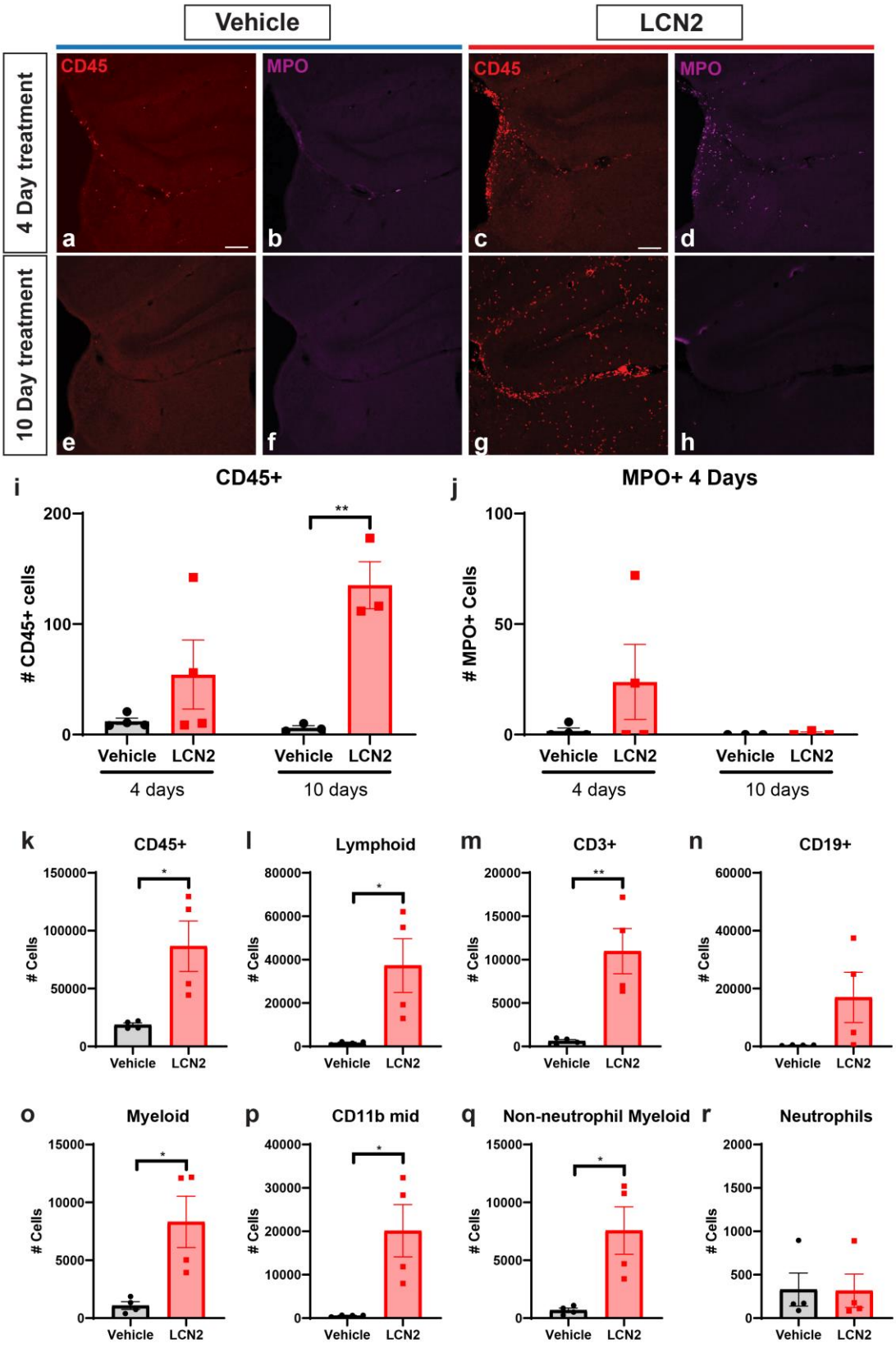
Vehicle
LCN2
4 Day treatment
10 Day treatment
CD45
MPO
a
b
c
d
e
f
g
h
i
CD45+
CD45+ cells
200
100
0
**
Vehicle
LCN2
4 days
10 days
j
MPO+ 4 Days
MPO+ Cells
100
50
0
k
CD45+
150000
100000
50000
*
Cells
l
Lymphoid
80000
60000
40000
20000
m
CD3+
20000
15000
10000
5000
n
CD19+
60000
40000
20000
o
Myeloid
15000
10000
5000
p
CD11b mid
40000
30000
20000
10000
q
Non-neutrophil Myeloid
r
Neutrophils
2000
1500
1000
500

Figure 6. Cerebral Lcn2 results in the recruitment of immune cells to the CNS. (a-h) Representative confocal images of the dentate gyrus and velum interpositum in mice treated with ICV vehicle or Lcn2 after 4 or 10 days. Scale bar = 300µm. (i-j) Imaging and quantification of CD45+ and MPO+ cells in mice treated with either ICV vehicle or Lcn2 after 4 or 10 days (n = 3-4 per group). (k-r) Flow cytometry analysis of immune cell populations using hemi-brains of mice treated with ICV vehicle or Lcn2 after 4 or 10 days (n = 4 per group). Data in i-r are expressed as mean ± SEM. Data represented in i-r were analyzed by two-tailed Students t-tests amongst treatment groups. *p ≤ 0.05, **p ≤ 0.01. MPO = myeloperoxidase.

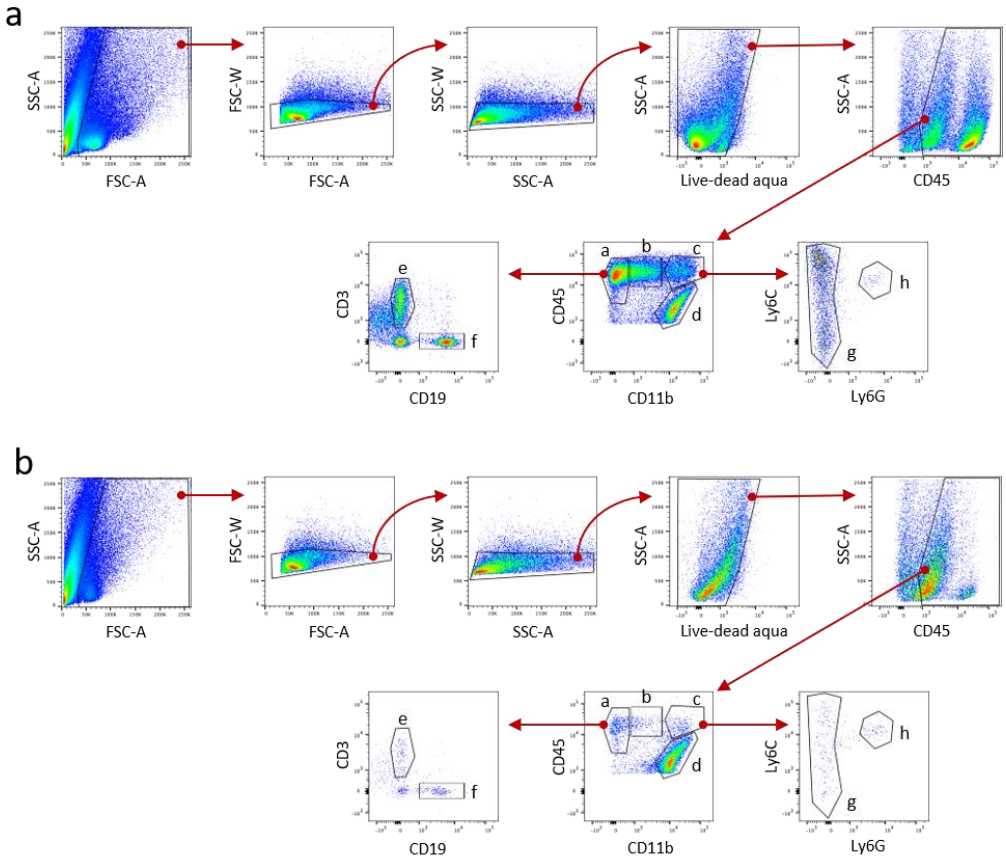

Supplementary figure 3. Related to Figure 6. Flow cytometry gating strategy for quantifying immune cell subpopulations in the CNS of mice receiving (a) Lcn2 or (b) vehicle. Cells were initially gated to remove debris, doublets and dead cells before gating on CD45+ cells. Immune cell markers were used to define the following subpopulations: (a) lymphoid cells = $CD45^{+}$ $CD11b^{-}$; (b) $CD45^{+}$ $CD11b^{mid}$; (c) myeloid cells = $CD45^{+}$ $CD11b^{+}$; (d) microglia = $CD45^{lo}$ $CD11b^{+}$; (e) T cells = $CD3^{+}$; (f) B cells = $CD19^{+}$; (g) myeloid cells (non-neutrophils) = $Ly6C^{+}$ $Ly6G^{-}$; (h) neutrophils = $Ly6C^{+}$ $Ly6G^{+}$.

Primary hippocampal neurons differentially respond to Lcn2 *in a time-dependent manner*

Previous literature suggests Lcn2 acts in a time-dependent fashion in mediating neuronal apoptosis(112, 139). However, an in-depth examination of neuronal gene expression in response to Lcn2 is outstanding. Since we observe a progressive response of hippocampal neurons to Lcn2 *in vivo,* we performed RNA sequencing of primary hippocampal neurons treated with Lcn2 or vehicle for either 1 or 4 days. After 1 day of Lcn2 treatment, neurons displayed an upregulation of several genes involved in transcriptional regulation and RNA splicing, including *Pcsk1n, Basp1, and Dact3* (Figure 7a). Furthermore, ontology analysis did not reveal a significant association between 1 day of Lcn2 treatment and cellular viability (Supplemental tables). These results are in contrast with the 4 day Lcn2 treatment condition, as *Hap1* (huntington-associated protein-1) and *Hpcal4* (hippocalcin-like protein 4; also known as VILIP-2) are amongst

the most up-regulated genes, and are known mediators of neurite development, calcium channel function, and synaptic release of neurotransmitter (Figure 7b)(600-603). The third most up-regulated gene, *Vgf,* is highly upregulated after peripheral nerve injury and is suggested to be secreted by damaged neurons to activate nearby microglia (Figure 7b; Supplementary tables)(604, 605). Gene ontology analysis of biological and cellular processes demonstrated a significant association between multiple processes of neuron morphology, axogenesis, and cytoskeletal rearrangement in genes up-regulated in the 4-day treatment condition (Figure 7c; Supplementary table X). Consistent with previous reports of Lcn2's apoptotic effects on neurons, several terms of programmed cell death were also significant, although both positive and negative regulation pathways were revealed (Supplementary tables) (112). Additionally, phenotypic ontology analysis of up-regulated genes in the 4-day treatment condition revealed a significant association with impaired synaptic plasticity, abnormal spatial learning, and hyperactivity (Figure 7c; Supplementary table X). These results demonstrate a strong temporal effect of Lcn2 on hippocampal neurons, with ontology analyses suggesting long-term exposure results in neuronal dysfunction.

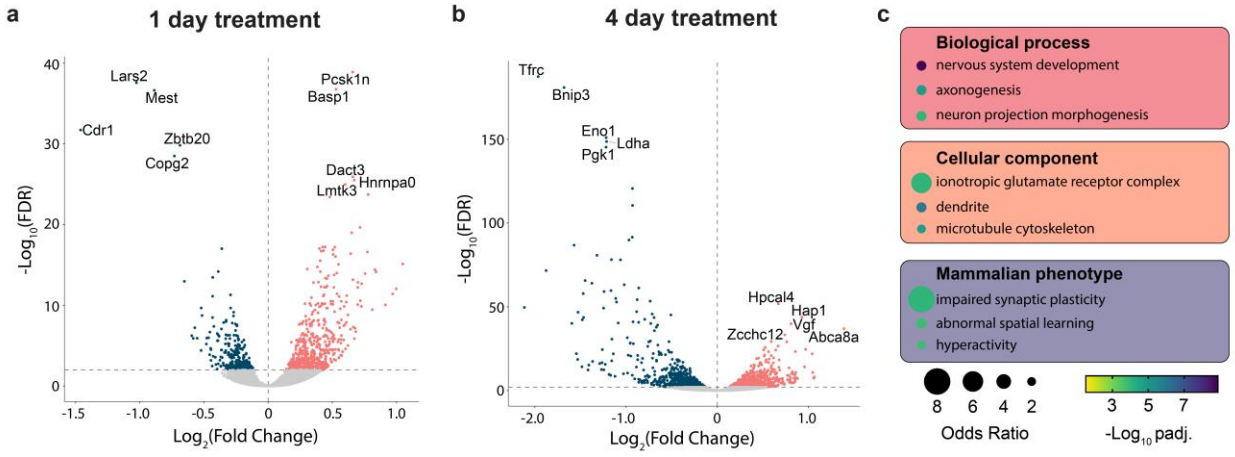

Figure 7. Primary hippocampal neurons respond to Lcn2 in a temporal fashion. Differential gene expression assessed by RNA-seq in primary hippocampal neurons treated with Lcn2 (100 ng/mL) or vehicle for either (a) 1 or (b) 4 days. (c) Gene ontology analysis performed on genes with increased expression after 4 days of Lcn2 treatment.

Prolonged cerebral Lcn2 *exposure results in impaired spatial recognition memory*

To determine whether cerebral Lcn2 mediates alterations in cognitive function, we performed a battery of behavioral and cognitive assessments in mice treated with central Lcn2. Specifically, we utilized an assessment paradigm that includes tests that present little or no intrinsic stress (except the final test of tail suspension), yet encompass several domains of cognitive and neuropsychiatric health(606-608). To study working memory, we utilized spontaneous alternation in the Y-maze, and observed no effect of cerebral Lcn2 treatment on percentage of alternation (Figure 8a). Similarly, Lcn2 treated mice displayed no change in visual object recognition memory or anxiety-like behavior as indicated by the object recognition test and light-dark box test, respectively (Figure 8b-c; Supplementary figure 4). We next utilized the two-trial Y-maze assessment to determine exploratory behavior and of a novel arm after a short inter-trial interval (ITI). Mice treated with central Lcn2 showed impaired spatial memory upon this test, spending significantly less time in the previously-blocked arm as vehicle treated

controls (Figure 8d). Finally, we assessed depressive-like behavior by the tail suspension test and observed no difference between Lcn2 and vehicle treated mice (Figure 8e). These data collectively suggest that increased cerebral Lcn2 does not influence anxiety and depressive-like behaviors, working memory, or object recognition memory, but negatively impacts spatial recognition memory, a cognitive task largely attributable to hippocampal-dependent processes (607).

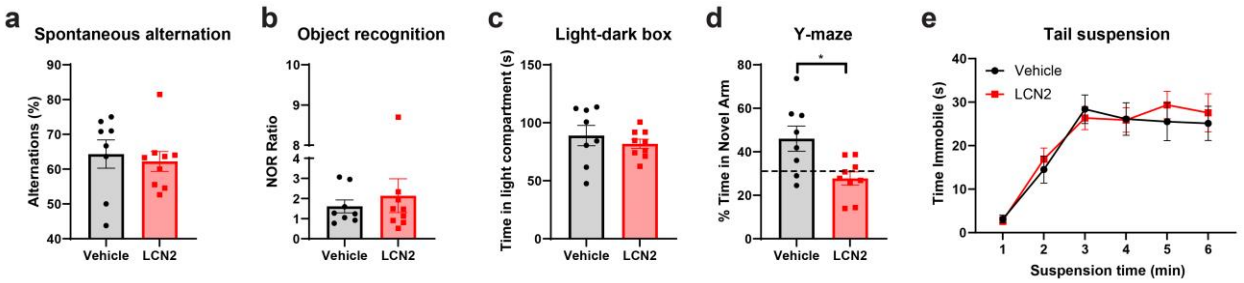

Figure 8. Chronic cerebral exposure to Lcn2 results in impaired spatial recognition memory. (a) Y-maze spontaneous alternation test reporting percentage of consecutive arm entry alternations (b) Novel object recognition test for recognition memory showing ratio of time spent with novel object to familiar object. (c) Time spent in the light compartment on light-dark box anxiety test. (d) Y-maze blocked arm test reporting % of time spent in previously blocked arm after a short inter-trial intermission. (e) Tail suspension test reporting time spent immobile over a 6-minute interval. n = 8-9 per group. *p ≤ 0.05.

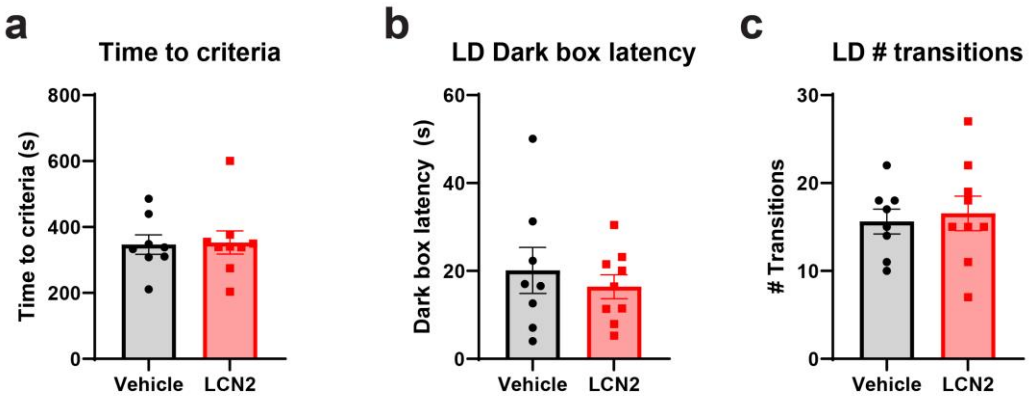

Supplementary figure 4. Related to Figure 8. (a) Time to achieve novel object recognition criteria as defined by a total of 20 seconds of exploration with novel or familiar objects. (b) Latency to enter dark compartment of the light-dark box. (c) Number of transitions between light and dark compartments in the light-dark box text.

3. Discussion

The purpose of this work was to evaluate the role of Lcn2 in the CNS, specifically as it relates to cognitive outcomes after prolonged exposure. Herein, we describe a pathologic role of Lcn2 in the CNS, in which Lcn2 mediates distinct neuronal, glial, and immune cell alterations in a time-dependent fashion, ultimately resulting in cognitive impairment. Our findings implicate Lcn2 as a pathologic molecule in the CNS during chronic inflammatory disease through its actions on the hippocampus, while the transient induction of Lcn2 in the CNS during acute inflammation is generally tolerable (Figure 9).

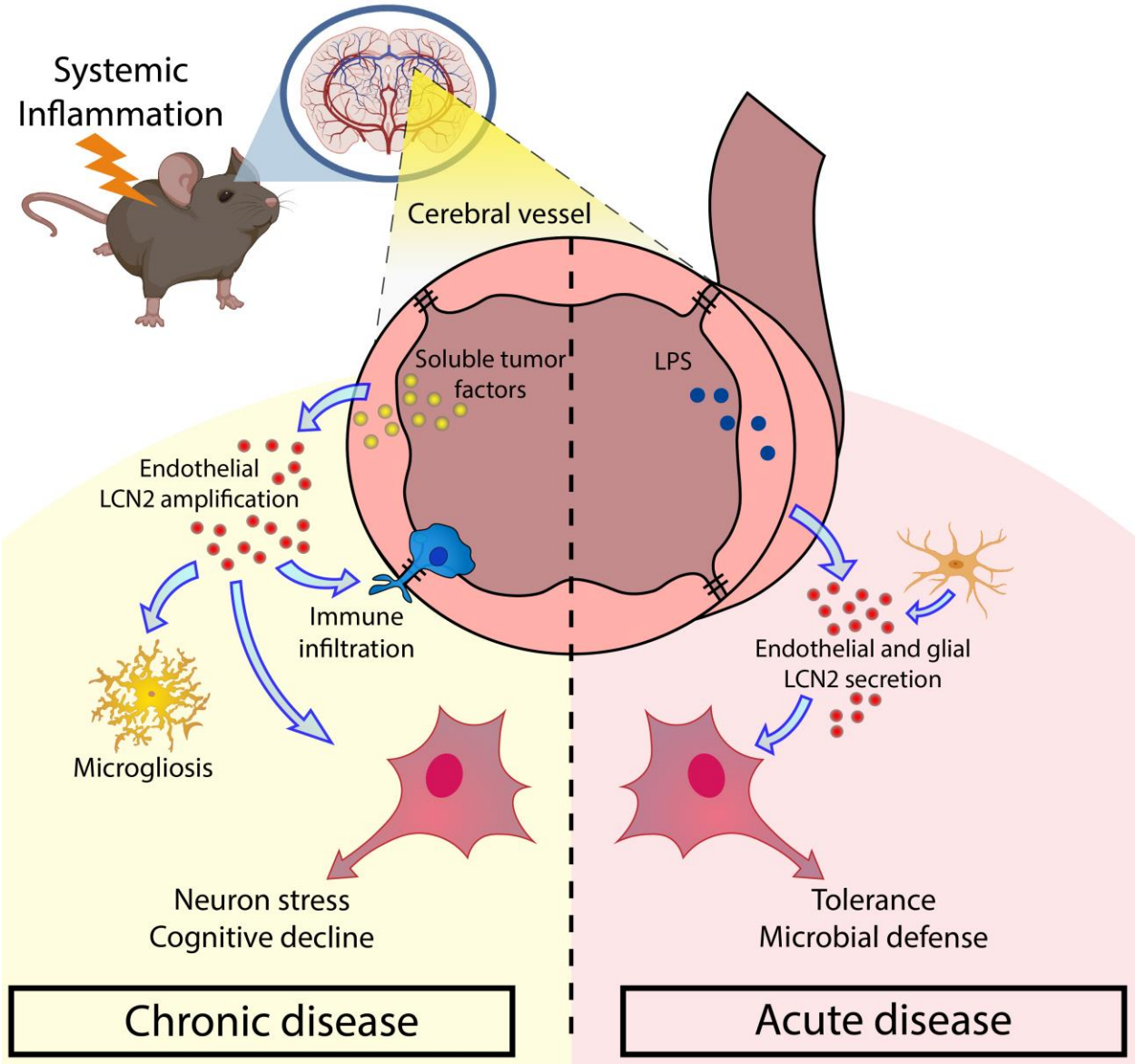

Figure 9. Graphical summary of the proposed role of Lcn2 in disease-associated neurocognitive decline. During acute inflammatory disease, Lcn2 is robustly induced by several CNS cells, including endothelium and glia, and protects the brain from invading pathogens. Acute exposure of Lcn2 in the brain is not harmful to neurons. Conversely, during prolonged inflammatory disease, Lcn2 is selectively produced and secreted by brain endothelium, particularly in pial vessels proximal to the hippocampus. This

continued production and secretion of Lcn2 during chronic disease results in a distinct microglial polarization phenotype, immune cell invasion, and prolonged neuronal stress, ultimately leading to neuronal dysfunction and cognitive impairment.

Using both *in vitro* and *in vivo* models, we observe a unique *lcn2* expression and production profile in the CNS dependent on the inflammatory insult. Specifically, the acute inflammatory model of LPS-based sepsis results in a large global induction of Lcn2 in the CNS, while the chronic inflammatory model of cancer cachexia results in a specific induction in cerebral endothelium. We observe a particularly robust expression of *lcn2* in the velum interpositum (VI), a double-layered invagination of the pia matter immediately ventral to the hippocampus. Since both acute and chronic inflammatory conditions result in a large induction of Lcn2 in the CNS, particularly in an area directly adjacent to the hippocampus, and Lcn2 is implicated in the regulation of neuronal health and cognition(127, 609), we sought to determine if genetic deletion of Lcn2 influences illness behaviors during LPS or cancer challenge. We observed improved nest building in *lcn2*-KO mice during cancer cachexia, but not LPS challenge, which led us to hypothesize that Lcn2 acts in a temporal fashion in the CNS, with the acute exposure of Lcn2 being less impactful on CNS processes than prolonged exposure. To formally test this hypothesis, we administered Lcn2 to the CNS of mice for either 4 or 10 days, and observed a progressive decrease in hippocampal neuron density, increased number of hippocampal microglia, and a robust infiltration of leukocytes. RNA sequencing analysis of primary hippocampal neurons were consistent with the time-dependent action of Lcn2 in the CNS observed *in vivo*, as neurons treated chronically demonstrated distinct

biological, cellular, and phenotypic ontologies compared to short-term Lcn2 treated neurons. Given these distinct alterations in hippocampal neuron, glia, and immune cell profiles in mice treated chronically with Lcn2, along with ontology analyses suggesting prolonged exposure of Lcn2 is associated with impaired synaptic plasticity and abnormal spatial learning, we performed behavioral and cognitive testing of mice after chronic central treatment of Lcn2. Mice treated with Lcn2 displayed an impairment in spatial memory, a cognitive process principally attributed to the hippocampus(607, 610). Our data also demonstrate that Lcn2 is not induced with meal intake which would be expected for a molecule with neurotoxic potential. These data are in contrast with previous reports, as we find a small but significant decrease in circulating Lcn2 after refeeding(82). It is currently unclear why these results are discordant at this time, but our data suggest this molecule may be a more robust mediator of appetite under pathological, rather than physiological, conditions.

Lcn2 is classically described as a neutrophil-derived protein with an evolutionarily conserved role in sequestering iron containing siderophores during infection, thereby limiting the proliferative capacity of siderophilic pathogens(89, 97). As such, it is generally accepted that the acute induction of Lcn2 evolved as a beneficial process, aimed at combating infection and maintaining tissue homeostasis in the short term, as the protein is rapidly cleared after resolution of the infection(611). Indeed, the acute induction of Lcn2 in the CNS is proposed to be beneficial to the host(127), although conflicting reports exist that suggest Lcn2 is dispensable during LPS challenge(565). In either case, it is clear that the central induction of Lcn2 during acute inflammatory challenge is not pathological, and our results are consistent with these findings in that

the cellular composition in the CNS and evolutionarily-conserved behaviors—specifically nest building—are broadly unaffected by short-term Lcn2 exposure. In addition to infection, Lcn2 is also upregulated in the brain during numerous non-infectious chronic diseases, during which the CNS would maintain continued exposure to high levels of Lcn2(123, 147, 551). Recent work by Llorens et al demonstrate a robust association between CSF Lcn2 levels and performance on clinical cognitive tests in patients with cerebrovascular disease, showing elevated CSF Lcn2 levels were associated with poorer performance on the Mini Mental Status Examination(122). Similar reports exist in examining peripheral Lcn2 levels, such that increasing plasma Lcn2 levels portends poorer neurocognitive testing performance(612). Despite the described role of Lcn2 in regulating cell viability in a temporal manner(112), along with reports of elevated Lcn2 in the CNS of patients with cognitive impairment(122), whether or not Lcn2 individually influences cognition has not been comprehensively examined. To our knowledge, this is the first report of the individual effects of Lcn2 in the CNS, in which we observe a time-dependent effect of Lcn2 on hippocampal cellular composition and cognition.

The cellular source of Lcn2 in the brain is also disparately reported in the literature, ranging from astrocytes, microglia, endothelium, and neurons depending on underlying pathologic condition(111, 112, 613-616). Furthermore, the cell-specific expression profile of Lcn2 may depend on cellular polarization, as microglial expression of *lcn2* was reported to be differentially expressed dependent on microglial inflammatory status(614). Using LPS and cancer cachexia models of systemic inflammation, we observe a robust vascular expression of *lcn2* in the CNS under both conditions, suggesting systemic

inflammatory mediators act at the point of contact between the periphery and brain to increase *lcn2* expression. Importantly, we confirm abluminal secretion or transmigration of Lcn2 by detection of the molecule in the CSF of mice, demonstrating peripheral inflammatory insults are not only capable of increasing expression and production of Lcn2 in the cerebral vasculature, but also result in release of the molecule into the CNS. Additionally, previous work has also demonstrated the ability of Lcn2 to cross the blood brain barrier (82). Therefore, our studies confirm that systemic inflammatory diseases can result in a robust induction of Lcn2 into the brain, and under chronic conditions, may be partially responsible for progressive cognitive decline through its actions in the hippocampus.

The effect of Lcn2 on cognitive function using various murine models was examined in the past, demonstrating variable effects of *lcn2* genetic deletion on cognition depending on model of study. In experimental models of vascular dementia and diabetic encephalopathy, *lcn2* knockout mice demonstrated improved spontaneous alternation in the Y-maze test(139), while our studies demonstrated that exogenous Lcn2 did not affect spontaneous alternation performance, suggesting a combinatorial role of Lcn2 and disease-specific factors in mediating a reduction in working memory. In a model of restraint stress, *lcn2* deficient mice displayed an enhancement of stress-induced anxiety as indicated by the elevated-plus maze and light-dark box tests(615). Our study did not demonstrate an effect of exogenous Lcn2 on anxiety using the light-dark box, suggesting that while a deficiency in CNS Lcn2 induces anxiety-like behaviors, an excess of the molecule does not appear protective against anxiety. These findings may also be reconciled by the clear role Lcn2 plays in hippocampal development, as *lcn2*

null mice display significantly altered hippocampal neuron spine density and morphology(617). Thus, while excessive CNS Lcn2 appears neuropathological in several disease conditions, basal expression of the molecule is critical in normal hippocampal development, suggesting whole-body knockout conditions may not represent a biologically-relevant setting for the study of Lcn2 on hippocampal function during disease. Using the J20 Alzheimer mouse model, Dekens et al observed no alterations in working and visual recognition memory by spontaneous alternation and novel-object recognition tests, respectively(616). In contrast to our study, the authors observe no differences in spatial recognition memory using the Morris water maze, although our studies utilized the blocked arm version of the Y maze(616). Collectively, these studies and more demonstrate that while Lcn2 is induced in the CNS during several diseases associated with cognitive decline, its effects on cognitive function are strongly dependent on the specific disease state. Since our study demonstrates an individual effect of Lcn2 on cognitive dysfunction in the absence of disease, it may be that the cognitive effects of Lcn2 are masked by more robust mediators of neuronal dysfunction during primary neuropathologies with profound cognitive impairment, such as hyperphosphorylated tau in the context of tauopathies(618).

Our study herein raises important questions, as well as limitations, concerning the precise mechanisms of Lcn2-induced neurocognitive decline. Since there are three putative receptors of Lcn2 (SLC22A17, megalin, and the type 4 melanocortin receptor [MC4R]), it remains to be determined which ligand-receptor interaction mediates which molecular, cellular, and behavioral consequences observed in our study(82, 85, 86). Secondly, while our RNA sequencing analyses of Lcn2-treated hippocampal neurons

suggest Lcn2 is individually detrimental to neurons, it is unclear whether the observed microgliosis and leukocyte infiltration into the CNS *in vivo* is beneficial or pathologic. In a recent report of HIV-1 induced neuropathology, it was demonstrated that Lcn2's neurotoxic effects were dependent on microglia(609). Conversely, microglial depletion during cancer worsens cachexia illness behaviors, demonstrating a protective effect of microglia during systemic inflammation(70). Similar to microglia, brain-infiltrating immune cells are reported to be either pathologic or beneficial depending on the disease state(45). Since we did not observe a change in expression of inflammation-related transcripts, including *Il-6, Tnf-α, Nos2,* and *Arg1* in Lcn2-treated microglia, it is plausible that the increased microglia, combined with their expression of chemokines, result in the recruitment of peripheral immune cells in attempt to repair the damaged hippocampus, although future investigation into these observations is warranted. Lcn2 is also known to modulate intracellular iron trafficking, as well as apoptosis depending on the iron-loading status of the molecule(85). In our studies, is likely that Lcn2 exists solely in the apo- form in our cachexia and LPS models, as we observe no evidence of bacterial infection (and therefore no bacterial siderophore production) during these conditions. Consistent with this ideology, our ICV experimental paradigm utilized the apo- form of Lcn2. Future studies should account for both apo- and holo- forms of Lcn2 when considering its effects on CNS function. Finally, our initial observations lead us to focus on the effects of Lcn2 on hippocampal biology, but it is conceivable that central Lcn2 mediates alterations elsewhere in the CNS. This remains an active area of investigation.

In summary, the data presented here demonstrate a temporal role of Lcn2 in mediating neuronal dysfunction and subsequent cognitive impairment. Given the evolutionarily-conserved role of Lcn2 in sequestering iron away from bacteria(97), along with recent reports of Lcn2's beneficial effect in the CNS during acute inflammation(127), it stands to reason that the rapid induction of Lcn2 in the CNS is an adaptive host response. Furthermore, recent evidence demonstrates that Lcn2 acts in a dose- and time-dependent fashion, as cells are able to tolerate high doses of Lcn2 acutely, but activate apoptosis after prolonged exposure(112, 139). These data demonstrate the dichotomous nature of Lcn2, having protective effects acutely, yet detrimental effects with prolonged exposure (Figure 9). Consistent with the notion of Lcn2 acting temporally, our study demonstrates Lcn2 chronically disrupts hippocampal cellular composition, ultimately leading to a concomitant decline in cognitive function. Together, our data implicate Lcn2 as a chronic mediator of CNS dysfunction and a potential therapeutic target for patients suffering from cognitive decline.

4. Methods

Mice

8-14 week-old C57BL/6J wild type (WT, JAX catalog number # 000664), Lipocalin 2 knockout (*lcn2-KO*, JAX catalog number # 024630), and Pomc-EGFP (JAX catalog number # 009593) mice were purchased from The Jackson Laboratory (Bar Harbor, ME) and maintained in our animal facility. *lcn2-KO* mice were generated on a C57BL/6J background. All mice were housed and bred in a dedicated mouse room with a

temperature 26˚C with a 12-hour light/dark cycle. Animals were provided *ad libitum* access to food and water (Rodent Diet 5001; Purina Mills). *lcn2-KO* mice were genotyped according to the standard protocol from The Jackson Laboratory. In behavioral studies, animals were individually housed for acclimation at least 7 days prior to interventional studies. Mouse studies were conducted in accordance with the National Institutes of Health Guide for the Care and Use of Laboratory animals, and approved by the Institutional Animal Care and Use Committee (IACUC) of Oregon Health & Science University.

Cell lines

The pancreatic cancer cell line used herein, generously provided by Dr. Elizabeth Jaffee, is derived from a C57BL/6J mouse with pancreatic-specific conditional alleles KRAS^{G12D} and TP53^{R172H} expression driven by the PDX-1-Cre promoter (KPC). The KPC model is a highly characterized and published model of PDAC cachexia due to its close biological semblance of human disease (38, 556, 585, 586). KPC cells were maintained in RPMI 1640 supplemented with 10% fetal bovine serum, 1% minimum essential medium non-essential amino acids, 1 mM sodium pyruvate, and 50 U/mL penicillin/streptomycin (Gibco). bEnd.3 cells were purchased from ATCC (ATCC CRL-2299) and maintained in DMEM supplemented with 10% fetal bovine serum, 1% minimum essential medium non-essential amino acids, 1 mM sodium pyruvate, and 50 U/mL penicillin/streptomycin (Gibco). All cells were grown in cell incubators maintained at 37˚ Celsius and 5% CO_2 and were routinely tested and confirmed negative for mycoplasma contamination prior to experimentation.

Primary glia culture and conditioned media studies

Primary mixed-glial cultures containing microglia and astrocytes were prepared from 1-3 day old WT C57BL/6J mouse pups. Briefly, cortices were dissected, freed of the meninges, and then digested with papain (Worthington Biochemical Corporation). Mixed cortical cells were passed through a 70-µm cell strainer and seeded in 75-cm^2 flasks for generating mixed-glia. Cultures were maintained 6 in DMEM media with low glucose supplemented with L-glutamine, 10% FBS and 1% penicillin/streptomycin. Media was refreshed every 3–4 days for 14–16 days. Primary microglia were isolated from mixed-glia by shaking flasks at 200 rpm for 2 hours in an incubator-shaker. More than 90% of the isolated cells were confirmed as microglia by Iba1 staining and flow cytometry (CD45+ CD11b+ cells, data not shown).

bEnd.3 cells, mixed-glia and isolated primary microglia were re-plated into 6-well plates (for mRNA analysis) and poly-D-lysine/laminin coated glass coverslips (Corning Biocoat,) in 24-well plates (for immunocytochemistry) for 1-2 days prior to treatment. KPC cells were cultured in a 75-cm^2 flask until 80-90% confluent. 24 hours prior to treatment, 13 ml fresh media (RPMI supplemented with 10% FBS and 1% penicillin–streptomycin) was added for generating KPC-conditioned media. On the treatment day, 4 parts KPC-conditioned media were mixed with 1 part fresh RPMI media prior to adding to mixed glia, primary microglia, and b3nd.3 cells plated in 6-well plates. Cells were treated with either KPC conditioned media, LPS (10 ng/mL), or control media (fresh RPMI media supplemented with 10% FBS and 1% penicillin–streptomycin). Each treatment condition was performed in triplicate. Cells were treated for 16 hours prior to

RNA extraction using a Qiagen RNAEasy kit or fixation with 4% paraformaldehyde for immunofluorescent staining with primary antibodies Lcn2 (R&D Systems, AF1857, goat, 1:500); GFAP (Calbiochem, IF03L-100UG, Mouse, 1:1000); Iba1 (Wako, 019-19741, Rabbit, 1:1000); CD31/PECAM (BD Pharmingen, 550274, Rat, 1:250); NeuN (Millipore, MAB377, Mouse, 1:1000). Secondary antibodies: donkey anti-goat AF630 (1:500); donkey anti-goat AF555 (1:500); donkey anti-mouse AF488 (1:1000); donkey anti-rabbit AF555 (1:1000); donkey anti-rat AF488 (1:500); goat anti-mouse AF594 (1:500). Cell nuclei were labeled with DAPI from the mount media (ProLong Gold Antifade media, Invitrogen).

Primary hippocampal neuronal culture

Wells of a 12-well plate were treated with Poly-D-Lysine (PDL, Sigma) overnight in a cell incubator on the day prior to hippocampal culturing. The morning of hippocampal dissection, PDL was aspirated from plates and wells were washed for 3 times with sterile water prior to adding hippocampal plating medium (NeuroQ basal medium [Global Stem] supplemented with 10% FBS, 1% GlutaMAX [Gibco], 1% Sodium pyruvate [Gibco], and 1% penicillin–streptomycin).

Pregnant (18 days post-fertilization) wild type C57BL/6J were rapidly killed by CO2 euthanasia and cervical dislocation. After sterilizing, an incision along the middle abdomen was made to expose uterine horns. Using sterile instruments, the uterus was opened and embryos were rapidly decapitated and heads placed in Hanks' balanced salt solution (HBSS) buffer (*Gibco 14175*). Whole brains were carefully removed from the skull base and immediately placed in fresh HBSS buffer. Ventrally, hippocampi were

freed from midbrain through gentle blunt dissection along meningeal foldings between the diencephalon and striatum (rostrally) to the caudal hippocampi (approaching base of the brain). Hippocampi were then blunt-dissected from the cortex and corpus callosum, and transferred to a 15 ml conical tube filled with 9 ml of HBSS. After hippocampi were allowed to settle to the bottom of the tube, 4.5 ml of HBSS was removed from the tube and replaced with 0.5 ml 2.5% trypsin (final concentration of 0.25%) and 50 µl of DNAse1 (final concentration of 1 mg/ml). Hippocampi were digested for 15 minutes in a 37C water bath swirling every 5 minutes. Supernatant was removed and enzymatic digestion was neutralized with plating medium (NeuroQ basal medium supplemented with 10% FBS, 1% GlutaMAX, 1% sodium pyruvate, and 1% penicillin–streptomycin). Hippocampi were dissociated and then passed through a 40 µm cell strainer. The resulting cell suspension was passed through another 40 µm cell strainer, and plated with plating medium in a 12-well plate at a density of 1-1.5 $x10^6$ cell/well (for mRNA analysis). 4 hours later after plating, plating medium was replaced with culture medium (NeuroQ basal medium supplemented with 1% GlutaMAX, 1% penicillin–streptomycin, and B-27 Plus supplement, Gibco). Day 3 after plating, half of the medium was replaced with culture medium containing 10 µM 5-fluoro-2'-deoxyuridine (FdU, Gibco). Day 6 after plating, one-third of the medium was replaced with fresh culture medium containing 10 µM FdU. All assays were started on day 7 after plating.

RNA Sequencing and bioinformatics analyses

Primary hippocampal neurons were treated with 100 ng/mL Lcn2 or vehicle control for either 1 or 4 days. Total RNA was purified with the RNeasy Mini Kit (Qiagen). Library

preparation and sequencing was performed by BGI Genomics at 100 base pair paired-end sequencing. Sequencing libraries were analyzed using the methods, parameters, and software versions, described this pipeline written in SnakeMake format. Briefly, reads were trimmed with bbduk and high-quality reads were screened for contamination with fastq_screen and aligned to the mm10 genome with STAR. Alignment features were filtered for protein-coding genes, and individual sample counts were aggregated into a counts table for input to DESeq2. Specific contrasts were constructed to facilitate differential expression analysis, such as Lcn2_1day-vs-Veh_1day and Lcn2_4day-vs-Veh_4day. Lowly-expressed genes with counts equal to or less than 1 across all samples were filtered away, and differential analysis was run with default settings. Results were extracted from the DESeq2 object by contrast and further analyzed with topGO with a BH p-value correction. Results were visualized using ggplot2. Below is a comprehensive list of bioinformatics tools utilized in the aforementioned pipeline, as well as hyperlinks to URL locations:

FastQ Screen: *https://pubmed.ncbi.nlm.nih.gov/30254741/*

Bbduk: *BBtools may be cited using the primary website: BBMap – Bushnell B. – sourceforge.net/projects/bbmap/*

STAR: ***https://www.ncbi.nlm.nih.gov/pmc/articles/PMC3530905/***

DESeq2:

https://genomebiology.biomedcentral.com/articles/10.1186/s13059-014-0550-8

topGO: ***https://bit.ly/3cHsbAz***

snake make:

https://snakemake.readthedocs.io/en/stable/project_info/citations.html

ggplot2: ***https://cran.r-project.org/web/packages/ggplot2/citation.html***

BH FDR adjustment: ***https://www.jstor.org/stable/2346101?seq=1***

Intracerebroventricular cannulation and injections

Mice were anesthetized using isoflurane and gently placed on a stereotactic alignment instrument (Kopf Instruments). Using sterile technique, bregma was exposed with a 3 mm incision and a 26-gauge lateral ventricle cannula was placed at 1.0 mm X, -0.5 mm Y, and -2.25 mm Z relative to bregma. Cannulas were secured to the skull with embedded screws and crosslinked flash acrylic. Mice were allowed 8 days for recovery after cannulation surgery. Recombinant mouse Lcn2 (R&D Systems, 40 ng) or vehicle were injected in a total volume of 2 uL. For repeated or single injection experiments of Lcn2 or vehicle, mice received injections under restriction, and received restriction training every day for 5 days prior to initial injections.

Cerebrospinal fluid extraction

Mice were anesthetized using isoflurane and placed on a stereotactic alignment instrument (Kopf Instruments). A 2 cm incision was made over the cisterna magna and the trapezius and paraspinal muscles were reflected. Blood and extracellular fluid lying over the cisterna magna were carefully removed to avoid CSF contamination. A glass micropipette (tip diameter of approximately 400-800 μm) was stereotactically inserted into the cisterna magna for capillary action-based CSF collection, transferred to a LoBind (Eppendorf) microcentrifuge tube, and immediately flash frozen.

In situ hybridization

Mice from control, LPS (acute inflammation, 24 hours after IP injection), or and pancreatic cancer (chronic inflammation, day 12 after tumor implantation) were sacrificed and underwent transcaridal perfusion with 20 mL PBS to ensure robust vasculature flushing. *In situ* hybridization was then performed on fresh frozen brains as previously described (325). Antisense ^{33}P-labeled mouse Lcn2 (*lcn2*) riboprobe (corresponding to bases 276-676 of murine *lcn2*; GenBank accession no. NM_008491.1 (.25 pmol/ml) was denatured, dissolved in hybridization buffer along with tRNA (1.7 mg/ml), and applied to slides. Slides were glass coverslipped, placed in a humidified chamber, and incubated overnight at 55 °C. The following day, slides were treated with RNase A and washed under conditions of increasing stringency. Slides were dipped in 100% ethanol, air dried, and then dipped in NTB liquid emulsion (Carestream Health Inc., Rochester, NY). Slides were developed 4d later and coverslipped.

Histology and Immunohistochemistry

Mice were deeply anesthetized using a ketamine/xylazine/acepromazine cocktail and sacrificed by transcardial perfusion with 20 mL PBS followed by ice cold 4% paraformaldehyde (PFA). Tissues were post-fixed in 4% PFA overnight at 4˚C prior to sectioning protocols. After post-fixation, brains were cryoprotected in 20% sucrose for 24 hours at 4˚C prior to 30 µM microtome sectioning. Free-floating sections were incubated in blocking solution for 1 hour at room temperature, followed by primary antibody incubation overnight at 4˚C. Sections were washed with PBS between steps.

Sections were then mounted on gelatin-coated slides and coverslipped with Prolong Gold anti-fade media (Thermofisher). Fluorescent-based images were acquired on a Nikon confocal microscope, while chromogen-based images were acquired using a Leica microscope (model DM 4000B).

Primary antibodies utilized above are listed with company, clone, host, species, and concentration defined in parentheses, respectively: Lcn2 (R&D Systems, AF1857, goat, 1:500); GFAP (Calbiochem, IF03L-100UG, Mouse, 1:1000); Iba1 (Wako, 019-19741, Rabbit, 1:1000); CD31/PECAM (BD Pharmingen, 550274, Rat, 1:250); NeuN (Millipore, MAB377, Mouse, 1:1000). Secondary antibodies: donkey anti-goat AF630 (1:500); donkey anti-goat AF555 (1:500); donkey anti-mouse AF488 (1:1000); donkey anti-rabbit AF555 (1:1000); donkey anti-rat AF488 (1:500); goat anti-mouse AF594 (1:500)

Image acquisition and analysis

Fluorescent images were acquired using a Nikon confocal microscope. 5-layer flattened Z-stack images of the hippocampus were procured using a 10× objective for wide view in the Lcn2 costains and CD45/MPO stain, 20x for the chronic Lcn2 gliosis staining, and 40x for the chronic Lcn2 NeuN quantification and Lcn2 costain insets. Images were 2048 x 2048 pixels, with a pixel size of 0.63 µm for 10x images, 0.32 µm for 20X images, and 0.16 µm for 40 X images. Images of POMC-GFP mice dentate gyri were taken using using a 40× objective. The hippocampus was identified by the granule cell layer of the dentate gyrus, which was positioned at the left end of each image.

Microglia, astrocytes, immune cells (CD45+ and MPO+), mature neurons, and GFP-positive newly born granule neurons dentate gyrus of POMC-GFP mice were quantified using the Fiji (ImageJ, NIH) plugin “Cell counter”. Microglia and astrocytic morphology were scored using a

validated activation scale described by Harrison et al(599). All images were quantified or scored by a blinded observer.

Quantitative real time PCR

Snap-frozen tissues or cell pellet were rapidly homogenized and RNA was purified with the RNeasy Mini Kit (Qiagen). Samples were then reverse-transcribed with the High Capacity cDNA Reverse Transcription Kit (Life Technologies). qRT-PCR was performed using reagents and TaqMan primer probes listed in **Supplementary table 1**. Tissues were normalized to 18S using the ddCT method.

Enzyme linked immunosorbent assay

Lcn2 concentrations in the CSF were assayed by ELISA according to the manufacturer's protocol (R&D Systems, Catalog # DY1857).

Flow cytometry

Contralateral brain halves from ICV treated, PBS-perfused mice were dispersed into a single cell suspension by straining through a steel mesh screen in RPMI. CNS mononuclear cells were isolated at the 40%-80% interface of a Percoll (Cytiva 17089101) step gradient after centrifugation at 500 x g for 45 minutes. Cells were washed, then resuspended in 100µl RPMI + 5%FBS and blocked for Fc receptor binding (TruStain FcX Plus, BioLegend 156604). Cells were stained with antibodies to the following surface markers for 1hr at 4^{o}C (cat. no., dilution): CD11b-BB515 from BD Biosciences (564454, 1:125). All remaining antibodies were obtained from BioLegend:

CD3-PE (100206, 1:100); CD45-PerCP-Cy5.5(103132, 1:125); CD19-APC (115512, 1:100); Ly6C-APC-Cy7 (128026, 1:200); Ly6G-BV421 (127628, 1:200). Live/Dead Fixable Aqua (ThermoFisher L34957) was used for the gating of viable cells. Samples were fixed (BD Cytofix, BD Biosciences 554655) for 15mins at 4^{o}C and run on the LSR II flow cytometer (BD Biosciences, San Jose, CA, USA). Gating and analysis were performed using FlowJo software version 10.1r7 (FlowJo LLC, Ashland, OR, USA).

Behavioral analysis

Y-maze spontaneous alternation assessment: 12-week old C57BL/6J mice were tested in a Y-maze apparatus consisting of three enclosed arms set at a 120˚ angle to one another, measuring 50 cm long, 11 cm wide, and 11 cm high. Visual cues were placed in the testing room around the Y-maze apparatus and kept constant throughout testing sessions. Mice were placed in the center of the maze and allowed to explore for a total of 5 minutes. Percentage alternation was calculated at the end of the study by the total number of successive alternations, defined as sequential entry into three different arms, divided by the total number of arm entries minus 2. **Y-maze blocked arm assessment:** utilizing the same Y-maze described above, mice were placed at the end of a randomly chosen arm and allowed to explore the maze for 5 minutes with one arm closed. After a 2-hour intertrial interval, mice were re-introduced to the maze (in the different arm than the acquisition trial, but not the novel arm) with all arms open and allowed to explore again for 5 minutes. Time spent in each arm was recorded, and the percentage of time spent in the novel arm was calculated (time spent in novel arm/total time spent in all three arms). **Novel object recognition:** Mice were subjected to a novel

object recognition test utilizing the well-established protocol by Leger et al with some minor modifications (619). Briefly, we tested mice with two identical objects placed in an open-field apparatus composed of a black wooden box measuring 33 × 33 × 20 cm. We utilized two different objects (Falcon tissue culture flask filled with sand and an equally-sized LEGO tower) in triplicate to minimize olfactory and sensory cues between the familiarization and test sessions. During the familiarization trial, mice were allowed to explore two identical objects in the open field until a total object exploration time of 20 seconds was achieved. After a 6-hour intertrial interval, mice were re-introduced to the open field with the familiar and novel object and allowed to explore for a total of 10 minutes. Preference index was calculated as time spent with novel object minus time spent with familiar object divided by total exploration time. **Light-dark box:** Mice were placed in the light compartment of a light-dark box and allowed to traverse the apparatus for 5 minutes. The test apparatus consisted of two equally-sized plexiglass compartments (one opaque/dark compartment, and one clear/light-penetrating compartment) with a small opening through which mice could enter and leave. Total time in each compartment, latency to enter the dark compartment after placement in the light compartment, as well as total number of transitions, were recorded. **Tail suspension test:** Four mice at a time were suspended by the tail using 17 cm tape strands (allowing for the last 2 cm to loop around the animal's tail) from a wooden dowel, separated by a wooden contraption that does not allow for mice to visualize one another. Prior to taping the tail, a small rigid plastic tube was placed proximal to the end of the tail where tape was then fastened to prevent mice from climbing. Mice were suspended for a total of 6 minutes with total time immobile being recorded. **Nest building:** Nest

building and blinded scoring was performed as previously reported(620). Briefly, mice were supplied a new 3.0 g nestlet along with the removal of used enrichment items one hour before the dark phase. The next morning (approximately 15 hours later unless otherwise indicated) nests were scored on a rating scale of 1-5 as described by Deacon(620). Where appropriate, all behavioral testing equipment was thoroughly cleaned with 70% ethanol between trials and mice to minimize olfactory cues.

Statistics

All statistical analyses for murine data were performed in GraphPad Prism 8.0 software. Quantitative data are reported as mean +/- standard error. Two-tailed Students t-tests were performed when comparing two groups. When comparing more than two groups of a single genotype, One-way ANOVA was utilized. Two-way ANOVA with Bonferroni multiple comparisons test was utilized when comparing multiple genotypes and treatment groups (sham and tumor; sham and LPS) unless otherwise specified in figure legends. For all analyses, a p value of < 0.05 was considered to be statistically significant.

Author contributions

BO and DM designed the study, analyzed the data, and wrote the manuscript with input from the other authors. BO, XZ, MN, PD, PL, AB and CH performed experiments and analyzed data. KB, KM, GK, and TB contributed with discussion, data abstraction, and data interpretation.

Acknowledgements

We are grateful for the help of several investigators and core laboratories, including Ashley J. Olson, Stephanie Krasnow, the OHSU flow cytometry core, and the OHSU advanced light microscopy core. This work was supported by NCI R01CA184324 (Marks), the Brenden-Colson Center for Pancreatic Care (Marks), and NIH F30CA254033 (Olson).

DM is a consultant for Pfizer, Inc. and Alkermes, Inc. DM is a consultant, has received grant funding, and has equity in Tensive Controls, Inc. All other authors declare no conflicts of interest.

Chapter 5: Physiologic and molecular characterization of a novel murine model of metastatic head and neck cancer cachexia

A manuscript under review at *Journal of Cachexia, Sarcopenia, and Muscle*

Physiologic and molecular characterization of a novel murine model of metastatic head and neck cancer cachexia

Brennan Olson[1,2], Mason A Norgard[1], Peter R Levasseur[1], Xinxia Zhu[1], *Daniel L Marks[1,3,4]

1. Papé Family Pediatric Research Institute, Oregon Health & Science University, Portland, OR USA
2. Medical Scientist Training Program, Oregon Health & Science University, Portland, OR USA
3. Brenden-Colson Center for Pancreatic Care, Oregon Health and & Science University Portland, OR USA
4. Knight Cancer Institute, Oregon Health & Science University, Portland, OR USA

*Corresponding Author Information

Daniel L. Marks, MD, PhD

3181 SW Sam Jackson Park Road

L 481

Portland, OR 97239

Email: marksd@ohsu.edu

Abstract

Background

Cancer cachexia is a metabolic disorder characterized by the progressive loss of fat and lean mass that results in significant wasting, ultimately leading to reduced quality of life and increased mortality. Effective therapies for cachexia are lacking, potentially owing to the mismatch in clinically relevant models of cachexia. Specifically, cachexia observed in a clinical setting is commonly associated with advanced or late-stage cancers that are metastatic, yet pre-clinical metastatic models of cachexia are limited. Furthermore, the prevalence of cachexia in head and neck cancer patients is high, yet few preclinical models of head and neck cancer cachexia exist. In addition to these shortcomings, cachexia is also heterogeneous amongst any given cancer, whereas patients with similar disease burden may experience significantly different degrees of cachexia symptoms. In order to address these issues, we characterize a metastatic model of human papilloma virus (HPV) positive head and neck squamous cell carcinoma that recapitulates the cardinal clinical and molecular features of cancer cachexia.

Methods

Male and female C57BL/6 mice were implanted subcutaneously with an oropharyngeal squamous cell carcinoma cells stably transformed with HPV16 E6 and E7 together with hRas and luciferase (mEERL) that metastasizes to the lungs (MLM). We then robustly characterize the physiologic, behavioral, and molecular signatures during tumor development in two MLM subclones.

Results

Mice injected with MLM tumor cells rapidly developed primary tumors and eventual metastatic lesions to the lungs. MLM3, but not MLM5, engrafted mice progressively lost fat and lean mass during tumor development despite the absence of anorexia ($p < 0.05$). Behaviorally, MLM3-implanted mice displayed decreased locomotor behaviors and impaired nest building ($p < 0.05$). Canonical muscle catabolism programs associated with cachexia, including E3 ubiquitin ligase and autophagy upregulation, along with progressive adipose wasting and accompanying browning gene signatures, were observed. Tumor progression also corresponded with hypothalamic and peripheral organ inflammation, as well as an elevation in neutrophil-to-lymphocyte ratio ($p < 0.05$). Finally, we characterize the fat and lean mass sparing effects of voluntary wheel running on MLM3 cachexia ($p < 0.05$).

Conclusions

This syngeneic MLM3 allograft model of metastatic cancer cachexia is reliable, consistent, and readily recapitulates key clinical and molecular features and heterogeneity of cancer cachexia. Since few metastatic models of cachexia exist—even though cachexia often accompanies metastatic progression—we believe this model more accurately captures cancer cachexia observed in a clinical setting, and thus is well suited for future mechanistic studies and preclinical therapy development for this crippling metabolic disorder.

Graphical Abstract

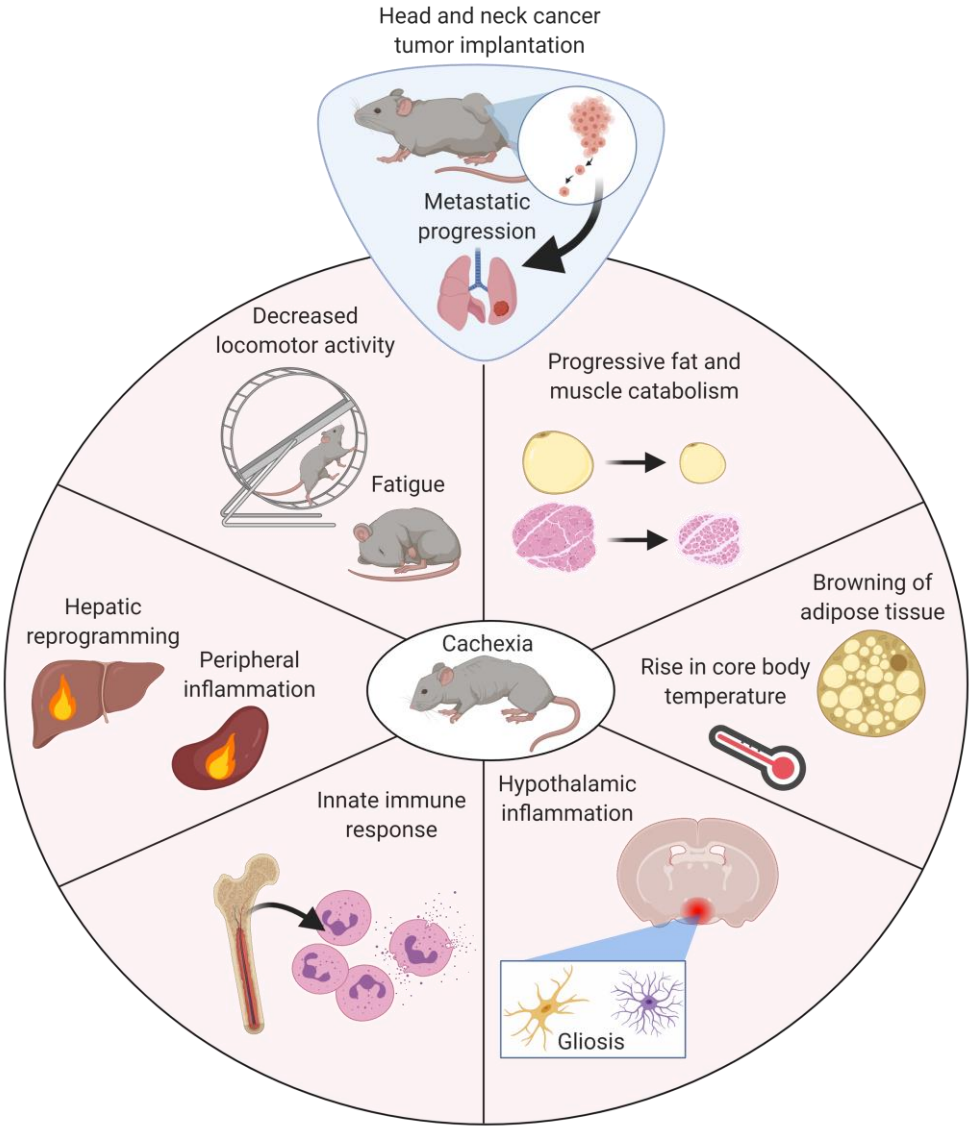

Keywords: cachexia, head and neck cancer, metastasis, inflammation, muscle wasting, fat wasting

1. Introduction

Cancer-associated cachexia is a metabolic disorder characterized by a progressive loss of body mass with preferential catabolism of muscle and adipose tissue (6, 15, 621). In addition to physical deterioration, cachexia manifests distinct behavioral adaptations, including anorexia, fatigue, anhedonia, and cognitive decline (15, 165). These signs and symptoms of cachexia significantly influence patients' quality of life, ability to tolerate treatment, and eventual mortality(622, 623). Despite the prevalence and clinical burden cancer-cachexia imposes, effective therapies are lacking. In fact, over one hundred clinical trials of human cancer cachexia have been conducted to date, yet none resulted in the approval of an effective therapy(166-170). This lack of translation from preclinical models of cachexia to human trials is not lost on those in the field of cachexia research, as there is a recent push to improve the predictive capacity of our commonly used rodent models of cachexia(624). Specifically, researchers are suggesting using older animals, mimicking clinical treatment modalities, and models of recurrent and/or metastatic disease(6, 166, 170, 625-627). The latter is a particularly noticeable feature lacking from current animal models, as metastatic disease and cachexia are closely associated in a clinical setting(628-631), and recent research suggests the metastatic cascade mediates unique systemic features of cachexia that cannot be solely explained by the biology of the primary tumor(632-634).

To this end, we sought to establish and characterize a model of cancer cachexia that is technically simple, reliable, reproducible, and addresses several of the aforementioned concerns of current cancer cachexia models posed by researchers in the field. Specifically, we characterize a metastatic HPV+ squamous cell carcinoma

model of head and neck cancer (HNC) cachexia that utilizes a metastatic cell line isolated from the lung from an animal that previously failed a cisplatin/radiation regimen(635). Since it is estimated that cachexia affects nearly half of patients diagnosed HNC(6, 14, 636, 637), and very few HNC or recurrent/metastatic animal models of cachexia exist, we believe this model helps bridge this important gap in cachexia research.

Herein, we robustly characterize the molecular and behavioral features mice injected with a syngeneic oropharyngeal squamous cell carcinoma cell line stably transformed with HPV16 E6 and E7 together with hRas and luciferase (mEERL) that metastasizes to the lungs (MLM)(635). Utilizing two MLM subclones with near identical tumor growth trajectories, we observed heterogenous cachexia responses to these two cell lines. Implantation of the MLM3 subclone resulted in significant muscle, fat, and body mass loss compared to the MLM5 subclone. Since MLM3-engraftment resulted in a significant wasting phenotype consistent with cachexia, we further characterized the behavioral and molecular features of MLM3 cachexia. Specifically, mice were assessed for gross fluctuations in body composition, including fat and lean mass atrophy, as well as commonly observed cachexia behaviors, including food intake and locomotor activities. Finally, we assess end-organ molecular adaptations associated with cancer-cachexia progression, including fast-twitch and slow-twitch fiber-enriched skeletal muscle groups, the central nervous system (CNS), heart, liver, spleen, brown (BAT) and white adipose tissue (WAT), as well as the blood/plasma.

2. Results

The MLM3 clone is uniquely cachexigenic

Since cachexia is broadly heterogenous and influenced by several host and tumor parameters, we first sought to determine if the equivalently growing MLM3 and MLM5 subclones induced a similar degree of cachexia-associated wasting(635). Consistent with studies performed by Vermeer and colleagues, the MLM3 and MLM5 clones display equivalent tumor growth in our studies (Figure 1A; Supplemental Figure 1A)(635). However, despite this nearly identical tumor growth, MLM5 implantation resulted in minimal body mass alterations compared to sham controls, while MLM3-implanted mice displayed a progressive loss of body mass (Figure 1B-C). We observed no differences in food consumption for MLM3-engrafted male mice compared to sham controls, yet MLM5-engrafted male mice demonstrated a modest hyperphagia phenotype (Figure 1D). Consistent with the progressive loss of body mass, MLM3-engrafted mice display a significantly increased fat wasting phenotype compared to MLM5-engrafted mice (Figure 1E-F). Additionally, whole-body lean mass, terminal gastrocnemius mass, and terminal cardiac tissue mass were significantly decreased in the MLM3-engrafted mice when compared to both sham and MLM5-engrafted mice (Figure 1G-I). The improvement in gross skeletal muscle mass in MLM5-engrafted mice was associated with decreased ubiquitin ligase expression in the gastrocnemius muscle (Supplemental Figure 1B). MLM5 mice displayed significantly increased blood glucose levels at the time of sacrifice compared to MLM3-engrafted mice, potentially owing to their improved caloric intake (Supplemental Figure 1C). MLM5-engrafted mice displayed

an intermediate hepatic inflammatory gene profile between sham and MLM-5 engrafted mice, as indicated by *Il-1β, Il-6,* and *Orm1* gene expression, although none of these were significantly altered compared to the MLM3 group alone (Supplemental Figure 1D). Interestingly, MLM5 engrafted mice displayed significantly larger spleens compared to the MLM3 group (Supplemental Figure 1E). Taken together, MLM3 and MLM5 cell lines display similar growth in vivo, yet demonstrate drastically different wasting phenotypes. These studies serve not only to validate the utility of MLM3 as a unique model of cancer cachexia, but also provides an invaluable non-cachexigenic comparator in MLM5. Future in vivo and in vitro studies comparing these two tumor models could prove useful for the identification of tumor-specific cachexia "factors" that may drive wasting in MLM3, but not MLM5.

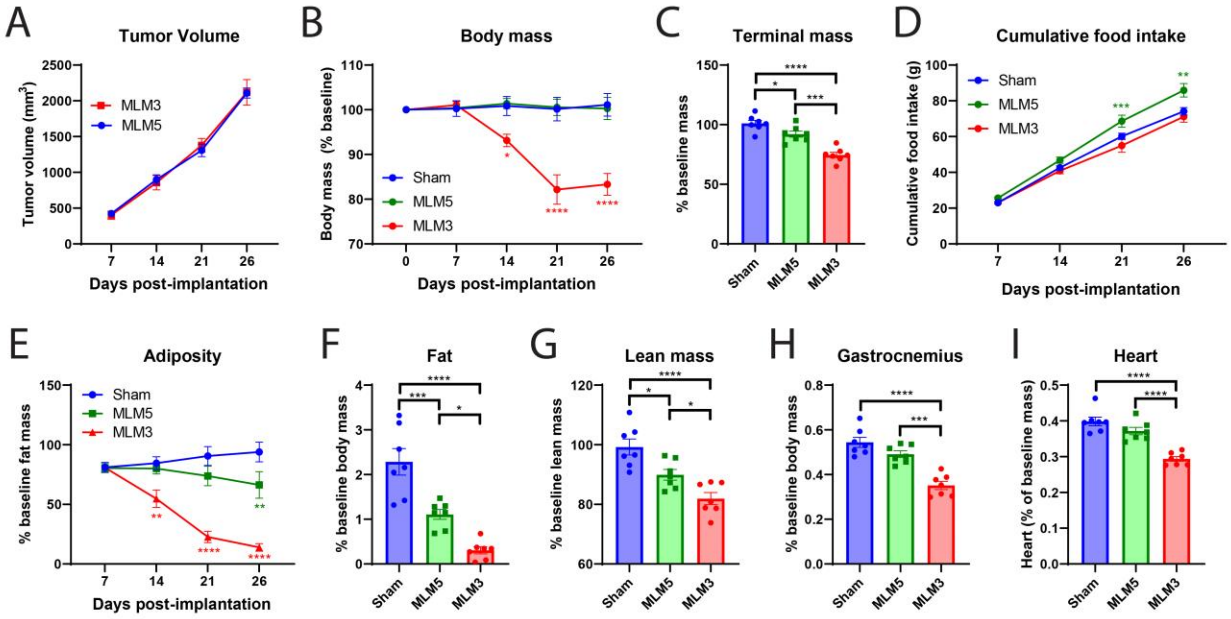

Figure 1. MLM3 engraftment results in significantly increased muscle and fat catabolism compared to the MLM5 subclone. (A) Tumor volume in MLM3 and MLM5

engrafted male mice. (B) Sequential and (C) tumor-free body mass in sham, MLM3-, and MLM5-implanted mice. (D) Cumulative food intake in sham, MLM3-, and MLM5-implanted mice. (E) Sequential NMR fat mass and (F) terminal gonadal WAT mass. (G) Terminal lean mass NMR, (H) gastrocnemius mass, and (I) cardiac tissue mass. All data are expressed as mean ± SEM. *p ≤ 0.05, **p ≤ 0.01, and ***p ≤ 0.001. N = 7 per group.

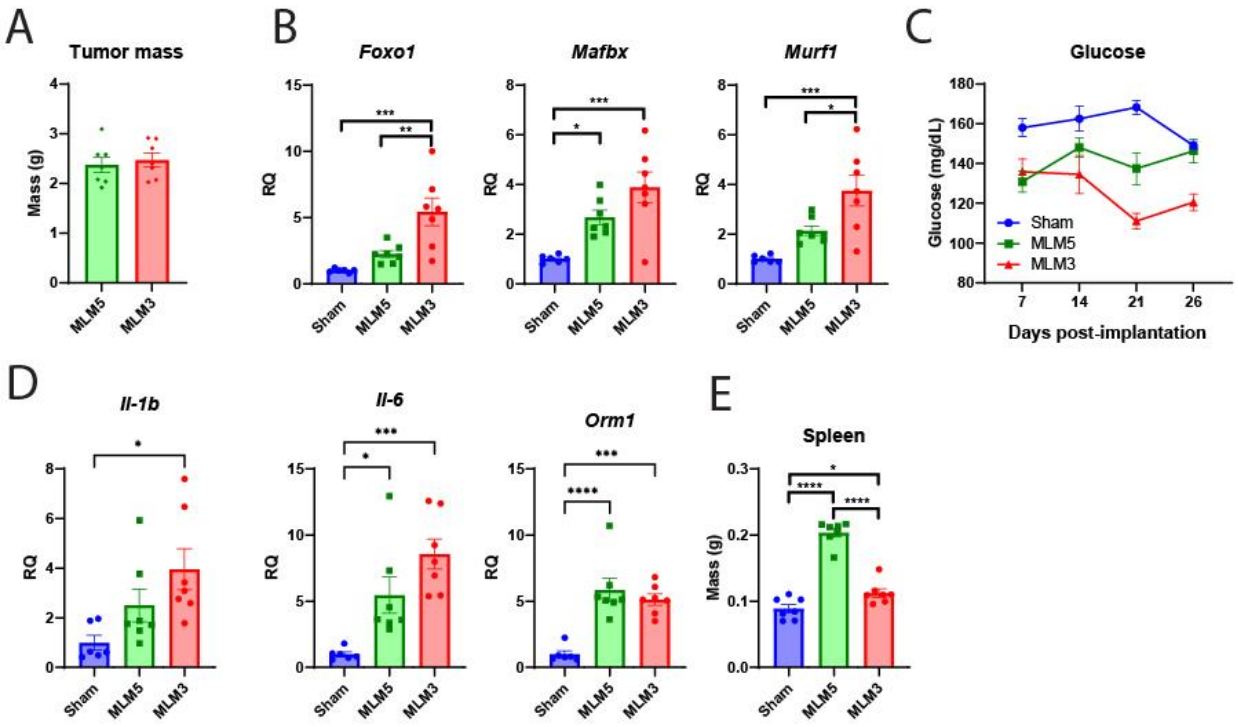

Supplemental Figure 1. Related to Figure 1. (A) Terminal tumor mass in MLM3 and MLM5 engrafted male mice. (B) Ubiquitin proteasome pathway gene expression in gastrocnemius muscle in sham, MLM3-, and MLM5-implanted mice. (C) Blood glucose levels in sham, MLM3-, and MLM5-implanted mice. (D) *IL-1β, Il-6, and Orm1* hepatic

gene expression in sham, MLM3-, and MLM5-implanted mice. (E) Terminal splenic mass in in sham, MLM3-, and MLM5-implanted mice.

MLM3 implantation results in the clinical signs and symptoms of cachexia in both male and female mice

With the identification of significant lean and fat mass catabolism in MLM3-engrafted male mice, we sought to further characterize the wasting features of MLM3 in both male and female mice. Indeed, subcutaneous implantation of MLM3 cells result in sickness behaviors associated with cachexia in both male and female models, including the progressive loss of body mass over the course of tumor development (Figure 2A, Supplemental Figure 2A-C). Both male and female MLM3-implanted mice displayed a significant loss of body mass at the necropsy as indicated by tumor-free mass (Figure 2B). When monitoring food daily food intake, male mice exhibited no alterations in food consumption between tumor and sham groups, while female tumor-bearing mice experienced a phase of relative hyperphagia starting at day 13 after tumor implantation (Figure 2C). Since cachexia is associated with preferential catabolism of fat and lean mass, we assessed both fat and lean compartments by nuclear magnetic resonance imaging (NMR). MLM3-engrafted males exhibited a progressive reduction in total-body fat mass, whereas tumor-bearing female mice lost a significant portion of their baseline fat mass early in the study (Figure 2D). Since portions of the tumor mass encode as lean mass by NMR, we assessed tumor-free lean mass at the study's end. Indeed, we observed a significant loss of total-body lean mass at the time of sacrifice in males, but

not females (Figure 2E). Finally, we assessed sham and tumor-implanted mice's willingness to build nests at 7-day intervals throughout the study. Since nest building is an enjoyable activity for mice, but also an evolutionarily-conserved behavior to insulate animals and conserve energy during sleep, nest building is a useful surrogate measure of anhedonia and overall well-being(620). Tumor-implanted mice displayed a significant reduction in nest-building behaviors at only advanced-stage disease (day 21 post-implantation). Collectively, we conclude that the MLM3 implantation results in a progressive loss of body mass, preferential catabolism of fat and lean mass, as well as decreased overall health and well-being, measures consistent with cachexia observed in a clinical setting.

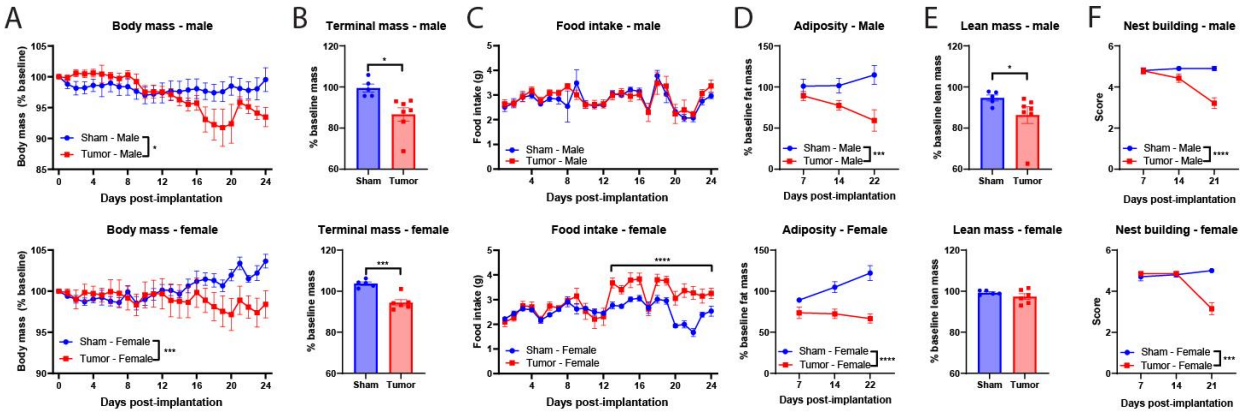

Figure 2. MLM3 implantation recapitulates key clinical signs and symptoms of cachexia. (A) Daily and (B) tumor-free body mass in MLM-engrafted and sham-operation controls in male and female cohorts. (C) Daily food intake in MLM-engrafted and sham-operation controls in male and female cohorts. (D) Sequential NMR fat mass and (E) terminal lean mass measures. (F) Sequential nest building scores. N = 5-7 per group. All data are expressed as mean ± SEM. *p ≤ 0.05, **p ≤ 0.01, and ***p ≤ 0.001.

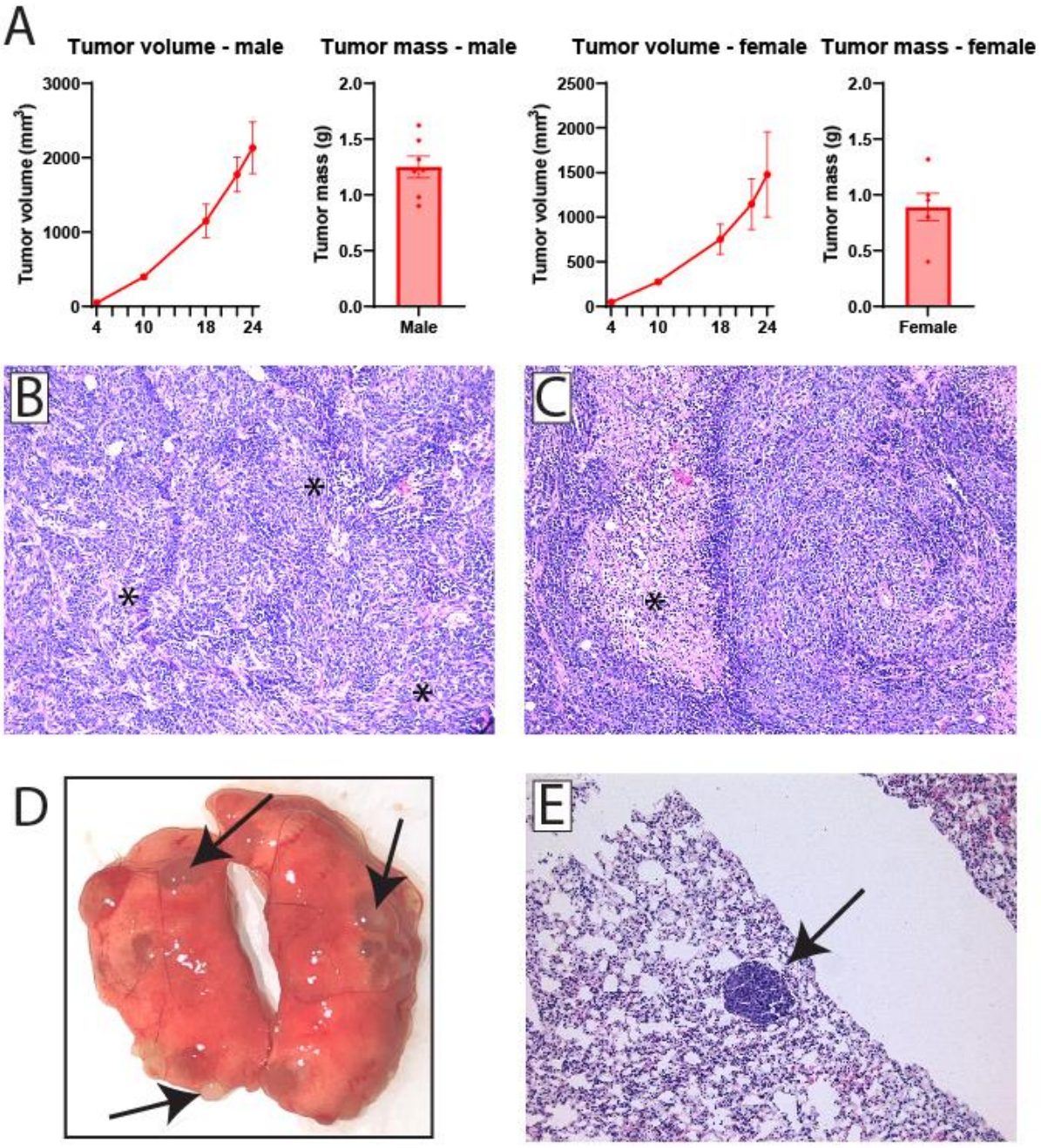

Supplemental Figure 2. Related to Figure 2. (A) Tumor volume and terminal tumor mass in MLM3-engrafted male and female mice. (B-C) Representative H&E histochemical images of primary MLM3 tumors, highlighting areas of (B) ragged stromal infiltration and

(C) focal necrotic loci. (D) Representative image of diseased lungs with metastatic lesions (arrows), and (E) representative histochemical image of microscopic metastatic MLM3 lesion (arrow).

MLM3 engraftment results in progressive reduction in locomotor behaviors

Since fatigue and lethargy produce significant impairments in patients' quality of life, future models of cancer cachexia should recapitulate these important clinical symptoms(6, 15). Thus, we sought to characterize home-cage locomotor activity (LMA) and voluntary wheel running throughout the course of MLM3 cachexia development. In assessing home cage LMA, we divided activity into 12 h light and dark cycles that correspond with sleep and wake cycles, and created tertile cachexia bins in accordance with the weight loss trajectory observed in Figure 2A (whereas minimal weight change is observed in the first third of the study). MLM3 tumor implantation resulted in a reduction of wake cycle activity beginning on day 8 post-implantation (Figure 3A-B), while sleep cycle activity was largely unaffected (Figure 3C-D). We also assessed voluntary wheel running behaviors in MLM3 implanted mice, as this behavior is not only a measure of tumor-associated fatigue, but also hedonic activity, as non-captive mice will elect to run on a wheel for long periods without incentive(638). Indeed, we observe a progressive reduction in wheel running in MLM3 implanted mice, with a significant and sustained reduction in wheel running starting day 7 post-implantation (Figure 3E-G). The consistent and progressive decline in both home-cage LMA and voluntary wheel

running in this cachexia model demonstrates its utility in studying this important facet of cancer cachexia.

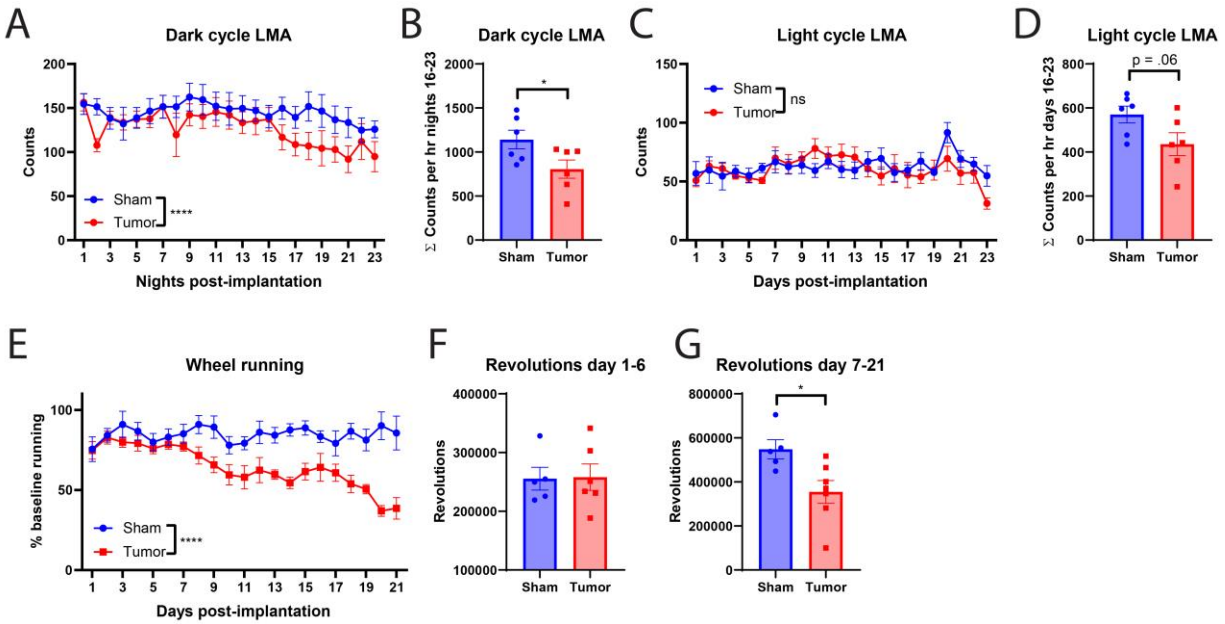

Figure 3. MLM3 implantation results a progressive decline in home-cage locomotion and voluntary wheel running behaviors. (A) Daily dark cycle locomotor activity in counts per hour, and (B) cumulative counts per hour from days 16-23 (late cachexia). (C) Daily light cycle locomotor activity in counts per hour, and (D) cumulative counts per hour from days 16-23 (late cachexia). (E) Daily voluntary wheel running as a percentage of baseline running. Cumulative revolutions from study days (F) 1-6 and (G) 7-21. (A-D) N = 6 per group. (E-G) N = 5-6 per group. All data are expressed as mean ± SEM. *p ≤ 0.05, **p ≤ 0.01, and ***p ≤ 0.001.

Lean mass catabolism associated with MLM3-cachexia is driven by autophagy and ubiquitin-ligase pathways

Since cardinal features of clinical cachexia include progressive muscle and fat catabolism, preclinical models should recapitulate these wasting trajectories, both grossly and molecularly. Here we characterized skeletal and cardiac tissue catabolism in MLM3-engrafted mice and observed significant lean mass wasting at the study's end. In the skeletal muscle compartment, MLM3-engrafted mice displayed significant wasting of fast-twitch fiber muscles, including the gastrocnemius, quadriceps, and tibialis anterior muscle (Figure 4A-C). The soleus, a slow twitch fiber muscle, also displayed significant catabolism (Figure 4D). Consistent with other preclinical models of cancer cachexia, including the $KRAS^{G12D}$ $P53^{R172H}$ $Pdx\text{-}Cre^{+/+}$ pancreatic ductal adenocarcinoma (KPC)(38), Lewis lung carcinoma (LLC)(639, 640), and C26 colorectal adenocarcinoma (C26)(641), MLM3-engrafted mice display a significant induction of the E3 ubiquitin ligase genes *Mafbx*, *Murf1*, and *Foxo1* in skeletal muscle (Figure 4E). Cardiac tissue atrophy was measurable in male tumor-bearing mice, whereas females were resistant to cardiac wasting (Figure 4F). Despite minimal alterations in gross cardiac wasting as indicated by organ mass, we observed a significant induction of autophagy genes *Cstl, Gabarapl,* and *Bnip3* in MLM3-engrafted mice (Figure 4G). While these autophagy-related genes were significantly regulated during MLM-cachexia in the heart, E3 ubiquitin ligase genes *Mafbx*, *Murf1*, and *Foxo1* were not significantly alerted in the heart between tumor and sham mice (Figure 4H). Collectively, the lean mass wasting observed in MLM3-engrafted mice is driven by activation of ubiquitin proteasome and autophagy pathways, two key catabolic pathways that drive cachexia-associated wasting in other highly studied murine models.

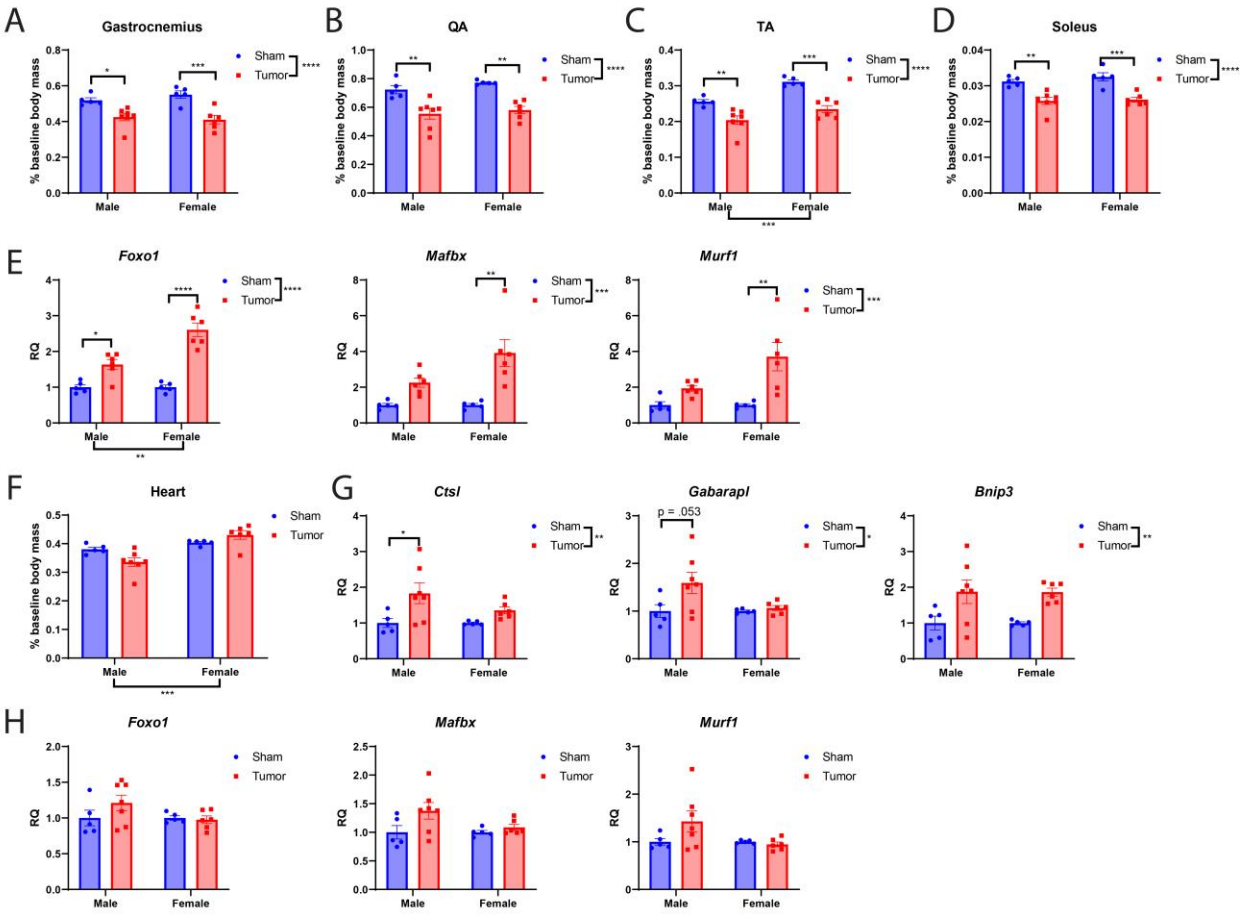

Figure 4. MLM engraftment results in skeletal and cardiac tissue catabolism and elevation of ubiquitin ligase and autophagy gene expression. (A) Gastrocnemius, (B) quadriceps, (C) tibialis anterior, and (D) soleus muscle mass normalized to body mass in MLM-engrafted and control mice. (E) Ubiquitin proteasome pathway gene expression in gastrocnemius muscle. (F) Cardiac muscle mass normalized to body mass. (G) Autophagy and (H) ubiquitin proteasome pathway gene expression in cardiac tissue. N = 5-7 per group. All data are expressed as mean ± SEM. *p ≤ 0.05, **p ≤ 0.01, and ***p ≤ 0.001. QA = quadriceps; TA = tibialis anterior.

MLM3-cachexia results in fat mass wasting, browning of white adipose tissue, and elevation of core body temperature

Another important facet of cancer cachexia that accompanies the progressive loss of fat mass is the metabolic reprogramming in this tissue that activates thermogenic pathways. In both pancreatic and lung cancer genetically engineered mouse models (GEMMs) of cachexia, the browning of white adipose tissue (WAT) corresponded with increased systemic energy expenditure(52). In the present model of MLM3 cachexia, we observe significant wasting of WAT (Figure 5A, Supplemental Figure 3A) and elevation of browning genes *Ucp1* and *Cidea*, yet decreased expression of *Prdm16* and *Ppar-γ* (Figure 5B). In brown adipose tissue (BAT), we also observe a significant increase in thermogenesis gene *Ucp1* (Figure 5C, Supplemental Figure 3B). The observed thermogenesis programs induced in in the fat of MLM3-engrafted mice was independent of PTHrP, as neither male nor female cohorts exhibited an increase in circulating levels (Supplemental Figure 3C-E). Since we observed an elevation in thermogenesis genes in both WAT and BAT, we next monitored core body temperature during the development of MLM3-cachexia. Tumor-bearing mice displayed an elevation in core body temperature during both light and dark cycles early- to mid-stage disease (days 7-14), while temperatures approached that of control mice during late-stage cachexia (days 15-22/23) (Figure 5D-E).

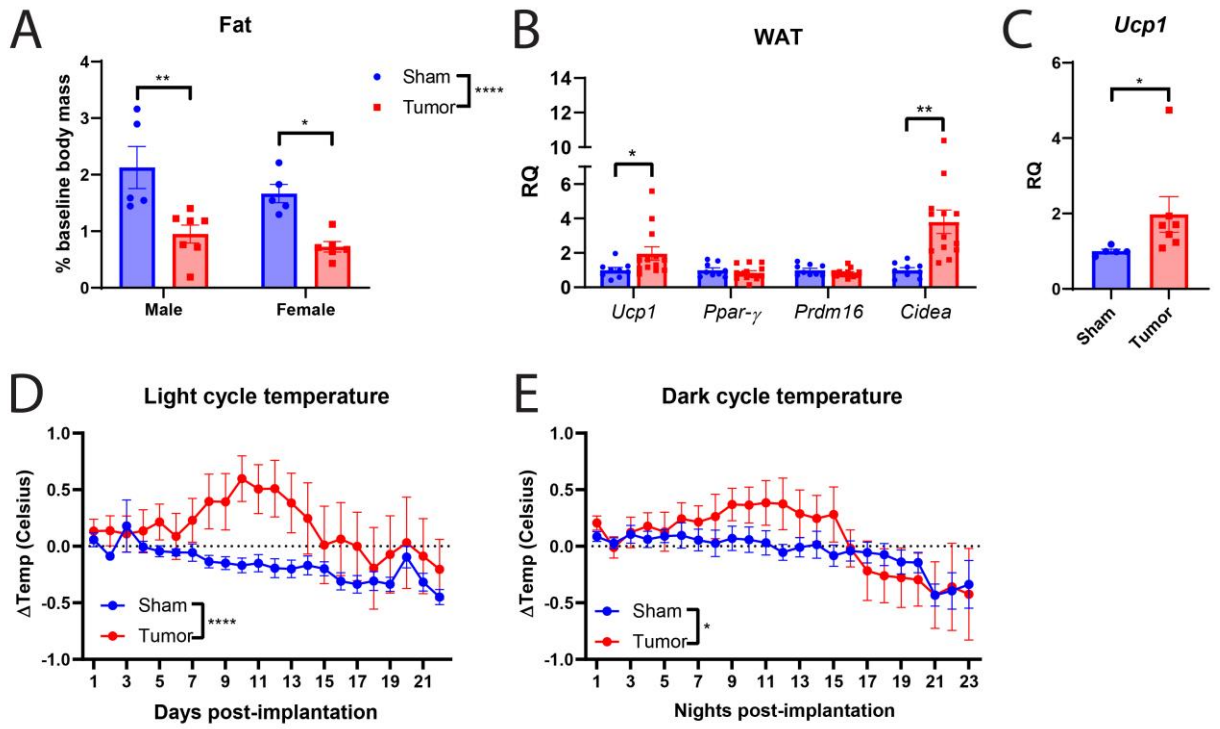

Figure 5. MLM-cachexia results in white adipose tissue browning, elevation of thermogenesis in brown adipose tissue, and increased core body temperature. (A) Gonadal WAT mass normalized to body mass at the time of sacrifice. (B) WAT browning gene expression and (C) BAT *Ucp1* gene expression in male mice engrafted with MLM3 tumors or sham-operation controls. (D) Light and (E) dark cycle body temperature change in male mice engrafted with MLM tumors or sham-operation controls. (A-C) N = 5-7 per group; (B) N = 8-12 per group. (D-E) N = 6 per group. All data are expressed as mean ± SEM. *p ≤ 0.05, **p ≤ 0.01, and ***p ≤ 0.001.

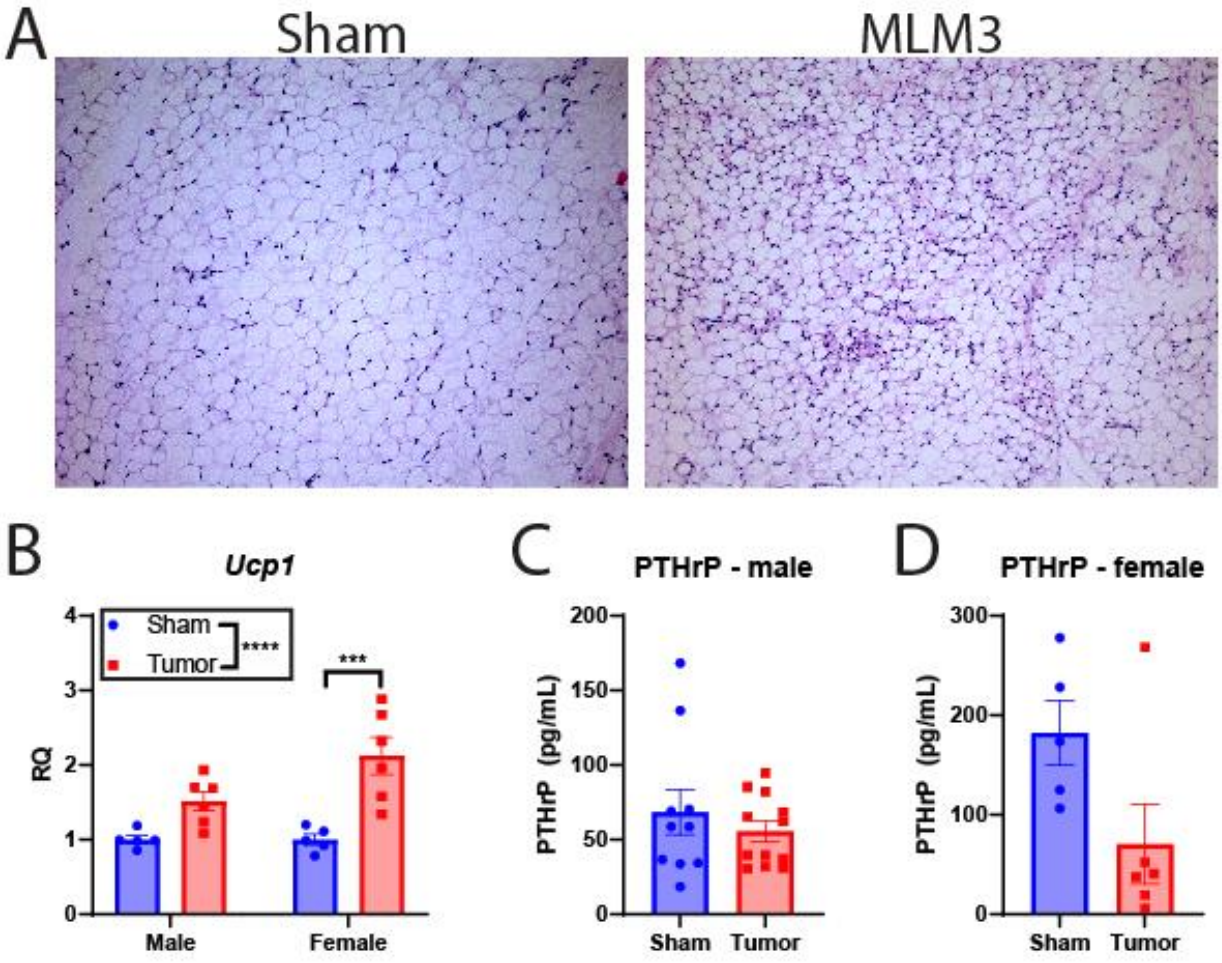

Supplemental Figure 3. Related to Figure 5. (A) Representative H&E histochemical images of gonadal white adipose tissue of male mice after sham operation or MLM3 tumor engraftment. (B) BAT *Ucp1* expression in male and female mice after sham operation or MLM3 tumor engraftment. Plasma PTHrP levels in (C) male and (D) female mice after sham operation or MLM3 tumor engraftment.

MLM3-cachexia results in hypothalamic inflammation

Since the hypothalamus is a critical central nervous system (CNS) structure in regulating metabolic and behavioral programs, and a growing body of evidence

implicate aberrant hypothalamic processes in cachexia pathology, we sought to determine if MLM-cachexia is associated with hypothalamic inflammation as observed in other models of cancer cachexia(13, 20, 38, 70). We observe a robust elevation of inflammatory cytokine *Il-1β,* but no alterations in *Il-6, Nos2, and Tnf-α* (Figure 6A). In addition to an elevation of inflammatory cytokine expression in the mediobasal hypothalamus (MBH) during cachexia, infiltration of peripheral immune cells was recently identified as a mediator of cachexia symptoms in the KPC pancreatic cancer model(20). We observe a significant elevation of cell adhesion molecule *Selp*, chemokines *Cxcl1,* and chemokine-inducer and neutrophil chemoattractant *lcn2*(96, 642), while *Cxcl10* is downregulated, and Cxcl2 and Ccl2 were unaffected by tumor engraftment (Figure 6B). Interestingly, the orexigenic peptide *Agrp* was significantly elevated in both male and female tumor-bearing mice, although only MLM3-engrafted females exhibited hyperphagia at the time of sacrifice (Figure 6C). In addition to the transcriptional inflammatory profile observed in the hypothalamus of MLM3-engrafted mice, we observed an increase in microglia and astrocytes in the median eminence, a circumventricular organ that contains an attenuated blood-brain barrier (Figure 6D-F). The arcuate nucleus and ventromedial hypothalamic nucleus demonstrated an increase in astrocytes in the MLM3 group, but no difference in the number of microglia (Figure 6D-F).

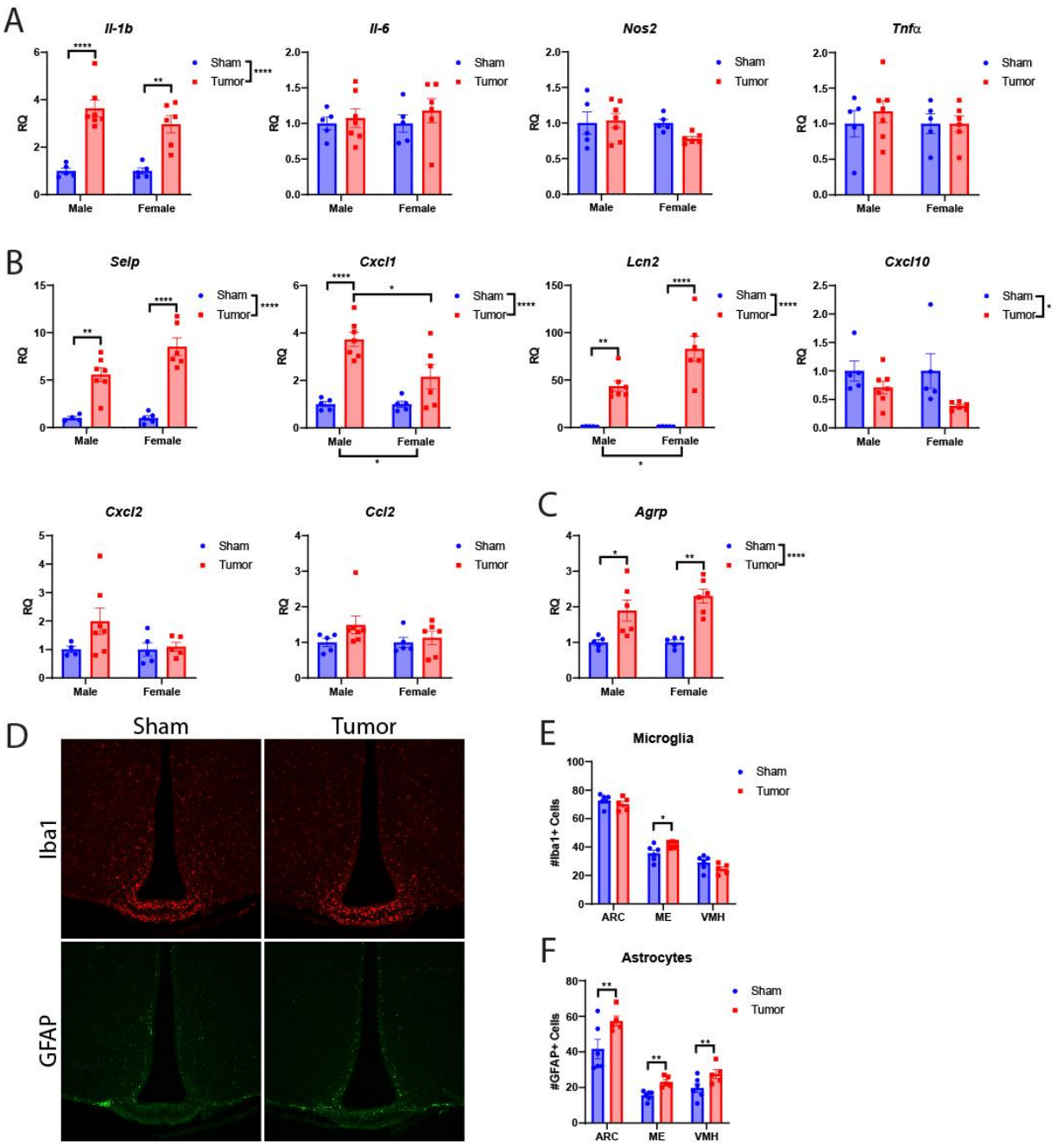

Figure 6. MLM cachexia is associated with hypothalamic inflammation and gliosis in the mediobasal hypothalamus. (A) Hypothalamic inflammatory gene expression in MLM-engrafted and control mice. (B) Hypothalamic cell adhesion and chemokine-related genes in MLM-engrafted and control mice. (C) *Agrp* gene expression in MLM-engrafted and control mice. (D) Representative fluorescent immunohistochemistry

images of the hypothalamus, staining for microglia (Iba1) and astrocytes (GFAP). (E) Microgliosis and (F) astrogliosis score in select hypothalamic regions in sham and tumor-bearing mice (N = 6 per group). N = 5-7 per group. All data are expressed as mean ± SEM. *p ≤ 0.05, **p ≤ 0.01, and ***p ≤ 0.001. ARC; Arcuate nucleus, ME; Median eminence, VMH; Ventromedial hypothalamus.

MLM engraftment results in neutrophil expansion and elevated neutrophil-to-lymphocyte ratio

A burgeoning area of cachexia research describes how the immune system influences biological processes, including metabolism, inflammation, and neuroendocrine function (20, 70, 557). Indeed, the emerging field of immunometabolism is now gaining traction in the field of cancer cachexia, as both immunologic and metabolic derangements contribute to the pathogenesis of cachexia. Thus, models of cachexia should recapitulate not only the behavioral and metabolic features of cancer progression, but also the immunologic features of advanced disease. To this end, decades of research describe an elevation of neutrophil to lymphocyte ratio (NLR) as a negative prognostic factor in several cancer types, including head and neck cancers(643), and recent studies link elevated NLR to significant weight loss and cachexia(644). MLM3 engraftment and subsequent development of cachexia results in a significant leukocytosis, which is largely driven by an absolute and relative increase in circulating neutrophils in both male and female models (Figure 7A-E). At the time of

sacrifice, both male and female engrafted mice display a large increase in neutrophil to lymphocyte ratio, with tumor-bearing females experiencing the highest ratio (Figure 7F). We also observed a significant decrease in mean corpuscular hemoglobin levels (MCH) for both males and females, while mean platelet volume (MPV) and total platelet count was elevated in tumor-bearing females, but not males (Supplemental table 1).

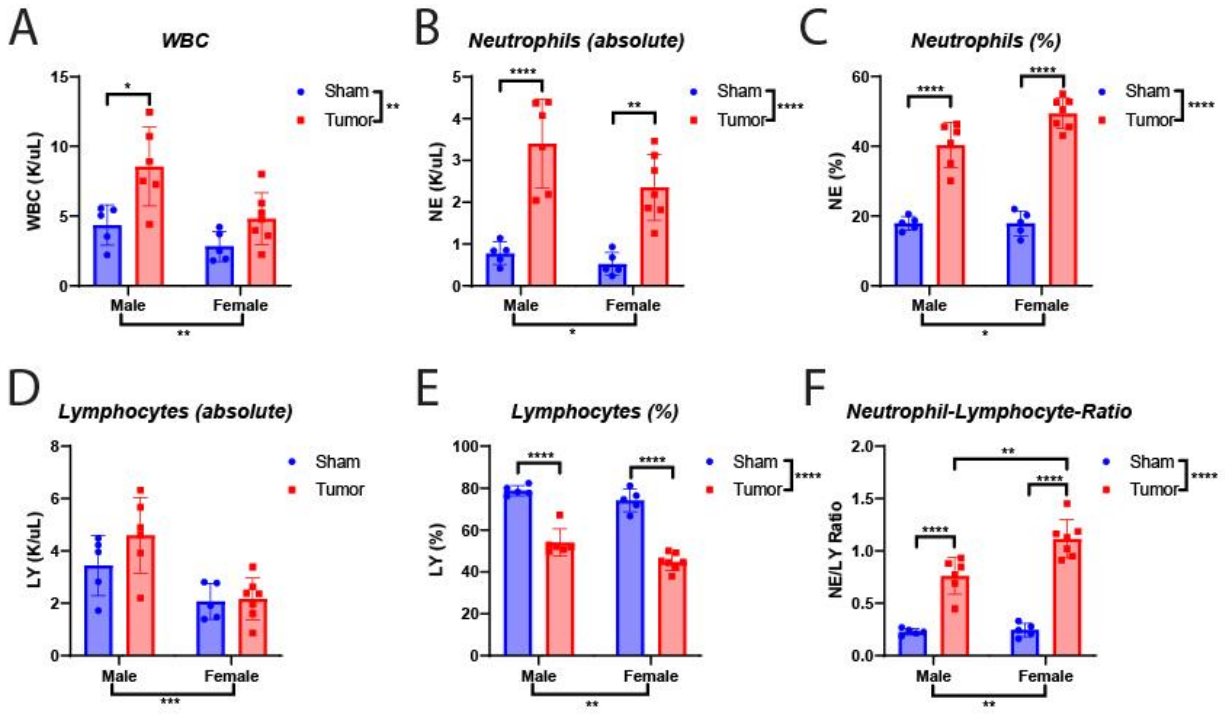

Figure 7. MLM cachexia results in a neutrophil-dominant leukocytosis and an elevated neutrophil-to-lymphocyte ratio. (A) Absolute white blood cell, (B) neutrophil, and (C) lymphocyte levels in male and female mice engrafted with MLM3 tumors or sham-operation controls. (D) Relative neutrophil levels, (E) relative lymphocyte levels, and (F) neutrophil-to-lymphocyte ratios in male and female mice engrafted with MLM3 tumors or sham-operation controls. N = 5-7 per group. All data are expressed as mean ± SEM. *p ≤ 0.05, **p ≤ 0.01, and ***p ≤ 0.001.

MLM3-cachexia results in systemic inflammation and alterations in hepatic metabolic gene expression

Hepatic processes are extensively involved in disease associated with cachexia through their ability to regulate both inflammatory and metabolic programs. Indeed, we observe a significant elevation of canonical inflammatory cytokines *Il-1β* and I*l-6* in MLM3-engrafted mice (Figure 8A). The acute-phase protein *Orm1,* a known mediator of inflammation and energy homeostasis through its actions on the leptin receptor, was also significantly elevated in MLM3-engrafted mice (Figure 8B)(645, 646). In addition to hepatic inflammation, the spleens of MLM-engrafted mice were larger than sham controls at the end of the study (Figure 8C). In the liver, tumor-implanted mice exhibited increased expression of key glycolytic *gene Hk2, enzyme Pck1,* and lactate metabolism gene *Mct4* (Figure 8D). Despite an elevated in gluconeogenesis (GNG) enzyme Pck1, hepatic G6pc was unchanged between tumor-bearing and control mice (Figure 8E). Expression of lipid metabolism gene Ppar-α was also unaffected by the presence of MLM3 tumors (Figure 8F). In addition to these alterations in glucose handling genes in the liver, both male and female MLM3-engrafted mice displayed progressive hypoglycemia during the development of cachexia (Figure 8G).

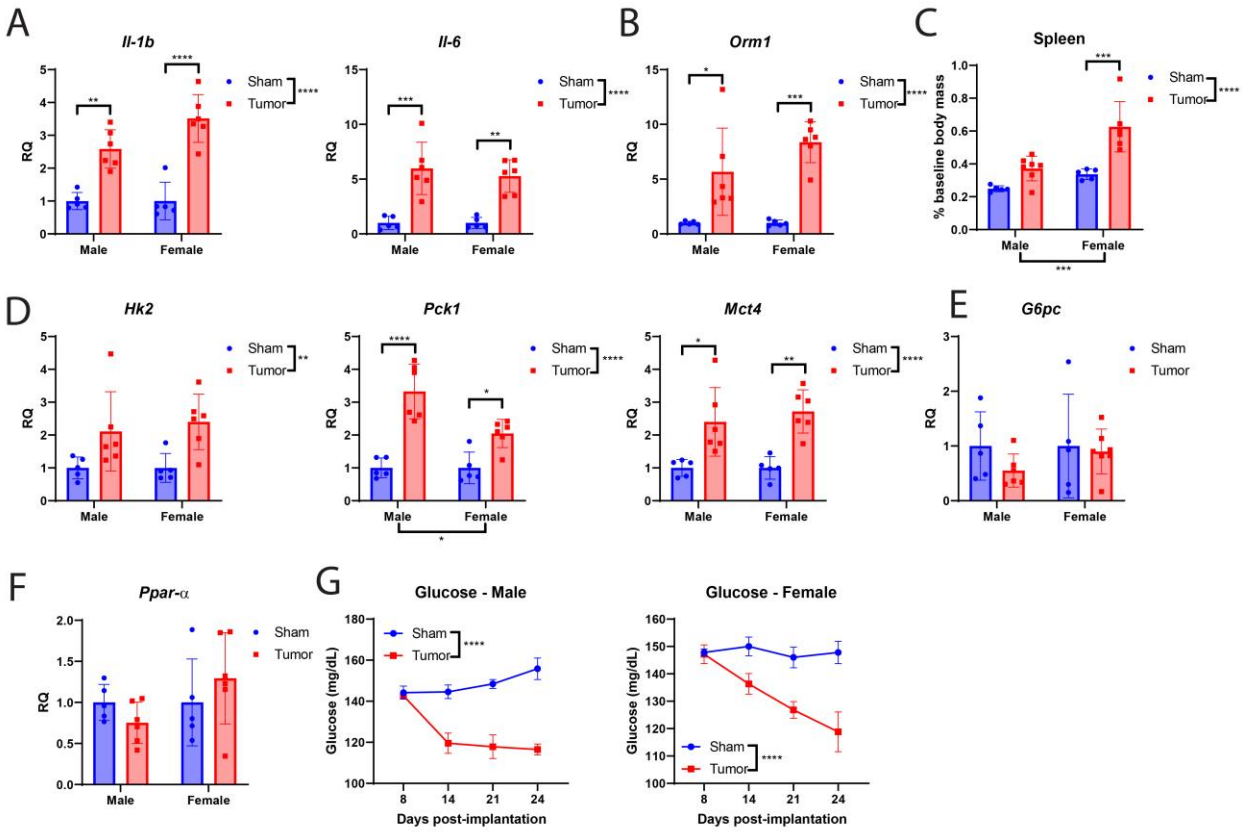

Figure 8. MLM-cachexia results in hepatic and splenic inflammation and alteration in metabolic gene expression. (A) *Il-1β, Il-6* and (B) *Orm1* hepatic gene expression in MLM3-engrafted and control mice. (C) Terminal spleen mass in MLM-engrafted and control mice. (D) Significantly regulated hepatic metabolic genes in MLM-engrafted and control mice. (E) *G6pc* and (F) *Ppar-α* gene expression in MLM-engrafted and control mice. (G) Repeated blood glucose measurements in male and female tumor-bearing and control mice. N = 5-7 per group. All data are expressed as mean ± SEM. *p ≤ 0.05, **p ≤ 0.01, and ***p ≤ 0.001.

Voluntary wheel running mitigates lean and fat mass wasting in MLM3-engrafted mice

The effect of voluntary wheel running was next explored in MLM3-engrafted mice to determine if aerobic exercise improves cachexia-related wasting, as is frequently reported in other murine cachexia models(647, 648). We observed a non-significant improvement in body mass loss in MLM3-engrafted mice with access to a wheel compared to those without (Figure 9A-B). Similarly, wheel running non-significantly improved food consumption in MLM3-engrafted mice (Figure 9C). Interestingly, we assessed fat mass throughout the study, and observed a significant sparing of baseline fat mass for tumor-bearing wheel mice compared to their no-wheel counterparts (Figure 9D-E). To our knowledge, this is the first report of voluntary wheel running demonstrating a fat-sparing effect during cancer cachexia, as most investigations are focused on lean mass sparing. Although total lean mass trended towards improvement in tumor-bearing wheel mice, terminal gastrocnemius and cardiac tissue mass was significantly improved (Figure 9H-I). This discrepancy could be explained by cancer-related organomegaly of tissues that encode as lean mass by NMR, including the liver and spleen, that is observed in both human and murine cancer progression(38, 649-651). On the molecular level, sparing of skeletal muscle in tumor-bearing wheel mice was associated with reduced ubiquitin ligase gene expression (Supplemental Figure 4). Finally, since voluntary wheel running is noted to have anti-tumor properties in a murine melanoma model, we measured both tumor volume and terminal tumor mass to determine if the fat and muscle sparing phenotype is attributable to reduced disease burden(652). In this study, access to a wheel did not significantly alter tumor growth, suggesting alternative mechanisms are responsible for fat and lean mass sparing in the wheel-running group (Figure 9J-K).

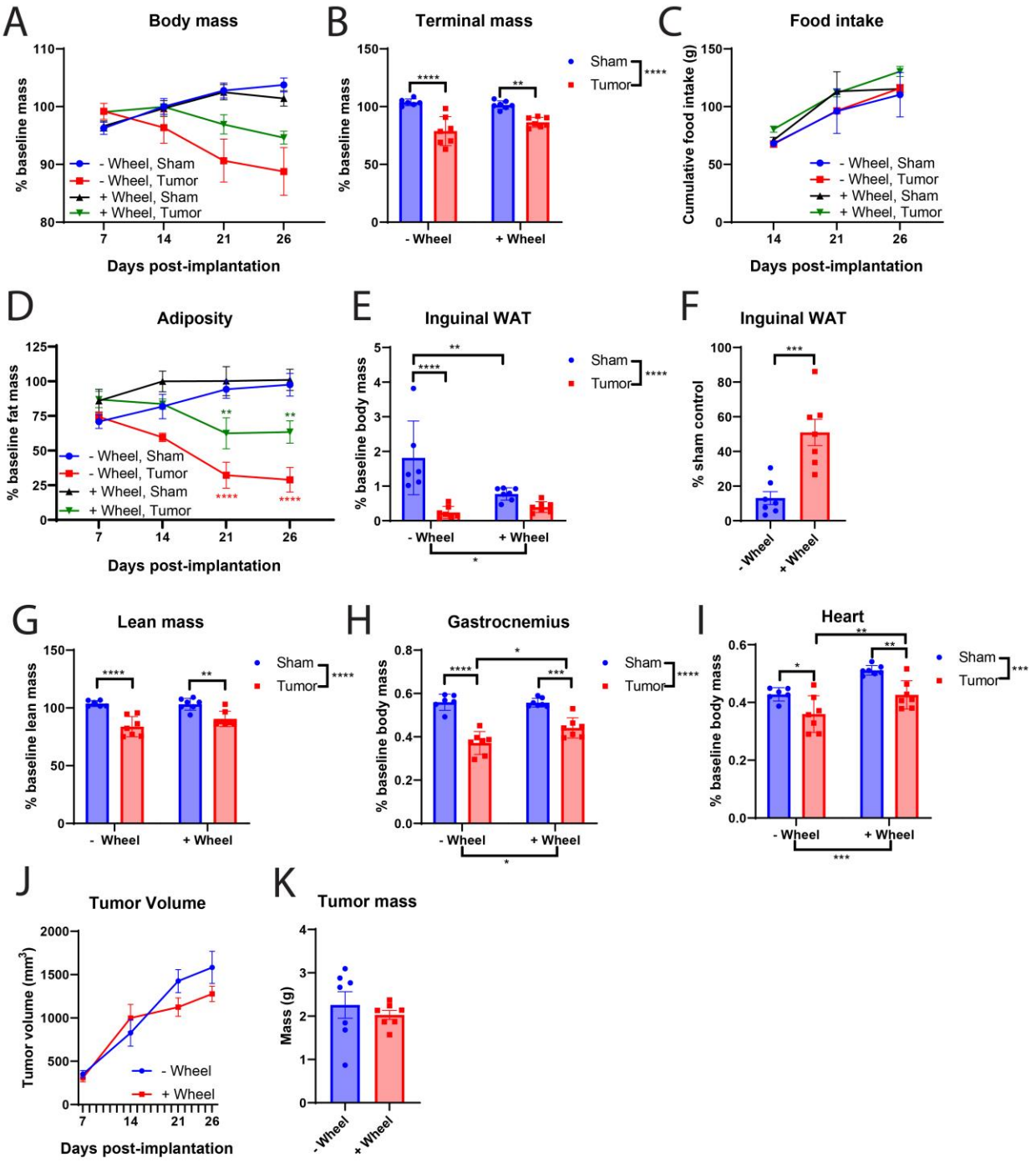

Figure 9. Voluntary wheel running abrogates cachexia-associated fat and lean mass wasting in MLM3-engrafted mice. (A) Daily body mass, (B) tumor-free body mass, and (C) cumulative food intake in MLM3-engrafted and sham-operation controls with or without access to wheel running. (D) Sequential NMR fat mass, (E) terminal

gonadal WAT mass, and (F) terminal sham-normalized WAT mass of MLM3-engrafted mice. (G) Terminal lean mass NMR, (H) gastrocnemius, and (I) cardiac tissue mass. (J) Tumor volume and (K) terminal tumor mass. N = 6-7 per group. All data are expressed as mean ± SEM. *p ≤ 0.05, **p ≤ 0.01, and ***p ≤ 0.001.

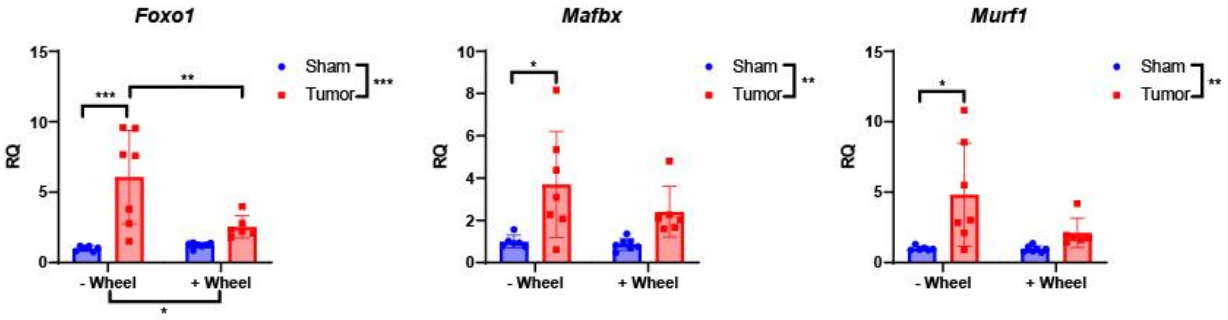

Supplemental Figure 4. Related to Figure 9. Ubiquitin proteasome pathway gene expression in gastrocnemius muscle in MLM3-engrafted and sham-operation controls with or without access to wheel running.

3. Discussion

Cancer cachexia is a devastating clinical entity that results in the progressive wasting of fat and lean mass. Despite the high prevalence of cachexia in oncologic patients, effective therapies are lacking. While several preclinical models of cachexia exist, all have limitations associated with their biological semblance of human disease. For instance, few rodent models of cancer cachexia include metastatic progression, even though cachexia in a clinical setting is almost always associated with metastatic and advanced-stage disease. Indeed, the ability of cancer cells to metastasize to host

organs and alter physiologic and metabolic outputs is a compelling area of cachexia research, yet therapeutic development in a preclinical setting is almost always performed on localized, early-stage cancers (for review, see(653)). Therefore, the development of clinically-relevant metastatic murine models of cachexia is a necessary step towards understanding cachexia in the context of advanced-stage disease. Utilizing a HPV+ oropharyngeal squamous cell carcinoma (SSC) cell line implanted in the flank of mice that readily metastasizes to the lungs, we robustly characterize the physiologic and behavioral parameters associated with cancer cachexia(635). Since these SSC clones are of epithelial origin, subcutaneous implantation in the flank confers the benefit of being orthotopic while also avoiding mechanical blockade of food intake that would occur if engrafted in the oropharynx. It is estimated that nearly 60 percent of patients with cancer of the head and neck develop cachexia, and since pulmonary metastases are most frequently observed in SSC of the head and neck, this model readily captures key oncologic features of clinically-observed head and neck cancer cachexia(6, 654). We therefore sought to determine if the present model also accurately reflects the molecular and behavioral features of cancer cachexia observed in both clinical and pre-clinical settings.

The MLM3 cachexia model recapitulates several behavioral features of cachexia observed in other preclinical models, including reductions in home-cage locomotion and voluntary wheel running. Since tumor-associated fatigue is the most common symptom of cancer at the time of diagnosis and significantly contributes to reduced quality of life, functional disability, and is associated with disease recurrence reduced overall survival in certain cancers, cachexia models should recapitulate this important behavioral

response associated with cancer progression(415, 655, 656). Alleviation of fatigue symptoms is not only an important behavioral endpoint of cachexia, but may also provide mechanistic insight in the context of pharmacologic intervention. Since it is generally accepted that inflammation is a critical mediator of cancer-related fatigue, an improvement in cancer-associated fatigue in this model infers improved inflammatory status associated with cachexia, and could lead to promising mechanistic insights into this metabolic disorder. Similarly, effective anabolic agents for cachexia should not only improve muscle mass and functionality, but may also results in improved locomotor behaviors, including fatigue(657). Collectively, the fatigue response associated with cancer cachexia is recapitulated in this MLM3 cancer cachexia model and mirrors that of human disease.

Since progressive wasting of muscle mass is a highly studied hallmark feature of human cachexia, it is critical that future murine cachexia models effectively demonstrate muscle catabolism(6). In the present model, we observe a significant lean-mass wasting phenotype that percolates to both fast- and slow-twitch muscle groups, including the gastrocnemius, tibialis anterior, and quadriceps (fast-twitch), as well as the soleus (slow-twitch). The wasting of skeletal muscle in this model corresponded with an elevated expression of E3 ubiquitin ligases *Murf1* and *Mafbx*, as well as their transcriptional regulator *Foxo1*. In addition to skeletal muscle catabolism, cardiac muscle catabolism and remodeling is also observed in select cases of cancer cachexia and represents a significant clinical challenge(658). In the present model, cardiac tissue was modestly wasted in males, but not females, and was associated with an elevation in autophagy-related genes *Ctsl, Gabarapl,* and *Bnip3*. Interestingly, while

other models of cancer cachexia report elevations in ubiquitin ligase genes in the heart, this axis of muscle wasting was not elevated in the MLM3 cachexia model in either male or female mice(38). Given the natural triaging of muscle catabolism in the context of both health and disease, with the preservation of cardiac tissue taking priority over that of skeletal muscle, and since cardiac wasting is regularly observed in other cancer cachexia models, it stands to reason that the present model represents a more modest muscle catabolism paradigm than that of other models(13, 38). Several plausible explanations could explain the cardiac-sparing in MLM3-cachexia in female mice, including the role of improved nutrition in cardiac cachexia (as anorexia is absent in the MLM3 model), unique inflammatory cytokine profiles and signaling, involvement (or lack thereof) of the sympathetic nervous system on cardiac tissue, and specific tumor-derived factors' influence on cardiac muscle pathophysiology. Additionally, female mice may experience lessened tissue catabolism due to their smaller tumor growth compared to their male counterparts. The decreased tumor growth may be explained, in part, by an immune mismatch of the implanted MLM cell line, as these clones were initially derived from a male mouse(635). Finally, we characterize the effects of voluntary wheel running on cachexia-associated wasting and observe a significant sparing of lean mass in tumor-bearing animals that have access to a wheel, consistent with other models of cancer cachexia(647, 648). Therefore, this model also represents a useful tool for the study of aerobic exercise during cancer cachexia. We believe the unique muscle wasting profile of this model represents a valuable approach to understanding divergent mechanisms in cardiac and skeletal muscle wasting during cachexia.

While muscle wasting remains the most studied facet of cachexia research, fat tissue physiology is increasingly recognized as a significant contributor the energy imbalance observed during cachexia. The importance of fat catabolism during cachexia is highlighted by the finding that white adipose tissue wasting frequently precedes that of muscle in patients suffering from cancer cachexia(659). In addition to WAT, BAT serves to produce heat through thermogenesis, an evolutionarily conserved response that enables mammals to regulate their body temperature in cold environments. While lipid depletion, fibrosis, and immune cell invasion represent mechanisms contributing to fat tissue wasting and inflammation, “browning” of white adipose, in which the expression of thermogenesis markers is elevated in WAT, remains a highly studied and debated topic of cachexia-related energy wasting(557, 660). Indeed, recent evidence for browning of WAT during cancer cachexia in humans and mice implores investigation into the contributions of fat to the pathogenesis of cachexia(52, 338). Interestingly, thermogenesis-related gene expression in WAT and BAT such as cell death-inducing DFFA-like effector A (CIDEA) and uncoupling protein 1 (UCP1), are inconsistently expressed amongst cachexia models. For instance, both C26 colonic adenocarcinoma and Lewis lung carcinoma (LLC) allografts result in elevation of UCP1 in WAT, while the KPC pancreatic ductal adenocarcinoma allograft results in decreased *Ucp1* expression(38, 52, 661). These discrepancies in thermogenesis gene expression across cancer cachexia models remains unclear, but could be partially explained by differences in nutritional status amongst these models, since caloric intake is a known mediator of adipose tissue browning(662-664). With this in mind, we characterized browning signatures in male mice, as food consumption in the male tumor cohort was equivalent

to that of sham controls, while female tumor-bearing mice exhibited significant hyperphagia near the end of our studies. We observed a significant elevation of browning markers *Ucp1* and *Cidea* in the WAT, with a concurrent increase in BAT *Ucp1,* in MLM3-engrafted male mice. Since tumor-derived parathyroid hormone-related protein (PTHrP) is a known mediator of adipose tissue browning in the LLC cachexia model, we assayed circulating levels of PTHrP in MLM-3 engrafted mice (338). We observed no alteration of circulating PTHrP in the context of MLM3 cachexia, demonstrating the browning programs induced by MLM3 progression is through alternative mechanisms. Furthermore, we observe a significant elevation of core body temperature in tumor-bearing mice compared to sham controls during middle stage disease, with a steady decline back to control animals toward end-stage disease. Although we observe increased thermogenesis gene expression in the BAT and WAT of MLM3-engrafted mice, along with a transient increase in core body temperature, these data are currently associative. Further mechanistic investigation is required to determine how (or if) browning of adipose tissue contributes to overall energy imbalance and cachexia progression in this model. Therefore, we believe this model represents a valuable resource for the study of adipose tissue biology and its respective contribution to the pathogenesis of cancer cachexia.

In addition to peripheral tissue catabolism and metabolic reprogramming, the CNS is a known mediator of metabolic dysfunction during cachexia. We and others described CNS-based mechanisms of cachexia in which systemic inflammatory signals are received and amplified by the hypothalamus, resulting in aberrant activity of weight- and activity-modulating neurons(16, 18, 165, 325, 665). To this end, we broadly

characterized the inflammatory status in the MBH of MLM3-engrafted mice, as this is an area that controls several metabolic and pathophysiologic processes involved in cachexia development. We observed an elevation of the inflammatory cytokine *IL-1β* in cachectic mice after MLM3 implantation, along with an increase in hypothalamic glial cells (astrocytes and microglia). Indeed, an increase in hypothalamic *IL-1β* expression is also observed in other murine cachexia models, and hypothalamic expression of *IL-1β* in fenestrated capillaries is sufficient to induce illness behaviors consistent with cachexia symptoms in mice(38, 44, 665, 666). Despite clear evidence for the role of IL1 signaling in the regulation of illness behaviors, the precise role of IL1 signaling during cachexia remains elusive. For example, while IL1 signaling is elevated during cancer cachexia and is individually capable of inducing fatigue, tumor-associated fatigue develops independently of IL1 signaling, suggesting alternative inflammatory signals in the CNS drive fatigue symptoms during cachexia(44, 665). While microglia and astrocyte activation can be either pro- or anti-inflammatory depending on the underlying condition, we recently reported the protective role of microglia in the hypothalamus in a murine model of pancreatic cancer cachexia(70). Therefore, it remains to be determined if the gliosis observed in the present model is protective or detrimental. We also observe a significant elevation of hypothalamic cell adhesion and chemokine gene expression, including *Selp, Cxcl1,* and *lcn2*. Recent work by Burfeind and colleagues demonstrate a clear role for myeloid cell invasion in the CNS in driving pancreatic cancer cachexia symptoms, including anorexia and lean mass catabolism, that is predominantly driven by the CCR2-CCL2 axis(20). While we observe an elevation in several immune recruitment transcripts in the MLM3 cachexia model, we observe no difference in

hypothalamic *Ccl2* expression. Given the unique immune recruitment gene expression profile we see in the hypothalami of MLM3-engrafted mice, whether or not immune cells invade the CNS, along with the specific role (if any) they serve in mediating cachexia symptoms, remain an exciting area of future investigation. Finally, we observe an elevation of the orexigenic peptide *Agrp* in MLM3-engrafted mice, consistent with previous work describing an increase in *Agrp* gene expression in the context of chronic inflammation(327). It is plausible that increased orexigenic peptide expression serves to prepare cachectic mice for a period of hyperphagia after inflammation subsides, ultimately in effort to replenish energy stores expended during the progression of cachexia.

From an immunologic perspective, the peripheral immune cell profile in the MLM3 model is consistent with that of cachectic patients. Decades of research describe an elevation in circulating neutrophils of patients with cancer, with an elevated neutrophil-to-lymphocyte ratio (NLR) being associated with poorer survival outcomes both before and after treatment(667, 668). Indeed, an elevation in NLR is associated with weight loss and cachexia in patients with advanced colon, lung, and prostate cancer(669). Despite the abundance of associative data concerning elevated NLR and patient outcomes, the influence of this immunologic shift during cachexia remains incompletely understood, ultimately highlighting the need for preclinical cachexia models that accurately reflect this immunologic shift for future mechanistic studies. Indeed, MLM3-engrafted mice display a neutrophil-dominant leukocytosis and elevated NLR, with tumor-bearing females exhibiting a significantly larger NLR than their male counterparts. This increased NLR in females may be explained by both baseline differences in

neutrophil and lymphocyte counts, as well as some degree of neoantigenicity to the MLM3 clone, as this cell line was originally derived from a male mouse(635). While it is generally appreciated that neutrophils play a vital role in the maintenance of lean muscle function through their interactions with tissue-resident macrophages, neutrophil invasion into muscle tissue after inflammatory challenge is associated with muscle membrane damage and reduced functionality(670-672). With the drastic increase in circulating neutrophils in both cachectic patients and mice, it is plausible that this immunologic shift alters tissue physiology during cachexia, including muscle and fat catabolism and remodeling. Since the MLM3 cachexia model accurately reflects the circulating immune cell profile of human cachexia, we believe this model is well suited for future mechanistic studies concerning the role of the immune system during cancer cachexia.

Cancer cachexia is also associated with a shift in hepatic processes that increase the overall energy deficit through both futile cycling of metabolic intermediates and activation of the acute phase response. It is well known that the lactate produced by tumor cell growth is reconverted to glucose in the liver via the Cori cycle. This axis is energetically demanding, as 6 ATP are consumed per glucose molecule produced, and it is hypothesized that these aberrant hepatic processes significantly contribute to the energy deficit incurred during the development of cachexia(673). In addition to glucose produced by the Cori cycle, an elevation in hepatic GNG during tumor progression ultimately provides more glucose substrate for the growing tumor. However, since the MLM3-engrafted mice exhibit an increase in both hepatic gluconeogenic (*Pck1)* and glycolytic (*Hk2*) gene expression, it is unclear if hepatic processes contribute to the

overall hypoglycemia observed during tumor progression. It is plausible that an internal competition between muscle and the growing tumor for the depleting glucose stores drives some of the behavioral features of cachexia we observe in this model, including fatigue(332). Notably, in contrast to our findings of increased GNG gene *Pck1*, Grossberg and colleagues observe a decrease in hepatic GNG genes in the parental non-metastatic cell line to MLM3, mEER, suggesting that MLM3 tumors differentially influence hepatic glucose handling from its parental cell line(332). Indeed, the livers of MLM3-engrafted mice displayed an elevation in inflammation and acute-phase response genes, as well as an increase in gluconeogenic and lactate metabolism gene expression, consistent with hepatic processes observed in human cancer cachexia(674-676). Since anorexia is not observed in MLM3 cachexia, this model provides a platform for the study the nutrition-independent effects of tumor progression on hepatic inflammation and metabolism.

While the MLM3 cachexia model recapitulates several key molecular and behavioral features of cancer cachexia, the model does have its limitations. Similar to other subcutaneous tumor models, positioning the tumor inoculum in an area in the flank that is not accessible to the mouse is imperative in preventing ulcerations and bleeding. Along these lines, the flank technically represents a heterotopic implantation site of the MLM3 cell line, as the parental cell line was generated from mouse tonsillar epithelium(677, 678). Although MLM3 implantation in the oropharynx may be possible to induce weight loss, it is likely that the wasting phenotype would be mostly attributable to the growth of the primary tumor directly in the aerodigestive tract and subsequent influence on caloric intake. However, subcutaneous engraftment of MLM3 cells still

represents an epithelial implantation site, and thus represents a more biologically relevant implantation site when compared to other commonly used subcutaneous allograft models, including LLC (lung adenocarcinoma) and C26 (colonic adenocarcinoma) to name a few. When implanted in the flank, this model of cachexia is not associated with anorexia, a cachexia symptom that is often observed in a clinical setting. However, while the absence of anorexia in this model may have its limitations, the nutrition-independent wasting phenotype observed has its advantages: (1) assessment of nutrition-influenced processes of cachexia, including adipose tissue thermogenesis, require technically challenging pair-feeding studies—this model circumvents the need for pair-feeding for accurate assessment of these parameters, and (2) not all models of cachexia accurately assess the contributions of food intake on fat and muscle wasting—our characterization of the MLM3 model provides clear evidence that significant fat and muscle wasting occurs in the context of adequate nutrition. To our knowledge, this is the first described syngeneic HNC cachexia model in C57BL/6 mice, the most widely used mouse strain with numerous genetically modified strains, ultimately enabling investigators wider access to knockout mouse variations for mechanistic studies. Finally, we also characterized an identically derived clone to MLM3, MLM5, with near-identical tumor growth(635). Despite equivalent disease burden, MLM5-engrafted mice were significantly spared from cachexia-associated fat and lean mass wasting when compared to their MLM3-engrafted counterparts. We believe that *in vivo* and *in vitro* comparisons of these two clones represent a unique resource for the identification of tumor-derived factors that may explain, in part, the cachexia inducing potential of MLM3.

The MLM3 model described herein is simple, reliable, and recapitulates key features of cachexia observed in humans with metastatic head and neck cancer. It is generally assumed that the wasting associated with human HNC is predominantly due to tumor-related dysphagia. This model produces cachexia symptoms in the absence of dysphagia and anorexia, allowing for the investigation of nutrition-independent mechanisms of HNC cachexia. Although resistant to a standard chemoradiation (e.g. cisplatin), as is often the case in HNC patients with disease recurrence and progression, the MLM3 model provides a platform for the assessment of both anti-tumor and cachexia-inducing effects of experimental drugs for refractory HNC(635). Given the large prevalence of cachexia in patients with HNC, yet development of very few preclinical models of metastatic and/or HNC cachexia, we believe this work helps bridge this gap in cachexia research. Collectively, our studies indicate that this metastatic HNC model accurately captures the signs and symptoms of clinically-observed cachexia, and provides the field a valuable tool for future mechanistic and therapeutic investigation.

4. Methods

Mice

Male and female C57BL/6J mice were purchased from The Jackson Laboratory (WT, JAX catalog number #000664) and maintained in our animal facility. All mice were housed and bred in a dedicated mouse room with a temperature 26˚C with a 12-hour light/dark cycle. Animals were provided *ad libitum* access to food and water (Purina rodent diet 5001; Purina Mills, St. Louis, MO, USA). For behavioral studies, animals were individually housed for acclimation for 7 days prior to tumor implantation. Tumor-

bearing animals were euthanized according to the end points of tumor study policy. All mouse studies were conducted in accordance with the National Institutes of Health Guide for the Care and Use of Laboratory animals, and approved by the Institutional Animal Care and Use Committee (IACUC) of Oregon Health & Science University.

HPV+ squamous cell carcinoma cell line and culturing

The models of HPV+ squamous cell carcinoma cachexia utilized herein are clonogenic cell lines derived from metastatic lung lesions from in a separate C57BL/6J mice implanted with a parental HPV+ squamous cell carcinoma (expressing HPV16 E6/E7, hRas, and luciferase [mEERL]) subcutaneously that failed cisplatin/radiation therapy(635). In this study, we perform cachexia analysis on four mEERL lung metastasis (MLM1, MLM3, MLM5, MLM10) described by Vermeer et al. and observe MLM3 as the only metastatic cell line associated with significant lean and fat mass loss (data not shown), thus we focus our subsequent analysis on this cell line(635). All cell lines were maintained in DMEM supplemented with 10% fetal bovine serum, 1% minimum essential medium non-essential amino acids, 1 mM sodium pyruvate, and 50 U/mL penicillin/streptomycin (Gibco), in cell incubators maintained at 37˚ Celsius and 5% CO_2. All cell lines were routinely tested and confirmed negative for mycoplasma contamination.

Generation of HNC model

C57BL/6 mice aged 10-12 weeks were inoculated subcutaneously with an inoculum of $3x10^6$ MLM tumor cells, while controls received heat-killed cells in the same volume.

Subcutaneous implantation was performed in the right hind flank with a 300 uL injection of cell suspension in DMEM under isoflurane anesthesia. Tumor growth was measured as previously described(678).

Analysis of cachexia

Food intake (with daily collection of spilled food mass with a bedding sieve), body mass, and post-procedure health status were monitored daily. Body temperature and voluntary locomotor activity were measured via implanted MiniMitter tracking devices on 5 min recording intervals (MiniMitter, Bend, OR, USA). Voluntary wheel running was measured continuously utilizing lab-constructed wheels with digital revolutions counter. Necropsy tissue analysis included tumor, gastrocnemius, soleus, tibialis anterior, quadriceps, and heart mass by observers blinded to treatment groups. Additionally, hypothalamus, heart, gastrocnemius, soleus, tibialis anterior, quadriceps, and liver tissues were immediately flash frozen for gene expression analysis.

Nuclear magnetic resonance imaging

Nuclear magnetic resonance (NMR) measurements were taken at the beginning of designated studies with concurrent balancing of weight and body composition measures between sham and tumor groups. For repeated measures studies, body composition was assessed at the designated time points, while terminal body composition was performed on animal carcasses after primary tumor excision.

Immunohistochemistry

At the end of a study, mice were deeply anesthetized using a ketamine/xylazine/acepromazine cocktail and sacrificed by transcardial perfusion with 20 mL PBS followed by ice cold 4% paraformaldehyde (PFA). Tissues were post-fixed in 4% PFA overnight at 4˚C prior to sectioning protocols. **Brain samples:** after post-fixation, brains were cryoprotected in 20% sucrose for 24 hours at 4˚C prior to 30 µM microtome sectioning. Free-floating sections were incubated in blocking solution (5% normal donkey serum in 0.01 M PBS and 0.3% Triton X-100) for 30 minutes at room temperature, followed by primary antibody incubation (listed below) overnight at 4˚C. Sections were thoroughly washed with PBS between steps. Sections were mounted on gelatin-coated slides and coverslipped with Prolong Gold anti-fade media with DAPI (Thermofisher).

Fluorescent-based images of the hypothalamus were acquired on a Nikon confocal microscope. Primary antibodies utilized above are listed with company, clone, host, species, and concentration defined in parentheses, respectively: mouse anti-GFAP (Millipore, GA5, 1:1000) and rabbit anti-Iba-1 (Wako, NCNP24, 1:1000). The following secondary antibodies were used, all derived from donkey: anti-mouse AF488 (1:500) and anti-rabbit AF555 (1:1000).

Enzyme-linked immunosorbent assay

Whole blood was harvested from mice by cardiopuncture and plasma was isolated using K_2EDTA tubes (BD 365974). Mouse plasma PTHrP concentrations were assayed by ELISA according to the manufacturer's protocol (LSBio, Catalog #LS-F15276).

Quantitative real time PCR

Snap-frozen tissues were rapidly homogenized and RNA was purified with an RNeasy Mini Kit (Qiagen). Samples were then reverse-transcribed with the High Capacity cDNA Reverse Transcription Kit (Life Technologies). qRT-PCR was performed using TaqMan primer probes and reagents detailed in **supplementary table 2**. Tissues were normalized to 18S using the ddCT method for analysis.

Clinical assays

Adaptive and innate immune cell counts were performed on EDTA-decoagulated plasma samples using HemaVet 950 (Drew Scientific). Blood glucose was measured immediately prior to euthanasia with electronic glucometer (OneTouch Ultra).

Statistics

All statistical analyses for murine data were performed in GraphPad Prism 8.0 software. Quantitative data are reported as mean +/- standard error. For comparison between tumor and control groups, data were assessed by Student's *t*-test, One-way ANOVA, or Two-way ANOVA if sex was a variable. For all analyses, a p value of < 0.05 was considered to be statistically significant. All measurements were from distinct samples and not taken from the same sample more than once.

Acknowledgements

We thank Dr. Paola Vermeer of Sanford Research for kindly providing MLM cells derived in her laboratory. This work was supported by NCI R01 CA184324 (Marks), the

Brenden-Colson Center for Pancreatic Care (Marks), as well as NIH F30CA254033 (Olson). The authors of this manuscript certify that they comply with the ethical guidelines for authorship and publishing in the *Journal of Cachexia, Sarcopenia and Muscle(679).*

DM is a consultant for Pfizer, Inc. and Alkermes, Inc. DM is a consultant, has received grant funding, and has equity in Tensive Controls, Inc. BO, MN, PL, and XZ declare that they have no conflict of interest.

Summary and Conclusions

Cachexia is a devastating wasting syndrome that occurs in many illnesses, with signs and symptoms including anorexia, weight loss, cognitive impairment, and fatigue. Cachexia severely limits quality of life and is the direct cause of death for nearly one third of all cancer patients, yet the mechanisms of cachexia remain poorly understood and there are no effective treatments. LCN2 is a secreted protein produced during numerous diseases, an important mediator of inflammation and able to access appetite regulating brain regions. However, its role in cachexia was unexplored. This dissertation focused on the physiologic and molecule role of LCN2 during the pathogenesis of cancer cachexia. My data lead me to focus on the LCN2's effect in the CNS, in which we identified distinct appetite-regulating and cognitive effects in the context of prolonged exposure.

Chapter 1 of this dissertation provided an extensive literature review of the disparate metabolic and behavioral adaptations during various states of undernutrition, including cachexia. I highlight the distinct biological state of cachexia, in which catabolic processes are activated and macronutrient intake is paradoxically suppressed, violating the rule of energy conservation. This review details basic mechanisms by which cachexia disobeys allostatic and homeostatic principles, signifying that while the cachexia field has made great leaps in understanding this metabolic syndrome, more work is needed.

Chapter 2 of this dissertation is a literature review on cancer-related cognitive decline. It reviews the clinical literature in which patients with non-central nervous system (CNS) tumors experience cognitive decline *prior* to treatment. This repeated

observation of diminished cognitive function in treatment-naïve cancer patients suggests a direct role for tumor-derived factors in modulating cognition and behavior. This review summarizes the state of the science of cancer-related cognitive impairment (CRCI) independent of treatment and focuses on biological mechanisms in which peripheral cancers modulate the CNS. Although this review focused on cognitive decline (a less-studied symptom of cancer), the principles described therein are well applied to the study of CNS mechanisms of cachexia-associated wasting, as various peripheral inflammatory, cellular, and endocrine mediators altered during CRCI are also are known to mediate cachexia symptoms when received by the brain.

Chapter 3 of this dissertation presented the appetite-regulating effects of LCN2 during pancreatic cancer-associated cachexia. In this chapter, we demonstrated a clear appetite-regulatory role of LCN2 during the progression of pancreatic cancer cachexia. We identified neutrophils as the predominant source of Lcn2 during pancreatic cancer progression, through both an increase in their absolute number and transcriptional regulation of *lcn2*. Bone marrow transplantation of Lcn2 replete marrow in a *lcn2*-KO mouse was sufficient in restoring the anorexia phenotype. We examined circulating LCN2 levels in patients with pancreatic cancer, and observed significant negative correlations between LCN2 and muscle mass, fat mass, and neutrophil-to-lymphocyte ratios. Finally, we noted that patients with elevated circulating LCN2 at diagnosis (>240 ng/mL) displayed increased mortality. These studies suggest LCN2 as an appetite-regulating molecule during pancreatic cancer cachexia, and may be a promising target for the improvement of appetite and weight loss during disease progression.

Numerous questions arise from the studies described in this Chapter. How is LCN2 modulating iron trafficking in the context of pancreatic cancer? And is the iron-loaded state of LCN2 important in its appetite regulating effects? Is peripherally-produced LCN2 able to directly modulate metabolism, as described in previous reports, during cachexia progression? Although the pancreatic cancer cachexia model we employ is rapidly progressive and allows for robust profiling of behavioral phenotypes, perhaps alternative cancer cachexia models would be better suited for the study of Lcn2 on peripheral tissues. Finally, are there permissive factors specific to pancreatic cancer that allow for the anorectic effects of LCN2 during cachexia? Specifically, is CNS inflammation requisite in LCN2's MC4R-dependent effects? This question largely stems from our experiment in which we administer Lcn2 directly into the brain of mice and observe a sustained, but delayed, anorectic effect; these mice received a highly invasive cannulation procedure, undoubtedly promoting a highly inflammatory environment in the CNS. Furthermore, if Lcn2 is truly a specific MC4R binding partner, we should have observed an immediate anorectic effect of the molecule when administered to the brain. Instead, we observed a delayed response, observing an anorectic effect only after 3-4 days of ICV injection. Another discordant observation across the Lcn2 literature is its basal level in a healthy, unperturbed C57BL6 mouse. Given that we identified neutrophils as the predominant producer of Lcn2 during cachexia and normal physiology, and a euthermic environment is critical for normal immune responses in mice (680), it is possible that rodent housing conditions significantly alters Lcn2 production, secretion, and even biological function. Whether or

not Lcn2 function is impacted by metabolic need or environment should be a focus of future research

It is especially worth noting a conflicting result from our work and that of the initial paper characterizing Lcn2's appetite regulating effect. Mosialou et al observe a large induction of Lcn2 after re-feeding fasted mice, suggesting Lcn2 is induced after a meal, traverses to the hypothalamus, binds to the MC4R to initiate feelings of satiety. We observed no such induction of Lcn2 in mice fasted and re-fed (Chapter 4; Supplementary figure 2e-f). Furthermore, I performed a fasting and refeeding study on myself, in which I abstained from food or liquid intake for 16 hours (from 6:30 PM to 10:30 the following morning). I drew my blood at this 16-hour fasted time point, then promptly consumed a large meal—in this case it was Chipotle leftovers. I then drew my blood 1 and 4 hours after this meal intake, isolated plasma, and performed an LCN2 ELISA. Similar to my rodent experiment, LCN2 was not markedly increased at the 1- and 4-hour timepoints after a meal (Figure 1; BGO timepoints in blue). These findings illuminate either a fundamental difference in our experiments (although I followed their published methodology as closely as possible), or that LCN2 represents more of a pathologic mediator of appetite, rather than a physiologic one.

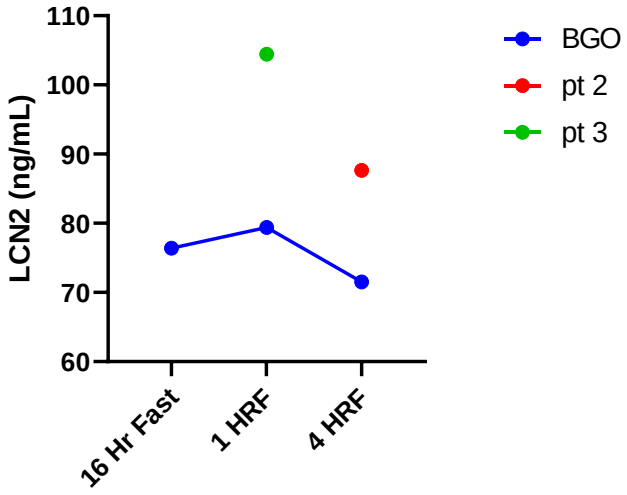

Figure 1. Plasma LCN2 levels in 3 humans. The blue line represents myself, Brennan Olson, after 16 hours of fasting, followed by 1 and 4 hours after a large meal (1 HRF and 4 HRF, respectively). Pt 2 and pt 3 are of other humans 1 and 4 hours after a meal not preceded by fasting.

As discussed in the Introduction of this thesis, there are numerous permutations through which Lcn2 can enact cellular change—bound or unbound to an iron-siderophore complex, through three distinct receptors with vastly different signaling properties, and temporally-driven effects (acute vs chronic exposure). Indeed, the literature paints a paradoxical picture of Lcn2, having either beneficial or detrimental actions during various inflammatory diseases (681), and this theme of chronicity is revisited several times in this thesis. However, the literature concerning Lcn2 is broadly conflicting, suggesting that our fundamental knowledge of Lcn2, including intracellular signaling, siderophore binding partners, and cell type-specific iron-trafficking, is grossly

deficient at this time. Hopefully future fundamental work on Lcn2 will allow for reconciliation of all of these conflicting reports.

Chapter 4 presented investigations into alternative functions of Lcn2 in the CNS, since Lcn2 also binds to two other receptors abundant in brain cell populations (SLC22A17 and megalin). After chronic, but not acute, administration of Lcn2 into the brain of healthy rodents, we observed distinct neuronal, glial, and immune cell alterations in the hippocampus, ultimately resulting in cognitive impairment. Our findings implicate Lcn2 as a pathologic mediator of cognitive decline in the CNS during chronic inflammatory disease through its actions on the hippocampus, while the transient induction of Lcn2 in the CNS during acute inflammation is generally tolerable.

And finally, Chapter 5 concludes this dissertation with an exciting route investigation that I hope to follow up on in the future. I extensively characterized a murine model of metastatic head and neck cancer cachexia, and inadvertently identified two identically-growing cell lines (*in vitro* and *in vivo*) that induce significantly different levels of cachexia as indicated by fat and muscle wasting. Not included in this Chapter is an experiment in which I implant MLM3 cells into WT or *lcn2*-KO mice, and in addition to *lcn2*-KO mice having mitigated muscle and fat wasting, they also grew significantly smaller tumors (Figure 2). This is in contrast with what we observed in our pancreatic cancer cachexia model, in which whole-body *lcn2* deletion did not influence tumorigenesis. I am planning to follow up these observations with a few *in vitro* and *in vivo* experiments. In addition to our well-established pancreatic cancer cachexia model, I plan to utilize these models for my future investigations into cancer cachexia.

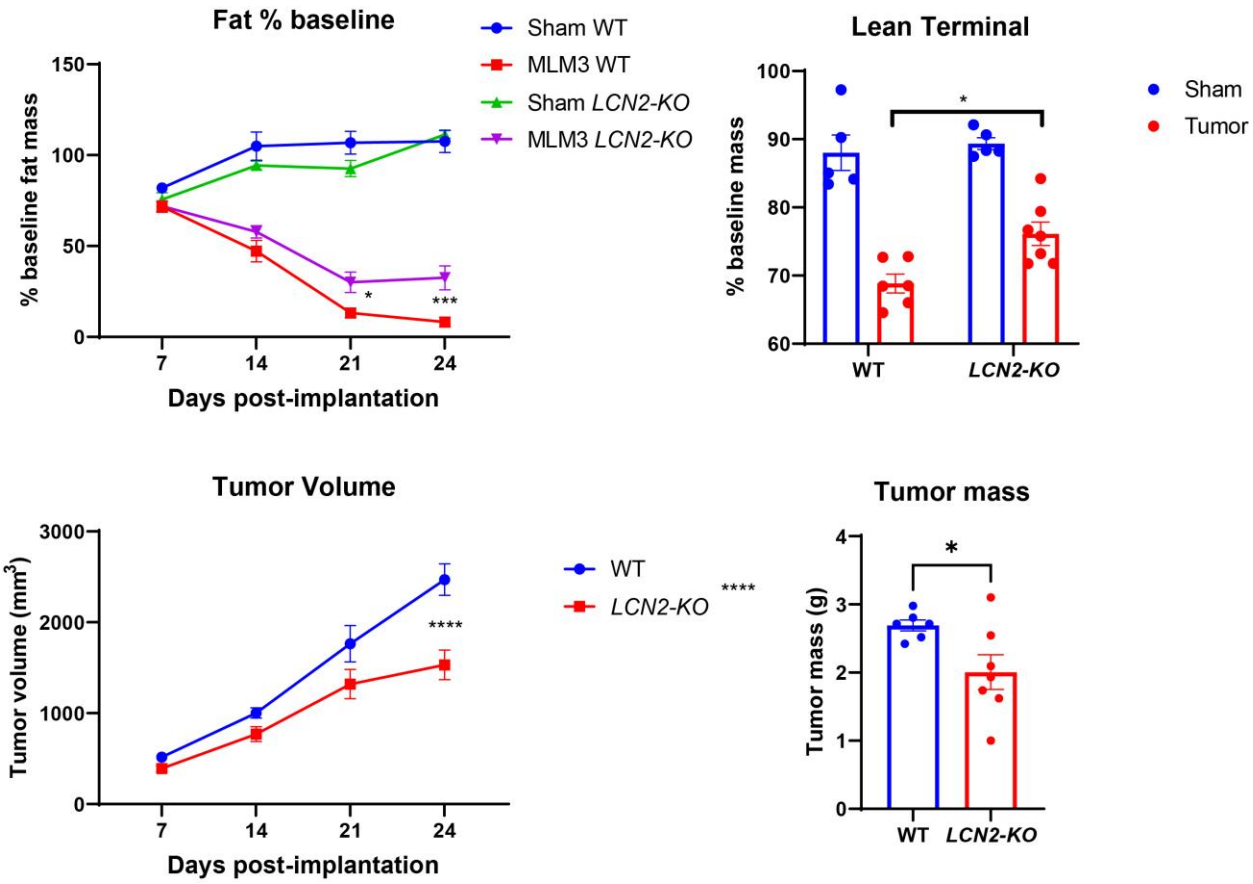

Figure 2. *lcn2*-KO mice engrafted with MLM3 tumors display improved fat and lean mass compared to their WT counterparts. *lcn2*-KO mice also had reduced terminal tumor volume and mass.

In conclusion, this dissertation identified LCN2 as a pathologic mediator of appetite suppression and cognitive decline. It also identified a clear temporal effect of this molecule in mediating these symptoms of cachexia, in which acute cerebral exposure to LCN2 is generally tolerable, while prolonged exposure results in anorexia and altered hippocampal function. I end this dissertation with the characterization of a novel model of head and neck cancer cachexia, which presents with a distinct

behavioral and wasting phenotype from our commonly used pancreatic cancer model. I believe this tool will serve the scientific community well, and I am eager to perform several follow up studies using this model when I am able to return to bench research. While several follow up studies are needed to further identify the precise cellular mechanism of LCN2, the results herein suggest this molecule could be a potential therapeutic target for the improvement of cachexia-associated anorexia and cognitive decline.

Appendix: Supporting first-authored manuscripts concerning cancer cachexia

The effect of sarcopenia on oncologic outcomes of primary surgery or definitive radiation therapy in localized oropharyngeal squamous cell carcinoma

A manuscript published in *JAMA Otolaryngology: Head and Neck Surgery*

Brennan Olson, BA[1]; Jared Edwards, BS[1]; Lucas Stone, BS[1]; Angie Jiang[1]; Xinxia Zhu, MD[2]; John Holland, MD[3]; Ryan Li, MD[4]; Peter Andersen, MD[4]; Stephanie Krasnow, PhD[2]; Daniel L. Marks, MD, PhD[2,5]; and Daniel Clayburgh, MD, PhD[4,6*]

1. School of Medicine, Oregon Health and Science University, Portland, OR
2. Papé Family Pediatric Research Institute, Oregon Health and Science University, Portland, OR
3. Department of Radiation Oncology, Oregon Health and Science University, Portland, OR
4. Department of Otolaryngology/Head and Neck Surgery, Oregon Health and Science University, Portland, OR
5. Brenden-Colson Center for Pancreatic Care, Oregon Health and Science University, Portland, OR
6. Operative Care Division, Portland Veterans Affairs Health Care System, Portland, OR

***Corresponding Author:**
Daniel Clayburgh MD PhD
Department of Otolaryngology Head and Neck Surgery
Oregon Health and Science University
3181 SW Sam Jackson Park Road, PV01
Portland, OR 97239
Phone: 503-494-5355; Fax: 503-346-6826
Email: clayburg@ohsu.edu

Key Points

Question: Does selection of primary treatment modality influence survival in sarcopenic patients with localized oropharyngeal squamous cell carcinoma (OPSCC)?

Findings: A matched analysis of sarcopenic patients with localized OPSCC demonstrated that patients treated by primary surgical resection had improved overall (HR, 0.33; 95% CI, 0.12-0.91) and disease-specific (HR, 0.17; 95% CI, 0.04-0.75) survival compared to patients treated by definitive radiotherapy.

Meaning: Upfront surgical resection may be associated with improved survival for sarcopenic patients with localized OPSCC.

Abstract

Importance: The negative effect of low lean muscle mass (sarcopenia) on survival outcomes in head and neck cancers, including oropharyngeal carcinoma, is established. However, it is not known if the choice of primary treatment modality (surgery or radiation) affects oncologic outcomes in oropharyngeal squamous cell carcinoma (OPSCC) patients with sarcopenia.

Objective: To determine if primary surgical resection or definitive radiotherapy is associated with improved survival for sarcopenic patients with localized OPSSC.

Design, setting, and participants: A cohort study was conducted of patients with clinically staged T1-2, N0-2 OPSCC with cross-sectional abdominal imaging within 60 days prior to treatment and treated between January 2005 and December 2017. Skeletal muscle mass was measured at the L3 level using previously defined techniques, and sarcopenia was defined as less than 52.4 cm2/m2 of muscle for men and less than 38.5 cm2/m2 for women. In addition, associated patient demographics, cancer data, treatment information, and survival outcomes were assessed.

Interventions: Measurement of the cross-sectional muscle area at the level of the third lumbar vertebrae.

Main outcomes and measures: Primary outcomes were overall and disease-specific survival.

Results: Among the 245 patients that met study inclusion, 209 were men (85.3%) and mean (SD) age was 62.3 (7.8) years. Sarcopenia was detected in 135 patients (55.1%), while normal skeletal muscle mass was detected in 110 patients (44.9%). For the 110 non-sarcopenic patients, primary treatment modality was not associated with improved survival. For patients with sarcopenia at diagnosis, primary surgical resection was associated with improved overall (hazard ratio [HR], 0.37; 95% CI, 0.17-0.82) and disease-specific (HR, 0.22; 95% CI, 0.07-0.68) survival. This effect persisted after propensity score matching, as upfront surgery was associated with improved overall (HR, 0.33; 95% CI, 0.12-0.91) and disease-specific (HR, 0.17; 95% CI, 0.04-0.75) survival.

Conclusions and relevance: Sarcopenia is a negative prognostic factor of survival for patients with OPSSC. Primary surgery and radiotherapy confer similar survival effects for patients with normal skeletal muscle mass in patients with localized OPSCC. However, upfront surgical resection may be associated with improved survival outcomes for sarcopenic patients.

Introduction

Patients with head and neck squamous cell carcinoma frequently experience changes in body weight prior to treatment, and a multitude of studies demonstrate that increased body mass index (BMI) is associated with increased survival in patients with solid tumors (682-685). However, recent research demonstrates that BMI incompletely describes the contributions of fat, muscle, and water compartments to the overall composition of the body (686, 687). Sarcopenia, defined as a degenerative loss of skeletal muscle (SM), was recently identified as a powerful prognostic marker of morbidity and mortality in patients with solid tumors, including patients with head and neck squamous cell carcinoma (581, 687-690). Indeed, the prognostic utility of sarcopenia is independent of BMI(687). This is exemplified by the subset of oncologic patients that are both sarcopenic and obese; these patients perform worse than their BMI matched non-sarcopenic counterparts(687). With the recent identification of sarcopenia as a strong independent predictor of outcomes for oncology patients, significant efforts are being made to improve detection methods of sarcopenia, understand its biological implications, and determine best clinical practices for treating cancer patients with excessive muscle catabolism.

For patients with localized oropharyngeal squamous cell carcinoma (OPSCC), primary surgery and definitive radiotherapy (RT) treatments historically demonstrate similar survival for both human papillomavirus (HPV) positive and negative disease (691-693). Thus, the decision between primary surgical treatment and definitive radiation therapy for localized OPSCC can be difficult, and is further complicated by uncertainties concerning whether adjuvant therapy is needed. As a result, the

identification of comorbidities and risk-factors that allow patients to differentially benefit from either primary surgical resection or definitive RT is an area of active research. To our knowledge, there are no published reports investigating the oncologic outcomes for localized OPSCC in a sarcopenic cohort receiving either primary surgery or definitive radiotherapy. Therefore, we sought to determine if selection of primary treatment modality for sarcopenic patients with localized OPSCC is associated with clinically meaningful changes in survival. Since the decision to add adjuvant therapy is typically made after pathologic staging and tumor features are made available after resection, we structured this analysis around the clinical decision-making involved in selecting a primary treatment modality, before the need for adjuvant therapy is known. Accordingly, the primary aim of this study was to characterize the association between sarcopenia and OPSCC survival for patients treated by either primary surgery or definitive RT.

Methods

Population Cohort and End Points

A retrospective review of the medical records for patients with OPSCC was performed between January 1, 2005 and December 31, 2017 at Oregon Health and Science University in Portland, Oregon. Study inclusion was restricted to patients treated with primary surgical resection or definitive RT with OPSCC clinically staged as T1-2, N0-2, M0 by AJCC eighth edition criteria. Furthermore, patients were required to have whole-body positron emission tomographic-computed tomographic (PET-CT) imaging or abdominal computed tomographic (CT) scans within 60 days prior to treatment initiation. Electronic health records were reviewed for data collection,

including: patient demographics, body mass and height, comorbidities, tumor staging and subsite, HPV/p16 status (defined by >75% of tumor cells displaying strong nuclear and cytoplasmic staining), smoking status, primary treatment modality details, evidence for recurrent disease, date and cause of death, and date of last follow up. After patient data was abstracted and correlated with imaging, data were de-identified for subsequent analysis. This study was approved by the institutional review board of Oregon Health and Science University, and requirement for informed consent was deemed unnecessary given the retrospective nature of the study. Overall survival was defined as the time from clinical diagnosis to the date of death as a result of any cause. Disease-specific survival was defined as the time from diagnosis to the date of death due to OPSCC. Morphological spread of disease was staged according to the American Joint Committee on Cancer using the eighth edition TNM system.

Computed Tomography Body Composition Analysis

Body composition analysis of skeletal muscle was conducted using previously described and widely-accepted methods(558). In brief, the cross-sectional area of skeletal muscle at the center of the third lumbar vertebrae was calculated for each patient by analyzing axial CT images of the abdomen. These CT images were often along with PET-CT imaging during the patient's clinical workup for neoplastic disease. Muscle tissue was defined as -29 to 150 Hounsfield units (Slice-o-Matic software, version 5.0; Tomovision) as described previously, and include the rectus abdominus, abdominal wall, psoas, and paraspinal muscles (694). After automated segmentation, each patient scan was examined for precise skeletal muscle labeling, and manual

corrections of mislabeled muscle were performed if necessary. The resulting cross-sectional muscle area was normalized to the patient's square of height in meters and used to calculate skeletal muscle index (SMI) (558). Sarcopenia was defined a priori as an SMI of less than 52.4 and 38.5 for males and females, respectively; these cutoffs are consistent with previous reports in head and neck cancer patients (688, 689).

Statistical Analysis

Data were analyzed between December 3, 2018, and August 28, 2019. Descriptive statistics were performed and differences between groups were assessed by Pearson chi-squared tests for categorical variables or 2-tailed *t* test for continuous variables. Odds ratios (OR) and 95% confidence intervals are reported for all appropriate calculations. Survival curves were generated using the Kaplan-Meier technique. Log-rank tests and hazard ratios (HRs) were calculated to compare both overall and disease-specific survival amongst groups. Univariable and multivariable analyses for overall survival were performed utilizing the Cox proportional hazards model, and variables with a *p* value of <0.20 by univariable analysis were included in multivariable analysis. Hazard ratios and corresponding 95% confidence intervals (CI) are reported. Propensity score matching (PSM) was performed amongst primary surgery and definitive RT groups to identify matched cohorts. Briefly, propensity scores were estimated using logistic regression of select covariates and matched utilizing nearest neighbor matching with a caliper of 0.2 (defined by units of standard deviations of the logit of the estimated propensity scores). The PSM was performed using the following covariates: age (<65 or ≥65), sex, clinical T stage (1 or 2), clinical N stage (0

or 1-2), smoking status (dichotomized by a 10 pack-year history cutoff), p16 reactivity, Charlson comorbidity score (<5 or ≥5), and BMI (<18.5, 18.5-24.9, and ≥25.0 kg/m2). All statistical analysis and graph construction was performed utilizing SPSS statistical software, version 25 (IBM).

Results

Baseline patient characteristics

A total of 245 patients met inclusion criteria for this study. Of these 245 patients, 209 (85.3%) of them identified as men and 36 (14.7%) identified as women, with a mean (SD) age of 62.3 (7.8) years. All of the 142 surgical patients included in the study had transoral resections with neck dissection, with 127 of those operations being robot assisted. Patients' smoking status was dichotomized as less than or ≥ 10 pack-year history, with 158 (64.5%) and 87 (35.5%) patients reporting less than or ≥ 10 pack-year history, respectively. Utilizing p16 reactivity as a surrogate for HPV positive disease, 28 (12.4%) of patients had p16-negative disease, with 197 (87.6%) patients with p16-positive disease. For the entire study, 135 (55.1%) of patients were sarcopenic and 110 (44.9%) were not. A Charlson Comorbidity Index (CCI) was calculated for each patient as previously described, and patients were stratified as either low-risk (CCI <5, 211 [86.1%]) and high-risk (CCI ≥5, 34 [13.9%])(695). The majority of patients in both groups (172 [70.2%] for the entire study) were overweight with a BMI greater than or equal to 25 (calculated as weight in kilograms divided by height in meters squared). Baseline characteristics for the entire study are shown in Table 1. Of the 142 patients treated by primary surgical resection, 43 went on to receive adjuvant RT, and 48

received adjuvant CRT. Of the 103 patients treated by primary RT, 83 also received concurrent chemotherapy.

We then analyzed the sarcopenic subset of patients prior to and after PSM. Specifically, Table 2 details the baseline characteristics of sarcopenic patients treated by either primary surgery or definitive RT before and after PSM to control for important survival covariates. Prior to PSM, primary surgery and definitive RT groups were clinically comparable in the following variables: age, N stage, HPV status CCI and BMI. After PSM, a comparison of the primary surgery and definitive RT groups did not show clinically meaningful differences with respect to age, sex, tumor stage, nodal stage, smoking status, HPV status, CCI, and BMI.

Sarcopenia and survival by primary treatment modality

Kaplan-Meier analysis of overall survival and disease-specific survival was performed for patients treated by either primary surgery or definitive RT and stratified by the presence or absence of sarcopenia (Figure 1). For non-sarcopenic patients, both overall survival and disease-specific survival were not statistically different between groups for patients treated by either primary surgical resection or definitive RT (Figure 1A, B). Similarly, there was no overall survival benefit observed for HPV-positive, non-sarcopenic patients treated by either surgical resection or definitive RT (Figure 1C). Prior to PSM, sarcopenic patients treated with upfront surgical resection demonstrated increased overall survival and disease-specific survival. This survival benefit was also observed when controlling for HPV status, as HPV-positive sarcopenic patients demonstrated increased overall survival when treated by primary surgical resection.

After PSM, these survival trends persisted for sarcopenic patients, as patients treated with primary surgical resection demonstrate an increase in overall survival and disease-specific survival (Figure 2). On univariable analysis of the matched sarcopenic patients, <10 pack year smoking history, negative HPV status, <18.5 BMI, and primary surgical resection were predictors of overall survival (Table 3). Multivariable analysis was then performed utilizing covariates of smoking status, HPV status, CCI, BMI, and primary treatment modality. This analysis demonstrated that <10 pack-year history smoking status and surgical resection were associated with improved overall survival, while negative HPV status and a BMI of less than 18.5 were negative predictors of overall survival.

Discussion

It is well established that skeletal muscle depletion is a significant indicator of surgical and oncologic outcomes across numerous cancer types (696-699), with a more recent identification of its prognostic utility in head and neck cancer treated by either primary surgical resection or definitive RT (688-690). However, to our knowledge, there are no published reports evaluating survival for sarcopenic patients treated by either upfront surgical resection or definitive RT in any oncologic setting. Thus, this study sought to evaluate if pre-treatment sarcopenia is associated with a differential survival benefit for patients with localized OPSCC treated by either primary surgical resection or definitive RT, as this disease is currently treated by either primary treatment modality with similar overall survival and recurrence-free survival (691, 692). To address this question, we identified 245 patients with localized OPSCC at clinical diagnosis and

performed CT imaging analysis to identify patients with and without sarcopenia. We found that patients with normal skeletal musculature at diagnosis demonstrate no difference in overall and disease-specific survival when treated by either primary surgery or definitive RT; however, when analyzing patients with sarcopenia at diagnosis, upfront surgical resection was associated with improved overall and disease specific survival in this study.

In the literature, the estimates of sarcopenia in the head and neck cancer population fluctuates significantly, with reports ranging from 35% to nearly 80%(688, 690). However, these reports vary in inclusion criteria and disease stage. In the present study, inclusion criteria were limited to patients with clinically staged T1-2, N0-2 disease, and we report 55.1% of the population was sarcopenic at diagnosis. This value is consistent with previous reports demonstrating skeletal muscle wasting could be present in nearly half of diagnosed HNC cases(689, 690, 700). Despite these large fluctuations in the prevalence of sarcopenia in patients with HNC, it is clear that a large portion of HNC patients present with sarcopenia at diagnosis. As current guidelines for patients with clinically staged T1-2, N0-2 OPSCC recommend a range of options, including primary surgery with pathologically-directed adjuvant therapy, definitive radiation therapy, concurrent chemoradiation, induction chemotherapy and RT, or clinical trials, clinicians are continually in search of risk-stratification methods to best determine which patients are most likely to benefit from these varied treatment modalities. Thus, identification of novel risk-factors that extend beyond tumor features have gained increased attention over the past decade, and include pre-treatment

measures of body composition, dietary patterns, and neurocognitive impairment (417, 701-703).

It is possible that sarcopenia is a consequence of other pathophysiological processes associated with cancer, including the unique biology of the primary tumor and the chronic disease-associated syndrome cachexia. In the case of the former, recent studies demonstrate the ability of HPV-positive cancers to secrete extracellular vesicles which increase tumor innervation and aggressiveness(525, 704). Furthermore, solid tumors may directly contribute to skeletal muscle wasting through release of heat shock proteins and extracellular vesicles that activate catabolic signaling pathways(705, 706). In this case, where the primary tumor biology is directly contributing to muscle catabolism, it is conceivable that sarcopenic patients would glean benefit from rapid surgical excision of the primary tumor. As mentioned previously, sarcopenia is also a sign of cachexia, a disease-associated metabolic syndrome which significantly reduces patients' quality of life and ultimate survival. Cachexia is a multi-organ wasting syndrome in which patients experience decreased appetite, yet have a paradoxical increase in basal metabolic rate (6, 15). Discriminating between simple nutritional deficiencies and cachexia in the clinic is especially challenging in HNC patients, as the primary tumor location is often directly positioned in the aerodigestive tract. As a result, determining the causative mechanism of sarcopenia (e.g. cachexia, malnutrition, dysphagia, old age, etc.) may lead to clearer risk-stratification methods for sarcopenic patients. Collectively, these data and more suggest that nutritional interventions for patients with sarcopenia would be beneficial, independent of the underlying muscle wasting etiology.

Taken together, these results highlight the unique biologic state of the sarcopenic patient, and suggest patients with excessive muscle loss at diagnosis may differentially respond to treatment modalities compared to their non-sarcopenic counterparts. There are many plausible explanations for this differential effectiveness of primary surgery versus radiation in sarcopenic patients. Baseline sarcopenia may limit HNC patients' ability to tolerate RT and chemo-RT, as sarcopenic patients are more likely to require treatment holidays than non-sarcopenic patients (707, 708). Similarly, the long-term effects of radiation, such as dysphagia, xerostomia, and other issues, may impact sarcopenic patients more significantly than non-sarcopenic patients, making surgery and subsequent de-escalation of radiation and/or chemotherapy a more viable treatment paradigm in these patients. While the recently published ORATOR trial demonstrates definitive RT patients had improved quality of life swallowing scores over transoral robotic surgery patients, the one year endpoint of this study may be too short to capture some of the long-term morbidities associated with RT, including dysphagia and aspiration(709). Alternatively, sarcopenia may be correlated with other host factors, such as reduced immune surveillance, that may render radiation therapy less effective. Further study into this observation will be required to better understand these factors and to test the utility of the clinical assessment of sarcopenia in clinical practice.

Limitations

As with any retrospective review, this study has important limitations to consider when interpreting the presented data. Retrospective studies are routinely subject to missing data and lack of patient follow-up data. As abdominal CT imaging is not always

performed during head and neck cancer workup or outside imaging may not have been available for analysis, several patients were excluded from analysis due to a lack of abdominal imaging. Thus, this selection of patients with abdominal imaging limits the overall power of the study and may introduce a selection bias. Additional treatment bias may be introduced as this was not a controlled study, and the choice of treatment modality was entirely up to the patients and treatment team. Similarly, precise clinical rationale on how or why a patient was selected for a given treatment modality was not easily captured in the health records. Finally, since this study was performed at a single tertiary care institution, care should be taken in interpreting these results, as they may not generalize to the broader head and neck oncology community.

Conclusions

OPSCC patients with depleted skeletal muscle mass, or sarcopenia, exhibit decreased overall and disease-specific survival, and patients with localized disease are routinely treated by primary surgical resection or definitive RT therapy. To our knowledge, no published reports have investigated the association between primary treatment modality and oncologic outcomes in patients with baseline skeletal muscle wasting. In this single-institution study, we report that patients with normal skeletal musculature at diagnosis benefit equally from primary surgical resection or definitive RT. However, upfront ablative surgery for sarcopenic patients was associated with an increase in overall and disease-specific survival compared to their definitive RT counterparts. As such, these data suggest sarcopenia may be a clinically significant variable when considering treatment modalities for patients with localized OPSCC.

Acknowledgements

Dr. Marks received personal fees from Pfizer and grants from the National Institutes of Health during the conduct of the study. No other disclosures were reported.

Figures and legends

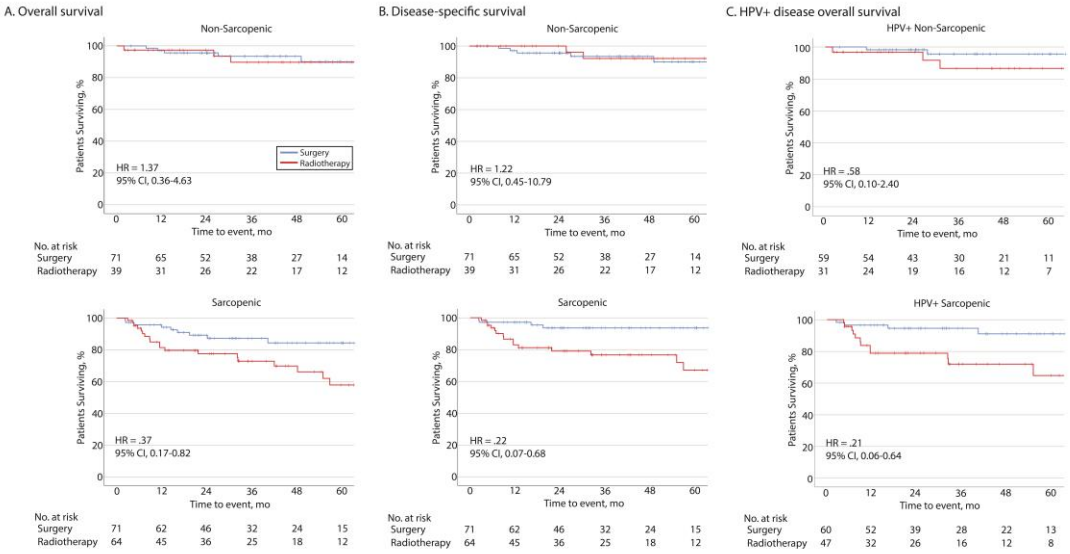

Figure 1. Survival in sarcopenic and non-sarcopenic patients. Overall (A) and disease-specific (B) survival for sarcopenic and non-sarcopenic patients treated by primary surgery or definitive RT. (C) Overall survival in sarcopenic and non-sarcopenic patients with HPV-positive disease.

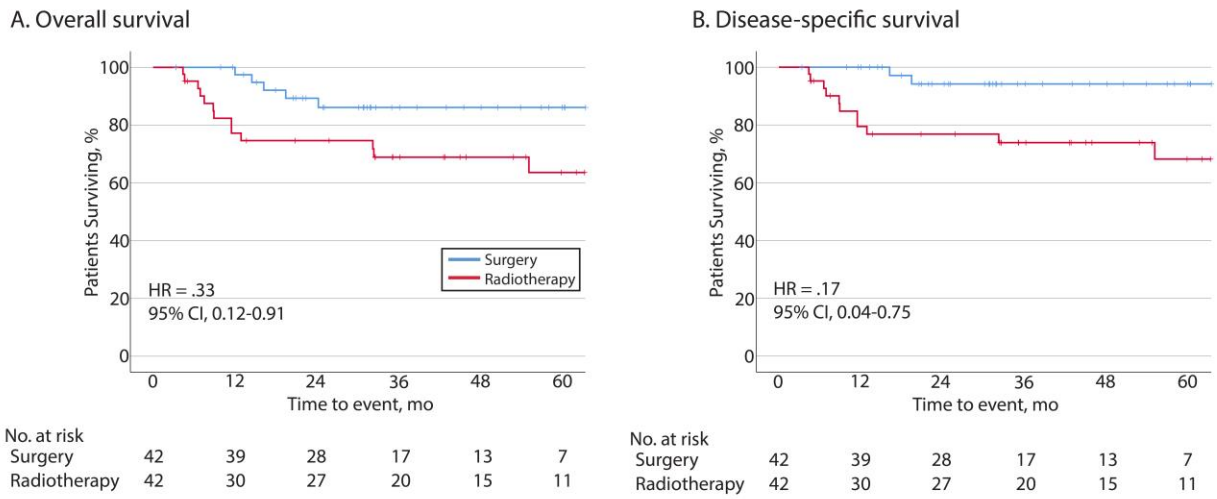

Figure 2. Survival analysis in a propensity score matched sarcopenic cohort. Overall (A) and disease-specific (B) survival for sarcopenic patients treated by either primary surgery or definitive RT.

Tables

Table 1. Patient Demographics

		Surgery *N = 142* No. (%)	Radiation *N = 103* No. (%)	Total *N = 245* No. (%)	Odds Ratio (95% CI)
Age					
	Mean (SD)	62.1 (7.5)	62.5 (8.2)	62.3 (7.8)	
	<65	107 (75.4)	60 (58.3)	167 (68.2)	2.2 (1.2-3.7)
	≥65	35 (24.6)	43 (41.7)	78 (31.8)	1
Sex					
	Male	111 (78.2)	98 (95.1)	209 (85.3)	0.2 (0.07-0.5)
	Female	31 (21.8)	5 (4.9)	36 (14.7)	1
Clinical Tumor Stage					
	1	62 (43.7)	33 (32.0)	95 (38.8)	1.6 (1.0-2.8)
	2	80 (56.3)	70 (68.0)	150 (61.2)	1
Clinical Nodal Stage					
	0	27 (19.0)	7 (6.8)	34 (13.9)	3.2 (1.3-7.7)
	1-2	115 (81.0)	96 (93.2)	211 (86.1)	1
Smoking					
	<10 pack year	108 (76.1)	50 (48.5)	158 (64.5)	3.4 (2.0-5.8)
	≥10 pack year	34 (23.9)	53 (51.5)	87 (35.5)	1
HPV Status					
	Negative	18 (13.1)	10 (11.4)	28 (12.4%)	1.2 (0.5-2.7)
	Positive	119 (86.9)	78 (88.6)	197 (87.6%)	1
Sarcopenic					
	No	71 (50.0)	39 (37.9)	110 (44.9)	1.7 (1.0- 2.8)
	Yes	71 (50.0)	64 (62.1)	135 (55.1)	1
CCI					
	<5	124 (87.3)	87 (84.5)	211 (86.1)	1.3 (0.6-2.6)
	≥5	18 (12.7)	16 (15.5)	34 (13.9)	1
BMI					
	<18.5	4 (2.8)	5 (4.9)	9 (3.7)	1.7 (0.4-6.4)
	18.5-24.9	40 (28.2)	24 (23.3)	64 (26.1)	0.8 (0.4-1.4)
	≥25	98 (69.0)	74 (71.8)	172 (70.2)	1

Abbreviations: HPV, Human papilloma virus p16 variant; CCI, Charlson Comorbidity Index; BMI, Body Mass Index; OR, odds ratio; CI, confidence interval.

Table 2. Sarcopenic Patient Demographics Before and After PSM

		Before PSM			
		Surgery	**Radiation**	**Total**	
		N = 71	*N = 64*	*N = 135*	
		No. (%)	No. (%)	No. (%)	Odds Ratio (95% CI)
Age					
	Mean (SD)	62.4 (8.6)	61.9 (8.1)	62.2 (8.4)	
	<65	44 (62.0)	48 (75.0)	92 (68.1)	0.5 (0.3-1.1)
	≥65	27 (38.0)	16 (25.0)	43 (31.9)	1
Sex					
	Male	59 (83.1)	61 (95.3)	120 (88.9)	0.2 (0.1-0.9)
	Female	12 (16.9)	3 (4.7)	15 (11.1)	1
Clinical Tumor Stage					
	1	34 (47.9)	19 (29.7)	53 (39.3)	2.2 (1.1-4.4)
	2	37 (52.1)	45 (70.3)	82 (60.7)	1
Clinical Nodal Stage					
	0	12 (16.9)	4 (6.3)	16 (11.9)	3.1 (0.9-10.0)
	1-2	59 (83.1)	60 (93.8)	110 (88.1)	1
Smoking Status					
	< 10 pack-year	49 (69.0)	25 (39.1)	74 (54.8)	3.5 (1.7-7.1)
	≥10 pack-year	22 (31.0)	39 (60.9)	61 (45.2)	1
HPV Status					
	Negative	8 (11.8)	10 (17.5)	18 (14.4)	0.62 (0.3-1.7)
	Positive	60 (88.2)	47 (82.5)	107 (85.6)	1
CCI					
	<5	59 (83.1)	58 (90.6)	117 (86.7)	0.5 (0.2-1.4)
	≥5	12 (16.9)	6 (9.4)	18 (13.3)	1
BMI					
	<18.5	3 (4.2)	4 (6.3)	7 (5.2)	1.3 (0.3-6.0)
	18.5-24.9	31 (43.7)	21 (32.8)	52 (38.5)	0.6 (0.3-1.3)
	≥25	37 (52.1)	39 (60.9)	76 (56.3)	1

Table 2 Continued

		After PSM			
		Surgery	**Radiation**	**Total**	
		N = 42	*N = 42*	*N = 84*	
		No. (%)	No. (%)	No. (%)	Odds Ratio (95% CI)
Age					
	Mean (SD)	62.1 (7.5)	62.5 (8.2)	62.3 (7.8)	
	<65	29 (69.0)	32 (76.2)	61 (72.6)	0.7 (0.3-1.8)
	≥65	13 (31.0)	10 (23.8)	23 (27.4)	1
Sex					
	Male	34 (81.0)	40 (95.2)	74 (88.1)	0.2 (0.04-1.1)
	Female	8 (19.0)	2 (4.8)	10 (11.9)	1
Clinical Tumor Stage					
	1	16 (38.1)	15 (35.7)	31 (36.9)	1.1 (0.5-2.7)
	2	26 (61.9)	27 (64.3)	53 (63.1)	1
Clinical Nodal Stage					
	0	7 (16.7)	4 (9.5)	11 (13.1)	1.9 (0.5-7.1)
	1-2	35 (83.3)	38 (90.5)	73 (86.9)	1
Smoking Status					
	< 10 pack-year	24 (57.1)	25 (59.5)	49 (58.3)	0.9 (0.4-2.2)
	≥10 pack-year	18 (42.9)	17 (40.5)	35 (41.7)	1
HPV Status					
	Negative	8 (19.0)	6 (14.3)	14 (16.7)	1.6 (0.5-5.1)
	Positive	34 (81.0)	36 (85.7)	70 (83.3)	1
CCI					
	<5	37 (88.1)	37 (88.1)	74 (88.1)	1.0 (0.3-3.7)
	≥5	5 (11.9)	5 (11.9)	10 (11.9)	1
BMI					
	<18.5	1 (2.4)	1 (2.4)	2 (2.4)	0.9 (0.1-14.4)
	18.5-24.9	18 (42.9)	14 (33.3)	32 (38.1)	0.7 (0.3-1.6)
	≥25	23 (54.8)	27 (64.3)	50 (59.5)	1

Abbreviations: HPV, Human papilloma virus p16 variant; CCI, Charlson Comorbidity Index; BMI, Body Mass Index; OR, odds ratio; CI, confidence interval.

Table 3. Univariable and Multivariable Analysis

Univariable			Multivariable		
		HR (95% CI)			HR (95% CI)
Age			Smoking Status		
	<65	0.15 (0.02-1.99)		< 10 pack-year	0.26 (0.08-0.86)
	≥65	1		≥ 10 pack-year	1
Sex			HPV Status		
	Male	0.39 (0.05-2.90)		Negative	1.29 (1.09-3.15)
	Female	1		Positive	1
Clinical Tumor Stage			CCI		
	1	0.92 (0.36-2.35)		<5	0.84 (0.09-7.54)
	2	1		≥5	1
Clinical Nodal Stage			BMI		
	0	0.62 (0.14-2.71)		<18.5	19.59 (2.64-145.55)
	1-2	1		18.5-24.9	1.76 (0.65-4.73)
Smoking Status				≥25	1
	< 10 pack-year	0.16 (0.05-0.50)	Primary Treatment		
	≥ 10 pack-year	1		Surgery	0.2 (0.08-0.81)
HPV Status				RT	1
	Negative	3.5 (1.30-10.25)			
	Positive	1			
CCI					
	<5	0.49 (0.19-1.21)			
	≥5	1			
BMI					
	<18.5	18.0 (3.62-89.96)			
	18.5-24.9	1.83 (0.71-4.75)			
	≥25	1			
Primary Treatment					
	Surgery	0.33 (0.12-0.91)			
	RT	1			

Abbreviations: HPV, Human papilloma virus p16 variant; CCI, Charlson Comorbidity Index; BMI, Body Mass Index; OR, odds ratio; CI, confidence interval.

Constructing and programming a cost-effective murine running wheel with digital revolution counter

A manuscript in review at *Nature Lab Animal*

Jared Edwards*[1,2], Brennan Olson*[2,3], and Daniel L. Marks[2,4,5]

* These authors contributed equally to this work

1. Department of General Surgery, Naval Medical Center San Diego, San Diego, CA USA
2. Papé Family Pediatric Research Institute, Oregon Health & Science University, Portland, OR USA
3. Medical Scientist Training Program, Oregon Health & Science University, Portland, OR USA
4. Knight Cancer Institute, Oregon Health & Science University, Portland, OR USA
5. Brenden-Colson Center for Pancreatic Care, Oregon Health and & Science University Portland, OR USA

Abstract:

Murine wheel running is a known voluntary behavior that has become well-established as a measure of physical activity in preclinical models of cancer cachexia. The cost of commercially-available revolution-tracking mouse running wheels are often expensive to the point of being fiscally-prohibitive due to per-wheel costs. We developed and tested a homemade revolution-counting mouse running wheel that is easily built from commercial-off-the-shelf (COTS) parts and an open-source C++-based program. Herein, we describe detailed assembly instructions and provide necessary resources for researchers to build their own running wheels. Multiple wheels can be built quickly and easily, and at less than a tenth of the cost of commercially-available mouse wheels. Testing data provided herein demonstrate comparability of homemade wheel data with recently-published data generated from commercially-available wheels.

Introduction:

Wheel running is a known voluntary murine behavior (710). Since voluntary wheel running is appreciated as a useful intervention in preclinical models of health and disease, technology to record wheel revolutions as a measure for mouse activity has been commercialized. These wheels often employ wireless transmission of data to a hub as well as low-friction bearings. However, the cost of commercially-available wheels can be prohibitive, costing several hundred dollars per wheel and almost a thousand dollars for a compulsory wireless hub. Furthermore, many experiments often require using several wheels simultaneously (as many as 12 wheels at a time(711)),

necessitating the purchase of numerous running wheels. These experiments can last for several weeks, making a staggered use of limited wheel resources less plausible for studies on a timeline. The upfront cost for a laboratory attempting such experiments can be prohibitively high, leaving this useful metabolic and behavioral intervention inaccessible to a large portion of the research community.

In contrast to other exercise models such as forced swimming(712) or treadmill running(713), wheel running does not require aversive stimuli to stimulate activity, suggesting that it may be distinctly useful in evaluating spontaneous murine behavior. Mice also prefer wheel running to other complex activities, such as mazes when provided with both(714), and even express preferences between different saucer shapes(715). Indeed, voluntary wheel running is seen in non-captive mice in the wild when they are provided running wheels(638). The natural predilection of mice to running on a wheel has been applied in translational research, allowing researchers to measure multiple factors contributing to both voluntary and motivated behaviors in preclinical models. Specifically, wheels offer a therapeutic exercise intervention shown to stimulate hippocampal neurogenesis(716), reduce tumor incidence and growth(652), and alter local EEG patterns during sleep(717) in murine models. Our laboratory has utilized this constructed wheel model to assess fatigue during the development of cancer cachexia with robust and consistent results, demonstrating the experimental reliability of these constructed wheels (597).

Given the clear utility of mouse running wheels in translational research and the high per-unit cost, lowering the barrier to their use is imperative in making this useful experimental intervention accessible to the broader research community. Thus, we set

out to design and construct a homemade running wheel that accurately and reliably counts wheel revolutions for several weeks with the combined benefits of low cost and simple construction. We were able to construct a durable wheel with a precise revolution counter for a fraction of the cost of commercially available wheels. This was achieved using commercial-off-the-shelf (COTS) parts and removing complex and redundant circuitry.

Materials:

An itemized list of both consumable and non-consumable materials required to assemble the mouse running wheel is enclosed in Appendix 1. The pre-fabricated printed circuit board (PCB) can be acquired by going to navigating to https://github.com/m141914/Mouse-Revolution-Counter and following the instructions to either independently manufacture or purchase the circuit boards from an independent manufacturer.

Procedure:

Wheel counter circuit board programming and soldering. Timing ~20 min

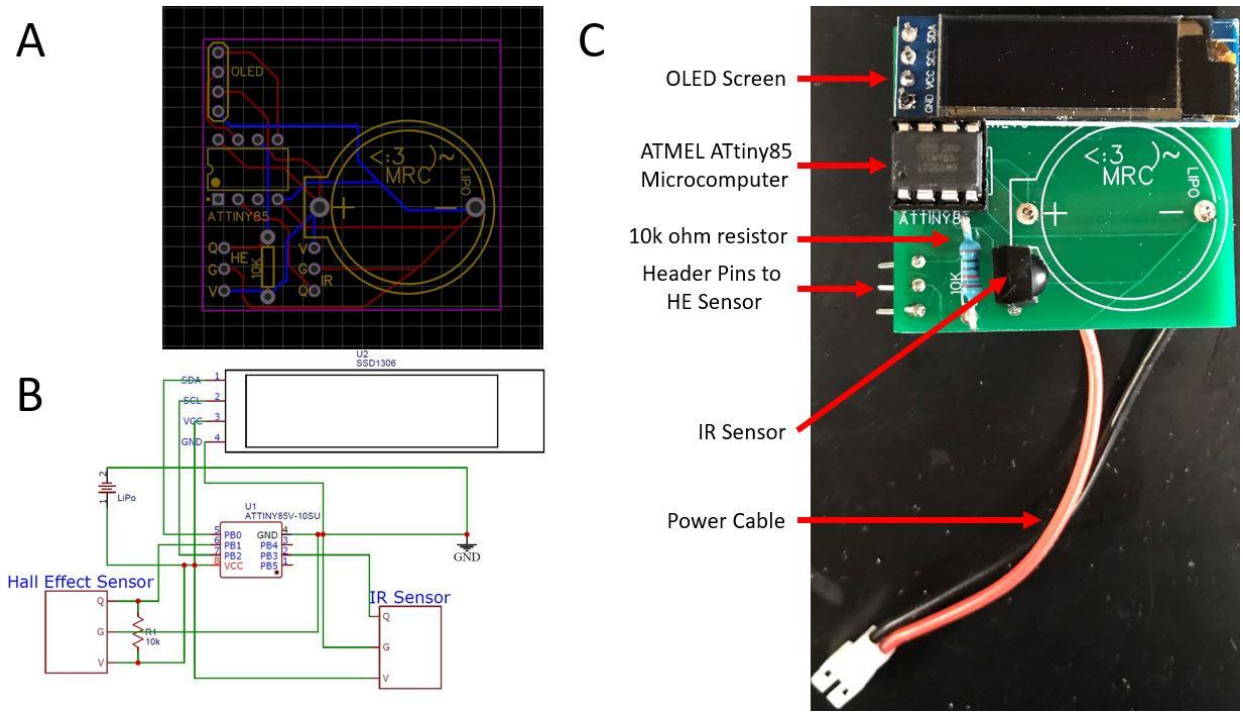

Figure 1: Mouse running wheel PCB schematics and parts layout. (A) Mouse wheel PCB diagram. (B) Electronic schematic. (C) Fully-constructed PCB with parts labelled.

1. Solder wires, header pins, optical light-emitting diode (OLED) screen, infrared (IR) sensor, and ATtiny85 socket onto the pre-fabricated circuit board as shown in Figure 1. !CAUTION Soldering electronic components involves high temperatures that can cause severe, permanent burn injury as well as property damage. Ensure that all manufacturer safety instructions are followed and that the heated soldering iron is placed in a safe and secure location when not actively used.

2. Insert the ATtiny85 into the TinyUSB programmer with static-free forceps and insert the programmer into a PC USB drive.

3. On the PC, open the Arduino integrated development environment (IDE; https://www.arduino.cc/en/main/software).

4. Under the “tools” header:

1. Select “Processor” and select “ATtiny85.”
2. Select “Clock” and select “Internal 1 MHz.”
3. Select “Burn Bootloader.”

5. Download both the TinyWireM and Tiny4kOLED Arduino libraries from the following links:

TinyWireM: https://github.com/adafruit/TinyWireM

Tiny4kOLED: https://github.com/datacute/Tiny4kOLED

6. Place both library files within the “libraries” folder in the Arduino directory that was made on installation of the Arduino IDE.

7. In the Arduino IDE, create a new Arduino file by selecting “file” on the toolbar and then “new.”

8. Copy the code from Appendix 2 and paste it into the blank file. Save this file.

9. Select the “Upload” button, which is the 2nd button from the left just below the toolbar, and appears as a right-facing arrow, in order to send the program to the ATtiny85 microcontroller.

10. Once “upload complete” is indicated, safely remove the TinyUSB programmer from the PC and remove the ATtiny85.

11. Place the ATtiny85 into the 8-pin socket on the assembled circuit board, ensuring that the depressed dot on the upper left of the microcontroller is on the side farthest from the OLED screen and on the same side as the semi-circular impression in the socket.

Wheel enclosure assembly. Timing ~10 min

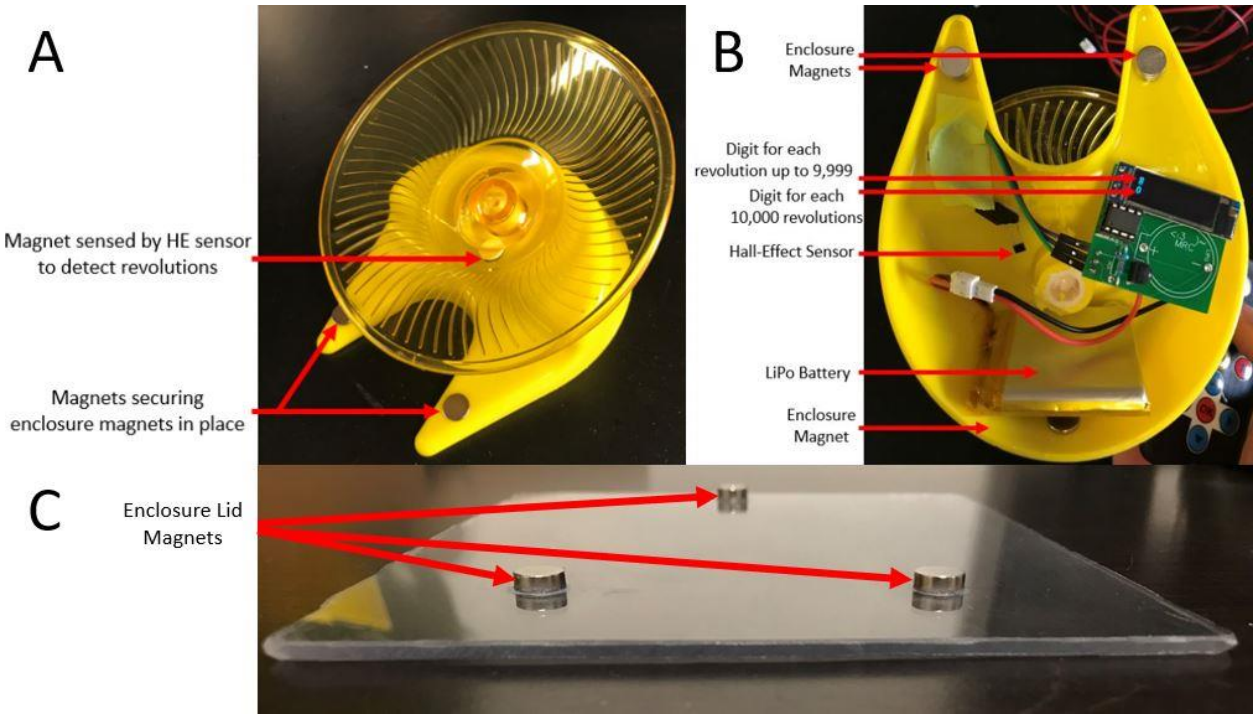

Figure 2: Running wheel construction and design. (A) Superior view of mouse running wheel with suggested magnet locations. (B) Bottom-side view of completed mouse running wheel enclosure). (C) Transparent enclosure lid with 3-point magnet placement.

12. Using a Dremel tool, cut and grind the underside of the mouse wheel base to remove the two midline plastic walls between the main body and white bottom of the wheel axle until it is flush with the yellow plastic bearing. !CAUTION The use of a Dremel tool can cause severe and permanent damage as well as wide dispersion of plastic. Ensure eye protection and an enclosed space such as a hood are used.

13. Glue neodymium magnets to the following areas on the wheel base:

1. 2 under each base strut (in addition to 1 on the upper side of each strut for increased adhesion).

2. 1 on the inner aspect of the real wall of the wheel base. Use and extra magnet on the outer side to hold the magnet in place while glue dries.

3. 1 magnet at the bottom of the rotating wheel. Ensure that the magnet is as close to the wheel base as possible so that the hall-effect sensor will be within range.

14. Secure the hall-effect sensor with the sensing (curved) side facing the wheel magnet through the plastic base. Ensure that it is as close to the magnet as possible to ensure reliable sensing.

15. Attach 3 female-to-female DuPont cables to the hall-effect sensor prongs.

16. Attach the other ends of the DuPont cables to the assembled circuit board. Correct wiring is such that the three header pins should line up with the hall-effect prongs if they are both face-up and the hall-effect prongs are pointing toward the header pins.

17. Place a charged lithium-ion battery into the base between the wheel bearing and rear wall of the wheel base.

18. Using a Dremel tool, cut a 12x14.5cm transparent rectangular pane from a large sheet of plastic.

19. Sandwich the plastic pane between the assembled wheel base and 3 neodymium magnets. Use adhesive to glue the 3 neodymium magnets in position on the plastic pane to ensure that they effectively secure the pane to the wheel via the wheel-base magnets glued on in step 13. When the adhesive dries, the wheel is ready to be used.

Wheel operation. Timing <5 min

20. Turn the wheel on by opening the enclosure to access the inside of the wheel base. Attach the male Japan Solderless Terminal (JST) coupling to the female JST coupling soldered to the circuit board and replace the enclosure lid.

21. Place the mouse running wheel within a murine subject habitat that has a transparent bottom.

22. In order to reset the counter, power must be disconnected from the microcontroller. The device does not have memory capability and should be checked regularly to record data.

23. To display the revolution count, a user can press any button on an IR-emitting remote control while it is facing the IR sensor, which includes most available television remote controls. The wheel displays 2 numbers:

1. The top number counts from 0-9,999. When a revolution occurs after 9,999, this number resets to 0.

2. The bottom number increments by 1 integer value once the top number resets. The bottom number represents 10,000 times its value in revolutions.

Timing:

Steps 1-11, wheel counter circuit board programming and soldering: 20 min

Steps 12-19, wheel enclosure assembly: 10 min

Steps 20-23, wheel operation: <5min

Results:

After a 2-week acclimation phase to the running wheels, we collected daily revolution counts for 12 days (post-acclimation running phase) and observed consistent daily revolution counts for all animals (n=4) in the study. We then introduced animals to a minimally invasive abdominal surgery in which pancreatic cancer cells were orthotopically implanted, abdominal musculature and fascia closed with absorbable sutures, and skin layers closed with small surgical clips as previously described (38). Mice significantly reduced wheel running activities the day after abdominal surgery,

followed by a steady recovery phase back to their baseline running prior to a slow decline due to previously-described tumor-induced fatigue (38) (Figure 3).

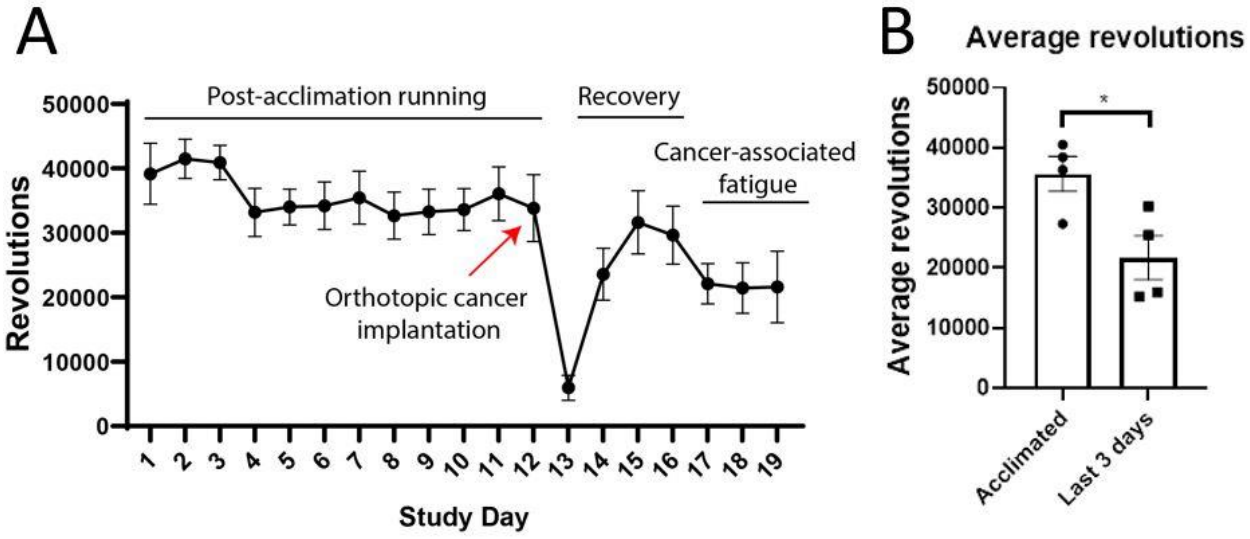

Figure 3: Experimental data utilizing mouse running wheel. (A) Daily running wheel revolutions for single-housed C57BL/6J mice after two weeks of wheel acclimation. Mice underwent a small abdominal surgery and orthotopic pancreatic cancer cell implantation on study day 12. (B) Average revolutions per day once acclimated versus final 3 days of experiment (days 17-19).

Conclusion:

The utility of voluntary wheel-running for preclinical modeling and murine behavior evaluation is well established(710). In order to make this valuable research modality available to the broader scientific community, we constructed an accurate and reliable running wheel out of cheap materials. We succeeded at designing a model that can be simply built for less than a tenth of the cost of commercially-available options. This design has been validated against industry standard running wheels in previous studies of pancreatic cancer cachexia. Additionally, the initial investment into required

tools (Dremel, pencil-tip soldering iron) becomes a smaller part of the overall cost with scaling to larger experiments requiring a higher number of wheels. The design is limited in comparison to commercially-available options due to required assembly and familiarization with soldering. Additionally, the lack of memory capacity combined with lack of wireless data transmission requires regular counter monitoring to prevent loss of data capture in the event of battery depletion. Despite its limitations, however, this design significantly lowers the barrier to entry for utilizing wheel-running in basic science research, making it accessible to a larger proportion of the scientific community. This will enable a rapid expansion of similar research, increasing volume of results and scientific knowledge.

Appendix 1: Parts list for mouse wheels per unit and non-consumable tools

Item	Approximate Cost (USD)
Parts	
Exercise Saucer	$6.29
12x14.5cmh clear plexiglass pane	$1.92
JST Power wire	$0.85
ATMEL Attiny85	$2.09
Pre-Printed MRC PCB	$5.00
3000mAh Lithium Polymer Battery	$12.50
10X3mm Neodymium Magnet x11	$1.43
SSD1306 OLED screen	$4.39
10kohm resistor	$0.06
Hall effect sensor	$0.40
IR sensor	$1.54
Header Pins x7	$0.10
Female-Female Dupont Cables x3	$0.38
Total Parts Cost	$36.95
Tools	
TinyAVR USB Programmer	$15.00
Electrical Tape	$6.50
Super Glue	$1.07
IR-emitting remote control	$6.00
Soldering Kit	$17.00
Dremel	$35.00
6-battery usb charger	$7.00
JST extension cables x6	$36.36
Arduino IDE	Free Download
TinyWireM library	Free Download
Tiny4kOLED library	Free Download
Total Tools Cost	$123.93

Appendix 2: Code to upload to Attiny85

```
#include <TinyWireM.h>
#include <Tiny4kOLED.h>
#include <avr/io.h>
#include <avr/interrupt.h>
#include <avr/sleep.h>
#ifndef cbi
#define cbi(sfr, bit) (_SFR_BYTE(sfr) &= ~_BV(bit))
#endif
#ifndef sbi
#define sbi(sfr, bit) (_SFR_BYTE(sfr) |= _BV(bit))
#endif
volatile int revs = 0;
volatile int cheddar = 0;
unsigned long bit;
void setup() {
  pinMode(0,OUTPUT); // Sets pin 0 as an output for the pin-change interrupt
  pinMode(1,INPUT);
  digitalWrite(1, LOW);
  pinMode(3,INPUT);
  digitalWrite(3, LOW);
  pinMode(2,OUTPUT); //SCL for OLED
  pinMode(4,INPUT); // removing floating variables by setting unused pins to input to
save power
  pinMode(5,INPUT);
  sbi(GIMSK,PCIE); // turns on pin change interrupt
  sbi(PCMSK,PCINT3); // defines pin 3 (IR Sensor) as affected by interrupt
  sbi(PCMSK,PCINT1); // defines pin 1 (Hall-Effect Sensor) as affected by interrupt
  oled.begin();
  oled.clear();
  oled.setFont(FONT8X16);
}
void loop() {//Main loop checks if IR sensor is triggered to either increase or display
count
bit=pulseIn(3,HIGH,50000UL);
if(bit<4000){
    revs++;
    if(revs>=20000){
    cheddar++; //if revolution number is at 10k, this variable goes up by 1
    revs=0;    //Resets counter variable to 0
    }
}
if(bit>4000){
     oled.on();
     oled.clear();
```

```
    oled.print(long((revs)/2)); //Displays revoltutions <10k
    oled.setCursor(0, 2);
    oled.print(long(cheddar)); //Displays multiples of 10k below <10k count
    delay(4000);
    }
digitalWrite(3,LOW);
system_sleep();
}
void system_sleep() {
  oled.off();
  cbi(ADCSRA, ADEN); // turns ADC off
  sleep_bod_disable();
  set_sleep_mode(SLEEP_MODE_PWR_DOWN); // sets the sleep mode
  sleep_mode(); // turns sleep mode on
  sbi(ADCSRA,ADEN); // turns ADC back on
}
ISR(PCINT0_vect){//Occurs whenever the HE or IR sensors sense pin-change
}
```

References

1. Dantzer R, Kelley KW. Twenty years of research on cytokine-induced sickness behavior. Brain Behav Immun. 2007;21(2):153-60.
2. Wang A, Luan HH, Medzhitov R. An evolutionary perspective on immunometabolism. Science (New York, NY). 2019;363(6423).
3. Stearns S. The Evolution of Life Histories Press OU, editor1992.
4. Kelley KW, Bluthé RM, Dantzer R, Zhou JH, Shen WH, Johnson RW, et al. Cytokine-induced sickness behavior. Brain Behav Immun. 2003;17 Suppl 1:S112-8.
5. Wang A, Huen SC, Luan HH, Yu S, Zhang C, Gallezot JD, et al. Opposing Effects of Fasting Metabolism on Tissue Tolerance in Bacterial and Viral Inflammation. Cell. 2016;166(6):1512-25.e12.
6. Baracos VE, Martin L, Korc M, Guttridge DC, Fearon KCH. Cancer-associated cachexia. Nat Rev Dis Primers. 2018;4:17105.
7. Katz AM, Katz PB. Diseases of the heart in the works of Hippocrates. Br Heart J. 1962;24(3):257-64.
8. Fearon K, Strasser F, Anker SD, Bosaeus I, Bruera E, Fainsinger RL, et al. Definition and classification of cancer cachexia: an international consensus. Lancet Oncol. 2011;12(5):489-95.
9. Wesseltoft-Rao N, Hjermstad MJ, Ikdahl T, Dajani O, Ulven SM, Iversen PO, et al. Comparing two classifications of cancer cachexia and their association with survival in patients with unresected pancreatic cancer. Nutrition and cancer. 2015;67(3):472-80.
10. Bachmann J, Buchler MW, Friess H, Martignoni ME. Cachexia in patients with chronic pancreatitis and pancreatic cancer: impact on survival and outcome. Nutrition and cancer. 2013;65(6):827-33.
11. McDonald MN, Wouters EFM, Rutten E, Casaburi R, Rennard SI, Lomas DA, et al. It's more than low BMI: prevalence of cachexia and associated mortality in COPD. Respiratory research. 2019;20(1):100.
12. Morley JE, Thomas DR, Wilson MM. Cachexia: pathophysiology and clinical relevance. The American journal of clinical nutrition. 2006;83(4):735-43.
13. Olson B, Marks DL, Grossberg AJ. Diverging metabolic programmes and behaviours during states of starvation, protein malnutrition, and cachexia. J Cachexia Sarcopenia Muscle. 2020;11(6):1429-46.
14. Anker MS, Holcomb R, Muscaritoli M, von Haehling S, Haverkamp W, Jatoi A, et al. Orphan disease status of cancer cachexia in the USA and in the European Union: a systematic review. J Cachexia Sarcopenia Muscle. 2019;10(1):22-34.
15. Grossberg AJ, Scarlett JM, Marks DL. Hypothalamic mechanisms in cachexia. Physiology & behavior. 2010;100(5):478-89.
16. Braun TP, Zhu X, Szumowski M, Scott GD, Grossberg AJ, Levasseur PR, et al. Central nervous system inflammation induces muscle atrophy via activation of the hypothalamic-pituitary-adrenal axis. The Journal of experimental medicine. 2011;208(12):2449-63.
17. Knoll JG, Krasnow SM, Marks DL. Interleukin-1beta signaling in fenestrated capillaries is sufficient to trigger sickness responses in mice. Journal of neuroinflammation. 2017;14(1):219.

18. Burfeind KG, Michaelis KA, Marks DL. The central role of hypothalamic inflammation in the acute illness response and cachexia. Seminars in cell & developmental biology. 2016;54:42-52.
19. Maldonado M, Molfese DL, Viswanath H, Curtis K, Jones A, Hayes TG, et al. The habenula as a novel link between the homeostatic and hedonic pathways in cancer-associated weight loss: a pilot study. J Cachexia Sarcopenia Muscle. 2018;9(3):497-504.
20. Burfeind KG, Zhu X, Norgard MA, Levasseur PR, Huisman C, Buenafe AC, et al. Circulating myeloid cells invade the central nervous system to mediate cachexia during pancreatic cancer. Elife. 2020;9.
21. Seelaender M, Laviano A, Busquets S, Püschel GP, Margaria T, Batista ML, Jr. Inflammation in Cachexia. Mediators of inflammation. 2015;2015:536954-.
22. Tsoli M, Robertson G. Cancer cachexia: malignant inflammation, tumorkines, and metabolic mayhem. Trends in Endocrinology & Metabolism. 2013;24(4):174-83.
23. Argilés JM, Stemmler B, López-Soriano FJ, Busquets S. Inter-tissue communication in cancer cachexia. Nature Reviews Endocrinology. 2019;15(1):9-20.
24. Scott HR, McMillan DC, Crilly A, McArdle CS, Milroy R. The relationship between weight loss and interleukin 6 in non-small-cell lung cancer. Br J Cancer. 1996;73(12):1560-2.
25. Nakashima J, Tachibana M, Ueno M, Miyajima A, Baba S, Murai M. Association between tumor necrosis factor in serum and cachexia in patients with prostate cancer. Clinical cancer research : an official journal of the American Association for Cancer Research. 1998;4(7):1743-8.
26. Derman BA, Macklis JN, Azeem MS, Sayidine S, Basu S, Batus M, et al. Relationships between longitudinal neutrophil to lymphocyte ratios, body weight changes, and overall survival in patients with non-small cell lung cancer. BMC cancer. 2017;17(1):141-.
27. Borish LC, Steinke JW. 2. Cytokines and chemokines. The Journal of allergy and clinical immunology. 2003;111(2 Suppl):S460-75.
28. Steinke JW, Borish L. 3. Cytokines and chemokines. The Journal of allergy and clinical immunology. 2006;117(2 Suppl Mini-Primer):S441-5.
29. Dranoff G. Cytokines in cancer pathogenesis and cancer therapy. Nature Reviews Cancer. 2004;4:11.
30. Seruga B, Zhang H, Bernstein LJ, Tannock IF. Cytokines and their relationship to the symptoms and outcome of cancer. Nat Rev Cancer. 2008;8(11):887-99.
31. Mantovani A, Allavena P, Sica A, Balkwill F. Cancer-related inflammation. Nature. 2008;454(7203):436-44.
32. Banks WA, Kastin AJ, Broadwell RD. Passage of cytokines across the blood-brain barrier. Neuroimmunomodulation. 1995;2(4):241-8.
33. Sonti G, Ilyin SE, Plata-Salamán CR. Anorexia induced by cytokine interactions at pathophysiological concentrations. Am J Physiol. 1996;270(6 Pt 2):R1394-402.
34. Plata-Salamán CR. Anorexia induced by activators of the signal transducer gp 130. Neuroreport. 1996;7(3):841-4.
35. Dinarello CA. The proinflammatory cytokines interleukin-1 and tumor necrosis factor and treatment of the septic shock syndrome. The Journal of infectious diseases. 1991;163(6):1177-84.
36. Turrin NP, Plata-Salamán CR. Cytokine-cytokine interactions and the brain. Brain Res Bull. 2000;51(1):3-9.

37. Carlson CD, Bai Y, Jonakait GM, Hart RP. Interleukin-1 beta increases leukemia inhibitory factor mRNA levels through transient stimulation of transcription rate. Glia. 1996;18(2):141-51.
38. Michaelis KA, Zhu X, Burfeind KG, Krasnow SM, Levasseur PR, Morgan TK, et al. Establishment and characterization of a novel murine model of pancreatic cancer cachexia. J Cachexia Sarcopenia Muscle. 2017;8(5):824-38.
39. Burfeind KG, Zhu X, Levasseur PR, Michaelis KA, Norgard MA, Marks DL. TRIF is a key inflammatory mediator of acute sickness behavior and cancer cachexia. Brain Behav Immun. 2018.
40. Liu X, Nemeth DP, McKim DB, Zhu L, DiSabato DJ, Berdysz O, et al. Cell-Type-Specific Interleukin 1 Receptor 1 Signaling in the Brain Regulates Distinct Neuroimmune Activities. Immunity. 2019.
41. Krasnow SM, Knoll JG, Verghese SC, Levasseur PR, Marks DL. Amplification and propagation of interleukin-1beta signaling by murine brain endothelial and glial cells. Journal of neuroinflammation. 2017;14(1):133.
42. Zhu X, Burfeind KG, Michaelis KA, Braun TP, Olson B, Pelz KR, et al. MyD88 signalling is critical in the development of pancreatic cancer cachexia. Journal of Cachexia, Sarcopenia and Muscle. 2019;0(0).
43. Ruud J, Backhed F, Engblom D, Blomqvist A. Deletion of the gene encoding MyD88 protects from anorexia in a mouse tumor model. Brain, behavior, and immunity. 2010;24(4):554-7.
44. Grossberg AJ, Vichaya EG, Christian DL, Molkentine JM, Vermeer DW, Gross PS, et al. Tumor-Associated Fatigue in Cancer Patients Develops Independently of IL1 Signaling. Cancer research. 2018;78(3):695-705.
45. Prinz M, Priller J. The role of peripheral immune cells in the CNS in steady state and disease. Nat Neurosci. 2017;20(2):136-44.
46. Jatoi A, Dakhil SR, Nguyen PL, Sloan JA, Kugler JW, Rowland KM, Jr., et al. A placebo-controlled double blind trial of etanercept for the cancer anorexia/weight loss syndrome: results from N00C1 from the North Central Cancer Treatment Group. Cancer. 2007;110(6):1396-403.
47. Hill AG, Jacobson L, Gonzalez J, Rounds J, Majzoub JA, Wilmore DW. Chronic central nervous system exposure to interleukin-1 beta causes catabolism in the rat. Am J Physiol. 1996;271(5 Pt 2):R1142-8.
48. Schafers M, Lee DH, Brors D, Yaksh TL, Sorkin LS. Increased sensitivity of injured and adjacent uninjured rat primary sensory neurons to exogenous tumor necrosis factor-alpha after spinal nerve ligation. J Neurosci. 2003;23(7):3028-38.
49. van Riemsdijk IC, Baan CC, Loonen EH, Knoop CJ, Navarro Betonico G, Niesters HG, et al. T cells activate the tumor necrosis factor-alpha system during hemodialysis, resulting in tachyphylaxis. Kidney international. 2001;59(3):883-92.
50. Takahashi N, Brouckaert P, Fiers W. Induction of tolerance allows separation of lethal and antitumor activities of tumor necrosis factor in mice. Cancer Res. 1991;51(9):2366-72.
51. Tsoli M, Moore M, Burg D, Painter A, Taylor R, Lockie SH, et al. Activation of thermogenesis in brown adipose tissue and dysregulated lipid metabolism associated with cancer cachexia in mice. Cancer Res. 2012;72(17):4372-82.

52. Petruzzelli M, Schweiger M, Schreiber R, Campos-Olivas R, Tsoli M, Allen J, et al. A switch from white to brown fat increases energy expenditure in cancer-associated cachexia. Cell Metab. 2014;20(3):433-47.
53. Herman JP, Flak J, Jankord R. Chronic stress plasticity in the hypothalamic paraventricular nucleus. Progress in brain research. 2008;170:353-64.
54. Brooks SL, Neville AM, Rothwell NJ, Stock MJ, Wilson S. Sympathetic activation of brown-adipose-tissue thermogenesis in cachexia. Bioscience reports. 1981;1(6):509-17.
55. Bing C, Brown M, King P, Collins P, Tisdale MJ, Williams G. Increased gene expression of brown fat uncoupling protein (UCP)1 and skeletal muscle UCP2 and UCP3 in MAC16-induced cancer cachexia. Cancer Res. 2000;60(9):2405-10.
56. Hundsberger T, Omlin A, Haegele-Link S, Vehoff J, Strasser F. Autonomic dysfunction in cancer cachexia coincides with large fiber polyneuropathy. Journal of pain and symptom management. 2014;48(4):611-8.e1.
57. Chauhan A, Sequeria A, Manderson C, Maddocks M, Wasley D, Wilcock A. Exploring autonomic nervous system dysfunction in patients with cancer cachexia: a pilot study. Autonomic neuroscience : basic & clinical. 2012;166(1-2):93-5.
58. Wang P, Loh KH, Wu M, Morgan DA, Schneeberger M, Yu X, et al. A leptin-BDNF pathway regulating sympathetic innervation of adipose tissue. Nature. 2020;583(7818):839-44.
59. Jiang Z, Rajamanickam S, Justice NJ. Local Corticotropin-Releasing Factor Signaling in the Hypothalamic Paraventricular Nucleus. J Neurosci. 2018;38(8):1874-90.
60. Kim MS, Yan J, Wu W, Zhang G, Zhang Y, Cai D. Rapid linkage of innate immunological signals to adaptive immunity by the brain-fat axis. Nat Immunol. 2015;16(5):525-33.
61. Stanley S, Pinto S, Segal J, Pérez CA, Viale A, DeFalco J, et al. Identification of neuronal subpopulations that project from hypothalamus to both liver and adipose tissue polysynaptically. Proc Natl Acad Sci U S A. 2010;107(15):7024-9.
62. Habecker BA, Sachs HH, Rohrer H, Zigmond RE. The dependence on gp130 cytokines of axotomy induced neuropeptide expression in adult sympathetic neurons. Developmental neurobiology. 2009;69(6):392-400.
63. Luan HH, Wang A, Hilliard BK, Carvalho F, Rosen CE, Ahasic AM, et al. GDF15 Is an Inflammation-Induced Central Mediator of Tissue Tolerance. Cell. 2019;178(5):1231-44.e11.
64. Lerner L, Hayes TG, Tao N, Krieger B, Feng B, Wu Z, et al. Plasma growth differentiation factor 15 is associated with weight loss and mortality in cancer patients. J Cachexia Sarcopenia Muscle. 2015;6(4):317-24.
65. Lerner L, Tao J, Liu Q, Nicoletti R, Feng B, Krieger B, et al. MAP3K11/GDF15 axis is a critical driver of cancer cachexia. J Cachexia Sarcopenia Muscle. 2016;7(4):467-82.
66. Suriben R, Chen M, Higbee J, Oeffinger J, Ventura R, Li B, et al. Antibody-mediated inhibition of GDF15-GFRAL activity reverses cancer cachexia in mice. Nat Med. 2020;26(8):1264-70.
67. Borner T, Shaulson ED, Ghidewon MY, Barnett AB, Horn CC, Doyle RP, et al. GDF15 Induces Anorexia through Nausea and Emesis. Cell Metab. 2020;31(2):351-62.e5.
68. Mendes MC, Pimentel GD, Costa FO, Carvalheira JB. Molecular and neuroendocrine mechanisms of cancer cachexia. The Journal of endocrinology. 2015;226(3):R29-43.

69. Laviano A, Inui A, Marks DL, Meguid MM, Pichard C, Rossi Fanelli F, et al. Neural control of the anorexia-cachexia syndrome. American journal of physiology Endocrinology and metabolism. 2008;295(5):E1000-8.
70. Burfeind KG, Zhu X, Norgard MA, Levasseur PR, Huisman C, Michaelis KA, et al. Microglia in the hypothalamus respond to tumor-derived factors and are protective against cachexia during pancreatic cancer. Glia. 2020;68(7):1479-94.
71. Braun TP, Grossberg AJ, Krasnow SM, Levasseur PR, Szumowski M, Zhu XX, et al. Cancer- and endotoxin-induced cachexia require intact glucocorticoid signaling in skeletal muscle. Faseb j. 2013;27(9):3572-82.
72. Braun TP, Szumowski M, Levasseur PR, Grossberg AJ, Zhu X, Agarwal A, et al. Muscle atrophy in response to cytotoxic chemotherapy is dependent on intact glucocorticoid signaling in skeletal muscle. PLoS One. 2014;9(9):e106489.
73. Waddell DS, Baehr LM, van den Brandt J, Johnsen SA, Reichardt HM, Furlow JD, et al. The glucocorticoid receptor and FOXO1 synergistically activate the skeletal muscle atrophy-associated MuRF1 gene. Am J Physiol Endocrinol Metab. 2008;295(4):E785-97.
74. Shimizu N, Yoshikawa N, Ito N, Maruyama T, Suzuki Y, Takeda S, et al. Crosstalk between glucocorticoid receptor and nutritional sensor mTOR in skeletal muscle. Cell Metab. 2011;13(2):170-82.
75. Burney BO, Garcia JM. Hypogonadism in male cancer patients. J Cachexia Sarcopenia Muscle. 2012;3(3):149-55.
76. Dev R. The assessment and management of cancer cachexia: hypogonadism and hypermetabolism among supportive and palliative care patients. Curr Opin Support Palliat Care. 2014;8(3):279-85.
77. Garcia JM, Li H, Mann D, Epner D, Hayes TG, Marcelli M, et al. Hypogonadism in male patients with cancer. Cancer. 2006;106(12):2583-91.
78. Rajagopal A, Vassilopoulou-Sellin R, Palmer JL, Kaur G, Bruera E. Symptomatic hypogonadism in male survivors of cancer with chronic exposure to opioids. Cancer. 2004;100(4):851-8.
79. Skipworth RJ, Moses AG, Sangster K, Sturgeon CM, Voss AC, Fallon MT, et al. Interaction of gonadal status with systemic inflammation and opioid use in determining nutritional status and prognosis in advanced pancreatic cancer. Supportive care in cancer : official journal of the Multinational Association of Supportive Care in Cancer. 2011;19(3):391-401.
80. Dev R, Hui D, Del Fabbro E, Delgado-Guay MO, Sobti N, Dalal S, et al. Association between hypogonadism, symptom burden, and survival in male patients with advanced cancer. Cancer. 2014;120(10):1586-93.
81. Biag J, Huang Y, Gou L, Hintiryan H, Askarinam A, Hahn JD, et al. Cyto- and chemoarchitecture of the hypothalamic paraventricular nucleus in the C57BL/6J male mouse: a study of immunostaining and multiple fluorescent tract tracing. J Comp Neurol. 2012;520(1):6-33.
82. Mosialou I, Shikhel S, Liu JM, Maurizi A, Luo N, He Z, et al. MC4R-dependent suppression of appetite by bone-derived lipocalin 2. Nature. 2017;543(7645):385-90.
83. Kjeldsen L, Cowland JB, Borregaard N. Human neutrophil gelatinase-associated lipocalin and homologous proteins in rat and mouse. Biochim Biophys Acta. 2000;1482(1-2):272-83.

84. Moschen AR, Adolph TE, Gerner RR, Wieser V, Tilg H. Lipocalin-2: A Master Mediator of Intestinal and Metabolic Inflammation. Trends Endocrinol Metab. 2017;28(5):388-97.
85. Devireddy LR, Gazin C, Zhu X, Green MR. A cell-surface receptor for lipocalin 24p3 selectively mediates apoptosis and iron uptake. Cell. 2005;123(7):1293-305.
86. Hvidberg V, Jacobsen C, Strong RK, Cowland JB, Moestrup SK, Borregaard N. The endocytic receptor megalin binds the iron transporting neutrophil-gelatinase-associated lipocalin with high affinity and mediates its cellular uptake. FEBS letters. 2005;579(3):773-7.
87. Xu SY, Carlson M, Engström A, Garcia R, Peterson CG, Venge P. Purification and characterization of a human neutrophil lipocalin (HNL) from the secondary granules of human neutrophils. Scand J Clin Lab Invest. 1994;54(5):365-76.
88. Kjeldsen L, Bainton DF, Sengeløv H, Borregaard N. Identification of neutrophil gelatinase-associated lipocalin as a novel matrix protein of specific granules in human neutrophils. Blood. 1994;83(3):799-807.
89. Kjeldsen L, Johnsen AH, Sengeløv H, Borregaard N. Isolation and primary structure of NGAL, a novel protein associated with human neutrophil gelatinase. J Biol Chem. 1993;268(14):10425-32.
90. Yang J, Goetz D, Li JY, Wang W, Mori K, Setlik D, et al. An iron delivery pathway mediated by a lipocalin. Mol Cell. 2002;10(5):1045-56.
91. van Renswoude J, Bridges KR, Harford JB, Klausner RD. Receptor-mediated endocytosis of transferrin and the uptake of fe in K562 cells: identification of a nonlysosomal acidic compartment. Proc Natl Acad Sci U S A. 1982;79(20):6186-90.
92. Yamashiro DJ, Tycko B, Fluss SR, Maxfield FR. Segregation of transferrin to a mildly acidic (pH 6.5) para-Golgi compartment in the recycling pathway. Cell. 1984;37(3):789-800.
93. Yamaguchi-Iwai Y, Stearman R, Dancis A, Klausner RD. Iron-regulated DNA binding by the AFT1 protein controls the iron regulon in yeast. The EMBO journal. 1996;15(13):3377-84.
94. Rouault T, Klausner R. Regulation of iron metabolism in eukaryotes. Curr Top Cell Regul. 1997;35:1-19.
95. Bachman MA, Miller VL, Weiser JN. Mucosal lipocalin 2 has pro-inflammatory and iron-sequestering effects in response to bacterial enterobactin. PLoS Pathog. 2009;5(10):e1000622.
96. Schroll A, Eller K, Feistritzer C, Nairz M, Sonnweber T, Moser PA, et al. Lipocalin-2 ameliorates granulocyte functionality. European journal of immunology. 2012;42(12):3346-57.
97. Flo TH, Smith KD, Sato S, Rodriguez DJ, Holmes MA, Strong RK, et al. Lipocalin 2 mediates an innate immune response to bacterial infection by sequestrating iron. Nature. 2004;432(7019):917-21.
98. Borkham-Kamphorst E, van de Leur E, Zimmermann HW, Karlmark KR, Tihaa L, Haas U, et al. Protective effects of lipocalin-2 (LCN2) in acute liver injury suggest a novel function in liver homeostasis. Biochim Biophys Acta. 2013;1832(5):660-73.
99. Haase M, Bellomo R, Devarajan P, Schlattmann P, Haase-Fielitz A. Accuracy of neutrophil gelatinase-associated lipocalin (NGAL) in diagnosis and prognosis in acute kidney injury: a systematic review and meta-analysis. Am J Kidney Dis. 2009;54(6):1012-24.
100. Verna EC, Brown RS, Farrand E, Pichardo EM, Forster CS, Sola-Del Valle DA, et al. Urinary neutrophil gelatinase-associated lipocalin predicts mortality and identifies acute kidney injury in cirrhosis. Dig Dis Sci. 2012;57(9):2362-70.

101. Grigoryev DN, Cheranova DI, Heruth DP, Huang P, Zhang LQ, Rabb H, et al. Meta-analysis of molecular response of kidney to ischemia reperfusion injury for the identification of new candidate genes. BMC Nephrol. 2013;14:231.
102. Kamińska D, Kościelska-Kasprzak K, Drulis-Fajdasz D, Hałoń A, Polak W, Chudoba P, et al. Kidney ischemic injury genes expressed after donor brain death are predictive for the outcome of kidney transplantation. Transplant Proc. 2011;43(8):2891-4.
103. Rubinstein T, Pitashny M, Putterman C. The novel role of neutrophil gelatinase-B associated lipocalin (NGAL)/Lipocalin-2 as a biomarker for lupus nephritis. Autoimmun Rev. 2008;7(3):229-34.
104. Mishra J, Dent C, Tarabishi R, Mitsnefes MM, Ma Q, Kelly C, et al. Neutrophil gelatinase-associated lipocalin (NGAL) as a biomarker for acute renal injury after cardiac surgery. Lancet. 2005;365(9466):1231-8.
105. Roth GA, Nickl S, Lebherz-Eichinger D, Schmidt EM, Ankersmit HJ, Faybik P, et al. Lipocalin-2 serum levels are increased in acute hepatic failure. Transplant Proc. 2013;45(1):241-4.
106. Ding L, Hanawa H, Ota Y, Hasegawa G, Hao K, Asami F, et al. Lipocalin-2/neutrophil gelatinase-B associated lipocalin is strongly induced in hearts of rats with autoimmune myocarditis and in human myocarditis. Circ J. 2010;74(3):523-30.
107. Leng X, Wu Y, Arlinghaus RB. Relationships of lipocalin 2 with breast tumorigenesis and metastasis. J Cell Physiol. 2011;226(2):309-14.
108. Leung L, Radulovich N, Zhu CQ, Organ S, Bandarchi B, Pintilie M, et al. Lipocalin2 promotes invasion, tumorigenicity and gemcitabine resistance in pancreatic ductal adenocarcinoma. PLoS One. 2012;7(10):e46677.
109. Lin CW, Tseng SW, Yang SF, Ko CP, Lin CH, Wei LH, et al. Role of lipocalin 2 and its complex with matrix metalloproteinase-9 in oral cancer. Oral Dis. 2012;18(8):734-40.
110. Martí J, Fuster J, Solà AM, Hotter G, Molina R, Pelegrina A, et al. Prognostic value of serum neutrophil gelatinase-associated lipocalin in metastatic and nonmetastatic colorectal cancer. World J Surg. 2013;37(5):1103-9.
111. Hamzic N, Blomqvist A, Nilsberth C. Immune-induced expression of lipocalin-2 in brain endothelial cells: relationship with interleukin-6, cyclooxygenase-2 and the febrile response. J Neuroendocrinol. 2013;25(3):271-80.
112. Bi F, Huang C, Tong J, Qiu G, Huang B, Wu Q, et al. Reactive astrocytes secrete lcn2 to promote neuron death. Proc Natl Acad Sci U S A. 2013;110(10):4069-74.
113. Lee S, Lee J, Kim S, Park JY, Lee WH, Mori K, et al. A dual role of lipocalin 2 in the apoptosis and deramification of activated microglia. J Immunol. 2007;179(5):3231-41.
114. Naudé PJ, Nyakas C, Eiden LE, Ait-Ali D, van der Heide R, Engelborghs S, et al. Lipocalin 2: novel component of proinflammatory signaling in Alzheimer's disease. Faseb j. 2012;26(7):2811-23.
115. Berard JL, Zarruk JG, Arbour N, Prat A, Yong VW, Jacques FH, et al. Lipocalin 2 is a novel immune mediator of experimental autoimmune encephalomyelitis pathogenesis and is modulated in multiple sclerosis. Glia. 2012;60(7):1145-59.
116. Nam Y, Kim JH, Seo M, Kim JH, Jin M, Jeon S, et al. Lipocalin-2 protein deficiency ameliorates experimental autoimmune encephalomyelitis: the pathogenic role of lipocalin-2 in

the central nervous system and peripheral lymphoid tissues. J Biol Chem. 2014;289(24):16773-89.
117. Howe CL, Kaptzan T, Magaña SM, Ayers-Ringler JR, LaFrance-Corey RG, Lucchinetti CF. Neuromyelitis optica IgG stimulates an immunological response in rat astrocyte cultures. Glia. 2014;62(5):692-708.
118. Chang CF, Cho S, Wang J. (-)-Epicatechin protects hemorrhagic brain via synergistic Nrf2 pathways. Ann Clin Transl Neurol. 2014;1(4):258-71.
119. Jin M, Kim JH, Jang E, Lee YM, Soo Han H, Woo DK, et al. Lipocalin-2 deficiency attenuates neuroinflammation and brain injury after transient middle cerebral artery occlusion in mice. J Cereb Blood Flow Metab. 2014;34(8):1306-14.
120. Lipina TV, Haque FN, McGirr A, Boutros PC, Berger T, Mak TW, et al. Prophylactic valproic acid treatment prevents schizophrenia-related behaviour in Disc1-L100P mutant mice. PLoS One. 2012;7(12):e51562.
121. Rathore KI, Berard JL, Redensek A, Chierzi S, Lopez-Vales R, Santos M, et al. Lipocalin 2 plays an immunomodulatory role and has detrimental effects after spinal cord injury. The Journal of neuroscience : the official journal of the Society for Neuroscience. 2011;31(38):13412-9.
122. Llorens F, Hermann P, Villar-Piqué A, Diaz-Lucena D, Nägga K, Hansson O, et al. Cerebrospinal fluid lipocalin 2 as a novel biomarker for the differential diagnosis of vascular dementia. Nat Commun. 2020;11(1):619.
123. Wu G, Li H, Fang Q, Jiang S, Zhang L, Zhang J, et al. Elevated circulating lipocalin-2 levels independently predict incident cardiovascular events in men in a population-based cohort. Arteriosclerosis, thrombosis, and vascular biology. 2014;34(11):2457-64.
124. Wang Q, Li S, Tang X, Liang L, Wang F, Du H. Lipocalin 2 Protects Against Escherichia coli Infection by Modulating Neutrophil and Macrophage Function. Front Immunol. 2019;10:2594.
125. Nairz M, Schroll A, Haschka D, Dichtl S, Sonnweber T, Theurl I, et al. Lipocalin-2 ensures host defense against Salmonella Typhimurium by controlling macrophage iron homeostasis and immune response. Eur J Immunol. 2015;45(11):3073-86.
126. Lee S, Kim JH, Kim JH, Seo JW, Han HS, Lee WH, et al. Lipocalin-2 Is a chemokine inducer in the central nervous system: role of chemokine ligand 10 (CXCL10) in lipocalin-2-induced cell migration. J Biol Chem. 2011;286(51):43855-70.
127. Kang SS, Ren Y, Liu CC, Kurti A, Baker KE, Bu G, et al. Lipocalin-2 protects the brain during inflammatory conditions. Molecular psychiatry. 2018;23(2):344-50.
128. Yahiro K, Ogura K, Goto Y, Iyoda S, Kobayashi T, Takeuchi H, et al. Subtilase cytotoxin induces a novel form of Lipocalin 2, which promotes Shiga-toxigenic Escherichia coli survival. Sci Rep. 2020;10(1):18943.
129. Ip JP, Noçon AL, Hofer MJ, Lim SL, Müller M, Campbell IL. Lipocalin 2 in the central nervous system host response to systemic lipopolysaccharide administration. J Neuroinflammation. 2011;8:124.
130. Schneider DS, Ayres JS. Two ways to survive infection: what resistance and tolerance can teach us about treating infectious diseases. Nature reviews Immunology. 2008;8(11):889-95.
131. Ferrandon D. Host tolerance versus resistance and microbial virulence in the host-pathogen equation. Cell Host Microbe. 2009;6(3):203-5.

132. Guo H, Jin D, Chen X. Lipocalin 2 is a regulator of macrophage polarization and NF-κB/STAT3 pathway activation. Mol Endocrinol. 2014;28(10):1616-28.
133. Zhang J, Wu Y, Zhang Y, Leroith D, Bernlohr DA, Chen X. The role of lipocalin 2 in the regulation of inflammation in adipocytes and macrophages. Mol Endocrinol. 2008;22(6):1416-26.
134. Jin M, Jang E, Suk K. Lipocalin-2 Acts as a Neuroinflammatogen in Lipopolysaccharide-injected Mice. Exp Neurobiol. 2014;23(2):155-62.
135. Jeon S, Jha MK, Ock J, Seo J, Jin M, Cho H, et al. Role of lipocalin-2-chemokine axis in the development of neuropathic pain following peripheral nerve injury. J Biol Chem. 2013;288(33):24116-27.
136. Jha MK, Jeon S, Jin M, Lee WH, Suk K. Acute Phase Protein Lipocalin-2 Is Associated with Formalin-induced Nociception and Pathological Pain. Immune Netw. 2013;13(6):289-94.
137. Chun BY, Kim JH, Nam Y, Huh MI, Han S, Suk K. Pathological Involvement of Astrocyte-Derived Lipocalin-2 in the Demyelinating Optic Neuritis. Invest Ophthalmol Vis Sci. 2015;56(6):3691-8.
138. Kim BW, Jeong KH, Kim JH, Jin M, Kim JH, Lee MG, et al. Pathogenic Upregulation of Glial Lipocalin-2 in the Parkinsonian Dopaminergic System. J Neurosci. 2016;36(20):5608-22.
139. Kim JH, Ko PW, Lee HW, Jeong JY, Lee MG, Kim JH, et al. Astrocyte-derived lipocalin-2 mediates hippocampal damage and cognitive deficits in experimental models of vascular dementia. Glia. 2017;65(9):1471-90.
140. Bhusal A, Rahman MH, Lee IK, Suk K. Role of Hippocampal Lipocalin-2 in Experimental Diabetic Encephalopathy. Front Endocrinol (Lausanne). 2019;10:25.
141. Bhusal A, Rahman MH, Lee WH, Lee IK, Suk K. Satellite glia as a critical component of diabetic neuropathy: Role of lipocalin-2 and pyruvate dehydrogenase kinase-2 axis in the dorsal root ganglion. Glia. 2021;69(4):971-96.
142. Shin HJ, Jeong EA, Lee JY, An HS, Jang HM, Ahn YJ, et al. Lipocalin-2 Deficiency Reduces Oxidative Stress and Neuroinflammation and Results in Attenuation of Kainic Acid-Induced Hippocampal Cell Death. Antioxidants (Basel). 2021;10(1).
143. Zhang J, Novakovic N, Hua Y, Keep RF, Xi G. Role of lipocalin-2 in extracellular peroxiredoxin 2-induced brain swelling, inflammation and neuronal death. Exp Neurol. 2021;335:113521.
144. Shao S, Cao T, Jin L, Li B, Fang H, Zhang J, et al. Increased Lipocalin-2 Contributes to the Pathogenesis of Psoriasis by Modulating Neutrophil Chemotaxis and Cytokine Secretion. J Invest Dermatol. 2016;136(7):1418-28.
145. Hau CS, Kanda N, Tada Y, Shibata S, Uozaki H, Fukusato T, et al. Lipocalin-2 exacerbates psoriasiform skin inflammation by augmenting T-helper 17 response. J Dermatol. 2016;43(7):785-94.
146. Ye D, Yang K, Zang S, Lin Z, Chau HT, Wang Y, et al. Lipocalin-2 mediates non-alcoholic steatohepatitis by promoting neutrophil-macrophage crosstalk via the induction of CXCR2. J Hepatol. 2016;65(5):988-97.
147. Wieser V, Tymoszuk P, Adolph TE, Grander C, Grabherr F, Enrich B, et al. Lipocalin 2 drives neutrophilic inflammation in alcoholic liver disease. Journal of hepatology. 2016;64(4):872-80.

148. Oberoi R, Bogalle EP, Matthes LA, Schuett H, Koch AK, Grote K, et al. Lipocalin (LCN) 2 Mediates Pro-Atherosclerotic Processes and Is Elevated in Patients with Coronary Artery Disease. PLoS One. 2015;10(9):e0137924.
149. Lin Y, Rajala MW, Berger JP, Moller DE, Barzilai N, Scherer PE. Hyperglycemia-induced production of acute phase reactants in adipose tissue. J Biol Chem. 2001;276(45):42077-83.
150. Yan QW, Yang Q, Mody N, Graham TE, Hsu CH, Xu Z, et al. The adipokine lipocalin 2 is regulated by obesity and promotes insulin resistance. Diabetes. 2007;56(10):2533-40.
151. Wang Y, Lam KS, Kraegen EW, Sweeney G, Zhang J, Tso AW, et al. Lipocalin-2 is an inflammatory marker closely associated with obesity, insulin resistance, and hyperglycemia in humans. Clin Chem. 2007;53(1):34-41.
152. Auguet T, Quintero Y, Terra X, Martínez S, Lucas A, Pellitero S, et al. Upregulation of lipocalin 2 in adipose tissues of severely obese women: positive relationship with proinflammatory cytokines. Obesity (Silver Spring). 2011;19(12):2295-300.
153. Zhang Y, Foncea R, Deis JA, Guo H, Bernlohr DA, Chen X. Lipocalin 2 expression and secretion is highly regulated by metabolic stress, cytokines, and nutrients in adipocytes. PLoS One. 2014;9(5):e96997.
154. Zhang Y, Guo H, Deis JA, Mashek MG, Zhao M, Ariyakumar D, et al. Lipocalin 2 regulates brown fat activation via a nonadrenergic activation mechanism. J Biol Chem. 2014;289(32):22063-77.
155. Meyers K, López M, Ho J, Wills S, Rayalam S, Taval S. Lipocalin-2 deficiency may predispose to the progression of spontaneous age-related adiposity in mice. Sci Rep. 2020;10(1):14589.
156. Mosialou I, Shikhel S, Luo N, Petropoulou PI, Panitsas K, Bisikirska B, et al. Lipocalin-2 counteracts metabolic dysregulation in obesity and diabetes. The Journal of experimental medicine. 2020;217(10).
157. Devireddy LR, Teodoro JG, Richard FA, Green MR. Induction of apoptosis by a secreted lipocalin that is transcriptionally regulated by IL-3 deprivation. Science (New York, NY). 2001;293(5531):829-34.
158. Boise LH, González-García M, Postema CE, Ding L, Lindsten T, Turka LA, et al. bcl-x, a bcl-2-related gene that functions as a dominant regulator of apoptotic cell death. Cell. 1993;74(4):597-608.
159. Richardson DR. 24p3 and its receptor: dawn of a new iron age? Cell. 2005;123(7):1175-7.
160. Wen X, Su B, Gao M, Chen J, Zhou D, You H, et al. Obesity-associated up-regulation of lipocalin 2 protects gastric mucosa cells from apoptotic cell death by reducing endoplasmic reticulum stress. Cell Death Dis. 2021;12(2):221.
161. Song E, Ramos SV, Huang X, Liu Y, Botta A, Sung HK, et al. Holo-lipocalin-2-derived siderophores increase mitochondrial ROS and impair oxidative phosphorylation in rat cardiomyocytes. Proc Natl Acad Sci U S A. 2018;115(7):1576-81.
162. Mackenzie IR, Neumann M, Baborie A, Sampathu DM, Du Plessis D, Jaros E, et al. A harmonized classification system for FTLD-TDP pathology. Acta Neuropathol. 2011;122(1):111-3.
163. Chen X, Qiu F, Zhao X, Lu J, Tan X, Xu J, et al. Astrocyte-Derived Lipocalin-2 Is Involved in Mitochondrion-Related Neuronal Apoptosis Induced by Methamphetamine. ACS Chem Neurosci. 2020;11(8):1102-16.

164. Liu J, Song X, Kuang F, Zhang Q, Xie Y, Kang R, et al. NUPR1 is a critical repressor of ferroptosis. Nat Commun. 2021;12(1):647.
165. Olson B, Marks DL. Pretreatment Cancer-Related Cognitive Impairment-Mechanisms and Outlook. Cancers (Basel). 2019;11(5).
166. Mueller TC, Bachmann J, Prokopchuk O, Friess H, Martignoni ME. Molecular pathways leading to loss of skeletal muscle mass in cancer cachexia--can findings from animal models be translated to humans? BMC cancer. 2016;16:75.
167. Morley JE, von Haehling S, Anker SD. Are we closer to having drugs to treat muscle wasting disease? J Cachexia Sarcopenia Muscle. 2014;5(2):83-7.
168. Le-Rademacher JG, Crawford J, Evans WJ, Jatoi A. Overcoming obstacles in the design of cancer anorexia/weight loss trials. Critical reviews in oncology/hematology. 2017;117:30-7.
169. Baracos VE. Clinical trials of cancer cachexia therapy, now and hereafter. Journal of clinical oncology : official journal of the American Society of Clinical Oncology. 2013;31(10):1257-8.
170. Penna F, Busquets S, Argilés JM. Experimental cancer cachexia: Evolving strategies for getting closer to the human scenario. Seminars in cell & developmental biology. 2016;54:20-7.
171. Cahill GF, Jr. Starvation in man. N Engl J Med. 1970;282(12):668-75.
172. Cahill GF, Jr. Fuel metabolism in starvation. Annual review of nutrition. 2006;26:1-22.
173. Heilbronn LK, Ravussin E. Calorie restriction and aging: review of the literature and implications for studies in humans. The American journal of clinical nutrition. 2003;78(3):361-9.
174. Lowell BB. New Neuroscience of Homeostasis and Drives for Food, Water, and Salt. N Engl J Med. 2019;380(5):459-71.
175. Edholm OG. Energy balance in man studies carried out by the Division of Human Physiology, National Institute for Medical Research. Journal of human nutrition. 1977;31(6):413-31.
176. Schwartz MW, Woods SC, Porte D, Jr., Seeley RJ, Baskin DG. Central nervous system control of food intake. Nature. 2000;404(6778):661-71.
177. Lowell BB, Goodman MN. Protein sparing in skeletal muscle during prolonged starvation. Dependence on lipid fuel availability. Diabetes. 1987;36(1):14-9.
178. Rennie MJ, Harrison R. Effects of injury, disease, and malnutrition on protein metabolism in man. Unanswered questions. Lancet (London, England). 1984;1(8372):323-5.
179. Murphy KG, Bloom SR. Gut hormones and the regulation of energy homeostasis. Nature. 2006;444(7121):854-9.
180. Kojima M, Kangawa K. Ghrelin: structure and function. Physiological reviews. 2005;85(2):495-522.
181. Nakazato M, Murakami N, Date Y, Kojima M, Matsuo H, Kangawa K, et al. A role for ghrelin in the central regulation of feeding. Nature. 2001;409(6817):194-8.
182. Cowley MA, Smith RG, Diano S, Tschop M, Pronchuk N, Grove KL, et al. The distribution and mechanism of action of ghrelin in the CNS demonstrates a novel hypothalamic circuit regulating energy homeostasis. Neuron. 2003;37(4):649-61.
183. Chen SR, Chen H, Zhou JJ, Pradhan G, Sun Y, Pan HL, et al. Ghrelin receptors mediate ghrelin-induced excitation of agouti-related protein/neuropeptide Y but not pro-opiomelanocortin neurons. J Neurochem. 2017;142(4):512-20.

184. Broberger C, Johansen J, Johansson C, Schalling M, Hokfelt T. The neuropeptide Y/agouti gene-related protein (AGRP) brain circuitry in normal, anorectic, and monosodium glutamate-treated mice. Proc Natl Acad Sci U S A. 1998;95(25):15043-8.
185. Chan JL, Heist K, DePaoli AM, Veldhuis JD, Mantzoros CS. The role of falling leptin levels in the neuroendocrine and metabolic adaptation to short-term starvation in healthy men. The Journal of clinical investigation. 2003;111(9):1409-21.
186. Pan WW, Myers MG. Leptin and the maintenance of elevated body weight. Nature Reviews Neuroscience. 2018;19(2):95-105.
187. Flak JN, Myers MG, Jr. Minireview: CNS Mechanisms of Leptin Action. Mol Endocrinol. 2016;30(1):3-12.
188. Fan W, Ellacott KL, Halatchev IG, Takahashi K, Yu P, Cone RD. Cholecystokinin-mediated suppression of feeding involves the brainstem melanocortin system. Nat Neurosci. 2004;7(4):335-6.
189. Turton MD, O'Shea D, Gunn I, Beak SA, Edwards CM, Meeran K, et al. A role for glucagon-like peptide-1 in the central regulation of feeding. Nature. 1996;379(6560):69-72.
190. Meeran K, O'Shea D, Edwards CM, Turton MD, Heath MM, Gunn I, et al. Repeated intracerebroventricular administration of glucagon-like peptide-1-(7-36) amide or exendin-(9-39) alters body weight in the rat. Endocrinology. 1999;140(1):244-50.
191. Halatchev IG, Cone RD. Peripheral administration of PYY(3-36) produces conditioned taste aversion in mice. Cell metabolism. 2005;1(3):159-68.
192. Batterham RL, Heffron H, Kapoor S, Chivers JE, Chandarana K, Herzog H, et al. Critical role for peptide YY in protein-mediated satiation and body-weight regulation. Cell metabolism. 2006;4(3):223-33.
193. Makimura H, Mizuno TM, Roberts J, Silverstein J, Beasley J, Mobbs CV. Adrenalectomy reverses obese phenotype and restores hypothalamic melanocortin tone in leptin-deficient ob/ob mice. Diabetes. 2000;49(11):1917-23.
194. Drazen DL, Wortman MD, Schwartz MW, Clegg DJ, van Dijk G, Woods SC, et al. Adrenalectomy alters the sensitivity of the central nervous system melanocortin system. Diabetes. 2003;52(12):2928-34.
195. Obici S, Feng Z, Karkanias G, Baskin DG, Rossetti L. Decreasing hypothalamic insulin receptors causes hyperphagia and insulin resistance in rats. Nat Neurosci. 2002;5(6):566-72.
196. Plum L, Ma X, Hampel B, Balthasar N, Coppari R, Münzberg H, et al. Enhanced PIP3 signaling in POMC neurons causes KATP channel activation and leads to diet-sensitive obesity. The Journal of clinical investigation. 2006;116(7):1886-901.
197. Brunstrom JM, Cheon BK. Do humans still forage in an obesogenic environment? Mechanisms and implications for weight maintenance. Physiology & behavior. 2018;193(Pt B):261-7.
198. Schuppli C, Graber SM, Isler K, van Schaik CP. Life history, cognition and the evolution of complex foraging niches. Journal of human evolution. 2016;92:91-100.
199. Ross CT, Winterhalder B. Sit-and-wait versus active-search hunting: A behavioral ecological model of optimal search mode. Journal of theoretical biology. 2015;387:76-87.
200. Miller JR, Ament JM, Schmitz OJ. Fear on the move: predator hunting mode predicts variation in prey mortality and plasticity in prey spatial response. The Journal of animal ecology. 2014;83(1):214-22.

201. Mistlberger RE. Neurobiology of food anticipatory circadian rhythms. Physiology & behavior. 2011;104(4):535-45.
202. Pirke KM, Broocks A, Wilckens T, Marquard R, Schweiger U. Starvation-induced hyperactivity in the rat: the role of endocrine and neurotransmitter changes. Neurosci Biobehav Rev. 1993;17(3):287-94.
203. Dietrich MO, Zimmer MR, Bober J, Horvath TL. Hypothalamic Agrp neurons drive stereotypic behaviors beyond feeding. Cell. 2015;160(6):1222-32.
204. Horvath TL, Diano S, van den Pol AN. Synaptic interaction between hypocretin (orexin) and neuropeptide Y cells in the rodent and primate hypothalamus: a novel circuit implicated in metabolic and endocrine regulations. J Neurosci. 1999;19(3):1072-87.
205. Horvath TL, Peyron C, Diano S, Ivanov A, Aston-Jones G, Kilduff TS, et al. Hypocretin (orexin) activation and synaptic innervation of the locus coeruleus noradrenergic system. The Journal of comparative neurology. 1999;415(2):145-59.
206. Choi JS, Kim JJ. Amygdala regulates risk of predation in rats foraging in a dynamic fear environment. Proc Natl Acad Sci U S A. 2010;107(50):21773-7.
207. Sclafani A, Rendel A. Food deprivation-induced activity in normal and hypothalamic obese rats. Behav Biol. 1978;22(2):244-55.
208. Jakubczak LF. Age differences in the effects of terminal food deprivation (starvation) on activity, weight loss, and survival of rats. J Gerontol. 1967;22(4):421-6.
209. Goodman MN, Larsen PR, Kaplan MM, Aoki TT, Young VR, Ruderman NB. Starvation in the rat. II. Effect of age and obesity on protein sparing and fuel metabolism. Am J Physiol. 1980;239(4):E277-e86.
210. Koubi HE, Robin JP, Dewasmes G, Le Maho Y, Frutoso J, Minaire Y. Fasting-induced rise in locomotor activity in rats coincides with increased protein utilization. Physiology & behavior. 1991;50(2):337-43.
211. Robin JP, Boucontet L, Chillet P, Groscolas R. Behavioral changes in fasting emperor penguins: evidence for a "refeeding signal" linked to a metabolic shift. Am J Physiol. 1998;274(3):R746-53.
212. Ferretti A, Maggini I, Lupi S, Cardinale M, Fusani L. The amount of available food affects diurnal locomotor activity in migratory songbirds during stopover. Sci Rep. 2019;9(1):19027.
213. Dulloo AG. Explaining the failures of obesity therapy: willpower attenuation, target miscalculation or metabolic compensation? International journal of obesity (2005). 2012;36(11):1418-20.
214. Kleitman N. BASAL METABOLISM IN PROLONGED FASTING IN MAN. American Journal of Physiology-Legacy Content. 1926;77(1):233-44.
215. Keys A, Brožek J, Henschel A, Mickelsen O, Taylor HL. The biology of human starvation. (2 vols). Oxford, England: Univ. of Minnesota Press; 1950. xxxii, 1385-xxxii, p.
216. Overton JM, Williams TD, Chambers JB, Rashotte ME. Cardiovascular and metabolic responses to fasting and thermoneutrality are conserved in obese Zucker rats. American journal of physiology Regulatory, integrative and comparative physiology. 2001;280(4):R1007-15.
217. Tanner JM, Kearns DT, Kim BJ, Sloan C, Jia Z, Yang T, et al. Fasting-induced reductions in cardiovascular and metabolic variables occur sooner in obese versus lean mice. Exp Biol Med (Maywood). 2010;235(12):1489-97.

218. Rosenbaum M, Hirsch J, Gallagher DA, Leibel RL. Long-term persistence of adaptive thermogenesis in subjects who have maintained a reduced body weight. The American journal of clinical nutrition. 2008;88(4):906-12.
219. Young JB, Landsberg L. Catecholamines and intermediary metabolism. Clin Endocrinol Metab. 1977;6(3):599-631.
220. Landsberg L, Young JB. Fasting, feeding and regulation of the sympathetic nervous system. N Engl J Med. 1978;298(23):1295-301.
221. Einhorn D, Young JB, Landberg L. Hypotensive effect of fasting: possible involvement of the sympathetic nervous system and endogenous opiates. Science (New York, NY). 1982;217(4561):727-9.
222. Swoap SJ. Altered leptin signaling is sufficient, but not required, for hypotension associated with caloric restriction. Am J Physiol Heart Circ Physiol. 2001;281(6):H2473-9.
223. Young JB, Landsberg L. Suppression of sympathetic nervous system during fasting. Science (New York, NY). 1977;196(4297):1473-5.
224. Cypess AM, Weiner LS, Roberts-Toler C, Franquet Elía E, Kessler SH, Kahn PA, et al. Activation of human brown adipose tissue by a β3-adrenergic receptor agonist. Cell metabolism. 2015;21(1):33-8.
225. Oelkrug R, Polymeropoulos ET, Jastroch M. Brown adipose tissue: physiological function and evolutionary significance. Journal of comparative physiology B, Biochemical, systemic, and environmental physiology. 2015;185(6):587-606.
226. Bartelt A, Bruns OT, Reimer R, Hohenberg H, Ittrich H, Peldschus K, et al. Brown adipose tissue activity controls triglyceride clearance. Nat Med. 2011;17(2):200-5.
227. van Marken Lichtenbelt WD, Vanhommerig JW, Smulders NM, Drossaerts JM, Kemerink GJ, Bouvy ND, et al. Cold-activated brown adipose tissue in healthy men. N Engl J Med. 2009;360(15):1500-8.
228. Cypess AM, Lehman S, Williams G, Tal I, Rodman D, Goldfine AB, et al. Identification and importance of brown adipose tissue in adult humans. N Engl J Med. 2009;360(15):1509-17.
229. Virtanen KA, Lidell ME, Orava J, Heglind M, Westergren R, Niemi T, et al. Functional brown adipose tissue in healthy adults. N Engl J Med. 2009;360(15):1518-25.
230. Saito M, Okamatsu-Ogura Y, Matsushita M, Watanabe K, Yoneshiro T, Nio-Kobayashi J, et al. High incidence of metabolically active brown adipose tissue in healthy adult humans: effects of cold exposure and adiposity. Diabetes. 2009;58(7):1526-31.
231. Zingaretti MC, Crosta F, Vitali A, Guerrieri M, Frontini A, Cannon B, et al. The presence of UCP1 demonstrates that metabolically active adipose tissue in the neck of adult humans truly represents brown adipose tissue. Faseb j. 2009;23(9):3113-20.
232. Puchalska P, Crawford PA. Multi-dimensional Roles of Ketone Bodies in Fuel Metabolism, Signaling, and Therapeutics. Cell metabolism. 2017;25(2):262-84.
233. Rothman DL, Magnusson I, Katz LD, Shulman RG, Shulman GI. Quantitation of hepatic glycogenolysis and gluconeogenesis in fasting humans with 13C NMR. Science (New York, NY). 1991;254(5031):573-6.
234. Felig P, Owen OE, Wahren J, Cahill GF, Jr. Amino acid metabolism during prolonged starvation. The Journal of clinical investigation. 1969;48(3):584-94.
235. Owen OE, Felig P, Morgan AP, Wahren J, Cahill GF, Jr. Liver and kidney metabolism during prolonged starvation. The Journal of clinical investigation. 1969;48(3):574-83.

236. Berg JM, Tymoczko JL, Stryer L. Food Intake and Starvation Induce Metabolic Changes. Biochemistry. 5th ed. New York: W H Freeman; 2002.
237. Garber AJ, Menzel PH, Boden G, Owen OE. Hepatic ketogenesis and gluconeogenesis in humans. The Journal of clinical investigation. 1974;54(4):981-9.
238. Henry CJ. Body mass index and the limits of human survival. European journal of clinical nutrition. 1990;44(4):329-35.
239. Wang T, Hung CC, Randall DJ. The comparative physiology of food deprivation: from feast to famine. Annual review of physiology. 2006;68:223-51.
240. Gahete MD, Córdoba-Chacón J, Luque RM, Kineman RD. The rise in growth hormone during starvation does not serve to maintain glucose levels or lean mass but is required for appropriate adipose tissue response in female mice. Endocrinology. 2013;154(1):263-9.
241. Marks V, Howorth N, Greenwood FC. Plasma Growth-hormone Levels in Chronic Starvation in Man. Nature. 1965;208(5011):686-7.
242. Duclos M, Corcuff JB, Roger P, Tabarin A. The dexamethasone-suppressed corticotrophin-releasing hormone stimulation test in anorexia nervosa. Clinical endocrinology. 1999;51(6):725-31.
243. Jaya Rao KS, Srikantia SG, Gopalan C. Plasma cortisol levels in protein-calorie malnutrition. Archives of disease in childhood. 1968;43(229):365-7.
244. Bajaj JS, Khardori R, Deo MG, Bansal DD. Adrenocortical function in experimental protein malnutrition. Metabolism: clinical and experimental. 1979;28(5):594-8.
245. Drott C, Svaninger G, Lundholm K. Increased urinary excretion of cortisol and catecholami-NES in malnourished cancer patients. Annals of surgery. 1988;208(5):645-50.
246. Lei J, Nowbar S, Mariash CN, Ingbar DH. Thyroid hormone stimulates Na-K-ATPase activity and its plasma membrane insertion in rat alveolar epithelial cells. Am J Physiol Lung Cell Mol Physiol. 2003;285(3):L762-72.
247. Williams LT, Lefkowitz RJ, Watanabe AM, Hathaway DR, Besch HR, Jr. Thyroid hormone regulation of beta-adrenergic receptor number. J Biol Chem. 1977;252(8):2787-9.
248. Croxson MS, Ibbertson HK. Low serum triiodothyronine (T3) and hypothyroidism in anorexia nervosa. The Journal of clinical endocrinology and metabolism. 1977;44(1):167-74.
249. Turkay S, Kus S, Gokalp A, Baskin E, Onal A. Effects of protein energy malnutrition on circulating thyroid hormones. Indian pediatrics. 1995;32(2):193-7.
250. Tancini G, Barni S, Crispino S, Paolorossi F, Lissoni P. A study of thyroid function in cancer cachexia. Tumori. 1989;75(2):185-8.
251. Kawane T, Saikatsu S, Akeno N, Abe M, Horiuchi N. Starvation-induced increase in the parathyroid hormone/PTH-related protein receptor mRNA of bone and kidney in sham-operated and thyroparathyroidectomized rats. European journal of endocrinology. 1997;137(3):273-80.
252. Kerstetter JE, Svastisalee CM, Caseria DM, Mitnick ME, Insogna KL. A threshold for low-protein-diet-induced elevations in parathyroid hormone. The American journal of clinical nutrition. 2000;72(1):168-73.
253. Kir S, Komaba H, Garcia AP, Economopoulos KP, Liu W, Lanske B, et al. PTH/PTHrP Receptor Mediates Cachexia in Models of Kidney Failure and Cancer. Cell metabolism. 2016;23(2):315-23.

254. Kir S, White JP, Kleiner S, Kazak L, Cohen P, Baracos VE, et al. Tumour-derived PTH-related protein triggers adipose tissue browning and cancer cachexia. Nature. 2014;513(7516):100-4.
255. Garnett ES, Cohen H, Nahmias C, Viol G. The roles of carbohydrate, renin, and aldosterone in sodium retention during and after total starvation. Metabolism: clinical and experimental. 1973;22(7):867-74.
256. Ljutić D, Raos V, Biocić M. Aldosterone and blood pressure in obese subjects during short-term starvation. Acta medica Croatica : casopis Hravatske akademije medicinskih znanosti. 1995;49(4-5):165-8.
257. Aldosterone secretion in infantile malnutrition. Nutrition reviews. 1974;32(10):296-8.
258. Anker SD, Sharma R. The syndrome of cardiac cachexia. International journal of cardiology. 2002;85(1):51-66.
259. Anker SD, Chua TP, Ponikowski P, Harrington D, Swan JW, Kox WJ, et al. Hormonal changes and catabolic/anabolic imbalance in chronic heart failure and their importance for cardiac cachexia. Circulation. 1997;96(2):526-34.
260. Zauner C, Schneeweiss B, Kranz A, Madl C, Ratheiser K, Kramer L, et al. Resting energy expenditure in short-term starvation is increased as a result of an increase in serum norepinephrine. The American journal of clinical nutrition. 2000;71(6):1511-5.
261. Gotoh M, Iguchi A, Tajima T, Ikari H, Hirooka Y. Starvation reduces norepinephrine activities in both hypothalamus and heart in rats. Brain research. 1996;706(2):351-4.
262. Petry CJ, Dorling MW, Wang CL, Pawlak DB, Ozanne SE. Catecholamine levels and receptor expression in low protein rat offspring. Diabetic medicine : a journal of the British Diabetic Association. 2000;17(12):848-53.
263. Günöz H, Neyzł O, Sencer E, Molvalilar S, Argun A. Growth hormone secretion in protein energy malnutrition. Acta paediatrica Scandinavica. 1981;70(4):521-6.
264. Svaninger G, Isaksson O, Lundholm K. Growth hormone and experimental cancer cachexia. Journal of the National Cancer Institute. 1987;79(6):1359-65.
265. Buchanan KD, Vance JE, Williams RH. Effect of starvation on insulin and glucagon release from isolated islets of Langerhans of the rat. Metabolism: clinical and experimental. 1969;18(2):155-62.
266. Das BK, Ramesh J, Agarwal JK, Mishra OP, Bhatt RP. Blood sugar and serum insulin response in protein-energy malnutrition. Journal of tropical pediatrics. 1998;44(3):139-41.
267. Bennegård K, Lundgren F, Lundholm K. Mechanisms of insulin resistance in cancer associated malnutrition. Clinical physiology (Oxford, England). 1986;6(6):539-47.
268. Edén E, Edström S, Bennegård K, Scherstén T, Lundholm K. Glucose flux in relation to energy expenditure in malnourished patients with and without cancer during periods of fasting and feeding. Cancer Res. 1984;44(4):1718-24.
269. Rofe AM, Bourgeois CS, Coyle P, Taylor A, Abdi EA. Altered insulin response to glucose in weight-losing cancer patients. Anticancer research. 1994;14(2b):647-50.
270. Rahmani J, Kord Varkaneh H, Clark C, Zand H, Bawadi H, Ryan PM, et al. The influence of fasting and energy restricting diets on IGF-1 levels in humans: A systematic review and meta-analysis. Ageing research reviews. 2019;53:100910.
271. Ammann P, Zacchetti G, Gasser JA, Lavet C, Rizzoli R. Protein malnutrition attenuates bone anabolic response to PTH in female rats. Endocrinology. 2015;156(2):419-28.

272. Costelli P, Muscaritoli M, Bossola M, Penna F, Reffo P, Bonetto A, et al. IGF-1 is downregulated in experimental cancer cachexia. American journal of physiology Regulatory, integrative and comparative physiology. 2006;291(3):R674-83.
273. Fontana L, Partridge L. Promoting health and longevity through diet: from model organisms to humans. Cell. 2015;161(1):106-18.
274. Laeger T, Henagan TM, Albarado DC, Redman LM, Bray GA, Noland RC, et al. FGF21 is an endocrine signal of protein restriction. The Journal of clinical investigation. 2014;124(9):3913-22.
275. Morrison CD, Xi X, White CL, Ye J, Martin RJ. Amino acids inhibit Agrp gene expression via an mTOR-dependent mechanism. American journal of physiology Endocrinology and metabolism. 2007;293(1):E165-71.
276. White BD, Porter MH, Martin RJ. Effects of age on the feeding response to moderately low dietary protein in rats. Physiology & behavior. 2000;68(5):673-81.
277. Zhu X, Krasnow SM, Roth-Carter QR, Levasseur PR, Braun TP, Grossberg AJ, et al. Hypothalamic signaling in anorexia induced by indispensable amino acid deficiency. American journal of physiology Endocrinology and metabolism. 2012;303(12):E1446-58.
278. Gietzen DW, Hao S, Anthony TG. Mechanisms of food intake repression in indispensable amino acid deficiency. Annual review of nutrition. 2007;27:63-78.
279. Koehnle TJ, Russell MC, Gietzen DW. Rats rapidly reject diets deficient in essential amino acids. J Nutr. 2003;133(7):2331-5.
280. Leung PM, Larson DM, Rogers QR. Food intake and preference of olfactory bulbectomized rats fed amino acid imbalanced or deficient diets. Physiology & behavior. 1972;9(4):553-7.
281. Mori M, Kawada T, Ono T, Torii K. Taste preference and protein nutrition and L-amino acid homeostasis in male Sprague-Dawley rats. Physiology & behavior. 1991;49(5):987-95.
282. Feurté S, Tomé D, Gietzen DW, Even PC, Nicolaïdis S, Fromentin G. Feeding patterns and meal microstructure during development of a taste aversion to a threonine devoid diet. Nutritional neuroscience. 2002;5(4):269-78.
283. Naito-Hoopes M, McArthur LH, Gietzen DW, Rogers QR. Learned preference and aversion for complete and isoleucine-devoid diets in rats. Physiology & behavior. 1993;53(3):485-94.
284. Sanahuja JC, Harper AE. Effect of amino acid imbalance on food intake and preference. Am J Physiol. 1962;202:165-70.
285. Griffioen-Roose S, Mars M, Siebelink E, Finlayson G, Tome D, de Graaf C. Protein status elicits compensatory changes in food intake and food preferences. The American journal of clinical nutrition. 2012;95(1):32-8.
286. Martens EA, Tan SY, Dunlop MV, Mattes RD, Westerterp-Plantenga MS. Protein leverage effects of beef protein on energy intake in humans. The American journal of clinical nutrition. 2014;99(6):1397-406.
287. Hao S, Sharp JW, Ross-Inta CM, McDaniel BJ, Anthony TG, Wek RC, et al. Uncharged tRNA and sensing of amino acid deficiency in mammalian piriform cortex. Science (New York, NY). 2005;307(5716):1776-8.

288. Rudell JB, Rechs AJ, Kelman TJ, Ross-Inta CM, Hao S, Gietzen DW. The anterior piriform cortex is sufficient for detecting depletion of an indispensable amino acid, showing independent cortical sensory function. J Neurosci. 2011;31(5):1583-90.
289. Hao S, Ross-Inta CM, Gietzen DW. The sensing of essential amino acid deficiency in the anterior piriform cortex, that requires the uncharged tRNA/GCN2 pathway, is sensitive to wortmannin but not rapamycin. Pharmacology, biochemistry, and behavior. 2010;94(3):333-40.
290. Gietzen DW, Aja SM. The brain's response to an essential amino acid-deficient diet and the circuitous route to a better meal. Mol Neurobiol. 2012;46(2):332-48.
291. Yokawa T, Tabuchi E, Takezawa M, Ono T, Torii K. Recognition and neural plasticity responding to deficient nutrient intake scanned by a functional MRI in the brain of rats with L-lysine deficiency. Obes Res. 1995;3 Suppl 5:685s-8s.
292. Leib DE, Knight ZA. Re-examination of Dietary Amino Acid Sensing Reveals a GCN2-Independent Mechanism. Cell reports. 2015;13(6):1081-9.
293. Bjordal M, Arquier N, Kniazeff J, Pin JP, Léopold P. Sensing of amino acids in a dopaminergic circuitry promotes rejection of an incomplete diet in Drosophila. Cell. 2014;156(3):510-21.
294. Zhu X, Krasnow SM, Roth-Carter QR, Levasseur PR, Braun TP, Grossberg AJ, et al. Hypothalamic signaling in anorexia induced by indispensable amino acid deficiency. American journal of physiology Endocrinology and metabolism. 2012;303(12):E1446-E58.
295. Du Y, Meng Q, Zhang Q, Guo F. Isoleucine or valine deprivation stimulates fat loss via increasing energy expenditure and regulating lipid metabolism in WAT. Amino acids. 2012;43(2):725-34.
296. Rozin P. Specific aversions as a component of specific hungers. J Comp Physiol Psychol. 1967;64(2):237-42.
297. Beverly JL, 3rd, Gietzen DW, Rogers QR. Protein synthesis in the prepyriform cortex: effects on intake of an amino acid-imbalanced diet by Sprague-Dawley rats. J Nutr. 1991;121(5):754-61.
298. Karnani MM, Apergis-Schoute J, Adamantidis A, Jensen LT, de Lecea L, Fugger L, et al. Activation of central orexin/hypocretin neurons by dietary amino acids. Neuron. 2011;72(4):616-29.
299. Xia T, Zhang Q, Xiao Y, Wang C, Yu J, Liu H, et al. CREB/TRH pathway in the central nervous system regulates energy expenditure in response to deprivation of an essential amino acid. International journal of obesity (2005). 2015;39(1):105-13.
300. Cheng Y, Meng Q, Wang C, Li H, Huang Z, Chen S, et al. Leucine deprivation decreases fat mass by stimulation of lipolysis in white adipose tissue and upregulation of uncoupling protein 1 (UCP1) in brown adipose tissue. Diabetes. 2010;59(1):17-25.
301. Cheng Y, Zhang Q, Meng Q, Xia T, Huang Z, Wang C, et al. Leucine deprivation stimulates fat loss via increasing CRH expression in the hypothalamus and activating the sympathetic nervous system. Mol Endocrinol. 2011;25(9):1624-35.
302. Yuan F, Jiang H, Yin H, Jiang X, Jiao F, Chen S, et al. Activation of GCN2/ATF4 signals in amygdalar PKC-δ neurons promotes WAT browning under leucine deprivation. Nat Commun. 2020;11(1):2847.

303. Xia T, Cheng Y, Zhang Q, Xiao F, Liu B, Chen S, et al. S6K1 in the central nervous system regulates energy expenditure via MC4R/CRH pathways in response to deprivation of an essential amino acid. Diabetes. 2012;61(10):2461-71.
304. Wang A, Huen SC, Luan HH, Yu S, Zhang C, Gallezot JD, et al. Opposing Effects of Fasting Metabolism on Tissue Tolerance in Bacterial and Viral Inflammation. Cell. 2016;166(6):1512-25 e12.
305. Dantzer R, O'Connor JC, Freund GG, Johnson RW, Kelley KW. From inflammation to sickness and depression: when the immune system subjugates the brain. Nature reviews Neuroscience. 2008;9(1):46-56.
306. Grossberg AJ, Scarlett JM, Zhu X, Bowe DD, Batra AK, Braun TP, et al. Arcuate nucleus proopiomelanocortin neurons mediate the acute anorectic actions of leukemia inhibitory factor via gp130. Endocrinology. 2010;151(2):606-16.
307. Suriben R, Chen M, Higbee J, Oeffinger J, Ventura R, Li B, et al. Antibody-mediated inhibition of GDF15-GFRAL activity reverses cancer cachexia in mice. Nat Med. 2020.
308. Marks DL, Ling N, Cone RD. Role of the central melanocortin system in cachexia. Cancer Res. 2001;61(4):1432-8.
309. Cheung W, Yu PX, Little BM, Cone RD, Marks DL, Mak RH. Role of leptin and melanocortin signaling in uremia-associated cachexia. The Journal of clinical investigation. 2005;115(6):1659-65.
310. Marks DL, Butler AA, Turner R, Brookhart G, Cone RD. Differential role of melanocortin receptor subtypes in cachexia. Endocrinology. 2003;144(4):1513-23.
311. Zhu X, Callahan MF, Gruber KA, Szumowski M, Marks DL. Melanocortin-4 receptor antagonist TCMCB07 ameliorates cancer- and chronic kidney disease-associated cachexia. The Journal of clinical investigation. 2020.
312. Scarlett JM, Bowe DD, Zhu X, Batra AK, Grant WF, Marks DL. Genetic and pharmacologic blockade of central melanocortin signaling attenuates cardiac cachexia in rodent models of heart failure. The Journal of endocrinology. 2010;206(1):121-30.
313. Markison S, Foster AC, Chen C, Brookhart GB, Hesse A, Hoare SR, et al. The regulation of feeding and metabolic rate and the prevention of murine cancer cachexia with a small-molecule melanocortin-4 receptor antagonist. Endocrinology. 2005;146(6):2766-73.
314. Carter ME, Soden ME, Zweifel LS, Palmiter RD. Genetic identification of a neural circuit that suppresses appetite. Nature. 2013;503(7474):111-4.
315. Campos CA, Bowen AJ, Han S, Wisse BE, Palmiter RD, Schwartz MW. Cancer-induced anorexia and malaise are mediated by CGRP neurons in the parabrachial nucleus. Nat Neurosci. 2017;20(7):934-42.
316. Campos CA, Bowen AJ, Schwartz MW, Palmiter RD. Parabrachial CGRP Neurons Control Meal Termination. Cell metabolism. 2016;23(5):811-20.
317. Paues J, Mackerlova L, Blomqvist A. Expression of melanocortin-4 receptor by rat parabrachial neurons responsive to immune and aversive stimuli. Neuroscience. 2006;141(1):287-97.
318. Emmerson PJ, Wang F, Du Y, Liu Q, Pickard RT, Gonciarz MD, et al. The metabolic effects of GDF15 are mediated by the orphan receptor GFRAL. Nat Med. 2017;23(10):1215-9.
319. Yang L, Chang CC, Sun Z, Madsen D, Zhu H, Padkjaer SB, et al. GFRAL is the receptor for GDF15 and is required for the anti-obesity effects of the ligand. Nat Med. 2017;23(10):1158-66.

320. Hsu JY, Crawley S, Chen M, Ayupova DA, Lindhout DA, Higbee J, et al. Non-homeostatic body weight regulation through a brainstem-restricted receptor for GDF15. Nature. 2017;550(7675):255-9.
321. Tsai VW, Husaini Y, Manandhar R, Lee-Ng KK, Zhang HP, Harriott K, et al. Anorexia/cachexia of chronic diseases: a role for the TGF-β family cytokine MIC-1/GDF15. J Cachexia Sarcopenia Muscle. 2012;3(4):239-43.
322. Lerner L, Tao J, Liu Q, Nicoletti R, Feng B, Krieger B, et al. MAP3K11/GDF15 axis is a critical driver of cancer cachexia. Journal of cachexia, sarcopenia and muscle. 2016;7(4):467-82.
323. Johnen H, Lin S, Kuffner T, Brown DA, Tsai VW, Bauskin AR, et al. Tumor-induced anorexia and weight loss are mediated by the TGF-beta superfamily cytokine MIC-1. Nat Med. 2007;13(11):1333-40.
324. Kozak W, Conn CA, Kluger MJ. Lipopolysaccharide induces fever and depresses locomotor activity in unrestrained mice. Am J Physiol. 1994;266(1 Pt 2):R125-35.
325. Grossberg AJ, Zhu X, Leinninger GM, Levasseur PR, Braun TP, Myers MG, Jr., et al. Inflammation-induced lethargy is mediated by suppression of orexin neuron activity. The Journal of neuroscience : the official journal of the Society for Neuroscience. 2011;31(31):11376-86.
326. Padilla SL, Qiu J, Soden ME, Sanz E, Nestor CC, Barker FD, et al. Agouti-related peptide neural circuits mediate adaptive behaviors in the starved state. Nature Neuroscience. 2016;19(5):734-41.
327. Scarlett JM, Zhu X, Enriori PJ, Bowe DD, Batra AK, Levasseur PR, et al. Regulation of agouti-related protein messenger ribonucleic acid transcription and peptide secretion by acute and chronic inflammation. Endocrinology. 2008;149(10):4837-45.
328. Arima Y, Yokota S, Fujitani M. Lateral parabrachial neurons innervate orexin neurons projecting to brainstem arousal areas in the rat. Sci Rep. 2019;9(1):2830.
329. Murphy KT, Chee A, Trieu J, Naim T, Lynch GS. Importance of functional and metabolic impairments in the characterization of the C-26 murine model of cancer cachexia. Dis Model Mech. 2012;5(4):533-45.
330. Voltarelli FA, Frajacomo FT, Padilha CS, Testa MTJ, Cella PS, Ribeiro DF, et al. Syngeneic B16F10 Melanoma Causes Cachexia and Impaired Skeletal Muscle Strength and Locomotor Activity in Mice. Front Physiol. 2017;8:715.
331. Kamei Y, Miura S, Suzuki M, Kai Y, Mizukami J, Taniguchi T, et al. Skeletal muscle FOXO1 (FKHR) transgenic mice have less skeletal muscle mass, down-regulated Type I (slow twitch/red muscle) fiber genes, and impaired glycemic control. J Biol Chem. 2004;279(39):41114-23.
332. Grossberg AJ, Vichaya EG, Gross PS, Ford BG, Scott KA, Estrada D, et al. Interleukin 6-independent metabolic reprogramming as a driver of cancer-related fatigue. Brain Behav Immun. 2020;88:230-41.
333. Hyltander A, Drott C, Körner U, Sandström R, Lundholm K. Elevated energy expenditure in cancer patients with solid tumours. European journal of cancer (Oxford, England : 1990). 1991;27(1):9-15.
334. Nixon DW, Kutner M, Heymsfield S, Foltz AT, Carty C, Seitz S, et al. Resting energy expenditure in lung and colon cancer. Metabolism: clinical and experimental. 1988;37(11):1059-64.

335. Lindmark L, Bennegård K, Edén E, Ekman L, Scherstén T, Svaninger G, et al. Resting energy expenditure in malnourished patients with and without cancer. Gastroenterology. 1984;87(2):402-8.
336. Rohm M, Zeigerer A, Machado J, Herzig S. Energy metabolism in cachexia. EMBO reports. 2019;20(4).
337. Cao DX, Wu GH, Zhang B, Quan YJ, Wei J, Jin H, et al. Resting energy expenditure and body composition in patients with newly detected cancer. Clin Nutr. 2010;29(1):72-7.
338. Kir S, White JP, Kleiner S, Kazak L, Cohen P, Baracos VE, et al. Tumour-derived PTH-related protein triggers adipose tissue browning and cancer cachexia. Nature. 2014;513(7516):100-4.
339. Konsman JP, Blomqvist A. Forebrain patterns of c-Fos and FosB induction during cancer-associated anorexia-cachexia in rat. Eur J Neurosci. 2005;21(10):2752-66.
340. Scarlett JM, Jobst EE, Enriori PJ, Bowe DD, Batra AK, Grant WF, et al. Regulation of central melanocortin signaling by interleukin-1 beta. Endocrinology. 2007;148(9):4217-25.
341. Ramage LE, Akyol M, Fletcher AM, Forsythe J, Nixon M, Carter RN, et al. Glucocorticoids Acutely Increase Brown Adipose Tissue Activity in Humans, Revealing Species-Specific Differences in UCP-1 Regulation. Cell metabolism. 2016;24(1):130-41.
342. Scotney H, Symonds ME, Law J, Budge H, Sharkey D, Manolopoulos KN. Glucocorticoids modulate human brown adipose tissue thermogenesis in vivo. Metabolism: clinical and experimental. 2017;70:125-32.
343. Kliewer KL, Ke JY, Tian M, Cole RM, Andridge RR, Belury MA. Adipose tissue lipolysis and energy metabolism in early cancer cachexia in mice. Cancer Biol Ther. 2015;16(6):886-97.
344. Legaspi A, Jeevanandam M, Starnes HF, Jr., Brennan MF. Whole body lipid and energy metabolism in the cancer patient. Metabolism: clinical and experimental. 1987;36(10):958-63.
345. Hansell DT, Davies JW, Shenkin A, Burns HJ. The oxidation of body fuel stores in cancer patients. Annals of surgery. 1986;204(6):637-42.
346. Bishop JS, Marks PA. Studies on carbohydrate metabolism in patients with neoplastic disease. II. Response to insulin administration. The Journal of clinical investigation. 1959;38(4):668-72.
347. Lang CH, Bagby GJ, Nowotny A, Spitzer JJ. Effects of toxic and nontoxic endotoxin derivatives on glucose kinetics. Circ Shock. 1985;17(4):301-11.
348. Dodesini AR, Benedini S, Terruzzi I, Sereni LP, Luzi L. Protein, glucose and lipid metabolism in the cancer cachexia: A preliminary report. Acta oncologica (Stockholm, Sweden). 2007;46(1):118-20.
349. Fukawa T, Yan-Jiang BC, Min-Wen JC, Jun-Hao ET, Huang D, Qian CN, et al. Excessive fatty acid oxidation induces muscle atrophy in cancer cachexia. Nat Med. 2016;22(6):666-71.
350. Fearon KC, Tisdale MJ, Preston T, Plumb JA, Calman KC. Failure of systemic ketosis to control cachexia and the growth rate of the Walker 256 carcinosarcoma in rats. British journal of cancer. 1985;52(1):87-92.
351. Flint TR, Janowitz T, Connell CM, Roberts EW, Denton AE, Coll AP, et al. Tumor-Induced IL-6 Reprograms Host Metabolism to Suppress Anti-tumor Immunity. Cell metabolism. 2016;24(5):672-84.

352. Fearon KC, Borland W, Preston T, Tisdale MJ, Shenkin A, Calman KC. Cancer cachexia: influence of systemic ketosis on substrate levels and nitrogen metabolism. The American journal of clinical nutrition. 1988;47(1):42-8.
353. Shukla SK, Gebregiworgis T, Purohit V, Chaika NV, Gunda V, Radhakrishnan P, et al. Metabolic reprogramming induced by ketone bodies diminishes pancreatic cancer cachexia. Cancer Metab. 2014;2:18.
354. Goncalves MD, Hwang SK, Pauli C, Murphy CJ, Cheng Z, Hopkins BD, et al. Fenofibrate prevents skeletal muscle loss in mice with lung cancer. Proc Natl Acad Sci U S A. 2018;115(4):E743-e52.
355. Lorite MJ, Cariuk P, Tisdale MJ. Induction of muscle protein degradation by a tumour factor. British journal of cancer. 1997;76(8):1035-40.
356. Beck SA, Tisdale MJ. Nitrogen excretion in cancer cachexia and its modification by a high fat diet in mice. Cancer Res. 1989;49(14):3800-4.
357. Yang QJ, Zhao JR, Hao J, Li B, Huo Y, Han YL, et al. Serum and urine metabolomics study reveals a distinct diagnostic model for cancer cachexia. J Cachexia Sarcopenia Muscle. 2018;9(1):71-85.
358. Reeds PJ, Fjeld CR, Jahoor F. Do the differences between the amino acid compositions of acute-phase and muscle proteins have a bearing on nitrogen loss in traumatic states? J Nutr. 1994;124(6):906-10.
359. Hall KD, Baracos VE. Computational modeling of cancer cachexia. Curr Opin Clin Nutr Metab Care. 2008;11(3):214-21.
360. Jeevanandam M, Horowitz GD, Lowry SF, Brennan MF. Cancer cachexia and the rate of whole body lipolysis in man. Metabolism: clinical and experimental. 1986;35(4):304-10.
361. Zuijdgeest-van Leeuwen SD, van den Berg JW, Wattimena JL, van der Gaast A, Swart GR, Wilson JH, et al. Lipolysis and lipid oxidation in weight-losing cancer patients and healthy subjects. Metabolism: clinical and experimental. 2000;49(7):931-6.
362. Klein S, Wolfe RR. Whole-body lipolysis and triglyceride-fatty acid cycling in cachectic patients with esophageal cancer. The Journal of clinical investigation. 1990;86(5):1403-8.
363. Fearon KC, Hansell DT, Preston T, Plumb JA, Davies J, Shapiro D, et al. Influence of whole body protein turnover rate on resting energy expenditure in patients with cancer. Cancer Res. 1988;48(9):2590-5.
364. McMillan DC, Preston T, Fearon KC, Burns HJ, Slater C, Shenkin A. Protein synthesis in cancer patients with inflammatory response: investigations with [15N]glycine. Nutrition (Burbank, Los Angeles County, Calif). 1994;10(3):232-40.
365. Melville S, McNurlan MA, Calder AG, Garlick PJ. Increased protein turnover despite normal energy metabolism and responses to feeding in patients with lung cancer. Cancer Res. 1990;50(4):1125-31.
366. Richards EW, Long CL, Nelson KM, Tohver OK, Pinkston JA, Navari RM, et al. Protein turnover in advanced lung cancer patients. Metabolism: clinical and experimental. 1993;42(3):291-6.
367. Glass DJ. Signaling pathways perturbing muscle mass. Curr Opin Clin Nutr Metab Care. 2010;13(3):225-9.
368. Eley HL, Tisdale MJ. Skeletal muscle atrophy, a link between depression of protein synthesis and increase in degradation. J Biol Chem. 2007;282(10):7087-97.

369. Lundholm K, Bennegård K, Edén E, Svaninger G, Emery PW, Rennie MJ. Efflux of 3-methylhistidine from the leg in cancer patients who experience weight loss. Cancer Res. 1982;42(11):4807-11.
370. Garcia JM, Boccia RV, Graham CD, Yan Y, Duus EM, Allen S, et al. Anamorelin for patients with cancer cachexia: an integrated analysis of two phase 2, randomised, placebo-controlled, double-blind trials. The Lancet Oncology. 2015;16(1):108-16.
371. Prado CM, Bekaii-Saab T, Doyle LA, Shrestha S, Ghosh S, Baracos VE, et al. Skeletal muscle anabolism is a side effect of therapy with the MEK inhibitor: selumetinib in patients with cholangiocarcinoma. British journal of cancer. 2012;106(10):1583-6.
372. MacDonald AJ, Johns N, Stephens N, Greig C, Ross JA, Small AC, et al. Habitual Myofibrillar Protein Synthesis Is Normal in Patients with Upper GI Cancer Cachexia. Clin Cancer Res. 2015;21(7):1734-40.
373. Winter A, MacAdams J, Chevalier S. Normal protein anabolic response to hyperaminoacidemia in insulin-resistant patients with lung cancer cachexia. Clin Nutr. 2012;31(5):765-73.
374. Prado CM, Sawyer MB, Ghosh S, Lieffers JR, Esfandiari N, Antoun S, et al. Central tenet of cancer cachexia therapy: do patients with advanced cancer have exploitable anabolic potential? The American journal of clinical nutrition. 2013;98(4):1012-9.
375. Temparis S, Asensi M, Taillandier D, Aurousseau E, Larbaud D, Obled A, et al. Increased ATP-ubiquitin-dependent proteolysis in skeletal muscles of tumor-bearing rats. Cancer Res. 1994;54(21):5568-73.
376. Fearon KC, Glass DJ, Guttridge DC. Cancer cachexia: mediators, signaling, and metabolic pathways. Cell metabolism. 2012;16(2):153-66.
377. Tisdale MJ. Mechanisms of Cancer Cachexia. Physiological reviews. 2009;89(2):381-410.
378. Bodine SC, Latres E, Baumhueter S, Lai VK, Nunez L, Clarke BA, et al. Identification of ubiquitin ligases required for skeletal muscle atrophy. Science (New York, NY). 2001;294(5547):1704-8.
379. Gomes MD, Lecker SH, Jagoe RT, Navon A, Goldberg AL. Atrogin-1, a muscle-specific F-box protein highly expressed during muscle atrophy. Proc Natl Acad Sci U S A. 2001;98(25):14440-5.
380. Llovera M, Carbó N, López-Soriano J, García-Martínez C, Busquets S, Alvarez B, et al. Different cytokines modulate ubiquitin gene expression in rat skeletal muscle. Cancer Lett. 1998;133(1):83-7.
381. Mizushima N, Levine B, Cuervo AM, Klionsky DJ. Autophagy fights disease through cellular self-digestion. Nature. 2008;451(7182):1069-75.
382. Mofarrahi M, Sigala I, Guo Y, Godin R, Davis EC, Petrof B, et al. Autophagy and skeletal muscles in sepsis. PLoS One. 2012;7(10):e47265.
383. Hermans G, Casaer MP, Clerckx B, Güiza F, Vanhullebusch T, Derde S, et al. Effect of tolerating macronutrient deficit on the development of intensive-care unit acquired weakness: a subanalysis of the EPaNIC trial. Lancet Respir Med. 2013;1(8):621-9.
384. Penna F, Costamagna D, Pin F, Camperi A, Fanzani A, Chiarpotto EM, et al. Autophagic degradation contributes to muscle wasting in cancer cachexia. Am J Pathol. 2013;182(4):1367-78.

385. Tardif N, Klaude M, Lundell L, Thorell A, Rooyackers O. Autophagic-lysosomal pathway is the main proteolytic system modified in the skeletal muscle of esophageal cancer patients. The American journal of clinical nutrition. 2013;98(6):1485-92.
386. Op den Kamp CM, Langen RC, Snepvangers FJ, de Theije CC, Schellekens JM, Laugs F, et al. Nuclear transcription factor κ B activation and protein turnover adaptations in skeletal muscle of patients with progressive stages of lung cancer cachexia. The American journal of clinical nutrition. 2013;98(3):738-48.
387. Johns N, Hatakeyama S, Stephens NA, Degen M, Degen S, Frieauff W, et al. Clinical classification of cancer cachexia: phenotypic correlates in human skeletal muscle. PLoS One. 2014;9(1):e83618.
388. Aversa Z, Pin F, Lucia S, Penna F, Verzaro R, Fazi M, et al. Autophagy is induced in the skeletal muscle of cachectic cancer patients. Sci Rep. 2016;6:30340.
389. Cosper PF, Leinwand LA. Cancer causes cardiac atrophy and autophagy in a sexually dimorphic manner. Cancer Res. 2011;71(5):1710-20.
390. Tian M, Asp ML, Nishijima Y, Belury MA. Evidence for cardiac atrophic remodeling in cancer-induced cachexia in mice. Int J Oncol. 2011;39(5):1321-6.
391. Manne ND, Lima M, Enos RT, Wehner P, Carson JA, Blough E. Altered cardiac muscle mTOR regulation during the progression of cancer cachexia in the ApcMin/+ mouse. Int J Oncol. 2013;42(6):2134-40.
392. Springer J, Tschirner A, Haghikia A, von Haehling S, Lal H, Grzesiak A, et al. Prevention of liver cancer cachexia-induced cardiac wasting and heart failure. European heart journal. 2014;35(14):932-41.
393. Das SK, Hoefler G. The role of triglyceride lipases in cancer associated cachexia. Trends in molecular medicine. 2013;19(5):292-301.
394. Das SK, Eder S, Schauer S, Diwoky C, Temmel H, Guertl B, et al. Adipose triglyceride lipase contributes to cancer-associated cachexia. Science (New York, NY). 2011;333(6039):233-8.
395. Bodnar RJ, Pasternak GW, Mann PE, Paul D, Warren R, Donner DB. Mediation of anorexia by human recombinant tumor necrosis factor through a peripheral action in the rat. Cancer Res. 1989;49(22):6280-4.
396. von Haehling S, Morley JE, Coats AJS, Anker SD. Ethical guidelines for publishing in the journal of cachexia, sarcopenia and muscle: update 2017. J Cachexia Sarcopenia Muscle. 2017;8(6):1081-3.
397. Ahles TA, Saykin AJ, Furstenberg CT, Cole B, Mott LA, Skalla K, et al. Neuropsychologic impact of standard-dose systemic chemotherapy in long-term survivors of breast cancer and lymphoma. Journal of clinical oncology : official journal of the American Society of Clinical Oncology. 2002;20(2):485-93.
398. Brezden CB, Phillips KA, Abdolell M, Bunston T, Tannock IF. Cognitive function in breast cancer patients receiving adjuvant chemotherapy. Journal of clinical oncology : official journal of the American Society of Clinical Oncology. 2000;18(14):2695-701.
399. Saykin AJ, Ahles TA, McDonald BC. Mechanisms of chemotherapy-induced cognitive disorders: neuropsychological, pathophysiological, and neuroimaging perspectives. Seminars in clinical neuropsychiatry. 2003;8(4):201-16.

400. Tannock IF, Ahles TA, Ganz PA, Van Dam FS. Cognitive impairment associated with chemotherapy for cancer: report of a workshop. Journal of clinical oncology : official journal of the American Society of Clinical Oncology. 2004;22(11):2233-9.
401. Jansen CE, Cooper BA, Dodd MJ, Miaskowski CA. A prospective longitudinal study of chemotherapy-induced cognitive changes in breast cancer patients. Support Care Cancer. 2011;19(10):1647-56.
402. Wefel JS, Lenzi R, Theriault RL, Davis RN, Meyers CA. The cognitive sequelae of standard-dose adjuvant chemotherapy in women with breast carcinoma: results of a prospective, randomized, longitudinal trial. Cancer. 2004;100(11):2292-9.
403. ACS. Cancer Facts and Figures. American Cancer Society. 2018.
404. Meyers C, & Perry, J. . Cognition and Cancer. Cambridge: Cambridge University Press; 2008.
405. Hickok JT, Roscoe JA, Morrow GR, Mustian K, Okunieff P, Bole CW. Frequency, severity, clinical course, and correlates of fatigue in 372 patients during 5 weeks of radiotherapy for cancer. Cancer. 2005;104(8):1772-8.
406. Bower JE. Cancer-related fatigue--mechanisms, risk factors, and treatments. Nature reviews Clinical oncology. 2014;11(10):597-609.
407. Meyers CA, Albitar M, Estey E. Cognitive impairment, fatigue, and cytokine levels in patients with acute myelogenous leukemia or myelodysplastic syndrome. Cancer. 2005;104(4):788-93.
408. Mock V, Atkinson A, Barsevick A, Cella D, Cimprich B, Cleeland C, et al. NCCN Practice Guidelines for Cancer-Related Fatigue. Oncology (Williston Park, NY). 2000;14(11A):151-61.
409. Feng LR, Espina A, Saligan LN. Association of Fatigue Intensification with Cognitive Impairment during Radiation Therapy for Prostate Cancer. Oncology. 2018;94(6):363-72.
410. Mustian KM, Sprod LK, Janelsins M, Peppone LJ, Mohile S. Exercise Recommendations for Cancer-Related Fatigue, Cognitive Impairment, Sleep problems, Depression, Pain, Anxiety, and Physical Dysfunction: A Review. Oncology & hematology review. 2012;8(2):81-8.
411. Biegler KA, Chaoul MA, Cohen L. Cancer, cognitive impairment, and meditation. Acta oncologica (Stockholm, Sweden). 2009;48(1):18-26.
412. Poulson MJ. Not just tired. Journal of clinical oncology : official journal of the American Society of Clinical Oncology. 2001;19(21):4180-1.
413. Boykoff N, Moieni M, Subramanian SK. Confronting chemobrain: an in-depth look at survivors' reports of impact on work, social networks, and health care response. Journal of cancer survivorship : research and practice. 2009;3(4):223-32.
414. Walker AK, Chang A, Ziegler AI, Dhillon HM, Vardy JL, Sloan EK. Low dose aspirin blocks breast cancer-induced cognitive impairment in mice. PloS one. 2018;13(12):e0208593-e.
415. Groenvold M, Petersen MA, Idler E, Bjorner JB, Fayers PM, Mouridsen HT. Psychological distress and fatigue predicted recurrence and survival in primary breast cancer patients. Breast cancer research and treatment. 2007;105(2):209-19.
416. Barnes EA, Bruera E. Fatigue in patients with advanced cancer: a review. International journal of gynecological cancer : official journal of the International Gynecological Cancer Society. 2002;12(5):424-8.

417. Hshieh TT, Jung WF, Grande LJ, Chen J, Stone RM, Soiffer RJ, et al. Prevalence of Cognitive Impairment and Association With Survival Among Older Patients With Hematologic Cancers. JAMA Oncol. 2018;4(5):686-93.
418. Baekelandt BMG, Hjermstad MJ, Nordby T, Fagerland MW, Kure EH, Heiberg T, et al. Preoperative cognitive function predicts survival in patients with resectable pancreatic ductal adenocarcinoma. HPB : the official journal of the International Hepato Pancreato Biliary Association. 2016;18(3):247-54.
419. Trachtenberg E, Mashiach T, Ben Hayun R, Tadmor T, Fisher T, Aharon-Peretz J, et al. Cognitive impairment in hodgkin lymphoma survivors. British journal of haematology. 2018;182(5):670-8.
420. Horowitz TS, Suls J, Trevino M. A Call for a Neuroscience Approach to Cancer-Related Cognitive Impairment. Trends in neurosciences. 2018;41(8):493-6.
421. Ahles TA, Saykin AJ, McDonald BC, Furstenberg CT, Cole BF, Hanscom BS, et al. Cognitive function in breast cancer patients prior to adjuvant treatment. Breast cancer research and treatment. 2008;110(1):143-52.
422. Wefel JS, Saleeba AK, Buzdar AU, Meyers CA. Acute and late onset cognitive dysfunction associated with chemotherapy in women with breast cancer. Cancer. 2010;116(14):3348-56.
423. Vardy JL, Dhillon HM, Pond GR, Rourke SB, Bekele T, Renton C, et al. Cognitive Function in Patients With Colorectal Cancer Who Do and Do Not Receive Chemotherapy: A Prospective, Longitudinal, Controlled Study. Journal of clinical oncology : official journal of the American Society of Clinical Oncology. 2015;33(34):4085-92.
424. Wefel JS, Vidrine DJ, Veramonti TL, Meyers CA, Marani SK, Hoekstra HJ, et al. Cognitive impairment in men with testicular cancer prior to adjuvant therapy. Cancer. 2011;117(1):190-6.
425. Hurria A, Rosen C, Hudis C, Zuckerman E, Panageas KS, Lachs MS, et al. Cognitive function of older patients receiving adjuvant chemotherapy for breast cancer: a pilot prospective longitudinal study. Journal of the American Geriatrics Society. 2006;54(6):925-31.
426. Hermelink K, Untch M, Lux MP, Kreienberg R, Beck T, Bauerfeind I, et al. Cognitive function during neoadjuvant chemotherapy for breast cancer: results of a prospective, multicenter, longitudinal study. Cancer. 2007;109(9):1905-13.
427. Janelsins MC, Heckler CE, Peppone LJ, Ahles TA, Mohile SG, Mustian KM, et al. Longitudinal Trajectory and Characterization of Cancer-Related Cognitive Impairment in a Nationwide Cohort Study. Journal of clinical oncology : official journal of the American Society of Clinical Oncology. 2018:Jco2018786624.
428. Simo M, Rifa-Ros X, Rodriguez-Fornells A, Bruna J. Chemobrain: a systematic review of structural and functional neuroimaging studies. Neurosci Biobehav Rev. 2013;37(8):1311-21.
429. Shiroishi MS, Gupta V, Bigjahan B, Cen SY, Rashid F, Hwang DH, et al. Brain cortical structural differences between non-central nervous system cancer patients treated with and without chemotherapy compared to non-cancer controls: a cross-sectional pilot MRI study using clinically-indicated scans. Proceedings of SPIE--the International Society for Optical Engineering. 2017;10572.
430. Scherling C, Collins B, MacKenzie J, Lepage C. Structural brain differences in breast cancer patients compared to matched controls prior to chemotherapy. International Journal of Biology. 2012;4(2):3-25.

431. McDonald BC, Conroy SK, Ahles TA, West JD, Saykin AJ. Gray matter reduction associated with systemic chemotherapy for breast cancer: a prospective MRI study. Breast cancer research and treatment. 2010;123(3):819-28.
432. Inagaki M, Yoshikawa E, Matsuoka Y, Sugawara Y, Nakano T, Akechi T, et al. Smaller regional volumes of brain gray and white matter demonstrated in breast cancer survivors exposed to adjuvant chemotherapy. Cancer. 2007;109(1):146-56.
433. Ruka W, Rutkowski P, Kaminska J, Rysinska A, Steffen J. Alterations of routine blood tests in adult patients with soft tissue sarcomas: Relationships to cytokine serum levels and prognostic significance. Annals of Oncology. 2001;12(10):1423-32.
434. Rutkowski P, Kaminska J, Kowalska M, Ruka W, Steffen J. Cytokine and cytokine receptor serum levels in adult bone sarcoma patients: correlations with local tumor extent and prognosis. Journal of surgical oncology. 2003;84(3):151-9.
435. Jiang XP, Yang DC, Elliott RL, Head JF. Reduction in serum IL-6 after vacination of breast cancer patients with tumour-associated antigens is related to estrogen receptor status. Cytokine. 2000;12(5):458-65.
436. Benoy IH, Salgado R, Van Dam P, Geboers K, Van Marck E, Scharpe S, et al. Increased serum interleukin-8 in patients with early and metastatic breast cancer correlates with early dissemination and survival. Clin Cancer Res. 2004;10(21):7157-62.
437. Ebrahimi B, Tucker SL, Li D, Abbruzzese JL, Kurzrock R. Cytokines in pancreatic carcinoma: correlation with phenotypic characteristics and prognosis. Cancer. 2004;101(12):2727-36.
438. Liao WC, Lin JT, Wu CY, Huang SP, Lin MT, Wu AS, et al. Serum interleukin-6 level but not genotype predicts survival after resection in stages II and III gastric carcinoma. Clin Cancer Res. 2008;14(2):428-34.
439. Ramsey S, Lamb GW, Aitchison M, McMillan DC. The longitudinal relationship between circulating concentrations of C-reactive protein, interleukin-6 and interleukin-10 in patients undergoing resection for renal cancer. British journal of cancer. 2006;95(8):1076-80.
440. Hoffmann TK, Sonkoly E, Homey B, Scheckenbach K, Gwosdz C, Bas M, et al. Aberrant cytokine expression in serum of patients with adenoid cystic carcinoma and squamous cell carcinoma of the head and neck. Head & neck. 2007;29(5):472-8.
441. Tsimberidou AM, Estey E, Wen S, Pierce S, Kantarjian H, Albitar M, et al. The prognostic significance of cytokine levels in newly diagnosed acute myeloid leukemia and high-risk myelodysplastic syndromes. Cancer. 2008;113(7):1605-13.
442. Lyon DE, Cohen R, Chen H, Kelly DL, McCain NL, Starkweather A, et al. Relationship of systemic cytokine concentrations to cognitive function over two years in women with early stage breast cancer. J Neuroimmunol. 2016;301:74-82.
443. Spangelo BL, Gorospe WC. Role of the cytokines in the neuroendocrine-immune system axis. Frontiers in neuroendocrinology. 1995;16(1):1-22.
444. Wu H, Li N, Jin R, Meng Q, Chen P, Zhao G, et al. Cytokine levels contribute to the pathogenesis of minimal hepatic encephalopathy in patients with hepatocellular carcinoma via STAT3 activation. Sci Rep. 2016;6:18528.
445. Andreotti C, King AA, Macy E, Compas BE, DeBaun MR. The Association of Cytokine Levels With Cognitive Function in Children With Sickle Cell Disease and Normal MRI Studies of the Brain. Journal of child neurology. 2015;30(10):1349-53.

446. Ma F, Wu T, Zhao J, Song A, Liu H, Xu W, et al. Folic acid supplementation improves cognitive function by reducing the levels of peripheral inflammatory cytokines in elderly Chinese subjects with MCI. Scientific reports. 2016;6:37486-.
447. Haroon E, Raison CL, Miller AH. Psychoneuroimmunology meets neuropsychopharmacology: translational implications of the impact of inflammation on behavior. Neuropsychopharmacology : official publication of the American College of Neuropsychopharmacology. 2012;37(1):137-62.
448. Cottrell GT, Ferguson AV. Sensory circumventricular organs: central roles in integrated autonomic regulation. Regulatory peptides. 2004;117(1):11-23.
449. John GR, Lee SC, Brosnan CF. Cytokines: powerful regulators of glial cell activation. The Neuroscientist : a review journal bringing neurobiology, neurology and psychiatry. 2003;9(1):10-22.
450. Vallieres L, Rivest S. Regulation of the genes encoding interleukin-6, its receptor, and gp130 in the rat brain in response to the immune activator lipopolysaccharide and the proinflammatory cytokine interleukin-1beta. J Neurochem. 1997;69(4):1668-83.
451. Ericsson A, Liu C, Hart RP, Sawchenko PE. Type 1 interleukin-1 receptor in the rat brain: distribution, regulation, and relationship to sites of IL-1-induced cellular activation. The Journal of comparative neurology. 1995;361(4):681-98.
452. Capuron L, Miller AH. Immune system to brain signaling: neuropsychopharmacological implications. Pharmacol Ther. 2011;130(2):226-38.
453. Serrats J, Schiltz JC, García-Bueno B, van Rooijen N, Reyes TM, Sawchenko PE. Dual roles for perivascular macrophages in immune-to-brain signaling. Neuron. 2010;65(1):94-106.
454. Fischer HG, Reichmann G. Brain dendritic cells and macrophages/microglia in central nervous system inflammation. J Immunol. 2001;166(4):2717-26.
455. Fabriek BO, Van Haastert ES, Galea I, Polfliet MM, Dopp ED, Van Den Heuvel MM, et al. CD163-positive perivascular macrophages in the human CNS express molecules for antigen recognition and presentation. Glia. 2005;51(4):297-305.
456. Ivanov, II, McKenzie BS, Zhou L, Tadokoro CE, Lepelley A, Lafaille JJ, et al. The orphan nuclear receptor RORgammat directs the differentiation program of proinflammatory IL-17+ T helper cells. Cell. 2006;126(6):1121-33.
457. Bailey-Bucktrout SL, Martinez-Llordella M, Zhou X, Anthony B, Rosenthal W, Luche H, et al. Self-antigen-driven activation induces instability of regulatory T cells during an inflammatory autoimmune response. Immunity. 2013;39(5):949-62.
458. Heneka MT, Carson MJ, El Khoury J, Landreth GE, Brosseron F, Feinstein DL, et al. Neuroinflammation in Alzheimer's disease. The Lancet Neurology. 2015;14(4):388-405.
459. Howland RH. Vagus Nerve Stimulation. Current behavioral neuroscience reports. 2014;1(2):64-73.
460. Steinberg BE, Silverman HA, Robbiati S, Gunasekaran MK, Tsaava T, Battinelli E, et al. Cytokine-specific Neurograms in the Sensory Vagus Nerve. Bioelectronic medicine. 2016;3:7-17.
461. Ronchi G, Ryu V, Fornaro M, Czaja K. Hippocampal plasticity after a vagus nerve injury in the rat. Neural regeneration research. 2012;7(14):1055-63.
462. Liu A-f, Zhao F-b, Wang J, Lu Y-F, Tian J, Zhao Y, et al. Effects of vagus nerve stimulation on cognitive functioning in rats with cerebral ischemia reperfusion. Journal of translational medicine. 2016;14:101-.

463. Jiang Y, Li L, Tan X, Liu B, Zhang Y, Li C. miR-210 mediates vagus nerve stimulation-induced antioxidant stress and anti-apoptosis reactions following cerebral ischemia/reperfusion injury in rats. J Neurochem. 2015;134(1):173-81.
464. Dunn AJ. Endotoxin-induced activation of cerebral catecholamine and serotonin metabolism: comparison with interleukin-1. J Pharmacol Exp Ther. 1992;261(3):964-9.
465. Zalcman S, Green-Johnson JM, Murray L, Nance DM, Dyck D, Anisman H, et al. Cytokine-specific central monoamine alterations induced by interleukin-1, -2 and -6. Brain research. 1994;643(1-2):40-9.
466. Muller N, Ackenheil M. Psychoneuroimmunology and the cytokine action in the CNS: implications for psychiatric disorders. Progress in neuro-psychopharmacology & biological psychiatry. 1998;22(1):1-33.
467. Luk WP, Zhang Y, White TD, Lue FA, Wu C, Jiang CG, et al. Adenosine: a mediator of interleukin-1beta-induced hippocampal synaptic inhibition. J Neurosci. 1999;19(11):4238-44.
468. Huang TL, O'Banion MK. Interleukin-1 beta and tumor necrosis factor-alpha suppress dexamethasone induction of glutamine synthetase in primary mouse astrocytes. J Neurochem. 1998;71(4):1436-42.
469. Tancredi V, Zona C, Velotti F, Eusebi F, Santoni A. Interleukin-2 suppresses established long-term potentiation and inhibits its induction in the rat hippocampus. Brain research. 1990;525(1):149-51.
470. Hanisch UK, Seto D, Quirion R. Modulation of hippocampal acetylcholine release: a potent central action of interleukin-2. J Neurosci. 1993;13(8):3368-74.
471. McQuiston AR. Acetylcholine release and inhibitory interneuron activity in hippocampal CA1. Frontiers in synaptic neuroscience. 2014;6:20-.
472. Ellison MD, Krieg RJ, Povlishock JT. Differential central nervous system responses following single and multiple recombinant interleukin-2 infusions. J Neuroimmunol. 1990;28(3):249-60.
473. Denicoff KD, Rubinow DR, Papa MZ, Simpson C, Seipp CA, Lotze MT, et al. The neuropsychiatric effects of treatment with interleukin-2 and lymphokine-activated killer cells. Ann Intern Med. 1987;107(3):293-300.
474. Spooren A, Kolmus K, Laureys G, Clinckers R, De Keyser J, Haegeman G, et al. Interleukin-6, a mental cytokine. Brain research reviews. 2011;67(1-2):157-83.
475. Satoh T, Nakamura S, Taga T, Matsuda T, Hirano T, Kishimoto T, et al. Induction of neuronal differentiation in PC12 cells by B-cell stimulatory factor 2/interleukin 6. Mol Cell Biol. 1988;8(8):3546-9.
476. Kunz D, Walker G, Bedoucha M, Certa U, Marz-Weiss P, Dimitriades-Schmutz B, et al. Expression profiling and Ingenuity biological function analyses of interleukin-6- versus nerve growth factor-stimulated PC12 cells. BMC genomics. 2009;10:90.
477. Cao Z, Gao Y, Bryson JB, Hou J, Chaudhry N, Siddiq M, et al. The cytokine interleukin-6 is sufficient but not necessary to mimic the peripheral conditioning lesion effect on axonal growth. J Neurosci. 2006;26(20):5565-73.
478. Zhang PL, Levy AM, Ben-Simchon L, Haggiag S, Chebath J, Revel M. Induction of neuronal and myelin-related gene expression by IL-6-receptor/IL-6: a study on embryonic dorsal root ganglia cells and isolated Schwann cells. Exp Neurol. 2007;208(2):285-96.

479. Qiu Z, Sweeney DD, Netzeband JG, Gruol DL. Chronic interleukin-6 alters NMDA receptor-mediated membrane responses and enhances neurotoxicity in developing CNS neurons. J Neurosci. 1998;18(24):10445-56.
480. Krady JK, Lin HW, Liberto CM, Basu A, Kremlev SG, Levison SW. Ciliary neurotrophic factor and interleukin-6 differentially activate microglia. J Neurosci Res. 2008;86(7):1538-47.
481. Heyser CJ, Masliah E, Samimi A, Campbell IL, Gold LH. Progressive decline in avoidance learning paralleled by inflammatory neurodegeneration in transgenic mice expressing interleukin 6 in the brain. Proc Natl Acad Sci U S A. 1997;94(4):1500-5.
482. Song C, Merali Z, Anisman H. Variations of nucleus accumbens dopamine and serotonin following systemic interleukin-1, interleukin-2 or interleukin-6 treatment. Neuroscience. 1999;88(3):823-36.
483. Damas P, Reuter A, Gysen P, Demonty J, Lamy M, Franchimont P. Tumor necrosis factor and interleukin-1 serum levels during severe sepsis in humans. Crit Care Med. 1989;17(10):975-8.
484. Pehlivan Y, Onat AM, Ceylan N, Turkbeyler IH, Buyukhatipoglu H, Comez G, et al. Serum leptin, resistin and TNF-alpha levels in patients with systemic sclerosis: the role of adipokines in scleroderma. International journal of rheumatic diseases. 2012;15(4):374-9.
485. Ma Y, Ren Y, Dai ZJ, Wu CJ, Ji YH, Xu J. IL-6, IL-8 and TNF-alpha levels correlate with disease stage in breast cancer patients. Advances in clinical and experimental medicine : official organ Wroclaw Medical University. 2017;26(3):421-6.
486. Michalaki V, Syrigos K, Charles P, Waxman J. Serum levels of IL-6 and TNF-alpha correlate with clinicopathological features and patient survival in patients with prostate cancer. British journal of cancer. 2004;90(12):2312-6.
487. Terrando N, Monaco C, Ma D, Foxwell BM, Feldmann M, Maze M. Tumor necrosis factor-alpha triggers a cytokine cascade yielding postoperative cognitive decline. Proc Natl Acad Sci U S A. 2010;107(47):20518-22.
488. Habbas S, Santello M, Becker D, Stubbe H, Zappia G, Liaudet N, et al. Neuroinflammatory TNFalpha Impairs Memory via Astrocyte Signaling. Cell. 2015;163(7):1730-41.
489. Licinio J, Kling MA, Hauser P. Cytokines and brain function: relevance to interferon-alpha-induced mood and cognitive changes. Seminars in oncology. 1998;25(1 Suppl 1):30-8.
490. Blank T, Detje CN, Spiess A, Hagemeyer N, Brendecke SM, Wolfart J, et al. Brain Endothelial- and Epithelial-Specific Interferon Receptor Chain 1 Drives Virus-Induced Sickness Behavior and Cognitive Impairment. Immunity. 2016;44(4):901-12.
491. Bradburn S, McPhee J, Bagley L, Carroll M, Slevin M, Al-Shanti N, et al. Dysregulation of C-X-C motif ligand 10 during aging and association with cognitive performance. Neurobiol Aging. 2018;63:54-64.
492. Croxson PL, Johansen-Berg H, Behrens TE, Robson MD, Pinsk MA, Gross CG, et al. Quantitative investigation of connections of the prefrontal cortex in the human and macaque using probabilistic diffusion tractography. J Neurosci. 2005;25(39):8854-66.
493. Kesler SR, Kent JS, O'Hara R. Prefrontal cortex and executive function impairments in primary breast cancer. Archives of neurology. 2011;68(11):1447-53.
494. Rezaie P, Trillo-Pazos G, Everall IP, Male DK. Expression of beta-chemokines and chemokine receptors in human fetal astrocyte and microglial co-cultures: potential role of chemokines in the developing CNS. Glia. 2002;37(1):64-75.

495. Deverman BE, Patterson PH. Cytokines and CNS development. Neuron. 2009;64(1):61-78.
496. Maartens G, Celum C, Lewin SR. HIV infection: epidemiology, pathogenesis, treatment, and prevention. Lancet (London, England). 2014;384(9939):258-71.
497. Zattoni M, Mura ML, Deprez F, Schwendener RA, Engelhardt B, Frei K, et al. Brain infiltration of leukocytes contributes to the pathophysiology of temporal lobe epilepsy. J Neurosci. 2011;31(11):4037-50.
498. Zenaro E, Pietronigro E, Della Bianca V, Piacentino G, Marongiu L, Budui S, et al. Neutrophils promote Alzheimer's disease-like pathology and cognitive decline via LFA-1 integrin. Nat Med. 2015;21(8):880-6.
499. Brochard V, Combadiere B, Prigent A, Laouar Y, Perrin A, Beray-Berthat V, et al. Infiltration of CD4+ lymphocytes into the brain contributes to neurodegeneration in a mouse model of Parkinson disease. The Journal of clinical investigation. 2009;119(1):182-92.
500. Dendrou CA, Fugger L, Friese MA. Immunopathology of multiple sclerosis. Nature reviews Immunology. 2015;15(9):545-58.
501. Reboldi A, Coisne C, Baumjohann D, Benvenuto F, Bottinelli D, Lira S, et al. C-C chemokine receptor 6-regulated entry of TH-17 cells into the CNS through the choroid plexus is required for the initiation of EAE. Nat Immunol. 2009;10(5):514-23.
502. Gelderblom M, Leypoldt F, Steinbach K, Behrens D, Choe CU, Siler DA, et al. Temporal and spatial dynamics of cerebral immune cell accumulation in stroke. Stroke. 2009;40(5):1849-57.
503. Dimitrijevic OB, Stamatovic SM, Keep RF, Andjelkovic AV. Absence of the chemokine receptor CCR2 protects against cerebral ischemia/reperfusion injury in mice. Stroke. 2007;38(4):1345-53.
504. Burfeind KG. Infiltrating and Resident Myeloid Cells in the Central Nervous System are Neuroinflammatory Mediators of Cachexia during Pancreatic Cancer: Oregon Health & Science University; 2019.
505. Varvel NH, Neher JJ, Bosch A, Wang W, Ransohoff RM, Miller RJ, et al. Infiltrating monocytes promote brain inflammation and exacerbate neuronal damage after status epilepticus. Proc Natl Acad Sci U S A. 2016;113(38):E5665-74.
506. Herz J, Sabellek P, Lane TE, Gunzer M, Hermann DM, Doeppner TR. Role of Neutrophils in Exacerbation of Brain Injury After Focal Cerebral Ischemia in Hyperlipidemic Mice. Stroke. 2015;46(10):2916-25.
507. Jordao MJC, Sankowski R, Brendecke SM, Sagar, Locatelli G, Tai YH, et al. Single-cell profiling identifies myeloid cell subsets with distinct fates during neuroinflammation. Science (New York, NY). 2019;363(6425).
508. D'Mello C, Le T, Swain MG. Cerebral microglia recruit monocytes into the brain in response to tumor necrosis factoralpha signaling during peripheral organ inflammation. J Neurosci. 2009;29(7):2089-102.
509. Johnstone RM, Adam M, Hammond JR, Orr L, Turbide C. Vesicle formation during reticulocyte maturation. Association of plasma membrane activities with released vesicles (exosomes). J Biol Chem. 1987;262(19):9412-20.

510. Yanez-Mo M, Siljander PR, Andreu Z, Zavec AB, Borras FE, Buzas EI, et al. Biological properties of extracellular vesicles and their physiological functions. Journal of extracellular vesicles. 2015;4:27066.
511. Harada T, Yamamoto H, Kishida S, Kishida M, Awada C, Takao T, et al. Wnt5b-associated exosomes promote cancer cell migration and proliferation. Cancer science. 2017;108(1):42-52.
512. Hendrix A, Hume AN. Exosome signaling in mammary gland development and cancer. The International journal of developmental biology. 2011;55(7-9):879-87.
513. Weidle UH, Birzele F, Kollmorgen G, Ruger R. The Multiple Roles of Exosomes in Metastasis. Cancer genomics & proteomics. 2017;14(1):1-15.
514. Paggetti J, Haderk F, Seiffert M, Janji B, Distler U, Ammerlaan W, et al. Exosomes released by chronic lymphocytic leukemia cells induce the transition of stromal cells into cancer-associated fibroblasts. Blood. 2015;126(9):1106-17.
515. Holm MM, Kaiser J, Schwab ME. Extracellular Vesicles: Multimodal Envoys in Neural Maintenance and Repair. Trends in neurosciences. 2018;41(6):360-72.
516. Grapp M, Wrede A, Schweizer M, Huwel S, Galla HJ, Snaidero N, et al. Choroid plexus transcytosis and exosome shuttling deliver folate into brain parenchyma. Nat Commun. 2013;4:2123.
517. Matsumoto J, Stewart T, Banks WA, Zhang J. The Transport Mechanism of Extracellular Vesicles at the Blood-Brain Barrier. Curr Pharm Des. 2017;23(40):6206-14.
518. Li JJ, Wang B, Kodali MC, Chen C, Kim E, Patters BJ, et al. In vivo evidence for the contribution of peripheral circulating inflammatory exosomes to neuroinflammation. Journal of neuroinflammation. 2018;15(1):8.
519. Balusu S, Van Wonterghem E, De Rycke R, Raemdonck K, Stremersch S, Gevaert K, et al. Identification of a novel mechanism of blood-brain communication during peripheral inflammation via choroid plexus-derived extracellular vesicles. EMBO Mol Med. 2016;8(10):1162-83.
520. Ridder K, Keller S, Dams M, Rupp AK, Schlaudraff J, Del Turco D, et al. Extracellular vesicle-mediated transfer of genetic information between the hematopoietic system and the brain in response to inflammation. PLoS biology. 2014;12(6):e1001874.
521. Su W, Hong L, Xu X, Huang S, Herpai D, Li L, et al. miR-30 disrupts senescence and promotes cancer by targeting both p16(INK4A) and DNA damage pathways. Oncogene. 2018;37(42):5618-32.
522. Song Y, Hu M, Zhang J, Teng ZQ, Chen C. A novel mechanism of synaptic and cognitive impairments mediated via microRNA-30b in Alzheimer's disease. EBioMedicine. 2019;39:409-21.
523. Magnon C, Hall SJ, Lin J, Xue X, Gerber L, Freedland SJ, et al. Autonomic nerve development contributes to prostate cancer progression. Science (New York, NY). 2013;341(6142):1236361.
524. Saloman JL, Albers KM, Li D, Hartman DJ, Crawford HC, Muha EA, et al. Ablation of sensory neurons in a genetic model of pancreatic ductal adenocarcinoma slows initiation and progression of cancer. Proceedings of the National Academy of Sciences of the United States of America. 2016;113(11):3078-83.
525. Madeo M, Colbert PL, Vermeer DW, Lucido CT, Cain JT, Vichaya EG, et al. Cancer exosomes induce tumor innervation. Nat Commun. 2018;9(1):4284.

526. Hawkins BT, Davis TP. The blood-brain barrier/neurovascular unit in health and disease. Pharmacol Rev. 2005;57(2):173-85.
527. Roher AE, Kuo YM, Esh C, Knebel C, Weiss N, Kalback W, et al. Cortical and leptomeningeal cerebrovascular amyloid and white matter pathology in Alzheimer's disease. Molecular medicine (Cambridge, Mass). 2003;9(3-4):112-22.
528. Vidal R, Calero M, Piccardo P, Farlow MR, Unverzagt FW, Méndez E, et al. Senile dementia associated with amyloid β protein angiopathy and tau perivascular pathology but not neuritic plaques in patients homozygous for the APOE-ε4 allele. Acta Neuropathologica. 2000;100(1):1-12.
529. Meucci G, Rossi G, Bettini R, Montanaro D, Gironelli L, Voci L, et al. Laser nephelometric evaluation of albumin, IgG and alpha 2-macroglobulin: applications to the study of alterations of the blood-brain barrier. J Neurol Sci. 1993;118(1):73-8.
530. Banks WA, Gray AM, Erickson MA, Salameh TS, Damodarasamy M, Sheibani N, et al. Lipopolysaccharide-induced blood-brain barrier disruption: roles of cyclooxygenase, oxidative stress, neuroinflammation, and elements of the neurovascular unit. Journal of neuroinflammation. 2015;12:223.
531. Iwase K, Miyanaka K, Shimizu A, Nagasaki A, Gotoh T, Mori M, et al. Induction of endothelial nitric-oxide synthase in rat brain astrocytes by systemic lipopolysaccharide treatment. J Biol Chem. 2000;275(16):11929-33.
532. Wang T, Town T, Alexopoulou L, Anderson JF, Fikrig E, Flavell RA. Toll-like receptor 3 mediates West Nile virus entry into the brain causing lethal encephalitis. Nat Med. 2004;10(12):1366-73.
533. Natah SS, Mouihate A, Pittman QJ, Sharkey KA. Disruption of the blood-brain barrier during TNBS colitis. Neurogastroenterology and motility : the official journal of the European Gastrointestinal Motility Society. 2005;17(3):433-46.
534. Farkas G, Márton J, Nagy Z, Mándi Y, Takács T, Deli MA, et al. Experimental acute pancreatitis results in increased blood–brain barrier permeability in the rat: a potential role for tumor necrosis factor and interleukin 6. Neuroscience Letters. 1998;242(3):147-50.
535. Rochfort KD, Collins LE, McLoughlin A, Cummins PM. Tumour necrosis factor-alpha-mediated disruption of cerebrovascular endothelial barrier integrity in vitro involves the production of proinflammatory interleukin-6. J Neurochem. 2016;136(3):564-72.
536. Rochfort KD, Cummins PM. Cytokine-mediated dysregulation of zonula occludens-1 properties in human brain microvascular endothelium. Microvascular research. 2015;100:48-53.
537. Lin R, Chen F, Wen S, Teng T, Pan Y, Huang H. Interleukin-10 attenuates impairment of the blood-brain barrier in a severe acute pancreatitis rat model. Journal of inflammation (London, England). 2018;15:4.
538. Tsao N, Hsu HP, Wu CM, Liu CC, Lei HY. Tumour necrosis factor-alpha causes an increase in blood-brain barrier permeability during sepsis. Journal of medical microbiology. 2001;50(9):812-21.
539. de Vries HE, Blom-Roosemalen MC, van Oosten M, de Boer AG, van Berkel TJ, Breimer DD, et al. The influence of cytokines on the integrity of the blood-brain barrier in vitro. J Neuroimmunol. 1996;64(1):37-43.

540. Daniels BP, Holman DW, Cruz-Orengo L, Jujjavarapu H, Durrant DM, Klein RS. Viral pathogen-associated molecular patterns regulate blood-brain barrier integrity via competing innate cytokine signals. mBio. 2014;5(5):e01476-14.
541. Hart BL. Biological basis of the behavior of sick animals. Neurosci Biobehav Rev. 1988;12(2):123-37.
542. Hart BL. Behavioral adaptations to pathogens and parasites: five strategies. Neurosci Biobehav Rev. 1990;14(3):273-94.
543. Mak RH, Cheung W, Cone RD, Marks DL. Mechanisms of disease: Cytokine and adipokine signaling in uremic cachexia. Nature clinical practice Nephrology. 2006;2(9):527-34.
544. von Haehling S, Anker SD. Prevalence, incidence and clinical impact of cachexia: facts and numbers-update 2014. J Cachexia Sarcopenia Muscle. 2014;5(4):261-3.
545. Bachmann J, Heiligensetzer M, Krakowski-Roosen H, Buchler MW, Friess H, Martignoni ME. Cachexia worsens prognosis in patients with resectable pancreatic cancer. Journal of gastrointestinal surgery : official journal of the Society for Surgery of the Alimentary Tract. 2008;12(7):1193-201.
546. Danai LV, Babic A, Rosenthal MH, Dennstedt EA, Muir A, Lien EC, et al. Altered exocrine function can drive adipose wasting in early pancreatic cancer. Nature. 2018;558(7711):600-4.
547. Katakami N, Uchino J, Yokoyama T, Naito T, Kondo M, Yamada K, et al. Anamorelin (ONO-7643) for the treatment of patients with non-small cell lung cancer and cachexia: Results from a randomized, double-blind, placebo-controlled, multicenter study of Japanese patients (ONO-7643-04). Cancer. 2018;124(3):606-16.
548. Nishie K, Yamamoto S, Nagata C, Koizumi T, Hanaoka M. Anamorelin for advanced non-small-cell lung cancer with cachexia: Systematic review and meta-analysis. Lung cancer (Amsterdam, Netherlands). 2017;112:25-34.
549. Currow DC, Skipworth RJ. The emerging role of anamorelin hydrochloride in the management of patients with cancer anorexia-cachexia. Future Oncol. 2017;13(20):1767-83.
550. Gomez-Chou SB, Swidnicka-Siergiejko AK, Badi N, Chavez-Tomar M, Lesinski GB, Bekaii-Saab T, et al. Lipocalin-2 Promotes Pancreatic Ductal Adenocarcinoma by Regulating Inflammation in the Tumor Microenvironment. Cancer Res. 2017;77(10):2647-60.
551. Viau A, El Karoui K, Laouari D, Burtin M, Nguyen C, Mori K, et al. Lipocalin 2 is essential for chronic kidney disease progression in mice and humans. The Journal of clinical investigation. 2010;120(11):4065-76.
552. Yndestad A, Landro L, Ueland T, Dahl CP, Flo TH, Vinge LE, et al. Increased systemic and myocardial expression of neutrophil gelatinase-associated lipocalin in clinical and experimental heart failure. European heart journal. 2009;30(10):1229-36.
553. Cone RD. Anatomy and regulation of the central melanocortin system. Nat Neurosci. 2005;8(5):571-8.
554. Zhao P, Elks CM, Stephens JM. The induction of lipocalin-2 protein expression in vivo and in vitro. The Journal of biological chemistry. 2014;289(9):5960-9.
555. Xu MJ, Feng D, Wu H, Wang H, Chan Y, Kolls J, et al. Liver is the major source of elevated serum lipocalin-2 levels after bacterial infection or partial hepatectomy: a critical role for IL-6/STAT3. Hepatology. 2015;61(2):692-702.

556. Zhu X, Burfeind KG, Michaelis KA, Braun TP, Olson B, Pelz KR, et al. MyD88 signalling is critical in the development of pancreatic cancer cachexia. J Cachexia Sarcopenia Muscle. 2019;10(2):378-90.
557. Baazim H, Schweiger M, Moschinger M, Xu H, Scherer T, Popa A, et al. CD8(+) T cells induce cachexia during chronic viral infection. Nature immunology. 2019;20(6):701-10.
558. Mourtzakis M, Prado CM, Lieffers JR, Reiman T, McCargar LJ, Baracos VE. A practical and precise approach to quantification of body composition in cancer patients using computed tomography images acquired during routine care. Appl Physiol Nutr Metab. 2008;33(5):997-1006.
559. Ogłuszka M, Orzechowska M, Jędroszka D, Witas P, Bednarek AK. Evaluate Cutpoints: Adaptable continuous data distribution system for determining survival in Kaplan-Meier estimator. Comput Methods Programs Biomed. 2019;177:133-9.
560. Burfeind KG, Zhu X, Norgard MA, Levasseur PR, Huisman C, Michaelis KA, et al. Microglia in the hypothalamus respond to tumor-derived factors and are protective against cachexia during pancreatic cancer. Glia. 2020.
561. Alwahsh SM, Xu M, Seyhan HA, Ahmad S, Mihm S, Ramadori G, et al. Diet high in fructose leads to an overexpression of lipocalin-2 in rat fatty liver. World J Gastroenterol. 2014;20(7):1807-21.
562. Stitt TN, Drujan D, Clarke BA, Panaro F, Timofeyva Y, Kline WO, et al. The IGF-1/PI3K/Akt pathway prevents expression of muscle atrophy-induced ubiquitin ligases by inhibiting FOXO transcription factors. Mol Cell. 2004;14(3):395-403.
563. Sandri M, Sandri C, Gilbert A, Skurk C, Calabria E, Picard A, et al. Foxo transcription factors induce the atrophy-related ubiquitin ligase atrogin-1 and cause skeletal muscle atrophy. Cell. 2004;117(3):399-412.
564. Milan G, Romanello V, Pescatore F, Armani A, Paik JH, Frasson L, et al. Regulation of autophagy and the ubiquitin-proteasome system by the FoxO transcriptional network during muscle atrophy. Nat Commun. 2015;6:6670.
565. Vichaya EG, Gross PS, Estrada DJ, Cole SW, Grossberg AJ, Evans SE, et al. Lipocalin-2 is dispensable in inflammation-induced sickness and depression-like behavior. Psychopharmacology (Berl). 2019;236(10):2975-82.
566. Eller K, Schroll A, Banas M, Kirsch AH, Huber JM, Nairz M, et al. Lipocalin-2 expressed in innate immune cells is an endogenous inhibitor of inflammation in murine nephrotoxic serum nephritis. PLoS One. 2013;8(7):e67693.
567. Barasch J, Hollmen M, Deng R, Hod EA, Rupert PB, Abergel RJ, et al. Disposal of iron by a mutant form of lipocalin 2. Nat Commun. 2016;7:12973.
568. Ishii A, Katsuura G, Imamaki H, Kimura H, Mori KP, Kuwabara T, et al. Obesity-promoting and anti-thermogenic effects of neutrophil gelatinase-associated lipocalin in mice. Sci Rep. 2017;7(1):15501.
569. Guo H, Jin D, Zhang Y, Wright W, Bazuine M, Brockman DA, et al. Lipocalin-2 deficiency impairs thermogenesis and potentiates diet-induced insulin resistance in mice. Diabetes. 2010;59(6):1376-85.
570. Law IK, Xu A, Lam KS, Berger T, Mak TW, Vanhoutte PM, et al. Lipocalin-2 deficiency attenuates insulin resistance associated with aging and obesity. Diabetes. 2010;59(4):872-82.

571. Jun LS, Siddall CP, Rosen ED. A minor role for lipocalin 2 in high-fat diet-induced glucose intolerance. American journal of physiology Endocrinology and metabolism. 2011;301(5):E825-35.
572. Hatori M, Vollmers C, Zarrinpar A, DiTacchio L, Bushong EA, Gill S, et al. Time-restricted feeding without reducing caloric intake prevents metabolic diseases in mice fed a high-fat diet. Cell Metab. 2012;15(6):848-60.
573. Chaix A, Zarrinpar A, Miu P, Panda S. Time-restricted feeding is a preventative and therapeutic intervention against diverse nutritional challenges. Cell Metab. 2014;20(6):991-1005.
574. Brandhorst S, Choi IY, Wei M, Cheng CW, Sedrakyan S, Navarrete G, et al. A Periodic Diet that Mimics Fasting Promotes Multi-System Regeneration, Enhanced Cognitive Performance, and Healthspan. Cell Metab. 2015;22(1):86-99.
575. Cheng H, Long F, Jaiswar M, Yang L, Wang C, Zhou Z. Prognostic role of the neutrophil-to-lymphocyte ratio in pancreatic cancer: a meta-analysis. Sci Rep. 2015;5:11026.
576. Chen Y, Yan H, Wang Y, Shi Y, Dai G. Significance of baseline and change in neutrophil-to-lymphocyte ratio in predicting prognosis: a retrospective analysis in advanced pancreatic ductal adenocarcinoma. Sci Rep. 2017;7(1):753.
577. Prado CM, Purcell SA, Laviano A. Nutrition interventions to treat low muscle mass in cancer. J Cachexia Sarcopenia Muscle. 2020.
578. Iwai N, Okuda T, Sakagami J, Harada T, Ohara T, Taniguchi M, et al. Neutrophil to lymphocyte ratio predicts prognosis in unresectable pancreatic cancer. Sci Rep. 2020;10(1):18758.
579. Giakoustidis A, Neofytou K, Costa Neves M, Giakoustidis D, Louri E, Cunningham D, et al. Identifying the role of neutrophil-to-lymphocyte ratio and platelets-to-lymphocyte ratio as prognostic markers in patients undergoing resection of pancreatic ductal adenocarcinoma. Ann Hepatobiliary Pancreat Surg. 2018;22(3):197-207.
580. Coffelt SB, Kersten K, Doornebal CW, Weiden J, Vrijland K, Hau CS, et al. IL-17-producing γδ T cells and neutrophils conspire to promote breast cancer metastasis. Nature. 2015;522(7556):345-8.
581. Prado CM, Lieffers JR, McCargar LJ, Reiman T, Sawyer MB, Martin L, et al. Prevalence and clinical implications of sarcopenic obesity in patients with solid tumours of the respiratory and gastrointestinal tracts: a population-based study. The Lancet Oncology. 2008;9(7):629-35.
582. Katz AM, Katz PB. Diseases of the heart in the works of Hippocrates. British heart journal. 1962;24:257-64.
583. Hofmann TJ, Otsuru S, Marino R, Rasini V, Veronesi E, Murgia A, et al. Transplanted murine long-term repopulating hematopoietic cells can differentiate to osteoblasts in the marrow stem cell niche. Molecular therapy : the journal of the American Society of Gene Therapy. 2013;21(6):1224-31.
584. Dominici M, Pritchard C, Garlits JE, Hofmann TJ, Persons DA, Horwitz EM. Hematopoietic cells and osteoblasts are derived from a common marrow progenitor after bone marrow transplantation. Proc Natl Acad Sci U S A. 2004;101(32):11761-6.
585. Burfeind KG, Zhu X, Levasseur PR, Michaelis KA, Norgard MA, Marks DL. TRIF is a key inflammatory mediator of acute sickness behavior and cancer cachexia. Brain Behav Immun. 2018;73:364-74.

586. Michaelis KA, Norgard MA, Zhu X, Levasseur PR, Sivagnanam S, Liudahl SM, et al. The TLR7/8 agonist R848 remodels tumor and host responses to promote survival in pancreatic cancer. Nat Commun. 2019;10(1):4682.
587. Kraus D, Yang Q, Kahn BB. Lipid Extraction from Mouse Feces. Bio Protoc. 2015;5(1):e1375.
588. Popuri K, Cobzas D, Esfandiari N, Baracos V, Jagersand M. Body Composition Assessment in Axial CT Images Using FEM-Based Automatic Segmentation of Skeletal Muscle. IEEE Trans Med Imaging. 2016;35(2):512-20.
589. Prado CM, Birdsell LA, Baracos VE. The emerging role of computerized tomography in assessing cancer cachexia. Curr Opin Support Palliat Care. 2009;3(4):269-75.
590. Kayser MS, Dalmau J. The emerging link between autoimmune disorders and neuropsychiatric disease. J Neuropsychiatry Clin Neurosci. 2011;23(1):90-7.
591. Gan L, Cookson MR, Petrucelli L, La Spada AR. Converging pathways in neurodegeneration, from genetics to mechanisms. Nat Neurosci. 2018;21(10):1300-9.
592. Zhao N, Xu X, Jiang Y, Gao J, Wang F, Xu X, et al. Lipocalin-2 may produce damaging effect after cerebral ischemia by inducing astrocytes classical activation. J Neuroinflammation. 2019;16(1):168.
593. Deacon RM, Croucher A, Rawlins JN. Hippocampal cytotoxic lesion effects on species-typical behaviours in mice. Behav Brain Res. 2002;132(2):203-13.
594. Deacon RM, Penny C, Rawlins JN. Effects of medial prefrontal cortex cytotoxic lesions in mice. Behav Brain Res. 2003;139(1-2):139-55.
595. Gaskill BN, Karas AZ, Garner JP, Pritchett-Corning KR. Nest building as an indicator of health and welfare in laboratory mice. Journal of visualized experiments : JoVE. 2013(82):51012.
596. Neely CLC, Pedemonte KA, Boggs KN, Flinn JM. Nest Building Behavior as an Early Indicator of Behavioral Deficits in Mice. Journal of visualized experiments : JoVE. 2019(152).
597. Olson B, Zhu X, Norgard MA, Levasseur PR, Butler JT, Buenafe A, et al. Lipocalin 2 mediates appetite suppression during pancreatic cancer cachexia. Nat Commun. 2021;12(1):2057.
598. Overstreet LS, Hentges ST, Bumaschny VF, de Souza FS, Smart JL, Santangelo AM, et al. A transgenic marker for newly born granule cells in dentate gyrus. J Neurosci. 2004;24(13):3251-9.
599. Harrison L, Pfuhlmann K, Schriever SC, Pfluger PT. Profound weight loss induces reactive astrogliosis in the arcuate nucleus of obese mice. Mol Metab. 2019;24:149-55.
600. Li SH, Li H, Torre ER, Li XJ. Expression of huntingtin-associated protein-1 in neuronal cells implicates a role in neuritic growth. Mol Cell Neurosci. 2000;16(2):168-83.
601. Few AP, Lautermilch NJ, Westenbroek RE, Scheuer T, Catterall WA. Differential regulation of CaV2.1 channels by calcium-binding protein 1 and visinin-like protein-2 requires N-terminal myristoylation. The Journal of neuroscience : the official journal of the Society for Neuroscience. 2005;25(30):7071-80.
602. Lautermilch NJ, Few AP, Scheuer T, Catterall WA. Modulation of CaV2.1 channels by the neuronal calcium-binding protein visinin-like protein-2. The Journal of neuroscience : the official journal of the Society for Neuroscience. 2005;25(30):7062-70.
603. Leal K, Mochida S, Scheuer T, Catterall WA. Fine-tuning synaptic plasticity by modulation of Ca(V)2.1 channels with Ca2+ sensor proteins. Proc Natl Acad Sci U S A. 2012;109(42):17069-74.

604. Moss A, Ingram R, Koch S, Theodorou A, Low L, Baccei M, et al. Origins, actions and dynamic expression patterns of the neuropeptide VGF in rat peripheral and central sensory neurones following peripheral nerve injury. Mol Pain. 2008;4:62.
605. Riedl MS, Braun PD, Kitto KF, Roiko SA, Anderson LB, Honda CN, et al. Proteomic analysis uncovers novel actions of the neurosecretory protein VGF in nociceptive processing. The Journal of neuroscience : the official journal of the Society for Neuroscience. 2009;29(42):13377-88.
606. Conrad CD, Galea LA, Kuroda Y, McEwen BS. Chronic stress impairs rat spatial memory on the Y maze, and this effect is blocked by tianeptine pretreatment. Behavioral neuroscience. 1996;110(6):1321-34.
607. Sarnyai Z, Sibille EL, Pavlides C, Fenster RJ, McEwen BS, Toth M. Impaired hippocampal-dependent learning and functional abnormalities in the hippocampus in mice lacking serotonin(1A) receptors. Proc Natl Acad Sci U S A. 2000;97(26):14731-6.
608. Messier C. Object recognition in mice: improvement of memory by glucose. Neurobiology of learning and memory. 1997;67(2):172-5.
609. Ojeda-Juárez D, Shah R, Fields JA, Harahap-Carrillo IS, Koury J, Maung R, et al. Lipocalin-2 mediates HIV-1 induced neuronal injury and behavioral deficits by overriding CCR5-dependent protection. Brain Behav Immun. 2020;89:184-99.
610. Winters BD, Forwood SE, Cowell RA, Saksida LM, Bussey TJ. Double dissociation between the effects of peri-postrhinal cortex and hippocampal lesions on tests of object recognition and spatial memory: heterogeneity of function within the temporal lobe. J Neurosci. 2004;24(26):5901-8.
611. Zhao H, Konishi A, Fujita Y, Yagi M, Ohata K, Aoshi T, et al. Lipocalin 2 bolsters innate and adaptive immune responses to blood-stage malaria infection by reinforcing host iron metabolism. Cell host & microbe. 2012;12(5):705-16.
612. Eruysal E, Ravdin L, Kamel H, Iadecola C, Ishii M. Plasma lipocalin-2 levels in the preclinical stage of Alzheimer's disease. Alzheimer's & dementia (Amsterdam, Netherlands). 2019;11:646-53.
613. Weng YC, Huang YT, Chiang IC, Tsai PJ, Su YW, Chou WH. Lipocalin-2 mediates the rejection of neural transplants. Faseb j. 2021;35(2):e21317.
614. Jang E, Lee S, Kim JH, Kim JH, Seo JW, Lee WH, et al. Secreted protein lipocalin-2 promotes microglial M1 polarization. Faseb j. 2013;27(3):1176-90.
615. Mucha M, Skrzypiec AE, Schiavon E, Attwood BK, Kucerova E, Pawlak R. Lipocalin-2 controls neuronal excitability and anxiety by regulating dendritic spine formation and maturation. Proc Natl Acad Sci U S A. 2011;108(45):18436-41.
616. Dekens DW, Naudé PJW, Keijser JN, Boerema AS, De Deyn PP, Eisel ULM. Lipocalin 2 contributes to brain iron dysregulation but does not affect cognition, plaque load, and glial activation in the J20 Alzheimer mouse model. Journal of neuroinflammation. 2018;15(1):330.
617. Ferreira AC, Pinto V, S DM, Novais A, Sousa JC, Correia-Neves M, et al. Lipocalin-2 is involved in emotional behaviors and cognitive function. Front Cell Neurosci. 2013;7:122.
618. Orr ME, Sullivan AC, Frost B. A Brief Overview of Tauopathy: Causes, Consequences, and Therapeutic Strategies. Trends Pharmacol Sci. 2017;38(7):637-48.
619. Leger M, Quiedeville A, Bouet V, Haelewyn B, Boulouard M, Schumann-Bard P, et al. Object recognition test in mice. Nature protocols. 2013;8(12):2531-7.

620. Deacon RM. Assessing nest building in mice. Nature protocols. 2006;1(3):1117-9.
621. Tisdale MJ. Biology of cachexia. Journal of the National Cancer Institute. 1997;89(23):1763-73.
622. von Haehling S, Anker SD. Cachexia as a major underestimated and unmet medical need: facts and numbers. J Cachexia Sarcopenia Muscle. 2010;1(1):1-5.
623. von Haehling S, Anker MS, Anker SD. Prevalence and clinical impact of cachexia in chronic illness in Europe, USA, and Japan: facts and numbers update 2016. J Cachexia Sarcopenia Muscle. 2016;7(5):507-9.
624. Tomasin R, Martin A, Cominetti MR. Metastasis and cachexia: alongside in clinics, but not so in animal models. J Cachexia Sarcopenia Muscle. 2019;10(6):1183-94.
625. Konishi M, Ebner N, von Haehling S, Anker SD, Springer J. Developing models for cachexia and their implications in drug discovery. Expert opinion on drug discovery. 2015;10(7):743-52.
626. Bennani-Baiti N, Walsh D. Animal models of the cancer anorexia-cachexia syndrome. Support Care Cancer. 2011;19(9):1451-63.
627. Argilés JM, Busquets S, Stemmler B, López-Soriano FJ. Cancer cachexia: understanding the molecular basis. Nat Rev Cancer. 2014;14(11):754-62.
628. Vanhoutte G, van de Wiel M, Wouters K, Sels M, Bartolomeeussen L, De Keersmaecker S, et al. Cachexia in cancer: what is in the definition? BMJ open gastroenterology. 2016;3(1):e000097.
629. Loberg RD, Bradley DA, Tomlins SA, Chinnaiyan AM, Pienta KJ. The lethal phenotype of cancer: the molecular basis of death due to malignancy. CA: a cancer journal for clinicians. 2007;57(4):225-41.
630. Consul N, Guo X, Coker C, Lopez-Pintado S, Hibshoosh H, Zhao B, et al. Monitoring Metastasis and Cachexia in a Patient with Breast Cancer: A Case Study. Clinical Medicine Insights Oncology. 2016;10:83-94.
631. Shiono M, Huang K, Downey RJ, Consul N, Villanueva N, Beck K, et al. An analysis of the relationship between metastases and cachexia in lung cancer patients. Cancer medicine. 2016;5(9):2641-8.
632. Waning DL, Mohammad KS, Reiken S, Xie W, Andersson DC, John S, et al. Excess TGF-β mediates muscle weakness associated with bone metastases in mice. Nat Med. 2015;21(11):1262-71.
633. Wang G, Biswas AK, Ma W, Kandpal M, Coker C, Grandgenett PM, et al. Metastatic cancers promote cachexia through ZIP14 upregulation in skeletal muscle. Nat Med. 2018;24(6):770-81.
634. Biswas AK, Acharyya S. Understanding cachexia in the context of metastatic progression. Nature Reviews Cancer. 2020;20(5):274-84.
635. Vermeer DW, Coppock JD, Zeng E, Lee KM, Spanos WC, Onken MD, et al. Metastatic model of HPV+ oropharyngeal squamous cell carcinoma demonstrates heterogeneity in tumor metastasis. Oncotarget. 2016;7(17):24194-207.
636. Olson B, Edwards J, Stone L, Jiang A, Zhu X, Holland J, et al. Association of Sarcopenia With Oncologic Outcomes of Primary Surgery or Definitive Radiotherapy Among Patients With Localized Oropharyngeal Squamous Cell Carcinoma. JAMA otolaryngology-- head & neck surgery. 2020;146(8):1-9.

637. Jager-Wittenaar H, Dijkstra PU, Dijkstra G, Bijzet J, Langendijk JA, van der Laan B, et al. High prevalence of cachexia in newly diagnosed head and neck cancer patients: An exploratory study. Nutrition (Burbank, Los Angeles County, Calif). 2017;35:114-8.
638. Meijer JH, Robbers Y. Wheel running in the wild. Proceedings Biological sciences. 2014;281(1786).
639. Cai D, Frantz JD, Tawa NE, Jr., Melendez PA, Oh BC, Lidov HG, et al. IKKbeta/NF-kappaB activation causes severe muscle wasting in mice. Cell. 2004;119(2):285-98.
640. Zhang G, Jin B, Li YP. C/EBPβ mediates tumour-induced ubiquitin ligase atrogin1/MAFbx upregulation and muscle wasting. The EMBO journal. 2011;30(20):4323-35.
641. Acharyya S, Ladner KJ, Nelsen LL, Damrauer J, Reiser PJ, Swoap S, et al. Cancer cachexia is regulated by selective targeting of skeletal muscle gene products. The Journal of clinical investigation. 2004;114(3):370-8.
642. Lee S, Kim JH, Kim JH, Seo JW, Han HS, Lee WH, et al. Lipocalin-2 Is a chemokine inducer in the central nervous system: role of chemokine ligand 10 (CXCL10) in lipocalin-2-induced cell migration. J Biol Chem. 2011;286(51):43855-70.
643. Xu C, Yuan J, Du W, Wu J, Fang Q, Zhang X, et al. Significance of the Neutrophil-to-Lymphocyte Ratio in p16-Negative Squamous Cell Carcinoma of Unknown Primary in Head and Neck. Front Oncol. 2020;10:39.
644. Barker T, Fulde G, Moulton B, Nadauld LD, Rhodes T. An elevated neutrophil-to-lymphocyte ratio associates with weight loss and cachexia in cancer. Scientific reports. 2020;10(1):7535-.
645. Sun Y, Yang Y, Qin Z, Cai J, Guo X, Tang Y, et al. The Acute-Phase Protein Orosomucoid Regulates Food Intake and Energy Homeostasis via Leptin Receptor Signaling Pathway. Diabetes. 2016;65(6):1630-41.
646. Lee YS, Choi JW, Hwang I, Lee JW, Lee JH, Kim AY, et al. Adipocytokine orosomucoid integrates inflammatory and metabolic signals to preserve energy homeostasis by resolving immoderate inflammation. J Biol Chem. 2010;285(29):22174-85.
647. Pigna E, Berardi E, Aulino P, Rizzuto E, Zampieri S, Carraro U, et al. Aerobic Exercise and Pharmacological Treatments Counteract Cachexia by Modulating Autophagy in Colon Cancer. Sci Rep. 2016;6:26991.
648. Khamoui AV, Park BS, Kim DH, Yeh MC, Oh SL, Elam ML, et al. Aerobic and resistance training dependent skeletal muscle plasticity in the colon-26 murine model of cancer cachexia. Metabolism: clinical and experimental. 2016;65(5):685-98.
649. Lieffers JR, Mourtzakis M, Hall KD, McCargar LJ, Prado CM, Baracos VE. A viscerally driven cachexia syndrome in patients with advanced colorectal cancer: contributions of organ and tumor mass to whole-body energy demands. The American journal of clinical nutrition. 2009;89(4):1173-9.
650. Bonetto A, Rupert JE, Barreto R, Zimmers TA. The Colon-26 Carcinoma Tumor-bearing Mouse as a Model for the Study of Cancer Cachexia. J Vis Exp. 2016(117).
651. Hojo H, Enya S, Arai M, Suzuki Y, Nojiri T, Kangawa K, et al. Remote reprogramming of hepatic circadian transcriptome by breast cancer. Oncotarget. 2017;8(21):34128-40.
652. Pedersen L, Idorn M, Olofsson GH, Lauenborg B, Nookaew I, Hansen RH, et al. Voluntary Running Suppresses Tumor Growth through Epinephrine- and IL-6-Dependent NK Cell Mobilization and Redistribution. Cell metabolism. 2016;23(3):554-62.

653. Biswas AK, Acharyya S. Understanding cachexia in the context of metastatic progression. Nat Rev Cancer. 2020;20(5):274-84.
654. Ferlito A, Shaha AR, Silver CE, Rinaldo A, Mondin V. Incidence and sites of distant metastases from head and neck cancer. ORL; journal for oto-rhino-laryngology and its related specialties. 2001;63(4):202-7.
655. Visser MR, van Lanschot JJ, van der Velden J, Kloek JJ, Gouma DJ, Sprangers MA. Quality of life in newly diagnosed cancer patients waiting for surgery is seriously impaired. Journal of surgical oncology. 2006;93(7):571-7.
656. Brown DJ, McMillan DC, Milroy R. The correlation between fatigue, physical function, the systemic inflammatory response, and psychological distress in patients with advanced lung cancer. Cancer. 2005;103(2):377-82.
657. Powers SK, Lynch GS, Murphy KT, Reid MB, Zijdewind I. Disease-Induced Skeletal Muscle Atrophy and Fatigue. Medicine and science in sports and exercise. 2016;48(11):2307-19.
658. Murphy KT. The pathogenesis and treatment of cardiac atrophy in cancer cachexia. American journal of physiology Heart and circulatory physiology. 2016;310(4):H466-77.
659. Fouladiun M, Körner U, Bosaeus I, Daneryd P, Hyltander A, Lundholm KG. Body composition and time course changes in regional distribution of fat and lean tissue in unselected cancer patients on palliative care--correlations with food intake, metabolism, exercise capacity, and hormones. Cancer. 2005;103(10):2189-98.
660. Batista ML, Jr., Henriques FS, Neves RX, Olivan MR, Matos-Neto EM, Alcântara PS, et al. Cachexia-associated adipose tissue morphological rearrangement in gastrointestinal cancer patients. J Cachexia Sarcopenia Muscle. 2016;7(1):37-47.
661. Rohm M, Schäfer M, Laurent V, Üstünel BE, Niopek K, Algire C, et al. An AMP-activated protein kinase-stabilizing peptide ameliorates adipose tissue wasting in cancer cachexia in mice. Nat Med. 2016;22(10):1120-30.
662. Kim KH, Kim YH, Son JE, Lee JH, Kim S, Choe MS, et al. Intermittent fasting promotes adipose thermogenesis and metabolic homeostasis via VEGF-mediated alternative activation of macrophage. Cell research. 2017;27(11):1309-26.
663. Li G, Xie C, Lu S, Nichols RG, Tian Y, Li L, et al. Intermittent Fasting Promotes White Adipose Browning and Decreases Obesity by Shaping the Gut Microbiota. Cell metabolism. 2017;26(5):801.
664. Rothwell NJ, Stock MJ. A role for brown adipose tissue in diet-induced thermogenesis. Obes Res. 1997;5(6):650-6.
665. Knoll JG, Krasnow SM, Marks DL. Interleukin-1β signaling in fenestrated capillaries is sufficient to trigger sickness responses in mice. Journal of neuroinflammation. 2017;14(1):219.
666. Liu X, Nemeth DP, McKim DB, Zhu L, DiSabato DJ, Berdysz O, et al. Cell-Type-Specific Interleukin 1 Receptor 1 Signaling in the Brain Regulates Distinct Neuroimmune Activities. Immunity. 2019;50(2):317-33.e6.
667. Howard R, Kanetsky PA, Egan KM. Exploring the prognostic value of the neutrophil-to-lymphocyte ratio in cancer. Sci Rep. 2019;9(1):19673.
668. Viñal D, Gutierrez-Sainz L, Martinez D, Garcia-Cuesta JA, Pedregosa J, Villamayor J, et al. Prognostic value of neutrophil-to-lymphocyte ratio in advanced cancer patients receiving immunotherapy. Clinical & translational oncology : official publication of the Federation of Spanish Oncology Societies and of the National Cancer Institute of Mexico. 2020.

669. Barker T, Fulde G, Moulton B, Nadauld LD, Rhodes T. An elevated neutrophil-to-lymphocyte ratio associates with weight loss and cachexia in cancer. Sci Rep. 2020;10(1):7535.
670. Frenette J, St-Pierre M, Côté CH, Mylona E, Pizza FX. Muscle impairment occurs rapidly and precedes inflammatory cell accumulation after mechanical loading. American journal of physiology Regulatory, integrative and comparative physiology. 2002;282(2):R351-7.
671. Tidball JG. Regulation of muscle growth and regeneration by the immune system. Nature reviews Immunology. 2017;17(3):165-78.
672. Dumont N, Bouchard P, Frenette J. Neutrophil-induced skeletal muscle damage: a calculated and controlled response following hindlimb unloading and reloading. American journal of physiology Regulatory, integrative and comparative physiology. 2008;295(6):R1831-8.
673. Friesen DE, Baracos VE, Tuszynski JA. Modeling the energetic cost of cancer as a result of altered energy metabolism: implications for cachexia. Theoretical biology & medical modelling. 2015;12:17.
674. Holroyde CP, Skutches CL, Boden G, Reichard GA. Glucose metabolism in cachectic patients with colorectal cancer. Cancer Res. 1984;44(12 Pt 1):5910-3.
675. Tisdale MJ. Mechanisms of cancer cachexia. Physiological reviews. 2009;89(2):381-410.
676. Holroyde CP, Gabuzda TG, Putnam RC, Paul P, Reichard GA. Altered glucose metabolism in metastatic carcinoma. Cancer Res. 1975;35(12):3710-4.
677. Spanos WC, Hoover A, Harris GF, Wu S, Strand GL, Anderson ME, et al. The PDZ binding motif of human papillomavirus type 16 E6 induces PTPN13 loss, which allows anchorage-independent growth and synergizes with ras for invasive growth. J Virol. 2008;82(5):2493-500.
678. Hoover AC, Spanos WC, Harris GF, Anderson ME, Klingelhutz AJ, Lee JH. The role of human papillomavirus 16 E6 in anchorage-independent and invasive growth of mouse tonsil epithelium. Archives of otolaryngology--head & neck surgery. 2007;133(5):495-502.
679. von Haehling S, Morley JE, Coats AJS, Anker SD. Ethical guidelines for publishing in the Journal of Cachexia, Sarcopenia and Muscle: update 2019. J Cachexia Sarcopenia Muscle. 2019;10(5):1143-5.
680. Karp CL. Unstressing intemperate models: how cold stress undermines mouse modeling. The Journal of experimental medicine. 2012;209(6):1069-74.
681. Bhusal A, Rahman MH, Lee WH, Bae YC, Lee IK, Suk K. Paradoxical role of lipocalin-2 in metabolic disorders and neurological complications. Biochemical pharmacology. 2019;169:113626.
682. Jager-Wittenaar H, Dijkstra PU, Vissink A, Langendijk JA, van der Laan BF, Pruim J, et al. Changes in nutritional status and dietary intake during and after head and neck cancer treatment. Head & neck. 2011;33(6):863-70.
683. Nejatinamini S, Debenham BJ, Clugston RD, Mawani A, Parliament M, Wismer WV, et al. Poor Vitamin Status is Associated with Skeletal Muscle Loss and Mucositis in Head and Neck Cancer Patients. Nutrients. 2018;10(9).
684. Jackson W, Alexander N, Schipper M, Fig L, Feng F, Jolly S. Characterization of changes in total body composition for patients with head and neck cancer undergoing chemoradiotherapy using dual-energy x-ray absorptiometry. Head & neck. 2014;36(9):1356-62.
685. Ghadjar P, Hayoz S, Zimmermann F, Bodis S, Kaul D, Badakhshi H, et al. Impact of weight loss on survival after chemoradiation for locally advanced head and neck cancer: secondary

results of a randomized phase III trial (SAKK 10/94). Radiation oncology (London, England). 2015;10:21.
686. Deurenberg P, Yap M, van Staveren WA. Body mass index and percent body fat: a meta analysis among different ethnic groups. International journal of obesity and related metabolic disorders : journal of the International Association for the Study of Obesity. 1998;22(12):1164-71.
687. Martin L, Birdsell L, Macdonald N, Reiman T, Clandinin MT, McCargar LJ, et al. Cancer cachexia in the age of obesity: skeletal muscle depletion is a powerful prognostic factor, independent of body mass index. Journal of clinical oncology : official journal of the American Society of Clinical Oncology. 2013;31(12):1539-47.
688. Grossberg AJ, Chamchod S, Fuller CD, Mohamed AS, Heukelom J, Eichelberger H, et al. Association of Body Composition With Survival and Locoregional Control of Radiotherapy-Treated Head and Neck Squamous Cell Carcinoma. JAMA Oncol. 2016;2(6):782-9.
689. Stone L, Olson B, Mowery A, Krasnow S, Jiang A, Li R, et al. Association Between Sarcopenia and Mortality in Patients Undergoing Surgical Excision of Head and Neck Cancer. JAMA otolaryngology-- head & neck surgery. 2019.
690. Achim V, Bash J, Mowery A, Guimaraes AR, Li R, Schindler J, et al. Prognostic Indication of Sarcopenia for Wound Complication After Total Laryngectomy. JAMA otolaryngology-- head & neck surgery. 2017;143(12):1159-65.
691. Pedro C, Mira B, Silva P, Netto E, Pocinho R, Mota A, et al. Surgery vs. primary radiotherapy in early-stage oropharyngeal cancer. Clinical and translational radiation oncology. 2017;9:18-22.
692. Kelly JR, Park HS, An Y, Contessa JN, Yarbrough WG, Burtness BA, et al. Comparison of Survival Outcomes Among Human Papillomavirus-Negative cT1-2 N1-2b Patients With Oropharyngeal Squamous Cell Cancer Treated With Upfront Surgery vs Definitive Chemoradiation Therapy: An Observational Study. JAMA Oncol. 2017;3(8):1107-11.
693. Kelly JR, Park HS, An Y, Yarbrough WG, Contessa JN, Decker R, et al. Upfront surgery versus definitive chemoradiotherapy in patients with human Papillomavirus-associated oropharyngeal squamous cell cancer. Oral oncology. 2018;79:64-70.
694. Mitsiopoulos N, Baumgartner RN, Heymsfield SB, Lyons W, Gallagher D, Ross R. Cadaver validation of skeletal muscle measurement by magnetic resonance imaging and computerized tomography. Journal of applied physiology (Bethesda, Md : 1985). 1998;85(1):115-22.
695. Charlson ME, Pompei P, Ales KL, MacKenzie CR. A new method of classifying prognostic comorbidity in longitudinal studies: development and validation. Journal of chronic diseases. 1987;40(5):373-83.
696. da Cunha LP, Silveira MN, Mendes MCS, Costa FO, Macedo LT, de Siqueira NS, et al. Sarcopenia as an independent prognostic factor in patients with metastatic colorectal cancer: A retrospective evaluation. Clinical nutrition ESPEN. 2019;32:107-12.
697. Ninomiya G, Fujii T, Yamada S, Yabusaki N, Suzuki K, Iwata N, et al. Clinical impact of sarcopenia on prognosis in pancreatic ductal adenocarcinoma: A retrospective cohort study. International journal of surgery (London, England). 2017;39:45-51.
698. Begini P, Gigante E, Antonelli G, Carbonetti F, Iannicelli E, Anania G, et al. Sarcopenia predicts reduced survival in patients with hepatocellular carcinoma at first diagnosis. Annals of hepatology. 2017;16(1):107-14.

699. Iritani S, Imai K, Takai K, Hanai T, Ideta T, Miyazaki T, et al. Skeletal muscle depletion is an independent prognostic factor for hepatocellular carcinoma. Journal of gastroenterology. 2015;50(3):323-32.
700. Wendrich AW, Swartz JE, Bril SI, Wegner I, de Graeff A, Smid EJ, et al. Low skeletal muscle mass is a predictive factor for chemotherapy dose-limiting toxicity in patients with locally advanced head and neck cancer. Oral oncology. 2017;71:26-33.
701. Olson B, Marks DL. Pretreatment Cancer-Related Cognitive Impairment-Mechanisms and Outlook. Cancers. 2019;11(5):687.
702. Brown JC, Cespedes Feliciano EM, Caan BJ. The evolution of body composition in oncology-epidemiology, clinical trials, and the future of patient care: facts and numbers. Journal of cachexia, sarcopenia and muscle. 2018;9(7):1200-8.
703. Crowder SL, Sarma KP, Mondul AM, Chen YT, Li Z, Pepino MY, et al. Pretreatment Dietary Patterns Are Associated with the Presence of Nutrition Impact Symptoms 1 Year after Diagnosis in Patients with Head and Neck Cancer. Cancer Epidemiology Biomarkers & Prevention. 2019.
704. Lucido CT, Wynja E, Madeo M, Williamson CS, Schwartz LE, Imblum BA, et al. Innervation of cervical carcinoma is mediated by cancer-derived exosomes. Gynecologic oncology. 2019;154(1):228-35.
705. Zhang G, Liu Z, Ding H, Zhou Y, Doan HA, Sin KWT, et al. Tumor induces muscle wasting in mice through releasing extracellular Hsp70 and Hsp90. Nat Commun. 2017;8(1):589.
706. Yang J, Zhang Z, Zhang Y, Ni X, Zhang G, Cui X, et al. ZIP4 Promotes Muscle Wasting and Cachexia in Mice With Orthotopic Pancreatic Tumors by Stimulating RAB27B-Regulated Release of Extracellular Vesicles From Cancer Cells. Gastroenterology. 2019;156(3):722-34.e6.
707. Ganju RG, Morse R, Hoover A, TenNapel M, Lominska CE. The impact of sarcopenia on tolerance of radiation and outcome in patients with head and neck cancer receiving chemoradiation. Radiotherapy and oncology : journal of the European Society for Therapeutic Radiology and Oncology. 2019;137:117-24.
708. Cho Y, Kim JW, Keum KC, Lee CG, Jeung HC, Lee IJ. Prognostic Significance of Sarcopenia With Inflammation in Patients With Head and Neck Cancer Who Underwent Definitive Chemoradiotherapy. Frontiers in oncology. 2018;8:457-.
709. Nichols AC, Theurer J, Prisman E, Read N, Berthelet E, Tran E, et al. Radiotherapy versus transoral robotic surgery and neck dissection for oropharyngeal squamous cell carcinoma (ORATOR): an open-label, phase 2, randomised trial. The Lancet Oncology. 2019;20(10):1349-59.
710. Goh J, Ladiges W. Voluntary Wheel Running in Mice. Curr Protoc Mouse Biol. 2015;5(4):283-90.
711. Sugihara M, Odagiri F, Suzuki T, Murayama T, Nakazato Y, Unuma K, et al. Usefulness of running wheel for detection of congestive heart failure in dilated cardiomyopathy mouse model. PLoS One. 2013;8(1):e55514.
712. Can A, Dao DT, Arad M, Terrillion CE, Piantadosi SC, Gould TD. The mouse forced swim test. J Vis Exp. 2012(59):e3638.
713. Bouganim S, Bergdahl A. Constructing an inexpensive and versatile homemade rodent treadmill. Lab Anim (NY). 2017;46(3):67-9.
714. Brant DH, Kavanau JL. 'Unrewarded' Exploration and Learning of Complex Mazes by Wild and Domestic Mice. Nature. 1964;204:267-9.

715. Yu K, Youshani AS, Wilkinson FL, O'Leary C, Cook P, Laaniste L, et al. A nonmyeloablative chimeric mouse model accurately defines microglia and macrophage contribution in glioma. Neuropathol Appl Neurobiol. 2018.
716. Garrett L, Lie DC, Hrabe de Angelis M, Wurst W, Holter SM. Voluntary wheel running in mice increases the rate of neurogenesis without affecting anxiety-related behaviour in single tests. BMC Neurosci. 2012;13:61.
717. Vyazovskiy VV, Ruijgrok G, Deboer T, Tobler I. Running wheel accessibility affects the regional electroencephalogram during sleep in mice. Cereb Cortex. 2006;16(3):328-36.